Use of hybrid iron oxide-silver nanoparticles for thermo-responsive drug delivery in pancreatic cancer

Mohsen Ali Asgari

A thesis submitted in partial fulfilment of the

Requirements of

Keele University

For the degree of Doctor of Philosophy

June 2020

Abstract

Pancreatic cancer is the 4th most aggressive cancer in the Western world. There are very little drugs available as chemotherapies for the treatment of pancreatic cancer. Of the ones used, most of them become eliminated by first pass metabolism before they reach their desired site of action. Nanoparticles which can work as drug delivery systems have huge potential for the treatment of different kinds of cancer such as pancreatic cancer. The qualities of silver nanoparticles applicable to human treatments are under investigation in assessing potential efficacy, laboratory and animal studies, toxicity, and costs. Coating Iron oxide with silver nanoparticles can lead increase silver performance and it can deliver the silver nano particles and cancer drugs to the target cells.

In this report, we focus on the design, synthesis, and characterization of hybrid iron oxide-silver core-shell nanostructures (HNPs). The HNP were characterised by various techniques such as magnetic properties, particle size, zeta potential, inductively coupled plasma (ICP), ultraviolet light (UV) and transmission electron microscopy (TEM). The laser mediated heating confirmed that the HNPs possessed surface plasmon resonance and hence highlights the potential of new HNP capability in thermo-responsive drug delivery.

The drug conjugation, stability and releasing of HNP- BNIPDSpm and HNP-BNIPDSpm-PEG Thiol were assessed by FTIR, zeta potential and high performance liquid chromatography (HPLC). HPLC results demonstrated new formulations have high physical and formulations stabilities. PEGylated formulations demonstrated greater release of drug in comparison with their unPEGylated counterparts. The drug release were assessed and optimised in biological media and aqueous environments.

The target peptide successfully conjugated in the novel drug formulations. *In vitro* drug uptake study also validated that hybrid formulations internalise and accumulate inside pancreatic cancer cells significantly higher than free drugs. The Cytotoxicity assays has shown the potential ability of BNIPDSpm novel formulations to accumulate and kill pancreatic cancer cells in comparison with free drugs, However there was not significant toxicity effect with naked HNP pancreatic cancer cells.

Key words: Iron oxide-silver nanoparticles, BNIPDSpm, surface plasmon resonance (SPR), polyethylene glycol (PEG), pancreatic cancer, thermo-responsive drug delivery, cytotoxicity assays, target peptide

ACKNOWLEGDEMENTS

Firstly, I would like to express my sincere gratitude to my supervisor Dr. Clare Hoskins for the continuous support of my Ph.D. study and related research, for her patience, motivation, and immense knowledge. Her guidance helped me in all the time of research and writing of this thesis. I could not have imagined having a better supervisor and mentor for my Ph.D. study. Besides my supervisor, I would like to thank the rest of my thesis committee and my advisor: Dr. Anthony Curtis for his insightful comments and encouragement, but also for the hard question which incanted me to widen my research from various perspectives.

I would also like to thank my very patient parents (Mr. Abolfazl Ali Asgari and Mrs. Badri Mohseni Seddigh) and my brother (Mr. Mehdi Ali Asgari) for being such a huge mental and financial support through my PhD! I have to mention that my dad has been one of the main encouragers on this way and he passed away because of the cancer on June 2017. This matter motivated me to research about cancer treatment and finds a beneficial way for preventing humans from death. I wish that this research will make my mother and father so happy and proud of me. My special gratitude also goes to my wife (Haniyeh Ebrahimi Fard), for her encouragement, help me to find best supervisor and love. She is the main reason that makes me sure about angel's existence.

And last but not least, completing this project would have been all the more difficult were it not for the support and friendship provided by the other members of the School of pharmacy at Keele University. I am indebted to them for their help.

Mohsen

Contents

List of Figures

List of Tables

List of abbreviations

5FU	*Fluorouracil*
AgNPs	*Silver nanoparticles*
AuNPs	*Gold nanoparticles*
BCRP	*Breast cancer resistance protein*
BNIDi	*Bis(naphthalimido)-1,20-diaminoicosane*
BNIPd	*Bis(naphthalimido)-1,12-diaminododecane*
BNIPDaoct	*Bis(naphtalimido propyl) di amino octane*
BNIPds	*Bis (naphthamimidopropyl)*
BNIPDSpm	*Bis(naphthalimidopropyl) spermine*
C(RGDfC)	*Cyclo(-Arg-Gly-Asp-D-Phe-Cys) peptide*
DMSO	*Dimethyl sulfoxide*
EPR	*Enhanced permeability and retention*
FTIR	*Fourier Transform Infrared spectroscopy*
HNPs	*Hybrid nanoparticles*
HPLC	*High performance liquid chromatography*
MNPs	*Magnetic nanoparticles*
MPS	*Mononuclear phagocyte system*

MRI	*Magnetic resonance imaging*
MTT	*3-(4,5-dimethylthiazol-2-yl)-2,5-diphenyltetrazolium bromide*
NPs	*Nanoparticles*
PDAC	*Pancreatic ductal adenocarcinoma*
PDI	*Polydispersity index*
PEG	*Polyethylene glycol*
PEI	*Poly (ethyleneimine)*
PCS	*Photon correlation spectroscopy*
RP	*Reversed-phase*
SDS	*Sodium dodecyl sulfate*
SERS	*Surface-enhanced Raman Scattering*
SH	*Thiol group*
SPIONs	*Super paramagnetic iron oxide nanoparticles*
SPM	*Scanning probe microscopy*
SPR	*Surface plasmon resonance*
TEM	*Transmission electron microscopy*
TB	*Trypan blue*

Chapter One

Introduction

1.1. Cancer

Cancer is characterised as unusual cell division in an uncontrolled manner. Some cancers may ultimately move and grew into other tissues and spread throughout the body. Cell growth and division are normal in all type of tissues, so cancer can initiate anywhere in the human body (Wilde *et al.,* 2012).

There are more than 200 different types of cancer. In all types of cancer, some of the body's cells begin to divide without stopping and spread into surrounding tissues. This may because of a growth called a tumour. The global cancer burden is evaluated to have risen to 18.1 million new cases and 9.6 million deaths in 2018 (International Agency for Research on Cancer, 2018). One in 6 women and one in 5 men worldwide develop cancer during their lifetime, and one in 11 women and one in 8 men die from the disease. There are some factors which can have an effect on causing cancer, including population growth and increasing number of older people (International Agency for Research on Cancer, 2018). The most causes of cancer related deaths in the world are lung, liver, bowl, breast, prostate and pancreatic cancer (ACS, 2011).

Risk factors relative to cancer are hereditary and can be classified as either preventable risk factors which include dietary habits (like high fat diet and alcohol), environmental factors (like ultraviolet radiation, chemical toxins and passive cigarette smoke inhalation) and non-preventable such as aging (patients over 75 account for more than 30% of all patients developing cancer (Yancik *et al.,* 2005). All these factors account for about 40% of cases in the United Kingdom (Surh *et al*., 2003; Yancik *et al.,* 2005; Moiseeva *et al.,* 2009; Cancer Research, 2016).

Pancreatic cancer

The pancreas is located within the abdomen surrounded by several other organs, major blood vessels and other tissue types (Zhi *et al.,* 2014). Pancreatic cancer is still remaining as the 4th cause of death associated with cancer in the Western world (Jemal *et al.,* 2007). Recently, CRUK have labelled pancreatic cancer as one of unmet need due to its poor patient survival rate and treatment progress in the last 40 years (Zhi *et al*., 2014).

Pancreatic cancer mostly increases with increased age and it most commonly diagnosed in the 65-75 year age group (Lowenfels and Maisonneuve, 2006). Every year, nearly 43,000 individuals diagnosed with pancreatic cancer will die of this disease in the U.S. The majority of cases are identified in the late stages of the cancer, when the likely hood of treatments to cure or indeed manage the disease is severely limited (Jiang *et al.,* 2019).

Surgical resection is currently the only potentially curable option for pancreatic cancer patients. Even though there are advanced surgeries for cancer tumours' resection, cancer recurrence is unavoidable in most patient and also relies on the patient being well enough for surgery which sadly is often not the case. Surgery often results in a median survival of approximately 11–15 months. Despite, the extraordinary advances have been occurred in chemotherapy and radiotherapy, death rates from pancreatic cancer has increased slightly in men and has levelled off in women (Jiang *et al.,* 2019).

Pancreatic cancer symptoms include pain in the upper or middle abdomen and back, jaundice, unexplained weight loss, loss of appetite and fatigue. Unfortunately, pancreatic cancer cannot be detected at early stages and most patients with localised disease have no detectable symptoms or signs. Therefore, it is not diagnosed until late stages, when cancer

has metastasised to other organs. This leads to poor prognosis and incidence equalling mortality (5 years survival rate) (Lowenfels and Maisonneuve, 2006).

There are very few drugs available as chemotherapies for the treatment of pancreatic cancer. Of the ones used, most of them become eliminated by first pass metabolism before they reach their desired site of action. Therefore, it is obvious that an improved method is required in order to transfer these drugs to their target sites which will increase efficacy and therapeutic effect. Ineffective absorption or problems of systemic drug circulation resulting in unwanted side effects are the main problems related to the treatment of cancer using traditional drugs. Therefore, the main rationale of this work is to produce drug carriers capable of improving drug efficacy by transferring them directly to the site of action (Lowenfels and Maisonneuve, 2006).

Pancreatic ductal adenocarcinoma (PDAC)

Pancreatic ductal adenocarcinoma (PDAC) is the most prevalent epithelial and one of the most lethal malignancies which occur. It can present anywhere in the pancreas but is most common is the pancreatic head. The late detection can lead to poor prognosis, however this is dependent on whether the cancer is localised or metastases have occurred. Overall survival rate for 5-years is just 3–5%. Pathologic variables associated with prognosis include tumour size and grade (Gui *et al*., 2019). Many physical barriers may affect efficient PDAC drug delivery which results from numerous pathological features. These barriers are leaky and disorganised with non-functional vasculature (Farrell et al. 2009), characteristically dense stroma (Neesse *et al*., 2011) and deregulated cellular transport proteins (Farrell *et al.,* 2009).

PDAC influences more developed countries than other parts of the world with more than 8000 cases diagnosed in the UK each year (Keane et al. 2014). It is now recognized that highly malignant and metastatic PDAC spreads from local precursor lesions called pancreatic intraepithelial neoplasia (PanIN). Molecular and pathological analysis has demonstrated an ordered series of genetic alterations during the progression of PanIN to PDAC. A general genetic analysis of 24 PDAC cases found an average of overexpression of 541 genes, which converge on 12 key cellular signalling pathways and 63 exotic alterations in this cohort (Song *et al*., 2019).

Clinical research has only displayed slight progress in the median overall survival of patients in the past 20 years ago (Lockhart *et al.,* 2005). Recent researches indicated that deregulated MicroRNAs (miRNAs) can play important role in PDAC development and progression by affecting multiple cellular processes, such as cell invasion, metastasis, proliferation, survival, apoptosis and chemotherapeutic resistance of PDAC (Sassen *et al*., 2008).

Treatments for pancreatic cancer

Surgical resection

Pancreatic Cancer surgery is the only possible way to remove the cancer and prevent to spread between other body organs. Even though, surgery can be effective in cancer treatment, surgery is only beneficial for patients in the early stages of the disease and it only prove to be effective in a rate ranging from 3-4% up to 27% as the 5 years survival rate report said (Ferrone *et al*., 2012; Shrikhande *et al*., 2007).

Unfortunately, there is no specific symptom in the cancer early stages. This can make the cancer diagnoses and treatment very hard. Whipple's procedure is the name of the surgical procedure for treating pancreatic cancer (Sa *et al.,* 2010; Kang *et al.,* 2016). Most of the failures of the surgery treatment of pancreatic cancer lead to recurrent relapse of the disease after operation. This is because of lack of appropriate detection techniques and failure of metastatic cancer removal within the pancreas at time of diagnosis. In this case, adjuvants chemotherapies can be useful method for completing cancer elimination. Adjuvants chemotherapies for pancreatic cancer are usually gemcitabine, capecitabine, paclitaxel, 5-fluorouracil and cisplatin (Ferrone *et al.,* 2012).

Cancer chemotherapy

Normal cells can grow and die in a controlled manner; however, cancerous cells keep growing without control. Chemotherapy works by killing the cancer, stopping them from dividing and reduce their growing speed. However, it can also harm healthy cells, which causes side effects. Depending on the sort and rate of chemotherapy, there are some side effects which may happen for patients. Some common side effects are fatigue, immunosuppression, nausea, vomiting, pain, and hair loss. Chemotherapy may be needed to be alone or with other treatments. The amount of chemotherapy is related to the level of cancer grows and the patients may get treatment every day, every week or every month (Nurgali *et al*., 2018).

Dosing of chemotherapy

Chemotherapeutic agents are mainly given in sequences to reduce the severity of side effects; the most of drug administration is normally several days to weeks (Avendano &

Menendez, 2008). However, chemotherapy is limited by considerable cytotoxicity which often leads to suspension of treatment or variation from the optimal treatment protocol to ensure adoption (Chabner and Longo, 2011). The dose of cytotoxic agent has to be exactly calculated according to the rate of tumour cells progress, sickness start time and patient ability to cope which such treatments.

Each chemotherapy regime can kill a certain percent of tumour cells and increasing dose of the agent will increase rate of cancer cell killing (Avendano & Menendez, 2008). However, high cytotoxic chemotherapy can lead to very bad side effects. Some of these side effects include gastrointestinal distress, alopecia, myelosuppression which can cause to blood cytopenia, immunosuppression and finally can induce a stroke-like syndrome that presents with transient neurological defects, for example alternating hemiparesis, aphasia, encephalopathy and seizures (Martino *et al.,* 1984; Walker *et al.,* 1986; Corrie *et al.,* 2008).

Gemcitabine

Gemcitabine was the first drug used as chemotherapeutic agent for pancreatic cancer treatment (Figure 1). Gemcitabine is a nucleoside analogue that mimics physiological nucleosides in terms of uptake and metabolism and is incorporated into newly synthesised DNA resulting in synthesis inhibition finally it can stop the chain and inhibit from tumour build-up (Cunha *et al.,* 2005). Gemcitabine has also been used for antiviral treatments aside from use in cancer therapy.

Although studies on patients demonstrate that this drug is only effective in 23.8% of patients, chemotherapy with gemcitabine is the only choice for the patients who surgical

resection is unable to remove the tumour (Neoptolemos *et al.,* 2010; O'Reilly *et al.,* 2011; Neoptolemos JP *et al.,* 2012; Tuveson & Neoptolemos, 2012; Vincent *et al*., 2011).

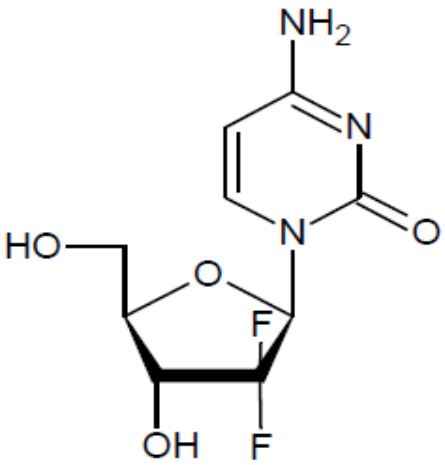

Figure 1: The structure of gemcitabine.

Capecitabine

Capecitabine IUPAC's name is Pentyl [1-(3, 4-dihydroxy-5-methyltetrahydrofuran-2-yl)-5-fluoro-2-oxo-1H-pyrimidin-4-yl] carba-mate (Figure 2). Capecitabine is a chemotherapy agent frequently used to treat solid cancers such as cancers, breast or pancreatic cancers (Akitake *et al.,* 2011).

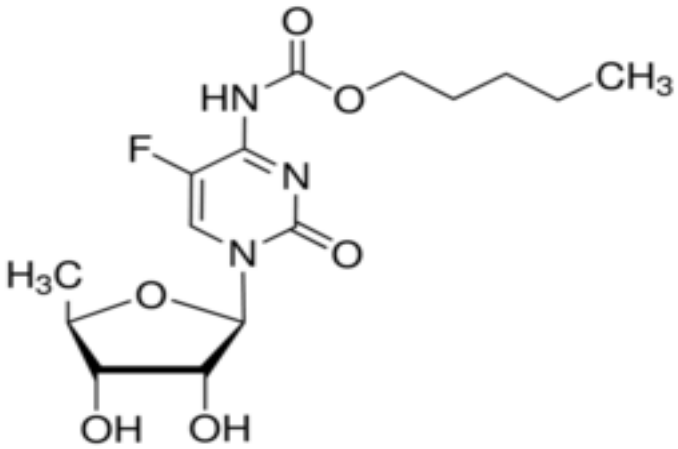

Figure 2: The structure of Capecitabine.

Capecitabine is active as single agent, but can also can be mixed with other cytotoxic agents, such as cisplatin (Lordick, *et al.,* 2014), Taxane (Naughton, 2010), Oxaliplatin and Irinotecan (Akitake et al., 2011). Capecitabine side effects are such as hair loss, fatigue, weakness, shortness of breath, headache (Okines, *et al.,* 2009). Capecitabine and intermittent 5-FU are known for a low prevalence of cardiovascular toxicity. In comparison between both drugs, the capecitabine is associated with a lower rate of neutropenia; however hand-foot syndrome (HFS) occurs far more regularly (Petrelli *et al.,* 2012).

Paclitaxel

Paclitaxel is an important member of the Taxane family of medications and without a doubt one of the most effective anti-cancer drugs of all time (Heinig *et al.,* 2013). Paclitaxel is the first microtubule-stabilizing agent identified and considered to be the most significant advance in chemotherapy of the past two decades (Figure 3). It is considered as one of most useful antineoplastic agents with widespread activity in various cancers including, endometrial cancer, bladder cancer, breast cancer, non-small-cell lung cancer and cervical carcinoma. It is also used for treating AIDS-related Kaposi sarcoma as a second line treatment (Heinig *et al.,* 2013).

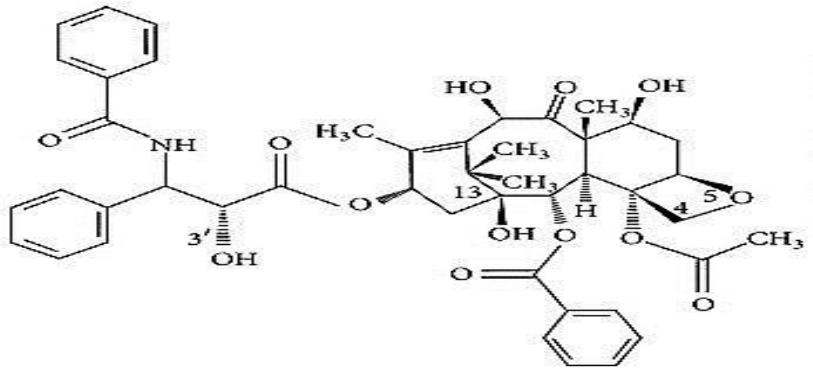

Figure 3: The structure of paclitaxel.

5-fluorouracil (5-FU)

5-fluorouracil (5-FU) is a thymidylate synthase inhibitor (Figure 4). This enzyme has responsible for the synthesis of thymidine. Thymidine is a nucleoside and it is crucial for DNA replication (Mohamed & Safwat, 2016). 5-FU has been extensively used for several decades to treat a variety of tumours including stomach, cervix, oesophagus, colon, breast and pancreas (Ajani *et al*., 2008; Rubinson *et al*., 2015; Takahari *et al.,* 2017).

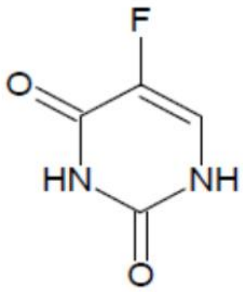

Figure 4: The structure of 5-fluorouracil (5-FU).

The primary mechanism of action of 5-FU is inhibition of thymidylate synthase. Thymidine is the main factor for DNA replication (Longley *et al.,* 2003). The ability of 5-FU to cross the blood brain barrier (BBB) may facilitate its central nervous system toxicity. 5-FU has second dangerous drug after anthracyclines. 5-FU Cardiac toxicity can manifest as chest pain, acute coronary syndrome/myocardial infarction, cardiac arrhythmias or rarely death (Chen *et al.,* 2014).

There are some factors which can lead to drug cardiac toxicity and two main likely factors are ischemia due to coronary vasospasm and drug-related myocardial toxicity. So impairment of executive function is the main issue which can be achieved by using 5-FU (Snyder, 2015).

Cisplatin

Cisplatin is a prototypic platinum chemotherapeutic agent and also first platinum which contain the anti-cancer drug. Cisplatin has four different mechanism for cancer removal include decreasing drug uptake, increasing DNA repair, defecting in apoptosis pathways, activation of pro-survival pathways and inhibition of pathways that promote cell death (Dai *et al.,* 2016; Fang *et al.,* 2017). Cisplatin structure includes a metallic coordination compound with two chlorine and two amine ligands in a cis conformation (Figure 5) (Dasari & Bernard Tchounwou, 2014).

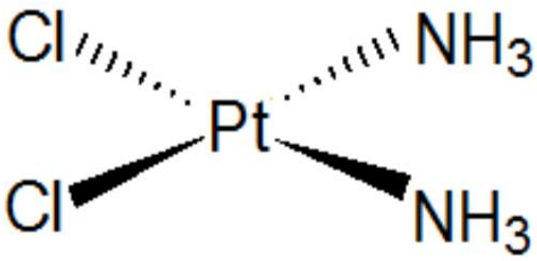

Figure 5: The structure of Cisplatin.

Cisplatin is useful drug for some of cancers including neck, lung and ovarian cancers. It also can be mix with some of chemotherapeutic drugs and use for breast, prostate and pancreatic cancers treatment (Dasari & Tchounwou, 2014).

Cisplatin must be activated by hydrolysis as it is chemically inert. In this case, chloride ions can replace with water molecules and make strong electrophile (Achkar, 2018). The amount of electrophile depending on the concentration difference of chloride ions between intracellular and extracellular milieu (approximately 2–10 mM, as compared to approximately 100mM in the extracellular space) (Michalke *et al.,* 2010). The electrophilic

forms of cisplatin can make bound to endogenous nucleophiles, such as metallothioneins, reduced glutathione (GSH) and methionine (Galluzzi, 2014).

Cisplatin interacts with nuclear DNA and mitochondria, which leads to the generation of inter- and intra-strand DNA crosslinks (Hu, 2018). This dativotes covalent binding forms DNA adducts which cause cancer cell DNA damage and block cell division which leads to apoptotic cell death (Dasari & Tchounwou, 2014). The studies demonstrate that the cancer cells can resistance against cisplatin treatment. There are many phytochemicals which are capable of reversing cisplatin resistance in various malignancies (Shahid *et al.,* 2018).

Naphthalimide and bisnaphthalimide based anticancer agents

In the early 1970s, the team of Brana published the first series of 1, 8 naphthal imides 1a-d possessing good cytotoxicity towards HeLa and KB cancer cells (Figure 6). The compounds were prepared by simple condensation of 3-nitro-1, 8-naphthalic anhydride with the amine side chain. Later, more derivative of naphthalimides were synthesised by changing ring substituents, and side chain (Roldan *et al*., 1973; Brana *et al.,* 1978; Brana *et al.,* 2001).

Studies demonstrate that the cytotoxicity of these compounds is very high as the presence of terminal amine functionality in the N-imide side chain. Specific substituent types on the naphthalic ring also play important role in increasing the cytotoxicity; for example, 3-amino, 3-nitro or 3-methoxy groups gave the best results. Activity was maximized when the amino group in side chain was two to three methylene groups from the 1, 8-naphthalimide unit. In addition, substitution at the C3 position of the naphthenic ring instead of C2 or C4 gave optimal results. According to the CPK model, the 3-nitro group lies in or nearer to then phthalic ring plane compared with a more sterically hindered nitro group at the C4 position

which rotates out of the plane (Paull and Nasr, 1984).This structure difference create stronger binding between binding of the3-nitro relative to the 4-nitro-1, 8-naphthalimide derivatives and DNA (National Cancer Institute, 1984).

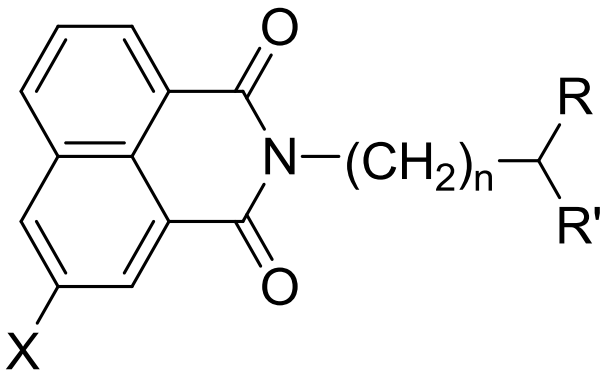

Figure 6: The structure of naphtha imides.

Mitonafide and Amonafide (Figure 7) were selected from a library of naphthal imides and thoroughly studied (go through Phase I and Phase II) because of their potent cytotoxic action against a group of cell lines. Both compounds use their action by binding to DNA by intercalation and inhibit Topoisomerase enzyme II action while, other naphthalimides are unable to inhibit Topoisomerase enzyme II (Lundberg *et al.,* 2011; Brana, 2001).

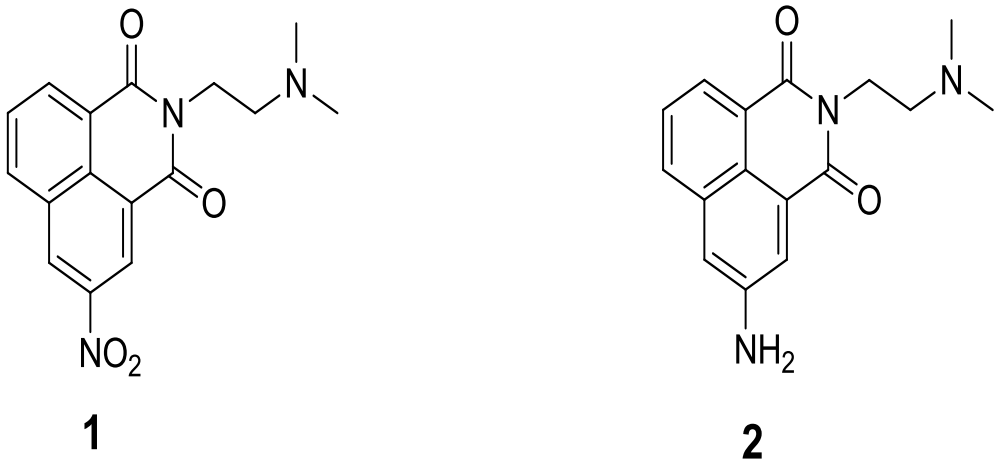

Figure 7: Chemical structure of Mitonafide (1) and Amonafide (2).

Changing both the chromophore substituents (in the order NO_2 > H > NH_2 > CH_3CONH) and the linker chain character (length and nature) can change biological activity of bisnaphthalimide compounds significantly. Derivatives of naphthalimides similar to Amonafide have been produced to increase the cytotoxic effects of the naphthalimides family. Bisnaphthalimides is one of these derivatives which have designed and synthesis to increase cytotoxic effect. This compound has stronger binding ability to DNA in comparison with the other naphthalimides derivatives (Brana et al., 2001).

Elinafide (Figure 8), a bisnaphthalimide derivative selected for phase I and phase II study, has no substituents in the chromophore and has seven methylene groups in the linker chain. Recent studies show that Elinafide has the highest cytotoxic effect in compare with the other bisnaphthalimide derivatives. Even though Elinafide cytotoxic effects are too high, it can lead to raising the side effect and restricting anti-cancer effects (Brana *et al.,* 2001).

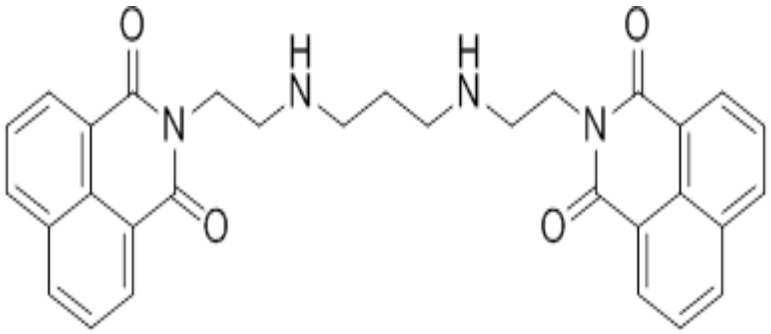

Figure 8: Chemical structure of Elinafide.

One of the problems for bisnaphthalimide using is the poor solubility property of bisnaphthalimide. In this case, asymmetric bisnaphthalimide derivatives were synthesised to solve the problem, however, cytotoxicity of these compounds decreased without great improvement of aqueous solubility of the parent compound (Braña & Ramos, 2001).

Lin and colleagues could synthesis new compounds by using polyamines into the linker chain of bisnaphthalimides in order to increase their aqueous solubility and activity (Lin & Pavlov, 2000) and (Pavlov *et al.,* 2001).

Combination therapy

Combination therapy is using multiple therapeutic agents with different mechanisms in combination for reducing the likelihood that resistant cancer cells will develop. In recent years, the combination therapy method has become the important strategy for cancer treatment. The varying pharmacokinetics of different drugs can lead to inconsistent drug uptake and suboptimal drug combination at the tumour sites and make them limit for cancer treatments. However, combination strategies in aim to maximize therapeutic efficacy is depend on the patient ability to cope this treatment, otherwise using combination therapy is impractical (Maiti *et al*., 2018).

Knox and his colleagues have published a significant research about combination of gemcitabine with Capecitabine efficacy on biliary cancer in 2005. They researched on forty-five patients were enrolled between July 2001 and January 2004. According to their research, "Eighty nine percent of patients had metastatic disease, 47% had gallbladder cancer and 43 percent had cholangiocarcinoma. The total objective response rate was 31%, with an additional 42% of patients with stable disease, for a disease control rate of 73%. The average of progression-free survival time was 7 months (95% CI, 4.6 to 11.8 months) and the average of total survival time was 14 months (95% CI, 7.3 months to not available)" (Knox *et al*., 2005). According to these data's, the chemotherapy combination was generally well tolerated. Even though some of side effects such as thrombocytopenia, fatigue, transient neutropenia and hand-foot syndrome were commonly observed but the rate of

side effects was very lower in compare with using single cancer drug and consequently, they could easily manage it without discontinuing further treatment (Knox *et al*., 2005).

1.2. Nanotechnology

Nanotechnology is concerned with the development, manufacture and use of materials that have structures, particles, fibers or platelets smaller than 100 nm. Hornyak and his colleagues argue that "it is not just about size, it is about the unique physical, chemical, biological and optical properties that emerge naturally at the nanoscale and the ability to manipulate and engineer such effects." Applications of nanotechnology are everywhere - it has helped make car bumpers lightweight, durable, and resilient; make fabrics resist wrinkling, staining, and body odour; improve shampoos, toothpaste, sunscreen, household cleaning products and food containers etc. (Hornyak *et al.,* 2008).

Nanotechnology accurately involves the making and application of biological, chemical and physical systems at scales ranging from single molecules or atoms to submicron dimensions, and also the integration of these resulting nanomaterials into larger systems. Scientists believe that nanotechnology has the potential to change and develop our perspectives about global issues and provide best resolve for future therapies. In the other words, nanotechnology has arisen as a multidisciplinary field, in which gaining a substantial understanding of the optical, electrical, mechanical and magnetic properties of nanostructures promises to deliver the next generation of functional materials with wide-ranging applications. Nanostructures have huge abilities to be used as a best solution in environmental and technological challenges such as solar energy conversion, water treatment catalysis and medicines (Zadeh *et al.,* 2019).

Nanotechnology in medicine

Human health is one of the most important subjects in the most of science research. In recent years, scientists constantly have considered nanoparticles as unique materials in medicine and especially in cancer treatment. Even though using nanoparticles are incredibly increasing for cancer treatment and little clinical translation has been realised, it is still believed that nanoparticles are on the verge of a new era in the near future (Li *et al.,* 2005).

Feynman is the person who was presented the concept of nanotechnology in his 1959 lecture. By saying "There's plenty of room at the bottom", defined the value of employing individual atoms using larger machines to creating smaller machines (Feynman, 1959). Nanoparticles are using in many different fields such as chemistry, engineering, biology and medicine. Nanoparticles are made by various physical and chemical methods such as photochemical (Li *et al.,* 2005) chemical reduction (Wang *et al.,* 2005) γ-radiation (Choi *et al.,* 2005) and laser ablation (Tsuji *et al.,* 2003).

There are two ways for drugs loading in the nano particulate systems. These are via incorporation technique or incubation techniques. In the incorporation technique, drug encapsulation is often achieved at the period of nanoparticle construction but in the incubation technique, adsorbing of the drug onto the nanoparticle surface is often carried out after the nanoparticles have been prepared (Shu *et al*., 2014).

Nano-drug delivery systems also have become a research hotspot in the field of drug delivery owing to the advantages of reduced drug toxicity and improved drug bioavailability. Be employing nano-drug delivery systems, drugs can be dissolved, adsorbed, and covalently bound to the surface of nanocarriers, or encapsulated and embedded inside nanocarriers.

Not only can this increase the solubility of the drug and improve its utilization in biological systems, it also targets the drug to the tumor site by exploiting the high permeability and retention effects of solid tumors, and by introducing surface modifications in the carrier. This helps avoid drug wastage by transportation to the normal tissues and enhances treatment safety (Kang *et al.,* 2018).

Nanoparticles can be comprised of organic or inorganic components. The organic nanoparticles consist of liposomes, amphiphilic polymers and dendrimers whilst the inorganic nanoparticles are often composed of metal oxides, gold and silver. Hybrid nanoparticles are constructed when two or more components are used to build more complex multifunctional systems conferring core-shell properties. The nano particles can be in different structure forms include micelles, vesicles, carbon nanotubes and metallic nanoparticles which are used for drug delivery systems (Islam & Miyazaki *et al.,* 2010; Salameh *et al*., 2014).

Research into NPs is in its infancy for pancreatic, liver, upper gastrointestinal and their use is becoming significantly popular as contrast media for radiological researches. On the other hands, more advanced technologies capable of active targeting are still in the first step of development for treatments in the clinics. Nanomedicines have many advantages for delivery, sensing and image-targeting agents (Andrén- Sandberg *et al.*, 2012).

Gregoria *et al.* prepared liposomes as drug carriers for the first time in 1974 (Gregoria *et al.* 1974). This was first study in cancer therapy by nanomedicine. The engineered NPs structure, shape, size and chemical properties open a huge range of technical applications and novel approaches in medical research (Yang *et al*., 2009).

In recent years most researches in NPs are based on polymeric (Thompson *et al*., 2008), liposomes (Park *et al.,* 2004), carbon nanotubes (Liu *et al*., 2007), quantum dots (Cai *et al.,* 2007), magnetic NPs (Thorek *et al.,* 2006), gold NPs (Huang *et al.,* 2011a) and silver NPs (Ferrari *et al.,* 2005; Grodzinski *et al*., 2006).

Polymeric and liposome NPs have been explored to encapsulate therapeutic agents in order to improve delivery efficiency, drug safety and increasing permeability of the cancerous tissues (Farokhzad and Langer, 2006; Moses *et al.,* 2003). Carbon-based NPs have been used for photo thermal therapy (Kam *et al.,* 2005) and drug delivery (Bekyarova *et al*., 2005; Bianco *et al.,* 2005; Lin *et al*., 2004).

Quantum dots have been exploited in biological finding and labelling because of their size dependent fluorescence properties (Bruchez *et al.,* 1998; Chan *et al.,* 1998; Lee, 2001). Magnetic NPs are suitable in magnetic hyperthermia therapy (Andra *et al.,* 1999; Hilger *et al.,* 2000; Kruse *et al.,* 2014), MRI and cell sorting (Liberti *et al.,* 2001; Lawaczeck *et al.,* 1997; Meyers *et al*., 1963; Schleich *et al.,* 2014) and drug delivery (Goodwin *et al.,* 1999; Joubert, 1997; Koppolu *et al.,* 2012).

Gold nanoparticles can enhance penetrability and retention (EPR) effect arising from the leaky vasculature and ineffective lymphatic drainage of the tumour tissue (Maeda *et al.,* 2000). In addition, the surface of gold nano particles can be changed and modified with active moieties such monoclonal antibodies, small molecules and peptides, to avoid from non-specific uptake, thus realizing tumour-specific targeting (Shakeri-Zadeh *et al.,* 2010; Sun *et al.,* 2014; Samadian *et al.,* 2016). Silver nano-particles (AgNPs) are widely used in a range of consumer products as a result of their antimicrobial properties (Xu *et al*., 2015).

Stimuli-responsive nano-carriers

Modifying of nanocarriers sensitive to exogenous or internal stimuli may indicate an attractive alternative to targeted drug delivery. The wide range of stimuli able to trigger the drug release at the right place and time, and the diversity of responsive materials that can be assembled in different architectures, allow great flexibility in the design of stimuli-responsive system. Nanoscale stimuli-responsive devices may be sentient to particular endogenous stimuli, like lowered interstitial pH, a greater glutathione concentration or an enhanced level of certain enzymes such as matrix metalloproteinases (Mura *et al*., 2013).

At the tissue level, one can take benefit of specific microenvironmental changes linked with neoplastic diseases (the treatment of which is the application of most of the research effort on stimuli-responsive nanocarriers) as well as pathological situations such as ischemia, inflammatory diseases or infections. At the cellular level, pH sensitivity can either trigger the release of the transported drug into late endosomes or lysosomes, or promote the escape of the nanocarriers from the lysosomes to the cell cytoplasm (Mura *et al*., 2013).

The consensus is that both the structural heterogeneity of the biological targets and the limited accessibility of the target cells are detrimental for drug targeting (often because of a combination of an exaggerate desmoplastic reaction, an excessive interstitial pressure and a poor status of endothelial blood vessels). Extracorporeal physical stimuli can be also applied.

For example, the targeted delivery of pharmacologically active molecules to a diseased area in the body can be magnetically guided by using ultrasmall iron oxide-based nanoparticles. Sustained drug release can also be achieved by thermo-, light- or ultrasound-sensitive nanoparticulate systems. Furthermore, the possibility of choosing between different routes

of administration (intravenous, oral, ocular or mucosal) is attractive (Mura *et al*., 2013). The thermosensitive liposomes, already in the clinical phase, are a good example. Consequently, immense progress in materials chemistry and drug delivery has led to the design of smart stimuli responsive concepts using well-engineered Nano systems (Mura *et al*., 2013).

Metallic nanoparticles

In 1857, Faraday first investigated the existence of metallic nano particles in solution. Metallic nano particle is nano sized metals with dimensions (length, width, thickness) within the size range of 1-100 nm. Nano materials can be prepared and adapted with huge different chemical structures and chemical functional groups. Metal nanoparticles include gold, palladium, copper, iron, zinc oxide, silver, selenium, platinum nanoparticles (Khande *et al*., 2016).

Nano materials can bind with antibodies, drugs and ligands. These materials applied in wide range of areas such as biotechnology, therapeutic area, vehicles for gene and drug delivery (Harish Kumar *et al.,* 2018). The advantages of metallic nanoparticles are diverse including the phenomenon possessed by some metallic nanoparticles (gold and silver) known as surface plasmon resonance (SPR). On the other hand, metallic nanoparticles have some disadvantages such as enhanced toxicity profiles, highly reactive nature, there can also be high chances of impurity from synthesis (Harish Kumar *et al.,* 2018).

Iron oxide metallic nanoparticles

In 200 BC, Chinese people discovered iron oxide magnetism properties by using rocks containing iron oxide for religious purposes. The advance of Fe_3O_4-based compasses for

navigation occurred in Europe as early as 850 AD. Fe_3O_4 was one of the first mineral structures produced by Bragg in 1915 (Bragg *et al*., 1915).

In the last decades, many different methods for the synthesis of iron oxide NPs have been published. Many reports have defined efficient green synthetic approaches to produce the biocompatible stable, shape controlled and monodispersed iron oxide NPs (Bharde *et al*., 2008). Some of most applied methods include sono-chemical, micro emulsion, coprecipitation, hydrothermal synthesises and thermal decomposition (Cabrera *et al.,* 2008).

Additionally, there are some biological methods for preparing there NPs which can be useful as well. These methods include microorganism or bacterial synthesis (especially the Magneto tactic bacteria and iron reducing bacteria) (Bharde *et al*., 2008; Roh *et al*., 2006), electrochemical synthesis (Pascal *et al.,* 1999) and laser pyrolysis techniques (Bomati Miguel *et al.,* 2011).

In recent years magnetic iron oxide NPs (MNPs) is the main subject of the researches because of they use for hyperthermia, imaging and many applications from utilising in the recovery of metal ions and dyes to drug delivery (Comoucka *et al.,* 2010; Neuberger *et al.,* 2005). Studies have highlighted MNPs offer the benefit of utilising both EPR effect (passive targeting) whilst also allowing for a direct, externally guided delivery to the tumour (active targeting) (Arruebo *et al.,* 2007). Iron oxide is used as a contrast agent in MRI scanners. Recently, scientists have focussed on coating magnetic nanoparticles with drugs, which can held the drug and deliver it to the desired site of action (Mejías *et al*., 2015; Dilnawaz *et al.,* 2011).

Iron oxide for magnetic resonance imaging (MRI)

Magnetic iron oxide nanoparticles (MNPs) are currently under research development to provide better diagnosis for a various range of diseases such as cancer (Ferrari *et al.,* 2005), cardiovascular disease (Wickline *et al.,* 2007) and neurological disease (Corot *et al.,* 2004).

Magnetic resonance imaging (MRI) is one of the major instruments used for clinical diagnosis due to its high soft tissue comparison, three-dimensional resolution (Ferrari *et al.,* 2005), depth penetration (Edelman, 1996) and ability to show contrast between healthy and diseased tissue (Wickline *et al.,* 2007).

Furthermore, MRI does not use ionizing radiation or radiotracers which can cause harmful side-effects. These days, magnetic iron oxide nanoparticles (MNPs) have become the in centre of attentions by scientists because of their great biomedical capability (Acar *et al.,* 2005). They have been used in targeted therapy, drug delivery and biological discovery by imaging (Corot *et al.,* 2004).

MNPs have large surface area in compared to their volume and low surface charge. MNPs cannot easily distribute in solution because of their magnetic property which causes of sedimentation of MNPs in solution. According to Neuberger, NPs can easily distributed in solution if coatings with polymers or other hydrophilic molecules are applied (Neuberger *et al.,* 2005). Magnetic nanoparticles can strongly adapted by various surface layers (Kalska Szostko *et al.,* 2014).

Interfacial reformation of the magnetic moment can lead to a rise in the magnetic hyperfine field and splitting of the MS spectra, which is in good agreement with data published for multilayers (Pan *et al.,* 1996). Particular chemical surface rectification is useful for further

bonding of biological particles. Recent researches demonstrate that some metals such as gold, copper and silver can play important role for surface modification. The noble metals have interesting type of functionalization in comparison to the oxidised one. This property can distinguish them with other metals. The layer of metals nature can lead to an enhancement in the district of the compounds able to connect to magnetic nanoparticles with special emphasis on bio application (Vekas *et al.,* 2006; Lu *et al.,* 2010; Sanvicens *et al.,* 2015; Weller *et al.,* 1996; O'Reilly *et al*., 2005).

Khana and their colleagues have studied about increasing gemcitabine therapeutic efficacy in pancreatic cancer by using superparamagnetic iron oxide nanoparticles in 2019. They could synthesize and develop a superparamagnetic iron oxide nanoparticle (SPION) formulation of curcumin (SP-CUR) (Khana *et al.*, 2019). This compound was characterized by different methods and confirmed that it's not toxic, bioactive anti-cancer or bioactive anti-inflammatory agents. The SP-CUR was played an important role in increasing drug delivery to the target cells (tumours). Moreover, their studies proved that Iron oxide could enhance gemcitabine (GEM) efficacy for reducing tumour growth and metastasis and pancreatic cancer treatment (Khana *et al.*, 2019).

Many nanoparticles, including superparamagnetic iron oxide nanoparticles (SPIONs) are using in different researches to delivery drugs to the desired site of action (tumour) or imaging. Vekas *et al.* could synthesise and preclinical evaluation of a multifunctional nano probe for dual MRI and optical imaging of pancreatic tumours. They synthesised a novel backbone cyclic core peptide targeting SSTR 1–5 with conjugating the Nano probe contains the magnetic ion cores for MRI and fluorescent dyes for fluorescence imaging and then they were anchored to FITC.PTR86 (Vekas *et al.,* 2006). The Nano probe demonstrated no

detrimental effect on the cellular viability as confirmed by FACS data analysis of DAPI stained cells. They researched results demonstrated the improved accumulation of targeted Iron oxide Nano worms had better performance in compare with non-targeted nano worms in mice bearing subcutaneous human pancreatic ductal adenocarcinoma (PANC-1). Consequently, the resulted hybrid nano probe can be used as multimodal diagnostic agents for targeted imaging with commercially available PET-MRI scanners (Vekas *et al.,* 2006).

Gold nanoparticles

In recent years significant progress in the design and application of numerous nanomaterials also improve and develop an understanding of the biomedical properties of nanoparticles for cancer treatment has occurred (Ferrari *et al*., 2005). In this area, gold nanoparticles (AuNPs) have recently emerged as promising agents. There are various types of AuNPs based on the physical properties, size and shape such as nano-rods, nano-shells, nanoparticles and nano-cages (Yang *et al.* 2015; Dreaden *et al.,* 2012).

AuNPs between 2 nm and 100 nm in diameter can be synthesised by wet chemical method, which is controlled reduction of an aqueous chloroauric acid ($HAuCl_4$) solution with different reducing agents under varying conditions (Cai *et al.* 2008).

Smaller Particle sizes have better chemical and physical properties, with interesting biomedical applications (Qian *et al.* 2008). AuNPs are useful for many different fields such as imaging (Zhang *et al.* 2009), cancer therapy (Jain *et al*. 2012), and drug delivery (Khan *et al.* 2014). Brazzale, Canaparo and their colleagues have discovered important evidences about AuNPs capabilities in generate cytotoxic reactive oxygen species (ROS) upon light and

ultrasound irradiation. They proved that AuNPs can promote in photodynamic therapy (PDT) and sonodynamic therapy (SDT), respectively (Brazzale *et al.* 2016).

Gold nanoparticles for cancer treatment

The enhanced permeability and retention (EPR) effect is a controversial concept by which molecules of certain sizes (typically liposomes, nanoparticles, and macromolecular drugs) tend to accumulate in tumor tissue much more than they do in normal tissues. This is highly dependent upon cancer type as solid tumours are widely regarded as being difficult to penetrate. The surface of AuNPs can detect tumour-specific targeting easily as their functionalized are similar with active targeting moieties such as monoclonal antibodies, proteins, small molecules and peptides (Shakeri-Zadeh *et al.* 2010), (Shakeri-Zadeh *et a*l. 2010) and (Sun *et al*. 2014).

AuNPs have high surface area-to-volume ratio and versatile surface chemistry. These properties make them suitable option to use as nano carriers for drug delivery (Ghosh *et al.* 2008). Moreover, AuNPs are qualified agents to be used as effective radio sensitizers for increasing cancer radiotherapy because gold nanoparticles have high atomic number to provide a larger X-ray absorption cross-section (Her *et al.* 2017).

Recent studies have demonstrated that the photo thermal conversion capability of AuNPs make them significantly beneficial to contribute for hyperthermia in cancer therapy (Ghaznavi *et al*., 2018). Surface Plasmon Resonance (SPR) is a phenomenon that happens when polarized light hits a metal film at the interface of media with various refractive indices. This is resultant from the surface plasmon resonance of gold a unique property which makes it highly desirable in tumour ablation (Hong *et al.* 2018).

Blood endothelial cells are leaky at the tumour site, which let penetration of NPs to the tumour milieu. However, the lymphatic endothelial cells are tight at the cancer site, which cause retention of the NPs at cancer site and prevent their departure from the surrounding tumour cells. Gold nanoparticles are able to preferentially remain at the tumour site via enhanced permeability and retention (EPR) effect arising from the leaky vasculature and ineffective lymphatic drainage of the tumour tissue (Maeda *et al.* 2000).

Biomedical application is the application of technology and engineering to living beings, especially the design and employment of medical equipment. Beik and colleagues studied on AuNPs in combinatorial cancer therapy strategies in 2019. They discovered that AuNPs could make a distinctive opportunity to combine various treatment modalities at the same time. Consequently, AuNPs have more applicability to cancer therapy in comparison with another nanostructure. “They provide a figure to show heat map the biomedical applications of some commonly used inorganic nanostructures. Red colour demonstrates that the respective nanostructure has not been reported to be applicable in a specific therapeutic modality. Bold blue colour indicates the extensive use of the respective nanostructure in a specific therapeutic modality” (Figure 9) (Beik *et al.,* 2019).

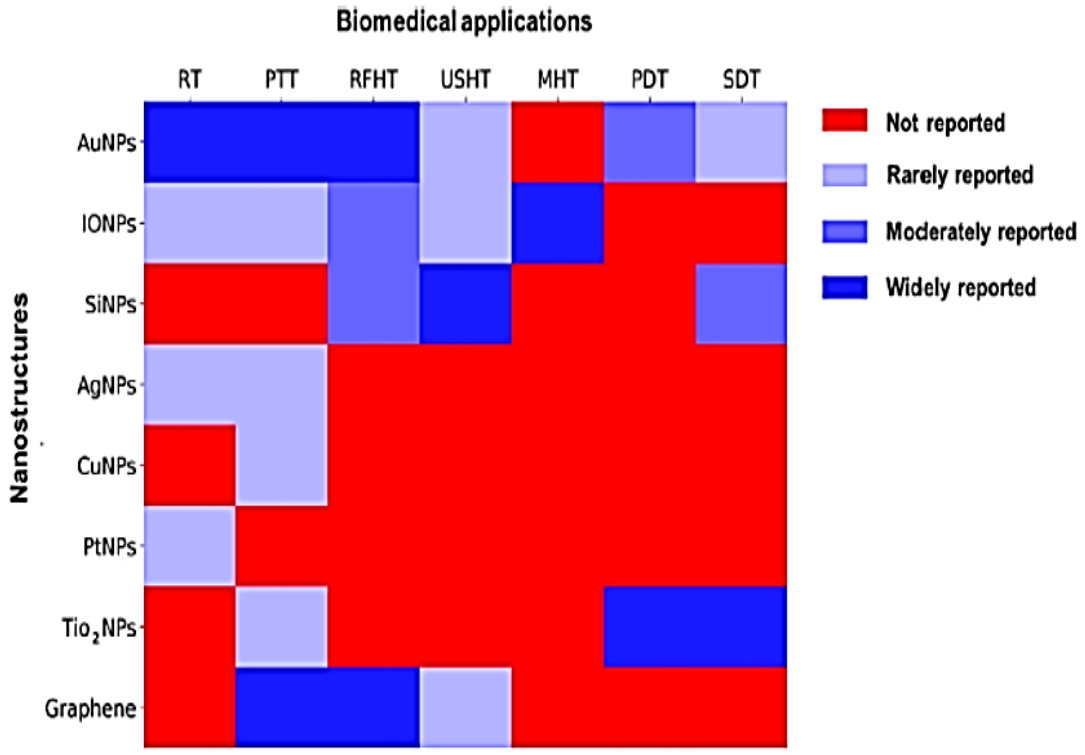

Figure 9: Various Nano structures biomedical applications (Beik *et al.,* 2019)

Xu and colleagues fabricated dumbbell-like iron oxide-gold NPs and coupled with Herceptin and a platin complex. The platin-gold-iron oxide-Herceptin complex as a target-specific nanocarrier was capable to deliver platin into Her2-positive breast cancer cells (Sk-Br3) with strong therapeutic effects (Xu et al. 2009). Moreover, literature has revealed that the oxidised maghemite form preferentially binds gold compared with the magnetite form and is more stable and biocompatible form of iron oxide (Lyon et al. 2004).

Silver Nanoparticles

Silver nanoparticles (AgNPs) demonstrate highest level of usage at market in compare to other nanoparticles (Xiu *et al.,* 2012). Almost 55.4% of the total nanomaterial- based consumer products are captured by AgNPs in the market (Wilson *et al.,* 2011; Asghari *et al.*, 2012). Colloidal silver in the nano-scale has taken part in as the significant amount of

functional nano-antimicrobial in consumer products such as surgical coatings, dietary supplements, cosmetics, textiles, food packaging, medical implants, and water sterilized applications (Monteiro *et al.,* 2009).

The earlier researches verified that it is hard to achieve nanoparticles with size below 10 nm with high mono distribution and stability (Shirtcliffe and Nickel, 1999; Caswell, 2003). Therefore, there are significantly important to synthesis AgNPs in smaller size. It is also modified the stability and distribution of the particles in the system (Pal *et al*., 2007; Steinigeweg *et al.,* 2003).

In most of the cases, borohydride-mediated reduction has been used for the synthesis of dispersible silver nanoparticles in wide range (Lin *et al.,* 2003; Tan *et al.,* 2003). However, $NaBH_4$ is not good desirable in the production of large silver nanoparticles where other basic solvents are preferred (Yang *et al.,* 2011). Another further weaker reducing agent is trisodium citrate (TSC) which contributes to manufacture of comparatively large silver nanoparticles. However, it has a wider size distribution (Creighton *et al.,* 1979). It is also significantly important to modify the shape of the nanoparticles for instance cubes, triangles and spherical nanoparticles are go supplemented with unwanted generation of rods (A. Pyatenko *et al.,* 2007; Sharma *et al*., 2009). The recent studies demonstrated that applying either of sodium boro hydride (NaBH4) and trisodium citrate (TSC) can be enough effective to synthesize silver nanoparticles with size below 10 nm (Arvizo *et al.,* 2012).

Silver nano particles stability

Konwarh *et al.* did significant research about silver stability. According their research, the mechanism of the AgNP formation is shown in Figure 10. They investigated that polyvinyl

acetate (PVA) and AgNPs mixture can lead to optical clarity which facilitates investigation of nanoparticles formation. In fact, PVA plays an important role in improving AgNPs stability because PVA prevents AgNPs from aggregation. Even though PVA concentration rising does not lead to the reduction of AgNP size, It is important to note that PVA as a protective agent plays a conclusive part in controlling the size distribution of AgNPs (Konwarh *et al.,* 2009).

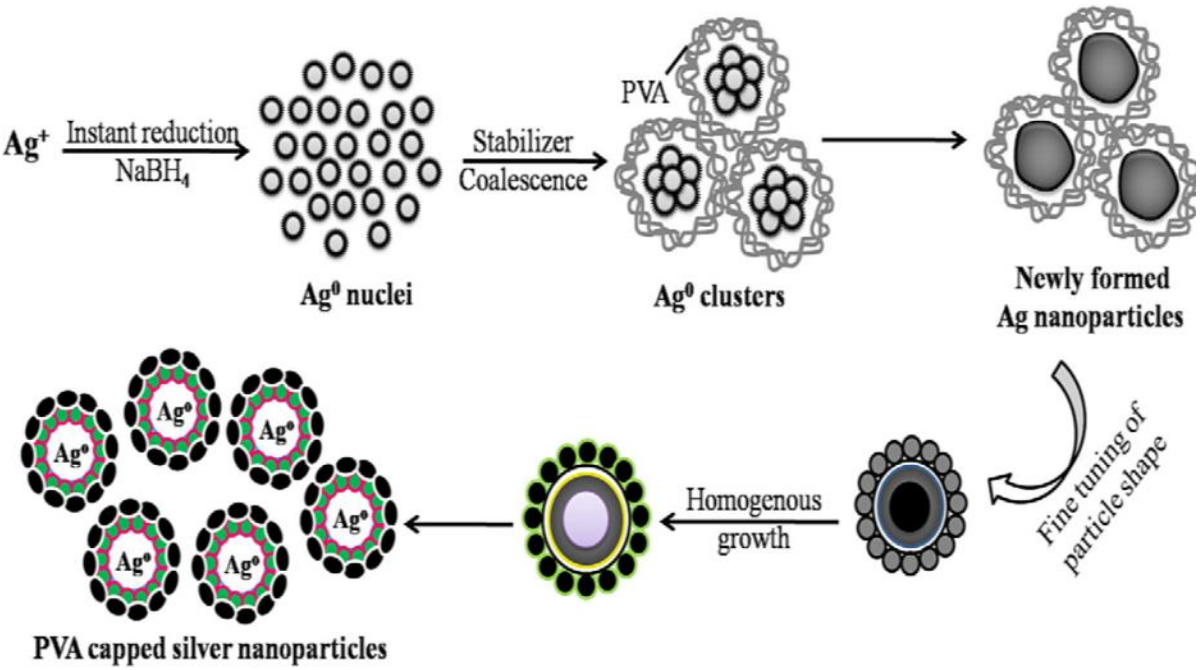

Figure 10: Schematic of size controlled AgNPs synthesis employing the chemical reduction method (Ajitha *et al*., 2015).

Silver nano particles antimicrobial properties

Silver nanoparticles have been expended in different fields such as surface enhanced Raman scattering (SERS), biosensors, optoelectronics and antimicrobials (Sun *et al*., 2002; Bois *et al.,* 2010; Dong *et al.* 2009).

Silver's antimicrobial property has been extensively applied because of to its oligo dynamic action broad (Thiel *et al.,* 2007), spectrum killing (Lok *et al.,* 2006) and minor possible danger for growth of microbial resistance against it (Gunawan *et al.,* 2011).

Earlier studies have verified that AgNPs antimicrobial activity is dependent to the variation of size and shape, in consequence; smaller nanoparticles are better antimicrobial activity than greater nanoparticles (Morones *et al.,* 2005). Different shape of the particle could produce different efficacy in different diseases, truncated-triangular nanoparticles appeared to be more effective for microbial killing. In comparison with different silver nanoparticles shapes, spherical nanoparticles have higher potential in antimicrobial activity (Agnihotri *et al*., 2013; Agnihotri *et al*., 2012; Mukherji *et al.,* 2012).

Recent studies have shown that silver nanoparticles have brilliant antimicrobial and antiviral properties in comparison with the other metal nanoparticles (Zhang and Wang, 2003; Claus *et al.,* 1999; Compagnini *et al.,* 1997; Elechiguerra *et al.,* 2005). Silver has high surface to volume ratio, this property cause to increase their biomedical activities. Consequently, silver is relatively free of adverse effects so this metal originally used as an effective anti-microbial agent. Recent studies demonstrate that this property using electron microscopy, which has revealed size dependent interaction of AgNPs with bacteria (Morones *et al*., 2015).

Ajitha and their colleges studied on Enhancing antimicrobial activity of silver nanoparticles with controlled particle size by pH variation in 2015. According to their studies "Silver nanoparticles of various sizes were synthesized through a simple reduction method at various pH values of the reaction solution (Ajitha *et al*., 2015). XRD results approved the decrement of crystallite size with the rise of pH. Morphological studies demonstrated the formation of spherical nanoparticles. The SPR peak is discovered to be shifted towards the

blue end with the increase of pH indicating the decrease in the particle size. A development in photoluminescence intensity was found with the increase of pH. Outcomes of antimicrobial studies demonstrated that the AgNPs efficiently inhibited different pathogenic organisms and reduced their viability in a pH-dependent manner". Their work infers that the fine-tuning of synthesis parameters will enhance possibilities of desired Nano product tailor-made for specific sensitive applications (Ajitha *et al*., 2015).

Silver nano particles toxicity

There are many ways of human exposure to AgNPs, including ingestion, dermalabsorption, inhalation and injection (Ahamed *et al*., 2010). Some of in vitro studies demonstarted AgNPs cytoxicities towards various types of human cells (Asharani *et al.,* 2012; kitti *et al*., 2013; Foldbjerg *et al.,* 2012; Gliga *et al.,* 2014). However, the scientists have not found clear and acurate answer about the AgNPs toxicity mechanisms so far (Browning *et al*.,2013).

This is very important to know that how specific physicochemical properties, such as particle size and surface chemistry can affect on cell viability (Ahlberg *et al.,* 2014; Comfort *et al*., 2014). There are some researches which have evaluated the amount of AgNPs toxic potential in different properties such as NP formulations (Boonkaew *et al.,* 2014), different AgNPs sizes (Kim *et al*., 2012), the storage environment (Ahlberg *et al*., 2014) and the duration of exposure (Comfortetal., 2014)however there is not many researches about decreasing AgNPs cytoxicity by coating them with polymers (Sharma *et al.,* 2009).

Numerous polymers have also been used to coat AgNPs, such as polyvinyl pyrrolidone (PVP) (Haberl *et al*., 2013) and poly (ethylene glycol) (PEG) (Lópezetal, 2009; Nymark *et al*., 2013). Some of researches has reported that coating silver nano particles with the polymers can

decrease silver toxicity, promote stability and avoid aggregation (Tao *et al.,* 2007; Lópezetal, 2009).

The few studies which have published the influence of coating on AgNPs toxicity stated conflicting information. It has been reported that the charged PVP coating improved the stability of AgNPs and decreased their toxicity (Zhang *et al.,* 2014), while other studies reported that PVP-coated AgNPs could be highly cytotoxic to mammalian cells (Grosse *et al*., 2013).

Polyethylene glycol (PEG) have low molecular weight and able to neutralize the surface charge and lead to stabilize NPS through steric hindrance. PEG coating has been reported to decrease NP reactivity (Povoski *et al*., 2013), improve penetration through the mucus layer and decrease Silver toxicity (Lópezetal, 2009). These results has caused to increase the interest in the use of this polymer for nanomedicine purposes(Suk *et al*., 2011; Tetley, 2013).

Silver nano particles for cancer treatment

Silver nano particles (AgNPs) has shown potential cytotoxicity against various number of cancer cells such as cervical cancer HeLa cells (Jeyaraj *et al*., 2013), lung cancer A549 cells (Gengan *et al*., 2013), Dalton's lymphoma ascites tumour (Sariram *et al*., 2010), breast cancer MCF-7 cells (Jeyaraj, 2013) and colon cancer HT29 cells (Sanpui, 2011).

Pharmaceutical application of nanomaterial is the most favourable way and also newest way for preparation of new biomedical sciences topic. nano formation of silver basically has significant characterises for suitable conductivity and outstanding therapeutic potential such as anti-inflammatory, antiplatelet, antimicrobial, antifungal, anti-angiogenesis and

anticancer activities and also chemical stability between different silver nanoparticles (AgNPs) (Austin *et al*., 2014; Vaidyanathan *et al*., 2009; Dar *et al*., 2013; Tolaymat *et al*., 2010).

Hsin *et al.* experiment was demonstrated in the mitochondrial pathway of apoptosis by AgNPs in NIH3T3 cells, which is mediated by a ROS- and JNK-dependent mechanism (Hsin, 2008). Gurunathan *et al.* furthermore determined evidence for AgNPs able anti-angiogenic influence due to the activation of PI3K/Akt signaling pathways (Gurunathan *et al.,* 2009).

One of the important abilities of AgNPs is to act selectively to inhibit creation of HeLa cells by caspase-3-mediated which causes cell death and DNA damage (Jeyaraj and Rajesh, 2013). Still, none of the molecular triggers have been revealed any of the underlying biochemical mechanisms (DeLima and Seabra, 2012). However, the toxicity of AgNPs developed noticeable to be driven by the escape of silver ions. Although AgNPs has great cytotoxicity rate alongside NSCLC A549 cells, some of latest researches has been demonstrated that there are not cytotoxicity toward normal healthy peripheral lymphocytes (PLs) (Gengan *et al*., 2013). Greulich *et al.* stated that silver ions were more cytotoxic toward bacteria and human cells than AgNPs (Greulich *et al*., 2012).

The AgNPs effects are not same as those of silver ions in inducing neurotoxicity through oxidative stress in rat cerebral astrocytes (Sun, 2016). Although, the recent researches have achieved the promising information's in this case, the toxicity effects of AgNPs are proven but the underlying molecular mechanisms inside the human cells still are not fully recognised up to now. The cellular events were untangle in human glioblastoma cells (U251) and normal human lung fibroblast cells (IMR-90), and they displayed mitochondrial dysfunction and induction of reactive oxygen species (ROS), which cause turning off

chromosomal deviation and DNA damage, as the possible mechanisms (Asharani *et al.,* 2009).

Regarding to José study *in vivo,* Intramuscular organization of AgNPs critically raised mice survival at day 35 in L5178Y-R tumour-bearing mouse model (José *et al.,* 2013).

Sriram *et al.* studies designated that, the efficacy of biologically synthesized AgNPs have significant ability in anticancer therapy. In metastasis of cancer the initiate cancer call travel through the blood cycles and lymphatic system and create another new cancer somewhere else in the body. In consequence, AgNPs have a strong inhibitory activity on disease development, metastatic cancer cell and a potent restorative effect in a Dalton's lymphoma ascites tumour-bearing mouse model (Sriram *et al.,* 2010).

Sanpui research demonstrated that "AgNPs showed a strong inhibitory effect on the growth of NSCLC cells (H1299) associated with their effects on bcl-2, caspase-3, and survivin. In a mouse H1299 xenograft tumour model, injection of mice with AgNPs potently suppressed the growth of H1299 tumours in SCID mice. AgNPs are better candidates for lung cancer chemoprevention than chemotherapy *in vivo*. Further researches should be carried out for the potential use of AgNPs in the treatment of NSCLCs" (Sanpui, 2011).

Hybrid nanoparticles

Hybrid nanoparticles have been reported in the literature consisting of metallic cores surrounded by additional coatings of another material. This could be polymeric based, lipid based or metallic based (Figure 11) (Chen *et al*., 2009).

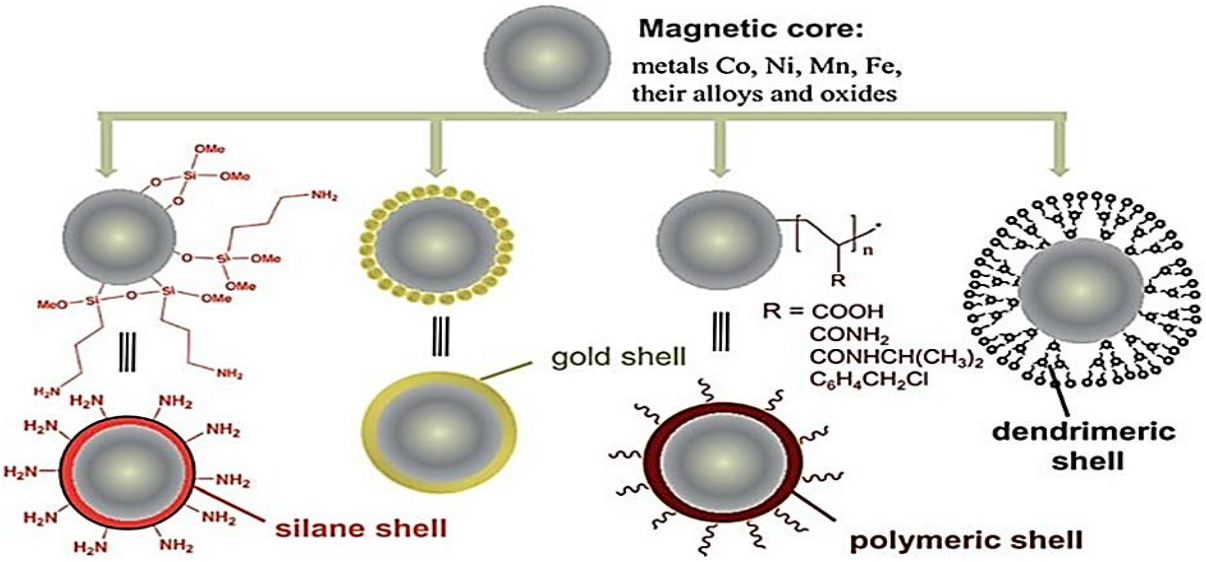

Figure 11: Magnetic nanoparticles with various shells (Chen *et al.,* 2009).

Shells structured from noble metals do not allow degradation of the internal core particularly protecting them from physiological conditions like pH. They can also cause to better and longer stability of nanoparticles core in different solvents (Ang *et al.,* 2014).

Stabilization by thiol ligands of Au and Ag shell can influence optical properties what directly can be applied in sensing devices. Sperling *et al*. were carried out significant study on the surface modification, functionalization and bio conjugation of colloidal inorganic nanoparticles on 2010. According the research, "gold nanoparticles stabilized by various thiol ligands with or without functional organic groups demonstrate that optical properties of the thiol-stabilized gold nanoparticles strongly relate on the composition of the ligand shell. Such dependence is a result of the ligand shell's direct influence on the electronic structure of the particle core" (Sperling *et al*., 2010).

Iron oxide coated gold hybrid

Magnetic nano particles (MNP's) can be coated with materials such as silica, polymers, silver and gold. These materials can make the safe MNP's safer. Iron oxide NPs coated with gold

are referred to as hybrid nanoparticle HNPs (Figure 12). Gold surfaces bind strongly with thiol (-SH) containing molecules via dative covalent linkages. This allows for ease of surface modification (Malekigorji *et al.,* 2014).

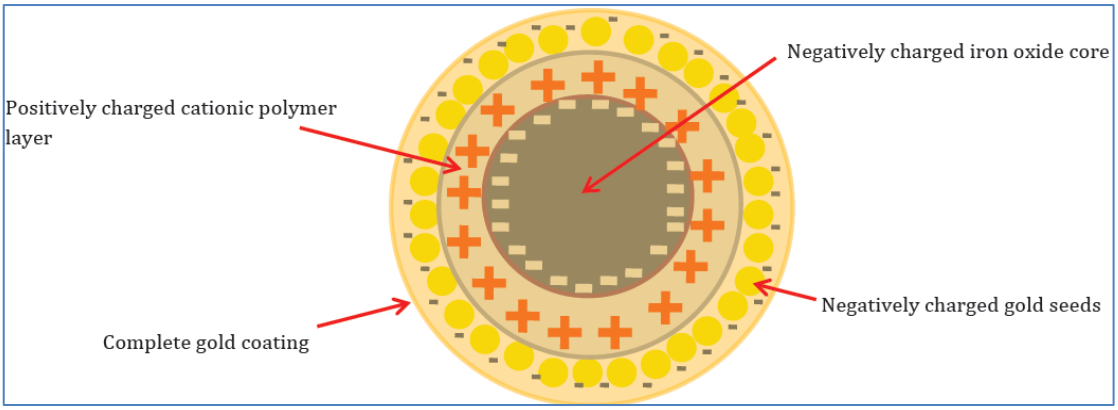

Figure 12: Schematic diagram of AuNPs surface charges (Malekigorji *et al*., 2014).

Some studies have exploited this for the treatment of pancreatic cancer. Kumagai and his colleagues studied on enhanced *in vivo* magnetic resonance imaging of tumours by PEGylated iron oxide - gold core shell nanoparticles with prolonged blood circulation properties in 2010 (Kumagai *et al*., 2010). In this study, high-density PEG coated iron oxide gold core shell nanoparticles with roughly 25 nm in diameter with a narrow distribution were synthesised as T2-weighted magnetic resonance imaging (MRI) contrast agents for cancer imaging (Kumagai *et al*., 2010). Bio distribution tests in mice bearing a subcutaneous colon cancer model prepared with C26 murine colon adenocarcinoma cells demonstrated high gathering of the PEG-AuIONs within the tumour mass and low nonspecific accumulation in the liver and spleen, resulting in high specificity to solid tumours. The research results demonstrated that PEG-AuIONs are a promising MRI contrast agent for diagnosis of malignant tumours, including pancreatic cancer (Kumagai *et al*., 2010).

Iron oxide coated silver hybrid

Iron oxide core- silver shell hybrid nanoparticles (HNPs) are of interest due to their multifunctional nature. Not only do these particles possess the magnetic benefits from the iron oxide but they also possess the antimicrobial properties as well as ease of functionalisation and heating ability of the colloidal silver (Sotiriou *et al*., 2010). Iron oxide core- silver shell hybrid structures add magnetic functionality to silver antimicrobial and anticancer properties (Jeyaraj *et al.,* 2013). Iron oxide is one of the best drug carriers, moreover silver nanoparticles can be unique assist to the drug for destroying the tumour for cancer treatment.

Coating Iron oxide with silver nanoparticles can lead increase silver performance and it can deliver the silver nano particles and cancer drugs to the target cells. Targeted drug delivery is more advantageous than conventional drug therapy as in targeted drug delivery only a desirable area in the body is affected, which can minimise the side effects caused by conventional drug therapy. The purpose of drug chemotherapy is to transport a drug to the targeted area and treat the disease without affecting surrounding healthy tissue (Seil *et al*., 2012). Recent researches demonstrate that anticancer and antibacterial efficiency of silver nanoparticles in Ag-Fe_3O_4 is stronger in compare with Ag-Fe_2O_3 heterodimers or plain Ag (Chen *et al*., 2013).

Eugênia and their colleges carried out significant research on Compact Ag-Fe_3O_4 Core-shell Nanoparticles in 2014 (Eugênia *et al*., 2013). They design capable and efficient synthetic route to produce novel compact core-shell structures of silver surrounded by magnetite. It consists in a parallel silver seed production in the same reaction medium of the iron thermal decomposition without vacuum application in a temperature-paused ramp (Eugênia *et al*.,

2013). The studies of the size, structure and magnetic properties of the multifunctional brick-like Ag-Fe_3O_4 NPs obtained reveal them as possible candidates for advanced medical purposes. They could discover that Ag-Fe_3O_4 NPs compact magnetite capping will help to increasing the biocompatibility as it helps to hinder the diffusion of silver ions to the surroundings (Eugênia *et al*., 2013).

1.3. Aims

To the best of my knowledge no research has focussed on the use of iron oxide and silver hybrid nanoparticles for cancer treatment. Following on from the success in Dr. Hoskins group with gold coated iron oxide in pancreatic cancer, I wanted to investigate whether switching the coating from gold to silver would result in a better delivery system. This is based on the assumption that silver has increased plasmonic properties compared with gold and may result in for efficient heat triggered delivery. To test this theory, we aimed conjugated novel bispnaphthalimido drug compounds electrostatically onto the surface of our fabricated particles and study their physical, chemical and biological properties in order to assess their potential as new therapies in pancreatic cancer treatment.

The hybrid iron oxide-silver nanoparticles research is consisting of different parts include synthesis and characterisation of HNPs. Firstly, the hybrid nanoparticles will be synthesised and characterised using inductively coupled plasma-optical emission spectroscopy (ICP/OES), fourier transform infrared spectroscopy (FTIR), transmission electron microscopy (TEM), UV/Visible spectroscopy and photon correlation spectroscopy and zeta potential measurement. Moreover, laser irradiation assess for thermos responsive drug delivery. In the second part drug loading (bisnaphthalimide based drugs), drug releasing assess and optimise and also HNP physical and chemical stability assess in various conditions.

Consequently, new formulations design and assess *in vitro* conditions. Third part is biological investigations of the novel formulations. In this part the hybrid nano particles cytotoxicity measure and compare with the drug and new formulations by MTT and trypan blue assays. *In vitro* cellular uptake of formulation comparison between only the drug and the new formulations will be conducted.

Chapter Two

Synthesis and characterisation of iron oxide-silver core-shell hybrid nanoparticles

2.1. Introduction

Silver nanoparticles (AgNPs) are capable to be used in various technologies such as nanoscale electronics (Yang, 2010), imaging (Lee *et al.,* 2006), catalysis (Christopher *et al*., 2008) and surface enhanced raman scattering (Baik *et al*., 2009). In recent years, silver nanoparticles are in centre of attention for many studies such as anticancer and anti-angiogenic agents in retinal endothelial cells (Sriram *et al*., 2010).

It is a well-known fact that silver ions and silver-based compounds are highly toxic to microorganisms which include major species of bacteria. This aspect of silver makes it an excellent choice for multiple roles in the medical field. Silver is generally used in the nitrate form to induce antimicrobial effect, but when silver nanoparticles are used, there is a huge increase in the surface area available for the microbe to be exposed to.

AgNPs demonstrated significant toxicity properties in various human cells such as human brain cells (U251) (AshaRani *et al*., 2009), endothelial cells (Kalishwaralal *et al.,* 2010), human lung fibroblast cells (IMR-90) and MDA-MB-231 human breast cancer cells (Gurunathan *et al*., 2013). Silver nanoparticles have the ability to anchor to the cancer intraceluular bacterial wall and subsequently penetrate it, thereby causing structural changes in the cell membrane like the permeability of the cell membrane and death of the cell. There is formation of 'pits' on the cell surface, and there is accumulation of the nanoparticles on the cell surface (Sondi *et al*., 2004). The formation of free radicals by the silver nanoparticles may be considered to be another mechanism by which the cancer cells die. There have been electron spin resonance spectroscopy studies that suggested that there is formation of free radicals by the silver nanoparticles when in contact with the

bacteria, and these free radicals have the ability to damage the cell membrane and make it porous which can ultimately lead to cell death (Danilcauk *et al.,* 2006)

There are some different methods for synthesising of silver nano particles with various sizes (Jau-RungChiou *et al.,* 2013; Agnihotr *et al*., 2012). Agnihotr synthesised silver nanoparticles with various sizes such as 5 nm, 7 nm, 10 nm, 15 nm, 20 nm, 30 nm, 50 nm, 63 nm, 85 nm and 100 nm (Agnihotr *et al*.2012). Silver nanoparticles were synthesized by using sodium borohydride ($NaBH_4$) as a primary reducing agent and trisodium citrate (TSC). Both of agents have grate potential to act as secondary reducing agent and the stabilizing agent. The reduction processes were accomplished in two stages thermal treatment involves 60 °C and 90 °C. The best pH of the solution was identified to be pH 10.5 using certain amount of sodium hydroxide (Agnihotr *et al*., 2012).

Controlled synthesis of nanoparticles was established on the co-reduction approach using a two stage thermal treatment (Figure 13) (Agnihotr *et al*., 2012). The initial reduction was accomplished using $NaBH_4$ at 60 °C (stage I). In this stage the large number of silver nanoparticles starts to be produced. At this stage, the reduction of silver cations leads to creation of new silver nuclei. Silver nanoparticles formed at the initial stage consequently participated in the growth process. In stage II the temperature should rise to be 90 °C. In this stage, TSC-mediated reduction of unspent Ag ions occurred. On the other hands, TSC presented with $NaBH_4$ during the initial stage. At the lower temperature dominating in stage I, TCS play important role in preventing silver nanoparticles agglomeration. An adequate NaBH4 to TSC ratio was acute to control the nucleation and progressing procedure in the two stage co-reduction approach (Agnihotr *et al*., 2012).

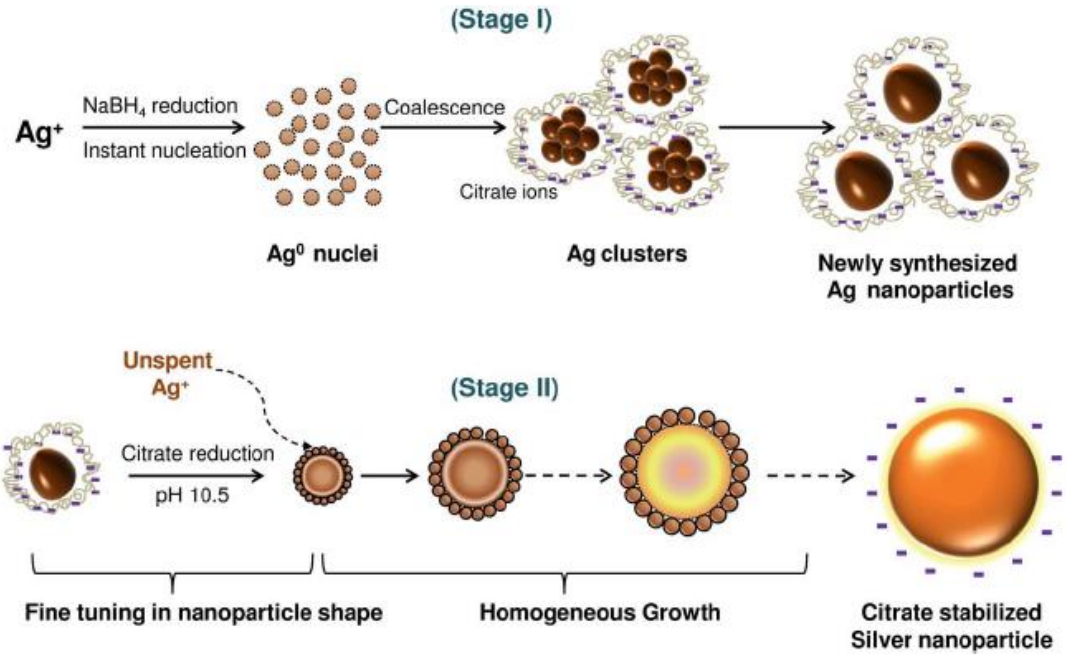

Figure 13: Different stages in synthesis of silver nanoparticles (Agnihotr *et al*., 2012).

Agnihotr and their colleague studies demonstrated that $NaBH_4$ is main factor for achieving silver nanoparticle smaller sizes. The AgNPs with range of 60- 100 nm can easily accumulate and TSC was the most important reducing agent for preventing silver nanoparticles agglomeration (Agnihotr *et al*., 2012). The silver nano particles were characterized by UV-Vis, TEM, XRD, zeta potential analyser. Consequently, the experiments shown that even though all AgNPs were found to be highly toxic to the bacterial strains, their antibacterial efficacy sharply increased with lowering particle size. This effect was considerably increased as the size of nanoparticles moved to the 5 nm range. AgNPs demonstrated 5nm size was the fastest bactericidal activity in compare to 7 nm and 10 nm (Agnihotria *et al.,* 2012).

The work in this chapter follows the synthetic route plans by Agnihotr and colleagues for the production of AgNPs for application in antibacterial and anti-cancer therapy (Agnihotria, *et al*., 2012).

Magnetic iron oxide NPs (MNPs) has significant potential in the recovery of metal ions and drug delivery systems (Comoucka *et al*., 2010; Neuberger *et al*., 2005). Coating iron oxide with silver nanoparticles can be an important step in cancer treatment. Iron oxide has shown great potential as a drug carrier, however covering this magnetic core in a silver shell can present unique multifunctional properties permitting for image guidance as well as triggered heating (Sotiriou *et al.,* 2010).

There are a few strategies reported for the synthesis and fabrication of iron oxide – silver nanoparticles such as facile one-pot green method (Jau-RungChiou *et al.,* 2013) and precipitation-deposition method (Sangili *et al.,* 2019). Jau-RungChiou and colleagues reported the one-pot green synthesis of silver/iron oxide compound nanoparticles for 4-nitrophenol reduction in 2013 (Jau-RungChiou *et al.,* 2013). They could successfully synthesize silver/iron oxide compound nanoparticles *via* a facile one-pot green method by the use of L-arginine. The green synthesis route is a noble way for synthesis metal nano particles by using harmless alternative bio compatible molecules such as vitamin B2, proteins, starch, amino acids, coffee and tea, d-glucose, peptides, cellulose, soybeans and extract as stabilizing and reducing agents (Nadagouda *et al.,* 2008).

Chiou and colleagues studies demonstrated that when ferrous chloride was used for the synthesis of iron oxide nanoparticles, silver chloride was designed instead of metallic silver in the followed silver coating (Chiou *et al.,* 2013). However, for synthesising iron oxide they used ferrous sulphate. The experimental data showed that, the action rate increased with escalating the reaction temperature. Therefore, the best temperature for synthesising was 70°C according to the research. The silver weight was 8.53% of total product and with a pH=10. The particle size for the final product was about 13.8 nm. It displayed acceptable

catalytic activity for the reduction 4-aminophenol from 4-nitrophenol by using sodium borohydride. The reduction reaction followed the pseudo-first-order kinetics. In addition, this product had quite good stability. In their research there was not considerable activity loss was happened after reuse for five cycles (Chiou *et al.,* 2013).

Sangili and colleagues worked on synthesis of silver nanoparticles decorated on core-shell structured tannic acid (TA)-coated iron oxide nano spheres (Sangilia *et al*., 2019). In first step, they synthesised TA-Fe_3O_4-AgNPs monohybrid. In this case, Fe_3O_4 nano spheres were organised by the solvo thermal method.

The average particle size for iron oxide was about 250 nm. The second step was coating Fe_3O_4 nano spheres by using a thin layer of carbon cell with TA as a carbon source *via* hydrothermal method. Hydroxyl and kenotic group play important role in immobilizing the catalytic active species (Sangilia *et al*., 2019). As the matter of fact, hydroxyl and kenotic compounds possess functional groups on the surface of the Fe_3O_4 nano sphere. In last step, Ag ions were added to the product and the ions were adsorbed by the hydroxyl/ ketonic group of TA present on the Fe_3O_4. Consequently, TA can act as an excellent stabilizer and green reducing agent to convert Ag ions to AgNPs (Sangilia *et al*., 2019).

Joshi *et al.* investigated the silver and gold nanoclusters have very similar optical properties (Joshi *et al.,* 2015). Silver and gold nanocluster's also have so similar crystal structure using X-ray diffraction. In this case, it would be possible to use synthesis of Fe_3O_4-Au core-shell HNPs for silver nanoparticles as well (Joshi *et al.,* 2015).

Barnett and colleagues studied on the synthesis of Fe_3O_4-Au core-shell HNPs with the core diameter of 70 nm, using a polymer intermediate ((poly (ethylenimine) (PEI)) (Barnett *et al*.,

2013a). These particles finally were PEGylated with PEG-thiol through dative covalent bonding between the gold shell of the NPs and the thiol groups (-SH) on the polymer (Barnett *et al.,* 2013a). Particles were characterised by the size of particles, Fourier transform infrared spectroscopy (FTIR), zeta potential, transmission electron microscopy (TEM) and T2 reflexivity. Moreover, The HNP heating potentials were checked to proof any physical degradation might happen since first measurement during 6 months (Barnett *et al.,* 2013a). HNPs were suspended in 3 different contains such as deionised water, the dialysis membrane and conical flasks containing 200 mL RPMI cell culture media (in sink condition). Media was pH modified from pH 7.2 and 4.5 to mimic blood and lysosomal physiological conditions.

The hybrid formulation was investigated for Fe and Au content by inductively coupled plasma-optical emission spectroscopy (ICP-OES). The metal concentration in HNP formulation was measured and ICP results demonstrated 3:1 ratio for Fe: Au (wt:wt). FTIR spectroscopy was shown the presence of characteristic the PEG coating peaks attributed. After six months, there were not any surface alteration and particle size modification which was confirmed by ICP and TEM, for the formulation. Zeta potential measurements test results also indicated that the gold shell did not degrade during the stability test. The ΔT values (change in temperature) achieved upon laser irradiation shown to be stable after six months, evaluated to the initial study (Barnett *et al.,* 2013a).

This work describes the synthesis and characterisation of silver coated iron oxide HNPs based on the techniques Barnett and colleagues reported for HNP assembly (Barnett *et al.,* 2013a). This method is able to synthesis magnetic nanoparticles and also capable coat the Iron oxide by AgNPs. As Iron oxide and AgNPs have negative surface charge so it would be

hard to stabilize coating, moreover, the iron oxide surface is to smooth. In this case, using PEI is so applied method as it had negative surface charge and the difference between the surfaces charges can steak the AgNPs strongly to the Fe_3O_4 coated with using PEI. Characterisation of the HNPs will be carried out using a number of analytical and microscopy techniques, photon correlation spectroscopy and zeta potential measurement, ICP-OES, UV/Visible spectroscopy, photon correlation spectroscopy, laser irradiation and transmission electron microscope (TEM). These methods are described below in relation to our work.

Inductively coupled plasma-optical emission spectroscopy (ICP-OES)

Inductively coupled plasma optical emission spectroscopy (ICP-OES) method has been used over the past three decades for various applications and particularly in the quantification of metal in nanoparticle synthesis (Parham *et al.,* 2009). This technique is ordinarily used in inorganic chemistry to quantify metallic element in systems such as metals concentration measurement in hybrid nanoparticles (Warra and Jimoh, 2011).

A schematic diagram of ICP- OES can be seen in Figure 14 (Boss and Fredeen, 1997). Fundamentally by injecting the samples into the ICP, the formation of solid samples modified to the liquid state and subsequently this material digest in the acids which mainly are hydrochloric and nitric acid. However, the gas and liquid state samples can be injected straight into the instrument (Mermet, 2005). In next step, the solution injected as a fine aerosol by combining it with a stream of argon gas which acting as a nebulizer (Todolí & Mermet, 2006). This aerosol is transferred with argon plasma of around 7000 °C to excite the outer electrons of the metals within the sample. After excited state, atoms will rest to the ground state through the emission of a photon, which have particular energy level. This

energy can be identified via the quantised energy level structure for the atoms or ions. Therefore, the wavelength of the photons determines the elements from which they originated. Finally, the concentration of element in the sample was calculated by considering the photons total numbers (Hou and Jones, 2000).

The work reported in this chapter will use ICP to confirm the ratio concentration of iron and silver in the novel hybrid nanoparticles.

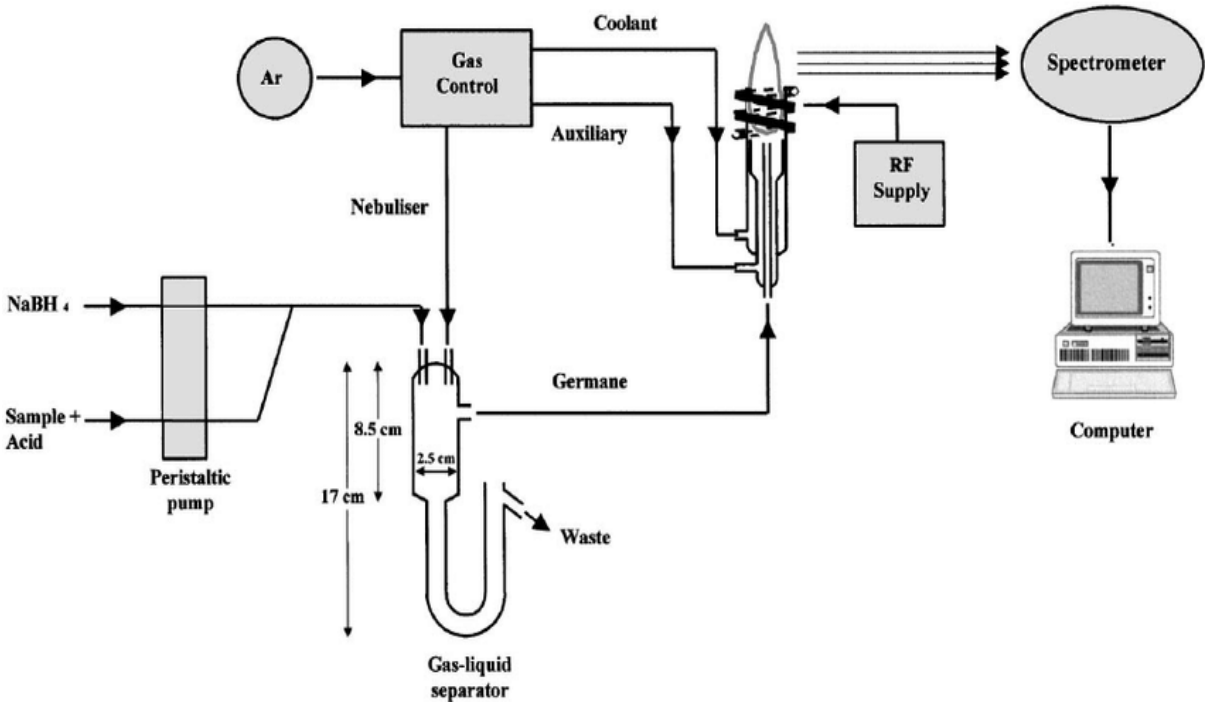

Figure 14: Schematic diagram of ICP-OES (Farias and Smichowski, 1999).

UV/Visible spectroscopy

Ultraviolet and visible (UV/Vis) spectroscopy is the main common analytical technique used to assess the absorbance of visible light and ultraviolet radiation of materials, usually organic compounds with conjugation and transition metals (Dean *et al*., 2002c).

UV/Vis is a valuable tool in most scientific research, to demonstrated metal or ligand binding and the stability of compounds and reaction kinetics (Mohamed *et al*., 2012; Alison and Bruce, 2010). The spectral variety is between 190 nm to 800 nm (Brian, 2002). When light is adsorbed after passing through the sample, outer electrons are pushed to higher states. This is because the electrons energy levels increase by electromagnetic radiation. The electrons are kept tightly in single bonds, making them hard to excite but the electrons take in double and triple bonds are kept less strong and can be exited even more. UV/Vis spectrometer includes of an appropriate wavelengths radiation source, tools for isolating light to a single wavelength (monochromator and optical geometry), a sample container for set up the test sample and convert them to the light beam and lastly a sensor to assess the light intensity (Figure 15).

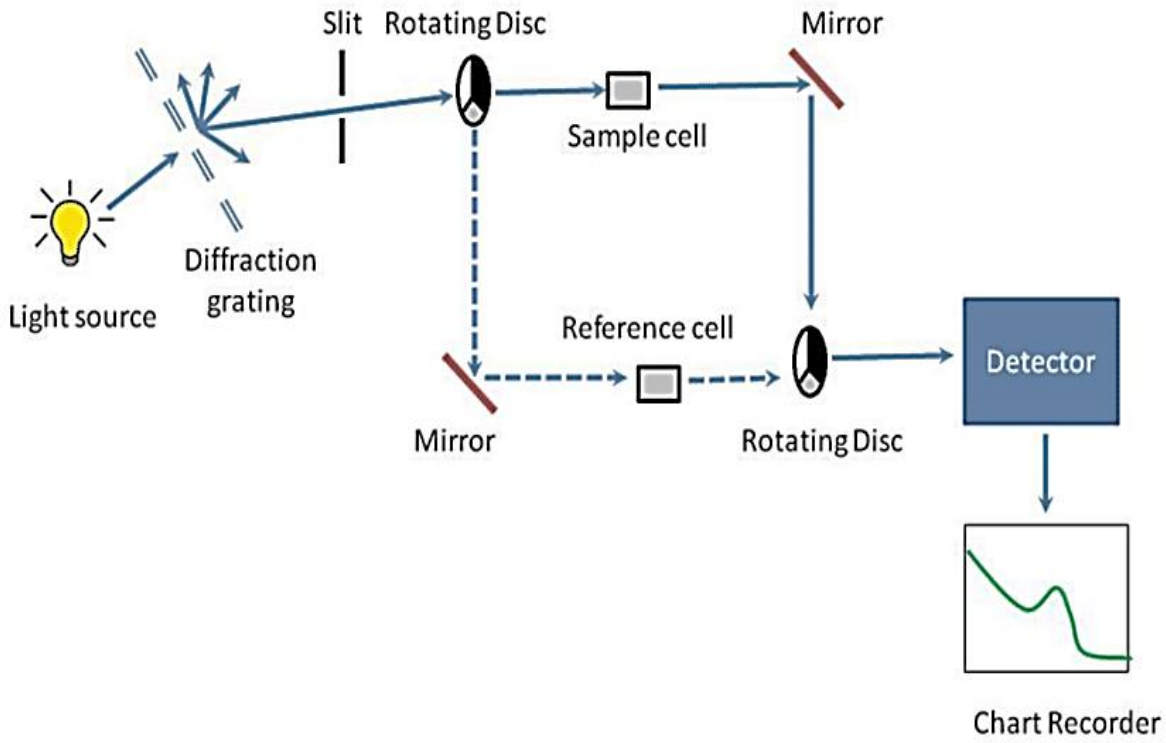

Figure 15: Simplified UV-vis diagram (Bordoloi, 2017)

Transmission electron microscopy (TEM)

Transmission electron microscopy (TEM) is a useful technique for detecting the surface of materials with more details based on shape and size. TEM has been used to image nanomaterials, measuring of particle and/or grain size, size distribution, and morphology. In this technique, a beam of electrons with high energy is allowed to pass through a very thin layer of specimen which causing scattered by the internal structures (Joyce *et al.,* 2015) (Figure 16).

TEM like other microscopic techniques is used for observing the surface of materials at a detail too high for the naked eye. Conventional optical microscopes use a series of lenses to magnify the images of materials to a size visible with the naked eye. However these lenses diffract visible light and are limited by the Abbe diffraction limit, which is the point where a microscope cannot distinguish two objects close to each other. The condition of images depends on the contrast of the sample relative to the background. The samples were made by drying NPs on a copper grid, which is coated with a thin layer of carbon. Chemicals with high electron densities such as carbon nanotubes, metals (copper, silver, gold and etc.) and metal oxides (iron, titanium and silica oxides), polymer NPs and quantum dots can be easily imaged compared with amorphous carbon. Consequently, TEM can be useful technique for observing size and shapes of nanoparticles in each step of synthesising (Douglas B, 2002).

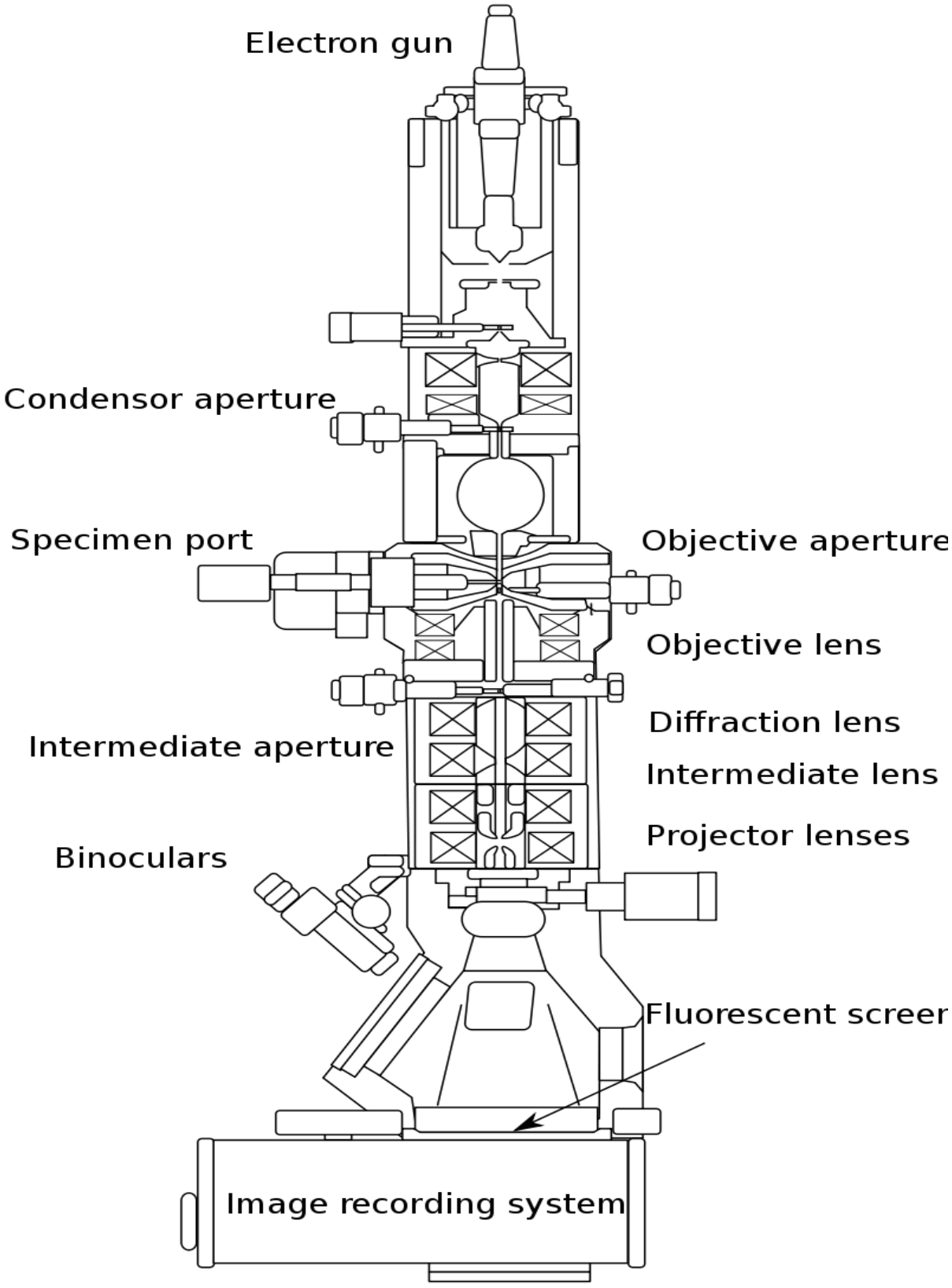

Figure 16: Schematic diagram of TEM (Wikimedia Website).

Photon correlation spectroscopy

Photon correlation spectroscopy (PCS) is based on the dynamic light scattering of a laser beam of a certain wavelength by particles or macro-molecules in a liquid medium. PCS known as dynamic light scattering (DLS) and this technique was developed by Robert Pecora in 1964 (Pecora, 1985). A schematic diagram of PCS can be seen in Figure 17.

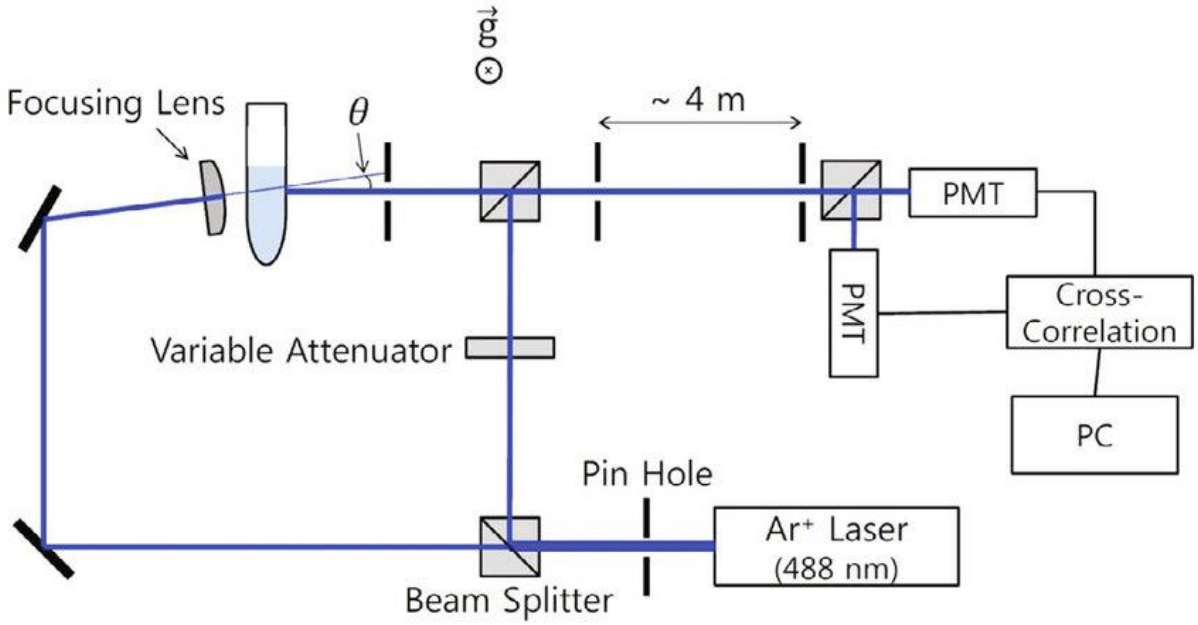

Figure 17: Schematic diagram of PCS (Lee *et al*., 2016).

PCS is used to identify macromolecule and nanoparticle size in solution. This technology is non-destructive and non-invasive. When small particles are exposed to the incoming light, the light will scatter in all directions. If the light supply coherent and monochromatic laser by moving particle and their speed level, PSC can detect dispersion intensity randomly in the solutions (Lee *et al*., 2016)

Large particles move more slowly in a liquid than smaller particles, speed of motion is used to measure by the PSC (Figure 18). The existed small particles in the liquid expose in PSC light, so the dispersion intensity of scattering light measure by the detector.

The dynamic data of the particles is originated by an auto-correlation of the intensity trace recorded all over the procedure (Sibilia, 1996).

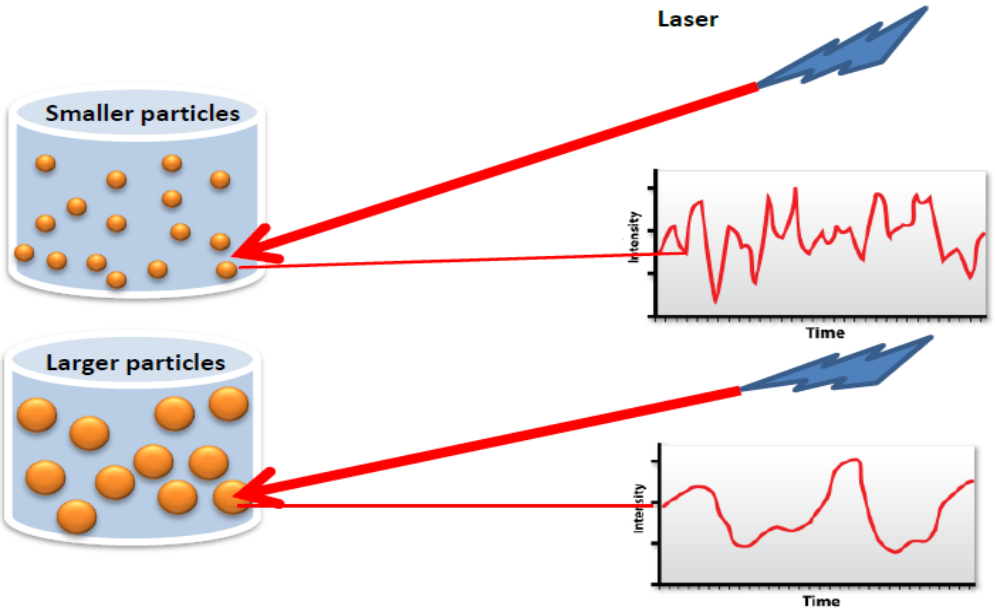

Figure 18: Particles size effect on the particles movement (Sibilia, 1996).

Zeta potential measurement

Zeta potential is a parameter that measures the electric potential energy of nanoparticles at their surface and compared with the charge of the particle-liquid interface and also standard technique to understand the stability of colloidal dispersions (Ruiz-Cabello *et al.* 2014).

When the potential is small, influence changings can be more than the revulsion and the light spreading may break simply. Colloids with higher zeta potential (negative or positive) are more and better electrically stabilised than colloids with low zeta potentials. For molecules and particles that are small enough, a high zeta potential will grant stability, i.e., the solution or diffusion will resist aggregation. Patel and Agrawal classified the zeta

potentials by stabilities, according their research the zeta potential between ±0-10 mV, 10-20 mV, 20-30 mV and 30+ mV are considered “highly unstable”, “relatively stable”, “moderately stable”, and “highly stable” respectively (Patel & Agrawal 2011). These particles will aggregate more, which leads to low stability. In contrast, high surface charge represents strong repulsive forces between particles, resulting less aggregation, and higher stability (Bhatta *et al.* 2016).

Laser irradiation

Laser irritation is putting the materials under fast and restricted energy for creating situation of electronic and thermodynamic non equilibrium. When a laser is irradiated to a sample surface, the surface reflects a ratio of the energy and also absorbs the rest of that. The reflection depends on the material and the laser wavelength (Zhigilei *et al.*, 2009). The adsorbed energy is transmitted from optical photons to electrons and subsequently to the lattice, resulting diffusion of the energy into the material (Liu, 2005). The laser-induced heat can be localized in the materials and lead to heat generation by the material. Metal oxides are of significant interest for Biological applications. Investigation of the localized heating effect due to the laser irradiation on the particle is required to prevent unwanted thermal effects (Palneedi *et al.,* 2018).

There are numerous researches about the metal nanoparticles thermal effects when exposued under laser irradiation. Tsuji *et al.* investigated morphological changes from spherical silver nanoparticles to cubes after laser irradiation in acetone–water solutions. According to the research, the shape changes of spherical AgNPs observed in acetone–water mixed solutions after they were laser-irradiated and left for 1–14 days. Results of observations of Ag NPs after preparation confirmed that AgNPs formation occurred

automatically after laser ablation and laser irradiation. The silver nanoparticle changes lead to increasing thermal properties and it can be useful for destroying cancer cells. Moreover, results suggest that acetone and ethanol would act only as stabilizing reagents. Instead, water plays an important role in atom transfer (Tsuji *et al.,* 2018).

Aims and objectives

The aim of this study is to synthesise hybrid iron oxide-silver core-shell NPs and characterise them in order to ensure the correct structures were fabricated. After synthesising the hybrid nanoparticles, they will be characterised for their surface charge, size, shape, concentration and the capability of HNPs to heat after laser irradiation.

2.2. Materials and methods

Materials used

Table1. Materials used in synthesis and characterisation of HNPs.

Materials	Suppliers
Potassium nitrate	Sigma-Aldrich Co., UK
Sodium Borohydride	ACROS Organics Co.,
Ethanol	Sigma-Aldrich Co., UK
Trisodium Citrate	Sigma-Aldrich Co., UK
Copper grid Agar	Scientific Co., UK
Iron III Sulphate Hydrate	ACROS Organics Co., USA
Chloroform	Sigma-Aldrich Co., UK
Silver Nitrate	Sigma-Aldrich Co., UK
Nitric Acid	Sigma-Aldrich Co., UK
Hydroxyl amine	Sigma-Aldrich Co., UK
Poly(ethyleneimine) (PEI) (ave. Mw=750 kDa)	Sigma-Aldrich Co., UK
Chloroauric acid	Sigma-Aldrich Co., UK
Hydrochloric acid	Sigma-Aldrich Co., UK
Poly(ethyleneimine) (PEI) (ave. Mw=2 kDa)	Sigma-Aldrich Co., UK
Sodium hydroxide	Fisher Scientific Co., UK
Sulphuric acid	Sigma-Aldrich Co., UK
Copper grid	Agar Scientific Co., UK
Iron and Gold standard for ICP	Fluka analytical

Methods

The synthesis and characterization of iron oxide and coating that with PEI and silver was inspired by Barnett *et al.* research in 2013 and also Goon and colleagues in 2009, which involved using a ‘‘polymer cushion’ of PEI between the magnetic iron core and the outer gold shell which called indirect gold coating (Goon *et al.,* 2009; Barnett *et al.,* 2013). Iron oxide core was synthesised through coprecipitation method (Sugimoto *et al.,* 1980).

Synthesis of iron oxide core

Sodium hydroxide (NaOH, 1.03 g) and 1.82 g potassium nitrate (KNO_3) were dissolved in 180mL deionised water at 90 °C under nitrogen (N_2) for 1 h. Iron (III) Sulphate heptahydrate ($FeSo_4.H_2O$, 3.89 g) was dissolved in 20 mL, 0.01 M sulphuric acid (H_2SO_4). The mixtures were added to the reaction with stirring for 24 h at 90 °C under N_2. After 12 h, the reaction was cooled in ice and the particles were magnetically separated from solution. The supernatant was removed after using a strong permanent magnet on the outside of a glass vial containing the iron oxide NPs to separate the magnetic material from the solvent. This magnetic fraction was washed 6 times and suspended in deionized water. Then particles were kept in 15 mL deionized water and after 1 week was characterised by zeta potential measurement and photon correlation spectroscopy and transmission electron microscopy for measuring and identifying the particle size and potential surface charge.

Polymer coating of iron oxide nanoparticles

The iron oxide nanaoparticles (5 mL) was added to 20 mL poly (ethylenimine) (PEI, MW 750,000) (5 mg mL^{-1}, pH=9) (C_2H_5N) and sonicated for 2 h. The particles were washed 6 times with deionised water and were magnetically separated from solution with magnet.

The final particles re-suspended in 5 mL deionized water. The surface charge of the particles was monitored *via* zeta potential measurement.

Synthesis of colloidal silver seed nanoparticles

The synthesis of AgNPs was according co-reduction method employing two different reductants (i.e., $NaBH_4$ and TSC) (Agnihotria *et al.,* 2012). In this case, 0.007 g sodium borohydride ($NaBH_4$) was added to 0.110 g trisodium citrate (TSC) in 100 mL deionised water. The mixture was mixed and heated to 60 °C for 0.5 h in the dark coated Erlenmeyer with maximum stirring to ensure a homogenous solution. 0.016 g silver nitrate solution was added drop wise to the mixture and subsequently, after adding silver nitrate the temperature was raised to 90 °C and pH of the solution was adjusted to pH 10.5 with using 0.1 M NaOH (0.04 g) for 20 min until a change of colour was evident.

The nanoparticles were cooled at room temperature to removing any unreacted starting material and also the bigger sized silver nano particulates. AgNPs suspensions were centrifuged (16128 RCF) for 15 min 3 times. After each centrifuge, 50 mL of top part of test tube was taken and 50 mL deionised water was added to tube. Finally, the AgNPs were kept at 4 °C. The AgNPs were characterised by zeta potential measurement and photon correlation spectroscopy and transmission electron microscopy for measuring and identifying the particle size and potential surface charge.

Polymer coating Fe_3O_4-PEI-AgNPs

Colloidal silver (50 mL) was added to 5 mL Fe_3O_4 – PEI and stirring for 2 h at room temperature. The magnetic particles were magnetically separated from solution and washed 6 times with deionised water. Deionised water (5 mL) was added to the mixture. By

coating Fe_3O_4 – PEI by AgNPs the surface charge must shift from the positive value toward the negative charge due to the presence of AgNPs coating. In this case, the hybrid nanoparticles were characterised by zeta potential measurement and photon correlation spectroscopy and transmission electron microscopy for measuring and identifying the particle size and potential surface charge and also the shape of hybrid nanoparticles which must not be smooth surface due presenting AgNPs.

Silver seeds coating of iron oxide nanoparticles-PEI

Fe_3O_4 – PEI –AgNPs (5 mL) were stabilised by stirring in a solution of 5 mL of 1 mg mL^{-1} PEI (MW 2000) for 20 min. The particles were washed extensively with deionised water 6 times and re-suspended in 5 mL deionised water. By coating HNPs by polymer the surface charge must shift from the negative value which has achieved from last step toward the positive charge due to the presence of PEI coating again.

Silver coating process

Sodium hydroxide (NaOH, 100 mL, 0.01 M) was mixed with the particle solution at 60 °C. In order to achieve a complete shell silver was reduced onto the particle surface. To do this 0.5 mL of 1% $AgNO_3$ was added followed by hydroxyl amine ($NH_2OH{\cdot}HCl$, 0.75 mL, 0.2 M). Two consecutive iterative reductions were carried out by addition of 1% $AgNO_3$ (0.5 mL) and 0.2 M $NH_2OH{\cdot}HCl$ (0.25 mL) with 10 min intervals for four times.

The final particle solution was stirred for 0.5 h then the product was washed at least five times by water and separated by magnetic. Final product was added by 5 mL of water and left for 1 week in case of confirming the product stability (Figure 19). The final product was characterized by zeta potential for potential surface charge, UV/Vis spectroscopy upon the

complete coating, photon correlation spectroscopy and transmission electron microscopy for measuring and identifying the particle size, ICP for the ratio between silver and Iron in the final product and also Laser irradiation in case of checking the HNPs thermos capabilities.

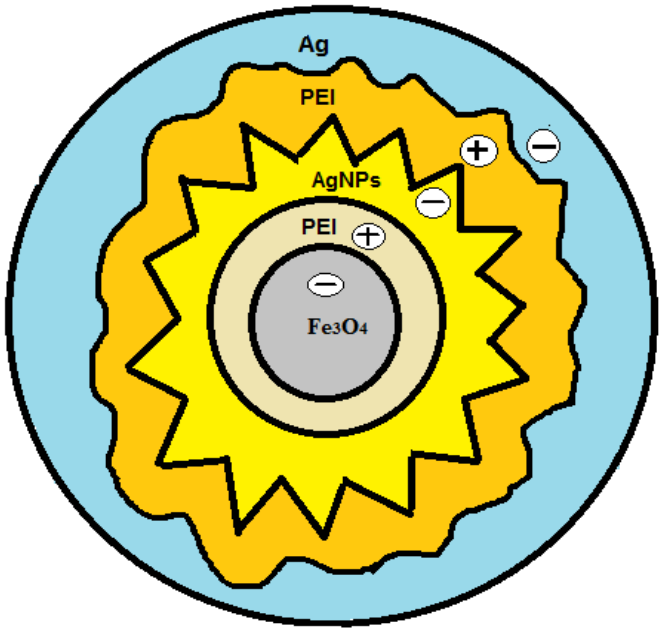

Figure 19: Schematic diagram of silver coating process.

Characterisation of hybrid nanoparticles

Photon correlation spectroscopy and zeta potential measurement

Hydrodynamic diameters and zeta potential measurements were carried out using a photon correlation spectrometer (PCS, Zetasizer nano-ZS, Malvern Instruments, UK). The amounts of particle size and zeta potential changes were investigated from first to last steps of iron oxide coatings.

Inductively Coupled Plasma - Optical Emission Spectroscopy (ICP-OES)

For determining the concentration of metal content in the HNPs, inductively coupled plasma-optical emission spectroscopy (ICP-OES, Optima 7000V DV, PerkinElmer, Wokingham, UK) was used. Before the HNP analysis; samples were dissolved using an acid digestion procedure (1:10 sample: acid). This digestion is carried out using a concentrated solution of hydrochloric acid: nitric acid (1:1) at 100 °C. Samples then diluted with deionised water (1:10) to be ready for analysis (Barnett *et al.,* 2012). Before testing the samples, a calibration was run using iron and silver standard solutions 0.05 – 10 ppm (R^2 = 0.9999). The concentration of HNPs used for all experiments indicates the concentration of Fe. Finally, the final sample concentrations were calculated by using standard curves data's by using the Microsoft Excel software package.

Transmission electron microscopy (TEM)

Transmission electron microscopy (TEM) is the one of the most powerful and popular technique to characterize nanoparticles (Wang *et al.,* 1999). TEM was used to visualize the particles. TEM grids were coated with chloroform and the grids were left to be dry for 1 day. Samples were pipetted onto formvar coated copper grids (2µL) and dried under a heat lamp for 4 h. The grids were directly imaged using a JEOL JEM-1230 microscope with Analysis software (JEOL, Japan).

Ultraviolet- visible spectroscopy (UV/VIS)

The samples include iron oxide NPs, Silver seeds and HNPs in deionised water was were aliquoted into quartz cuvettes and their absorbance monitored on Ultraviolet- visible spectroscopy (UV-VIS) system and scanned between 200 – 800 nm (Agilent Technologies,

Cary 60). All measurements were run in triplicate at room temperature (25 °C) and recorded as average values.

Laser Irradiation

The ability of the HNPs to act as localised nano-heaters was determined using laser irradiation. Agar (2 g) was diluted in 100 mL water and heated up to 60^{o}C until the mixture changed to the clear solution. The gel (0.076 mm diameter, T-type, PFA coated, Omega, UK) has been used in various studies as a mimic for biological tissues (Curtis *et al.* 2015).

We used the gel to provide the conditions like tumour environment for indicating the HNP heating capability. The particles were suspended in 2 % agar at both 25 µgmL^{-1} and 50 µgmL^{-1}. The dispersed HNPs in agar were allowed to cool to form gels in 35 mm diameter plastic petri dishes. Samples were exposed to pulsed laser beam (10 ns, 1 W, 6 Hz) emitted by a solid state laser system (Ng: YAG pulsed 1064 nm). It is assumed that laser irradiation at 1064 nm should cause localised heating of the HNPs without heating of biological tissues. Moreover, laser systems using 1064 nm pulsed sources are widely used both in the cosmetic industry for tattoo removal and hair removal and also in clinical settings for ophthalmic treatment (Tanaka *et al.,* 2011). In first step, simple gel was equilibrated to 37^{o}C to mimic body temperature by oven. The gels were then exposed to wave laser beam for 30 s and the temperature monitored using an Optris PI640 Thermal Imaging Camera (Optris, Germany). The data was recorded on Optris PI Connect software (Optris, Germany). The temperature changes for HNP was suspended in 2 % agar at both 25 µgmL^{-1} and 50 µgmL^{-1} were compared to control gels with no HNPs present and the thermal changes were calculated within the Microsoft Excel software package ($\Delta T = (T_{final} – T_{initial}) - \Delta T_{control}$).

For measuring the heat dissipation the samples were exposed to laser irradiation at 1064nm using a ML- LASER-YB5 Q-switched Nd:YAG Laser Treatment System (WeiFang MingLiang Electronics Company Ltd, China). Heat dissipation analysis away from the laser culmination point was measured and analysed for 0s, 10s, 20s and 30s. In this case the thermal imaging camera (Optris PI640) was positioned 5 cm away from the gel and focussed on the irradiation site. The laser culmination point possessed at the highest temperature and the heat in the gel at set distances (1, 2, 3, … 10 mm) from this were recorded in order to give an indication of how localised the heating would be *in vivo*.

2.3. Results

The iron oxide cores and subsequent PEI coating were successfully achieved as per the literature and confirmed with PCS, zeta potential measurement and TEM. TEM imaging represented a precise view of the Fe_3O_4 shape and size, which was 80 nm (n = 20, SD = ± 4.88) (Figure 20). The TEM micrograph demonstrated the smaller particle sizes in compare with photon correlation spectroscopy (PCS). This phenomenon is possible due to the very small fraction of the sample represent in TEM image. On the other hands, a number of factors have a great influence on the hydrodynamic diameter of the particles measured by dynamic light scattering such as polymer shells, hydration layer or other stabilisers, which lead the particles size to be seen larger by PSC (Heinz et al., 2014).

Basically PSC has been used in each step of coating to demonstrate the size changes in each level. The particle size was decreased from Iron oxide to HNP in each step of synthesis and it could be due to decreasing particle agrigation.

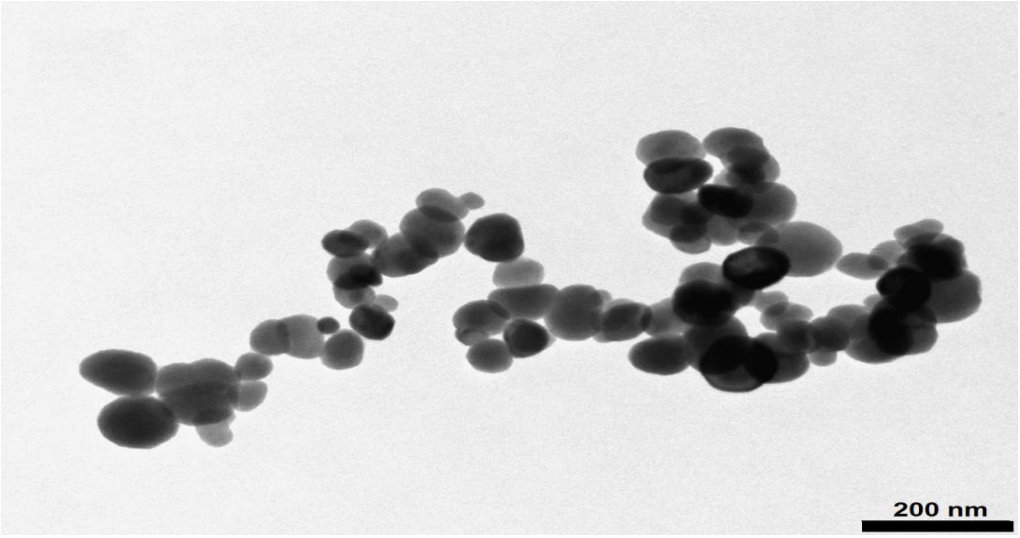

Figure 20: Size and shape estimations of Fe_3O_4 nanoparticles analysed by TEM.

The Iron oxide had negative surface charge of -22.67 ± 0.96 mV which due to the surface sulphate associations from the synthetic procedure (Hoskins *et al*., 2012a). The surface charge potential was changed to + 46.40 ± 0.68 mV when iron oxide core coated with PEI and the main reason is the presence of the positively charged primary amine groups in the PEI backbone (Table 2).

Table2. Hydrodynamic Radius, polydispersity index and zeta potential analysis for 1 mg mL^{-1} aqueous polymer solutions n=3, ave (SD).

Particle	**Hydrodynamic Radius nm ± SD**	**Polydispersity Index ± SD**	**Zeta Potential mV ± SD**
Fe_3O_4	846.97± 0.21	0.30±0.05	- 22.67±0.96
Fe_3O_4-PEI	590.77±59.01	0.31±0.06	+ 46.40±0.68

Synthesis of silver nanoparticles and silver coating characterisation

One major difficulty faced in this work was the repeatable synthesis of silver seed nanoparticles for attachment onto the Fe_3O_4-PEI which act as anchor points for subsequent coating. Silver nanoparticles have high surface area which might be lead to poor colloidal stability and aggregation in solution (Wu *et al*., 2010).

Hence, the method development took a long time to complete. Multiple attempts at synthesis were hindered mainly by the aggregation of the silver seeds, whereby, particle sizes at approximately 30 nm were formed. This was far above the size required for seeding onto the Fe_3O_4-PEI. Moreover just a little number of AgNPs was attached on the Fe3O4-PEI surface after washing the particles.

The main concern regarding the particle size was in order to make the 'seeds' small enough to attach onto the Fe_3O_4-PEI for subsequent coating. If the particles were too large the final silver coat would be very thick, studies have shown for gold hybrid NPs that the thinner the coat the better plasmonic properties observed (Barnett *et al.,* 2012). Hence, a smaller seed particle size was desirable but this was very difficult to achieve in reality and a lot of method development was required at this stage. Previous researches demonstrated that they could achieve gold nanoparticles by 2 – 5nm size; however the lowest size of silver nanoparticles was around 25 – 30 nm by using this method (Barnett *et al.,* 2012). Table 4 demonstrated some of attempts for synthesising silver nanoparticles which were failed in different dates by PCS. In this case some of factors like temperature or mixing substances time were changed but it did not have significant change in the silver particle size (Table 3).

Table3. Failed attempts in synthesising silver nanoparticles by PCS.

Different Batches	Hydrodynamic Radius nm ± SD	Polydispersity Index ± SD	Zeta Potential mV ± SD
Batch 1	25.56± 3.58	0.25±0.15	- 13.6±14.58
Batch 2	36.61±5.55	0.35±0.18	- 25.69±0.93
Batch 3	24.6±1.25	0.21±0.05	- 1.68±1.52
Batch 4	12.57±26.81	0.25±0.62	+ 1.19±0.37
Batch 5	12.68±1.65	0.32±0.25	- 3.58±1.55
Batch 6	66.02± 0.56	0.31±0.20	- 1.58±1.89
Batch 7	11.09±2.08	0.28±1.77	+11±4.81
Batch 8	39.15±3.55	0.32±2.11	- 60.57±2.58
Batch 9	10.57±8.20	0.12±4.81	+ 1.19±0.37
Batch 10	13.55±1.74	0.33±1.17	- 41.77±0.91
Batch 11	80.17± 3.10	0.39±4.10	- 20.20±12.71

The other concern was about silver stability. In other studies, silver nanoparticles were synthesised around 8 nm in diameter, even though, silver was not stable and the particle were aggregated after couple of weeks (Kholoud & Abou, 2010). When we tried this methodology the silver seeds were highly unstable aggregated after couple of weeks. TEM results demonstrated the aggregated silver nano particles with bigger sizes than PSC results for silver nano particle size after 8 weeks from synthesising (Figure 21A and 21B).

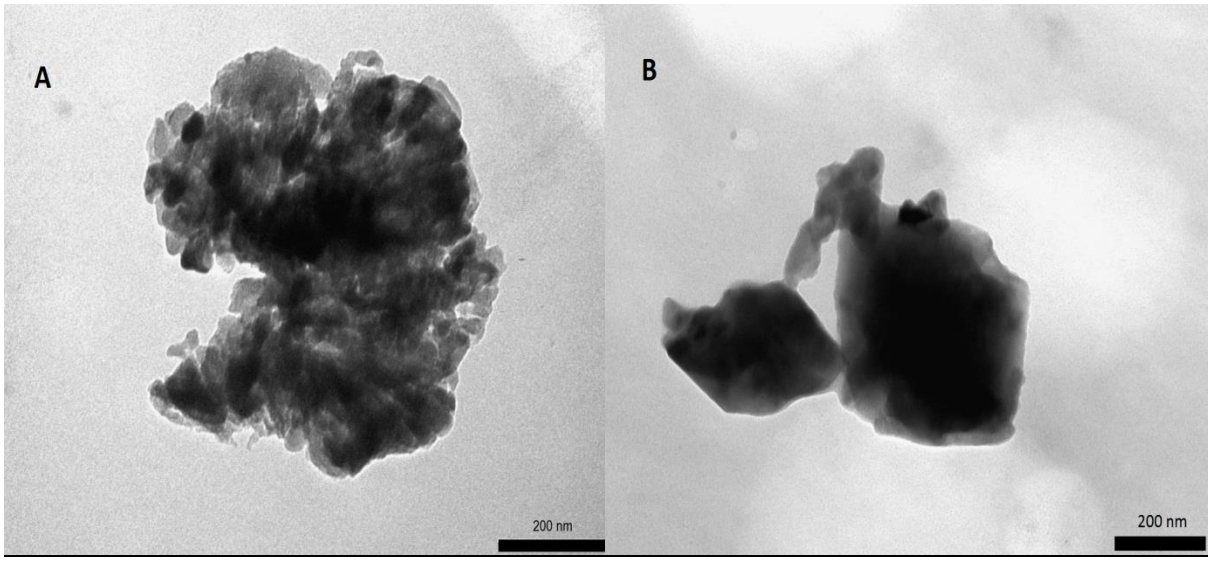

Figure 21A and 21B: TEM micrographs of aggregated silver seeds.

This stability issues was not really an issue for this work as the seed particles could be synthesised and then immobilised onto the Fe_3O_4 surface for subsequent coating. However, The TEM demonstrated that the lower numbers of silver nanoparticles were attached on Fe_3O_4-PEI surface charge by using this method as well (Figure 22A and 22B) (Kholoud & Abou, 2010).

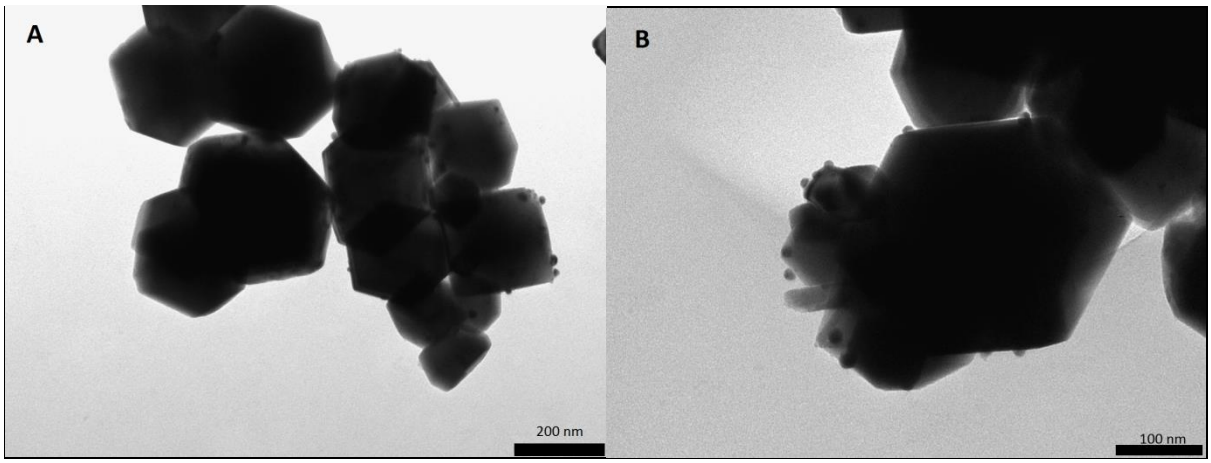

Figure 22A and 22B: Failed TEM result for attached AgNPs on Fe_3O_4-PEI.

The optimal synthesis of AgNPs in this work was carried out as Agnihotr and colleagues described (Agnihotria, *et al.* 2012). The method involves the synthesis of AgNPs with different size and demonstrated that AgNPs with 5 -10 nm was using co-reduction method employing two different reductants (i.e., $NaBH_4$ and TSC) (Agnihotria, *et al*., 2012).

Once the silver colloid methodology was deduced the HNP synthesis was easily achieved as evidenced by PCS, zeta potential measurement, ICP and TEM as described in the sections below. The change in physical appearance can be seen in Figure 23.

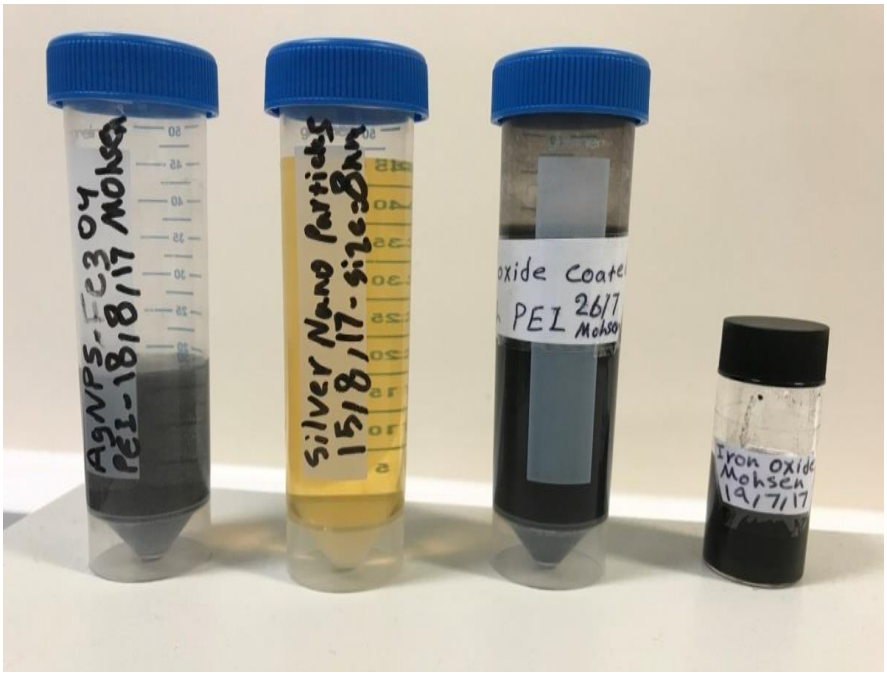

Figure 23: Colour changes from Fe_3O_4 to Fe_3O_4-PEI-AgNPs.

ICP allowed for the measurement of elements of Fe and Ag presented within the HNPs and their ratios in order to quantify their concentration and ratios (Malekigorji *et al,* 2017). Water blanks were analysed against the calibration curves to ensure all false positives were removed. In first step standard solutions were created for standard carve and the formulation of y = ax ± b were used to find the final concentration for silver and iron. The

maintained regression linearity (R^2) was 0.99 over the calibration range of 0 – 10 µg L^{-1} in single particle analysis mode (Barnett *et al.,* 2013a) and (Hoskins *et al.,* 2012b) (Figure 24).

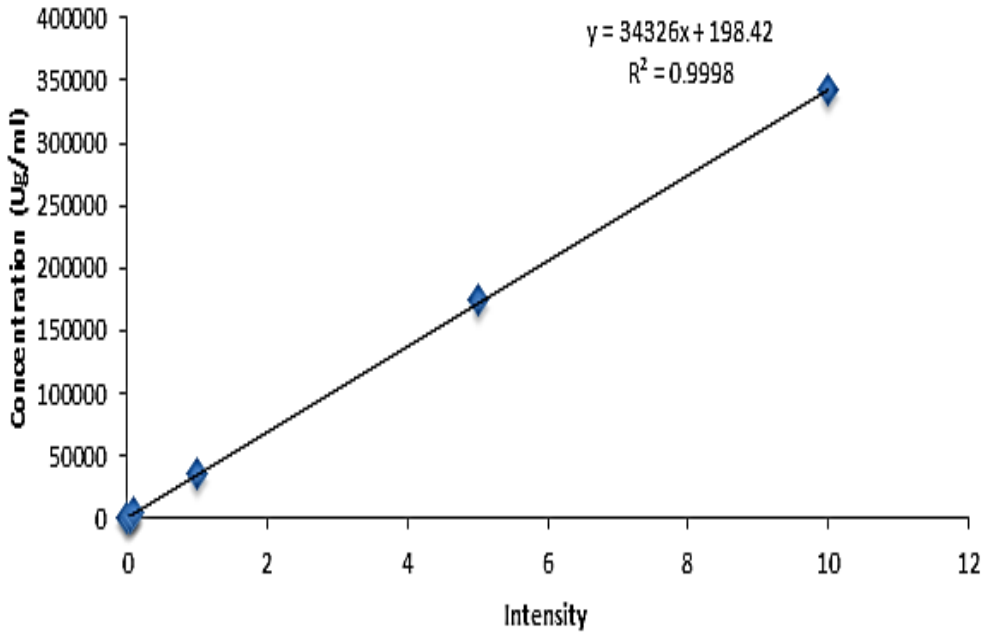

Figure 24: ICP standard curve.

The second major difficulty faced in this work was the repeatable synthesis of silver coating process. For the silver coating, some ICP data demonstrated that the ratio of iron to silver was much greater than 3:1 in the HNP. The ICP result wasn't same as previous researches (Barnett *et al.,* 2013a; Hoskins *et al*., 2012b) (Table 4). In this case the silver coating process method was repeated to achieve ratio of 3:1 for Fe and Au. This ratio was desirable as the data agrees with the TEM images, whereby a coating of similar thickness was obtained for both particles in this ratio. The ICP test was repeated 6 times for 3 different batches of HNPs showing that the standard deviations and means are reliable and the synthesis protocol is reproducible.

Table4. Failed attempts in synthesising HNP by ICP.

Batches	Silver Concentration (mg mL^{-1} ± SD)	Iron Concentration (mg mL^{-1} ± SD)
Batch 1	0.29±13.63	54.93±1.36
Batch 2	0 0.28±0.94	68.69±0.88
Batch 3	0.45±2.51	254.17±0.73
Batch 4	0.13±9.91	24.59±22.47
Batch 5	0.93±0.57	98.32±21.50
Batch 6	0.61±3.22	14.83±0.66
Batch 7	0.26±3.27	68.10±0.81
Batch 8	0.27±1.02	43.53±0.40
Batch 9	0.29±1.88	54.93±0.72

According to the three different batches ICP results, the average iron concentration was 2.865± 3.18 mg mL^{-1} and silver concentration was 0.733 ± 2.44 mg mL^{-1}.

The ICP data demonstrates that iron oxide core was successfully coated with silver forming the HNPs with a ratio between Fe and Ag of 3:1. ICP analysis for Fe and Ag was run 6 times for 3 different batches of HNPs showing that the standard deviations and means are reliable and the synthesis protocol is reproducible.

Photon correlation spectroscopy and zeta potential measurement

The hydrodynamic radius of Fe_3O_4 core and HNP was 846.97 ±0.21 nm and 100.29 ± 0.91 nm respectively, which determined by photon correlation spectroscopy (Figure 25).

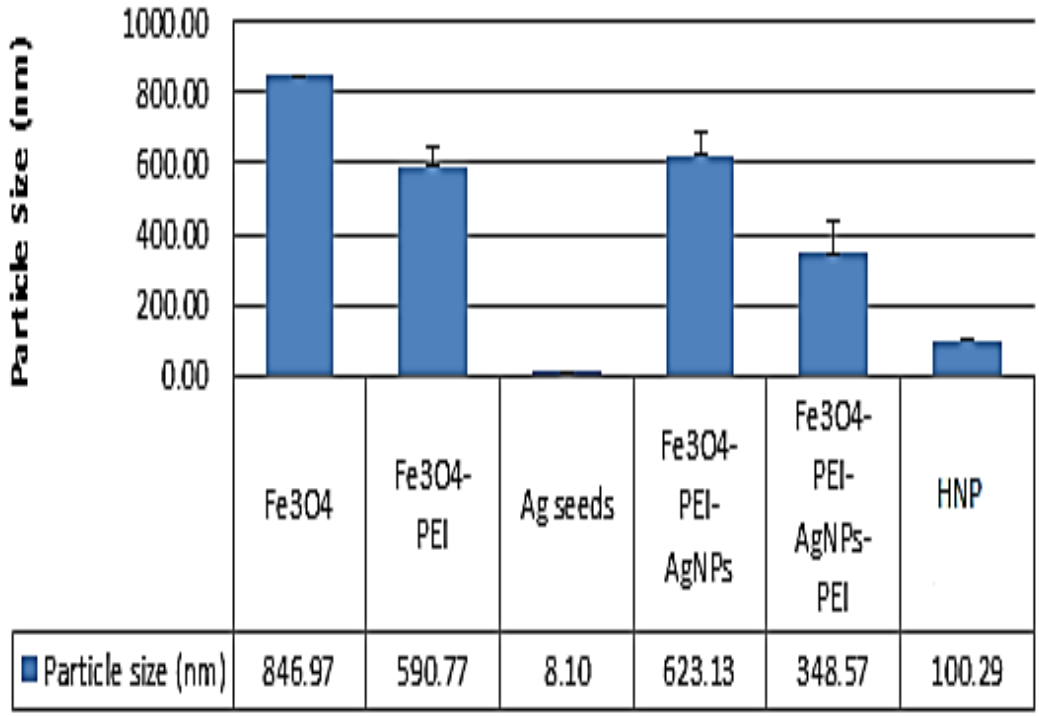

Figure 25: Particle size from F_3O_4 to HNP and AgNPs.

For iron oxide to HNP, a large diameter was obtained due to the inherent magnetic properties of the iron oxide cores. Silver nanoparticle did not have magnetic properties. The particle size for AgNPs were synthesised with 8.1 nm± 1.07 nm. The particle size was shift to smaller size as the coatings in each step decreased the aggregation of the particles.

The reactions were monitored using zeta potential measurements. The zeta surface potential also was shown the amount of changes from Fe_3O_4 to HNP (Figure 26).

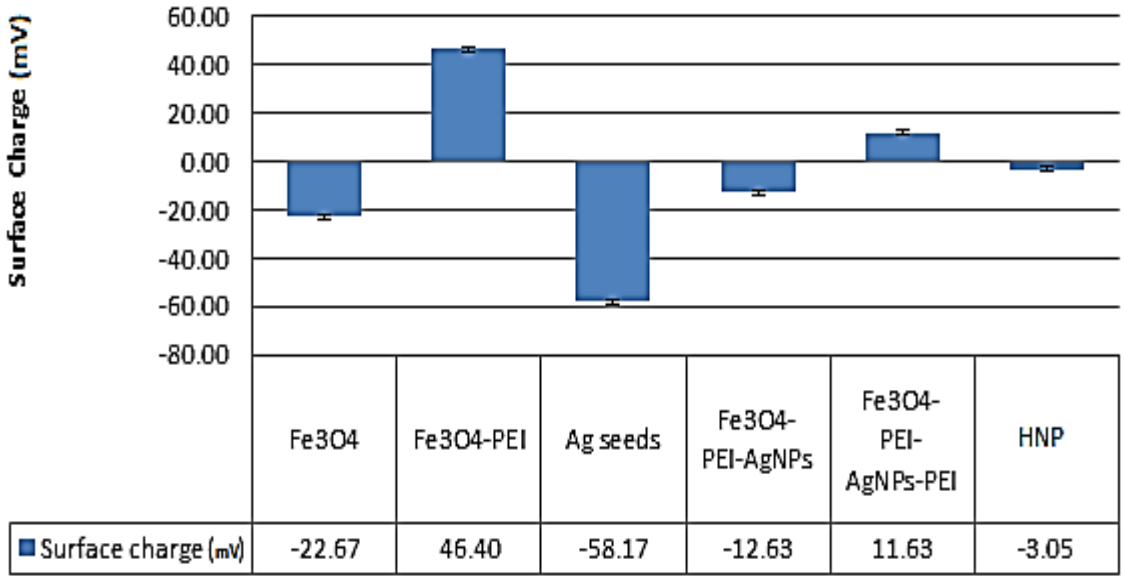

Figure 26: Surface charge from F_3O_4 to HNP and AgNPs

The Fe_3O_4 had negative surface charge of -22.67 ± 0.96 mV which due to the surface sulphate associations from the synthetic procedure (Hoskins *et al*., 2012a). The surface charge potential was changed to + 46.40 ± 0.68 mV when iron oxide core coated with PEI and the main reason is the presence of the positively charged primary amine groups in the PEI backbone (Table 2). The silver nanoparticles surface charge was -58.17 ± 0.68 mV because of the negatively charged silver atoms and this negativity amount was reduced to -12.63 ± 1.02mV when the AgNPs were added to Fe_3O_4-PEI. As the data shows, the surface charge was changed to +11.63 ± 0.68 mV after coating Fe_3O_4-PEI-AgNPs with PEI, and finally the HNP product possessed a surface charge of -3.05 mV ± 0.29 mV (Figure 26). The surface charge potential changes indicated that the HNPs were successfully synthesised.

The poly dispersity index (PDI) of particles demonstrated that they possess homogeneous distribution within the formulation as PDI from Fe_3O_4 to Fe_3O_4-PEI-Ag seeds-PEI were 0.3 to 0.381 respectively and also the PDI was 0.4 for final product. This increase could be due to the presence of small fraction of free silver seeds in formulation leading to more

polydispersity samples; these could easily be removed by centrifugation or magnetic separation (Table 5).

Table 5. Hydrodynamic Radius, polydispersity index and zeta potential analysis for 1 mg mL^{-1} aqueous polymer solutions n=3, ave (SD).

Particle	Hydrodynamic Radius nm ± SD	Polydispersity Index ± SD	Zeta Potential mV ± SD
Fe_3O_4-PEI-Ag seeds	623.13±64.07	0.37±0.04	- 12.63±1.02
Fe_3O_4-PEI-Ag seeds-PEI	348.57±87.87	0.38±0.08	+ 11.63±0.68
HNP	100.29±0.91	0.40±0.01	- 3.05±0.29

Transmission electron microscopy imaging (TEM)

The TEM micrograph represented a precise view of the Fe_3O_4 (Figure 20) (refer to page 65), AgNPs (Figure 27), Fe_3O_4-PEI-AgNPs (Figure 28A) and HNP (Figure 28B), sizes and shapes.

Silver nanoparticles (Figure 27) were represented the size of 5 nm. The shapes demonstrated that AgNPs were not aggregated after 6 weeks from synthesising.

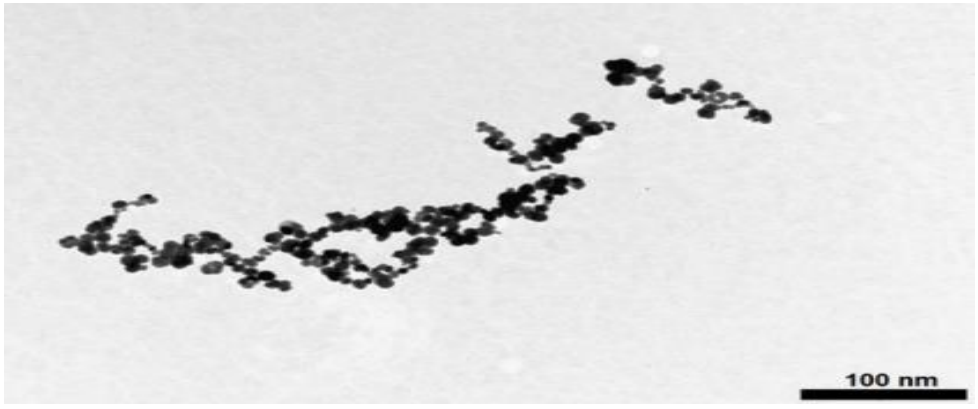

Figure 27: Size and shape estimations of silver nano-seeds analysed by TEM

Figure 28A was demonstrated the TEM image of the fully coated Fe_3O_4-PEI coated with Ag seeds displayed unique shape and different from the iron oxide core and the size is 85 nm (n = 20, SD = ± 3.29) and finally we could get the particle size with 90 nm (n = 20, SD = ± 3.90) for the HNPs (Figure 28B).

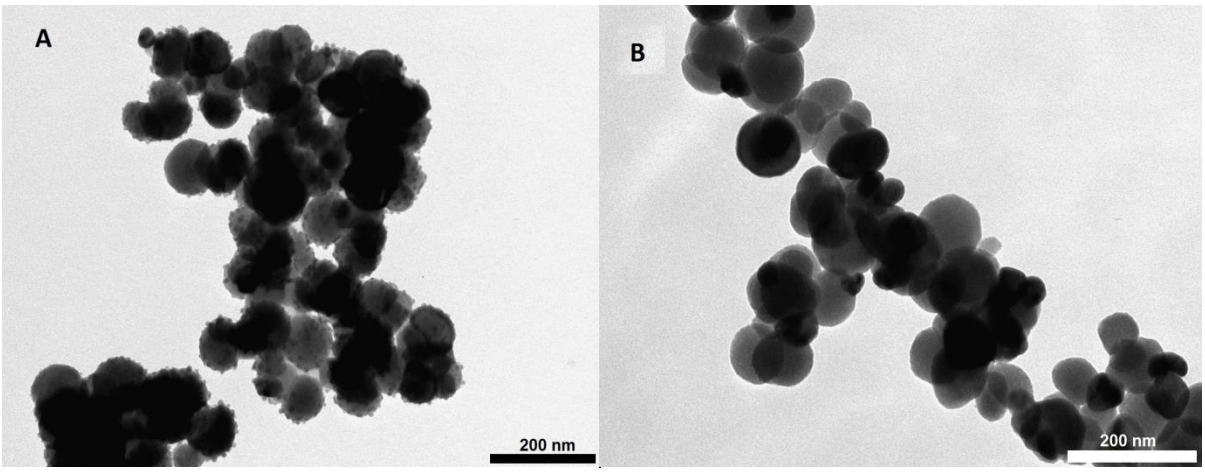

Figure 28: TEM micrographs of A) Fe_3O_4-Auseed and B) HNPs.

Ultraviolet- visible spectroscopy (UV-VIS)

The use of Ultraviolet- visible spectroscopy (UV-VIS) is one method to identify the presence of an absorbing species in solution. UV-Vis is based on the Beer–Lambert law. This law state that the absorbance of a solution is directly related to the concentration of the absorbing molecules in the solution (Bouguer, 1729). UV-visible spectroscopy was carried out to achieve absorption spectra of the particles (Figure 29) in order to determine the wavelength at which maximum absorbance occurred (λ_{max}). This value is indicative of the wavelength which is required for maximum efficiency of laser mediated heating at the surface plasmon resonance of the particles.

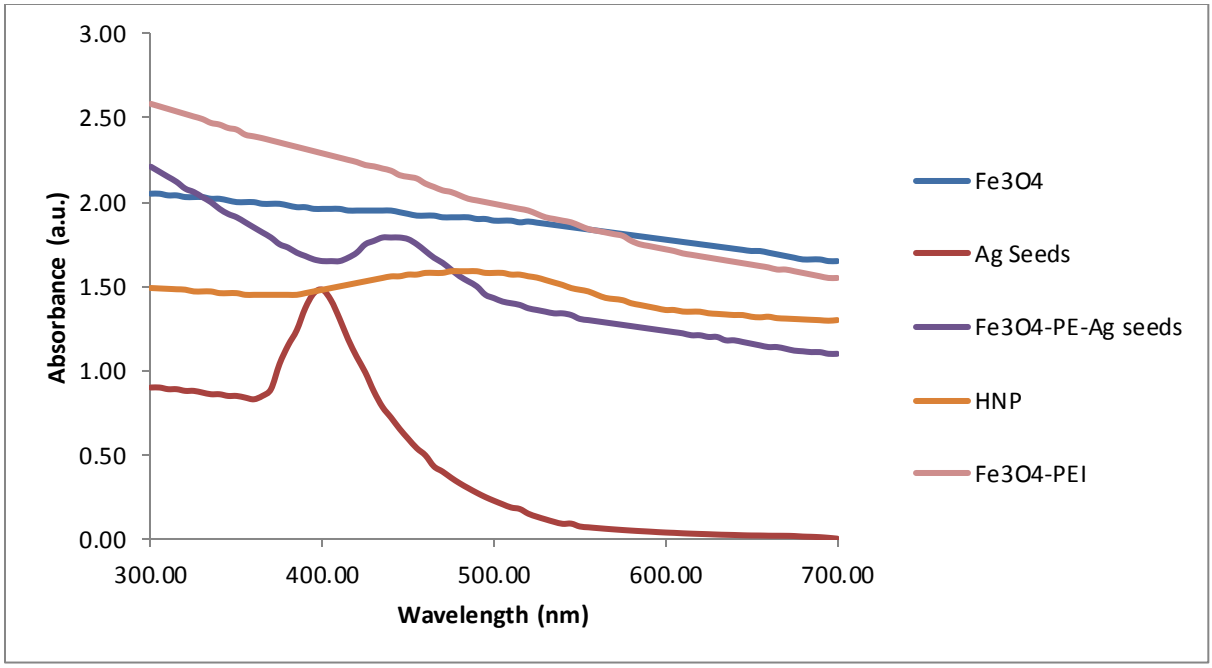

Figure 29: UV/Vis spectra of Fe_3O_4, Fe_3O_4-PEI, Ag seed, Fe_3O_4-PEI-Ag seeds and HNP.

According to the UV chart there is no plasmon resonance appears for Fe_3O_4 and Fe_3O_4-PEI because of lack of presence of silver in these particles. Ag seeds have λ_{max} of 400 nm. Fundamentally, when UV light is applied to the AgNPs, polarization of free electrons occurs which can lead to a charge separation. Consequently, the surface plasmon resonance (SPR) persuades a strong absorption of the applied light which can be measured by using a UV/Vis spectrometer (Xiaohua and Mostafa, 2010). The Fe_3O_4-PEI-Ag seeds indicate λ_{max} shift to 450 nm which might be due to the interaction between solute and solvent or Ag shell and PEI polymer. The λ_{max} of 490 nm was observed for HNP. According to the previous researches the different NPs size and shape can effect on light absorption range (John *et al.,* 2013; Hainfeld *et al.,* 2014). The λ_{max} shift is confirmation that the HNPs were successfully synthesised. However, the value of 490 nm was somewhat lower than expected. The peak although very broad did not appear to spread into the region of 1064 nm which was the wavelength of the laser system used for subsequent heating studies. Ideally a laser around

490 nm may result in better heating of the particles. However caution is advised as this sits below the biological near infrared window whereby tissue is not damaged. At 490 nm laser irradiation would likely result in tissue ablation which is not the focus of this study. Absorbance is measured in absorbance units (Au), which relate to transmittance as seen in figure 29. A silver nano particle has less than 1.0 Au and the other nano particles have 1.5 – 2.6 Au. In fact, higher concentrations at the other particles (In comparison with silver nanoparticle) can lead to decreasing transmittance inherently. It can lead to have higher absorbance units in comparison with silver nanoparticle.

Laser irradiation

Despite the low λ_{max} value, the laser irradiation studies were carried out in order to evaluate whether using a laser of 1064 nm (known to be safe for use in cosmetics) could induce localised heating in the HNPs. The rationale was that thermo-responsive drug delivery would result in localised drug release resulting in localised tumour damage with minimum damage to the surrounding normal tissues. The hybrid nanoparticles with different concentrations (25 μgmL^{-1} and 50 μgmL^{-1}) were dispersed within the agar phantom. This particular agar phantom was used as it mimics the stiffness and physiology of human tissue (Tanaka *et al.,* 2011). The particles were initially equilibrated to body temperature before being irradiated (Ng: YAG pulsed 1064 nm, 1000 V, 6 Hz) at oven. The change in temperature was monitored both inside beam and outside beam using an infrared camera.

Initially, the experiment was set up for 60 s irradiation, however, it was observed that the agar phantom began to melted and rip inside laser beam point when the temperature exceeded 47 – 50 °C. Therefore, in order to be confident that the measurements taken were

not subject to phase change in the agar the experiment was conducted over 30 s duration to overcome this issue.

The amount of temperature change for simple agar (control) was maximum 2.3 °C. All data's have subtracted from the control temp. All tests were carried out for three different batches of 25 μgmL^{-1} and 50 μgmL^{-1} of the HNPs in 37 °C for 30 s. Figure 30 demonstrates the laser irradiation for 25 μgmL^{-1} and 50 μgmL^{-1} HNPs in 37 °C for 30 s (subtracted from the control temperature).

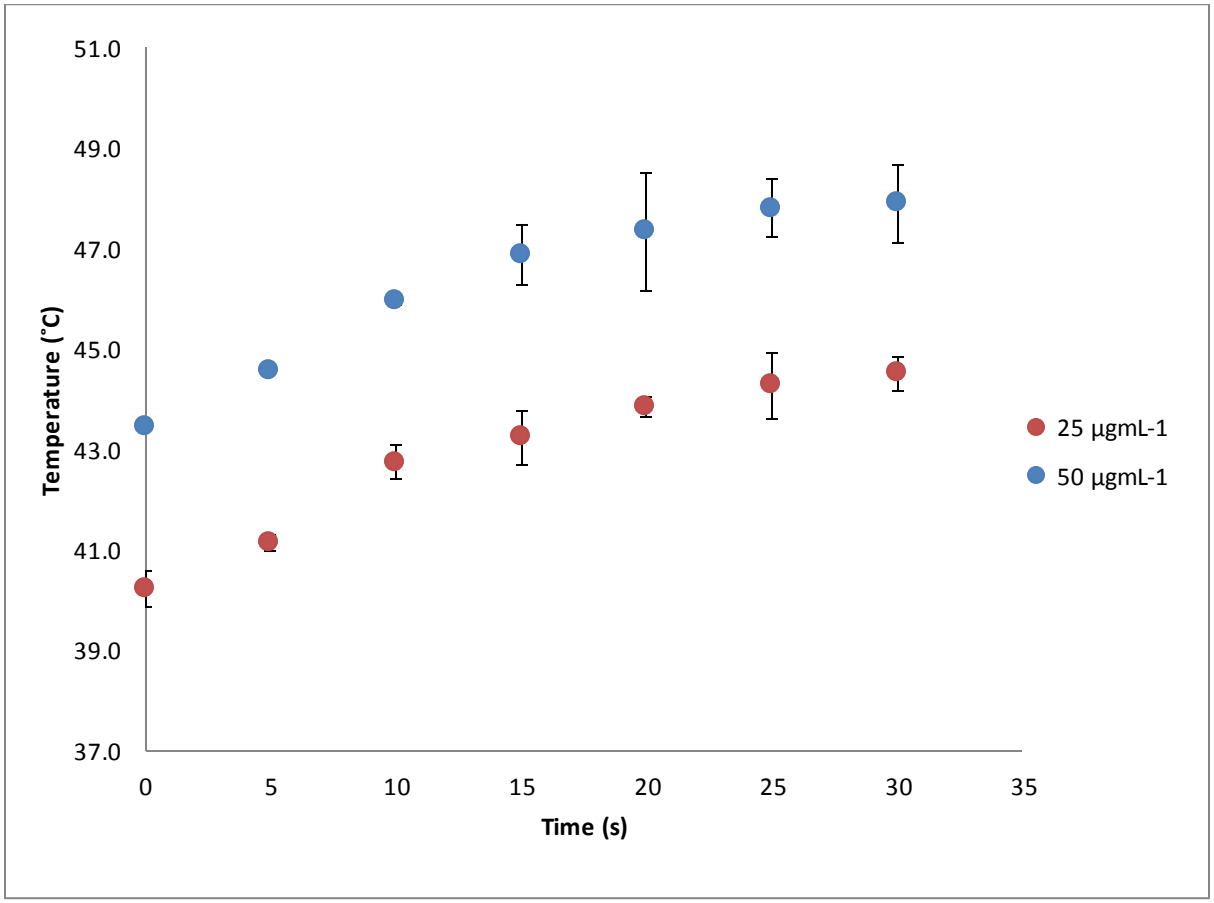

Figure 30: Laser Irradiations for 25 μgmL^{-1} and 50 μgmL^{-1} HNPs dispersed in 2 % agar gel in 37 °C for 30 s.

When the samples exposed to laser irradiation, the 25µgmL^{-1} HNP has sharp increased (4 ^{o}C) in first 5 s. The temperature went up to more than 7 ^{o}C in 25 s. The temperature appeared to plateau towards 30 s. At concentrations 25 µgmL^{-1} HNP temperature was increased to 44.5 °C ± 0.35 at 37 °C for 30 s ($p > 0.05$). According to the data there were minimal deviations which occurred between different batches of 25 µgmL^{-1} HNP = $p > 0.05$ or 50 µgmL^{-1} HNP = $p > 0.05$. However, the results demonstrate that there are significant changes between times, concentration between different HNPs in compare with the control ($p < 0.05$).

At concentrations 50 µgmL^{-1} HNP temperatures increased to 48 °C ± 0.56 in after 25 s ($p > 0.05$) The data demonstrates high increasing temperature in first 5 sec followed by a more discrete rise up to 15 s, after which a plateau was observed.

According to the data, the steepest rise in temperature increase occurred consistently within the first 5 s of irradiation. The temperature went up for 5.8 ^{o}C at 25 µgmL^{-1} HNP and 9.2 ^{o}C at 50 µgmL^{-1} after 10 s ($p < 0.05$). The temperature in the 25 µgmL^{-1} sample increased 7 ^{o}C and 11 ^{o}C in the 50 µgmL^{-1} after 25 s and the temperature were stable during 30 s ($p > 0.05$). A similar trend was observed across the irradiation duration. Consequently it could be concluded that the extend of temperature change is dependant less on time of irradiation, given that most samples heated within the first 10 s and also increased concentration does result in increased temperature rises, though the extent of which may not be significant for application.

The heat dissipation analysis away from the laser culmination point was measured and analysed for 0, 10, 20 and 30 s. It was assumed that since the HNPs were spherical that heat distribution was equal at all points of the spheres exterior resulting in a uniform halo like

effect (Curtis *et al.,* 2015). In this case, the laser culmination point possessed the highest temperature and the heat in the gel at set distances from this were recorded in order to give an indication of how localised the heating would be *in vivo*. Figure 31 indicated the temperature changes of the different HNP concentration on the agar across the 10mm.

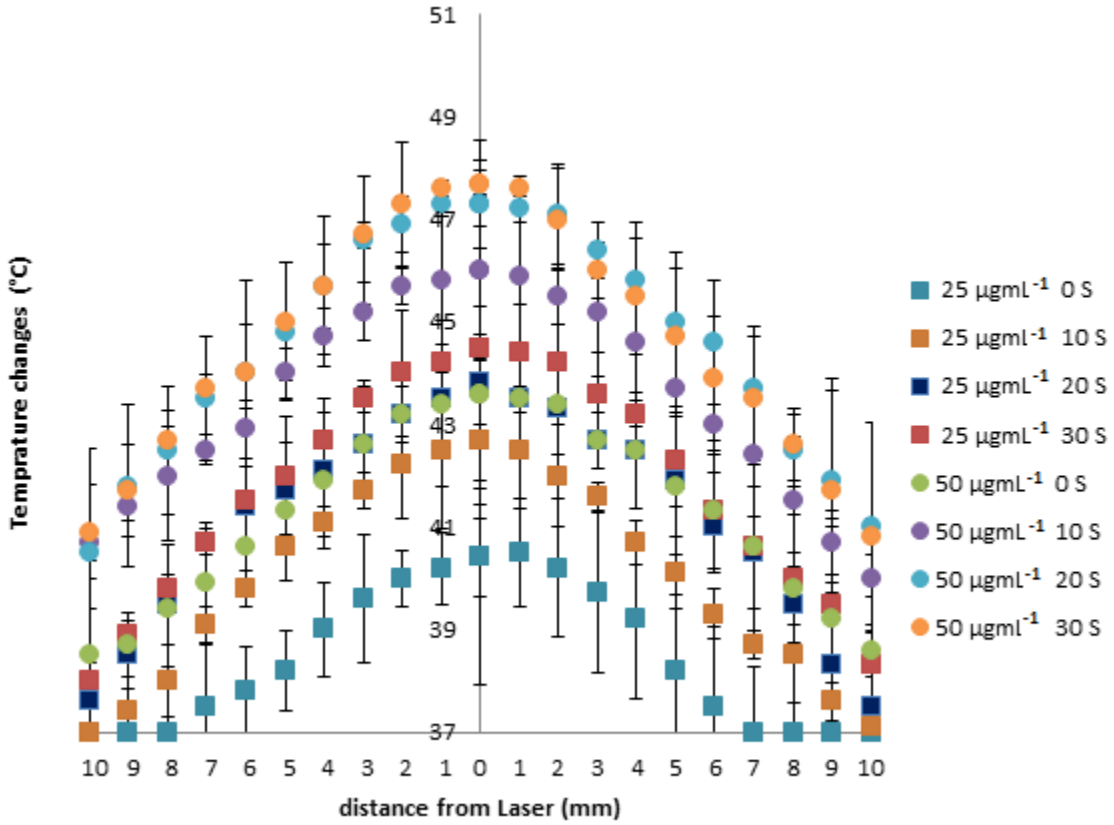

Figure 31: The heat dissipation between 25 µgmL^{-1} HNP and 50 µgmL^{-1} HNP (n=3, ±SD).

According to the chart, at 25 µgmL^{-1} HNP there is not heating effect occurred in 8 mm from the laser irradiation site in 0 s. Moreover when 25µgmL^{-1} HNP exposed in laser irradiation for 10 s, heat dropped from 43^{o}C and there is not heating effect in 10 mm. At same HNP concentration, there are small heating effect in 10 mm distance from laser irradiation and the temperature were 0.3 ^{o}C and 1 ^{o}C higher than body temperature in 20 and 30 s respectively ($p > 0.05$).

At 50 µgmL^{-1} HNPs there are still experiencing heating effects at 10 mm distance. The graph showed that in 1 mm distance from laser irradiation the temperatures were 43.5^{o}C, 46^{o}C, 47.3 ^{o}C and 47.5 ^{o}C in 0 s, 10 s, 20 s and 30 s respectively. The temperatures were dropped to 38.5 ^{o}C, 40 ^{o}C, 41 ^{o}C and 41.2 ^{o}C in 0 s, 10 s, 20 s and 30 s, respectively ($p < 0.05$). According to the chart the heating distribution was too wide and it can damage to surround healthy tissue.

According to the graph even though the increasing concentration can raise the heating generation ability, it can spread heating more and it cause to damage to the surrounding cells from laser point. Generally, these data's can proof that the HNPs can be useful for thermal applications such as for ablation or thermal responsive switches for drug delivery. However, the heating spreads was better performance in lower concentration and it can cause to lower damage to surround healthy tissue.

2.4. Discussion

The results demonstrated that the hybrid iron oxide-silver nanoparticles were successfully synthesised. As discussed in the results section the synthesis of the silver colloids was the rate limiting step for this whole study with the method development taking up to 1.5 years. Eventually, the Agnihotr and colleague method was identified as the optimal synthetic route for synthesis silver nanoparticles in 5 nm size. This method helps to connect silver seeds on the Iron oxide smooth surface and also increase the silver properties to act as strong anti-cancer agent (Agnihotria, *et al*., 2012). The iron oxide synthesis and coated with PEI by using Barnett *et al.* research in 2013 and also Goon and colleagues in 2009 methods.

Generally, the colour was changed in each step of iron oxide coating according to the Figure 23 which can be indicated the chemical reaction in each step. In each step of synthesising the sample were characterised by photon correlation spectroscopy and zeta potential measurement. The particle sizes were measured in each step for checking and confirming the nanoparticle size. The surface charge constantly shifted between positive and negative surface charges between iron, silver and PEI during coating as expected and in agreement with the Barnett and Malekigorji gold-iron oxide HNP studies (Barnett *et al., 2013;* Malekigorji *et al.,* 2014).

The iron oxide surface charge was - 22.67 ±0.96 mV and by coating iron oxide with PEI the surface charge shift to + 46.40 ± 0.68 mV. The silver seeds and the surface charge when it coated on the Fe_3O_4 - 12.63 ±1.02 mV and then by coating silver seed by PEI the surface charge shift to positive again (+ 11.63 ±0.68 mV). The silver coating process in final step leads to shift the surface charge to - 3.05 ±0.29 mV. The changing zeta surface charge demonstrates that the surface charge changes make the stronger bonds and better between different layers. Patel and Agrawal classified the zeta potentials by stabilities. According to their work a zeta potential (Patel & Agrawal, 2011) (Table 6).

Table 6. Nanoparticle stability Classification according to the surface charge level.

Surface Charge	**Stability**
±0 mV	Highly Unstable
From -10 mV to +10 mV	Relatively Stable
From -20 mV to +20 mV	Moderately Stable
≤ -30 mV to +30+ mV ≥	Highly Stable

Therefore, the HNPs developed can be considered to be highly stable. Moreover, nanoparticles with high surface charge indicate strong repulsive forces between particles, resulting less aggregation, and higher stability (Bhattacharjee, 2016).

The TEM images indicated that the silver seeds were successfully anchored onto the surface of the Fe_3O_4-PEI and also that subsequent coating had been achieved. The TEM micrograph demonstrated the smaller particle sizes in compare with photon correlation spectroscopy (PCS). This phenomenon is possible due to the very small fraction of the sample represent in TEM image. On the other hand, a number of factors have a great influence on the hydrodynamic diameter of the particles measured by dynamic light scattering such as polymer shells, hydration layer or other stabilisers, which lead the particles size to be seen larger (Heinz *et al.,* 2014). In comparison with naked iron oxide, polymer coated iron oxide NPs tend to be smaller and more uniform; this result correlates well with the aim of using the polymer layer as stabiliser (Heinz *et al.,* 2014). Increase of the solution stability leads to decrease of particle agglomeration and size. However, iron oxide NPs agglomerates and form large clusters due to the hydrophobic interactions between the NPs because of its large surface area-to-volume ratio and hydrophobic surfaces properties (Wei *et al.,* 2012).

UV/Visible spectroscopy was carried out in order to identify the presence of colloidal silver in HNP. The λ_{max}, measured via UV/Visible spectroscopy, the λ_{max} shift occurred from λ_{max} of 400 nm for silver NPs, λ_{max} of 450 nm for Fe_3O_4-PEI-Ag seeds and finally λ_{max} of 490 nm for HNP. There was not observed plasmon resonance for Fe_3O_4 and Fe_3O_4-PEI (Figure 29). The UV results demonstrate that silver iron oxide HNP was successfully coated.

The ratio between iron and silver were identified by using ICP. The ratio demonstrated the silver and iron existing ratio in the HNP is 1: 3.1 respectively. In general, previous studies

have shown that the ratio of iron oxide in HNPs formulations was 4-fold of gold (Malekigorji *et al.,* 2017; Curtis *et al.,* 2015).

There has not published any article about thermal effects of iron oxide-silver (HNPs) so far. However, there are few investigations which have been performed for the thermal effects of iron oxide-gold HNPs (Hirsch *et al*., 2003). Hirsch *et al.* transferred their novel HNPs into a tumour tissue in mice, which was exposed to laser irradiation (820 nm, 4 Wcm^{-2}, 5 mm spot diameter) for around 6 min. The result demonstrated that irradiation of this novel particles inside the tumours raised the temperature to 37.4 °C after 4 - 6 min irradiation. Hirsch reported that this temperature increase was above the threshold temperature at which irreversible tissue damage occurs (Hirsch *et al*., 2003).

Malekigorji *et al.* studied on gold-iron oxide HNP thermal ability in 2014 (Malekigorji *et al.,* 2014). They compared heat changes between 50 μgmL^{-1} and 100 μgmL^{-1} for gold-iron oxide HNP were dispersed in agar gel and irradiated with continuous wave laser (Ng:YAG pulsed 1064 nm, 1000 V, 6 Hz) in room temperature and 37 °C for 60 s. According to their work at concentrations of 50 μgmL^{-1} at room temperature and 37 °C, ΔT was 5.57 °C ± 1.43 and at 100 μgmL^{-1}, ΔT was 7.70 °C ± 0.80 which were significantly higher than the temperature increase achieved outside the beam ($p < 0.05$). They also observed a small time dependant rise in temperature upon longer laser exposure, which was not significant ($p > 0.05$). The experiment was repeated at 37 °C and around the same ΔT was achieved for samples at this temperature ($p < 0.05$) (Malekigorji *et al.,* 2014).

In comparison with the previous research, the silver-iron oxide HNPs demonstrates significantly greater thermal capability in lower concentrations (25 μgmL^{-1}). Here, at concentrations of 25 μgmL^{-1}, ΔT was 7 °C ± 0.35 and at 50 μgmL^{-1}, ΔT was 11 °C ± 0.56 at

37 °C in 30 s ($p < 0.05$.). The charts clearly demonstrated that there is not differ between 2 points in any concentrations or times. At 25 μgmL^{-1} and 50 μgmL^{-1}, the heat dissipation changes were not significant for 0 -2 mm but the changes were dropped significantly from 2 to 10mm. There interestingly, the study had to be curtailed after only 30 s due to agar melting, again highlighting the great efficiency of laser induced heating. The SPR optimal wavelength of the particles was 500 nm and our HNPs observed heat generation up to 11°C at 50 μgmL^{-1} and dissipation up to 10 mm away from radiation site for 25 μgmL^{-1} (0 s and 10 s). Consequently HNPs may also be useful in tumour ablation however due care is required in order to minimize heat dissipation to healthy tissues.

This excellent heating ability was somewhat unexpected due to the λ_{max} of the silver HNPs being so low and the broad peak disappearing before the 1064 nm of the laser. However, our UV-Vis instrument only recorded absorbance 300 - 700 nm. Nevertheless, the laser irradiation data demonstrated that the HNPs have capability in increasing temperature which may be exploited in thermally-triggered drug release.

All the data also showed that maximum heating occurred after 10 s. Interestingly, this was also observed in Malekigorji's work where the sharp temperature rise was followed by a plateau. In this case, the temperature rise was sufficient theoretically to induce drug release according to her study. In the next chapter this will be explored further. It is pertinent to note that Malekigorji only irradiated her tumours *in vivo* for 20 s (Malekigorji *et al.,* 2014). Therefore the data collected in this study over 30s is still very relevant for application.

In next chapter the pancreatic cancer drug (bis (naphthalimidopropyl)spermine (BNIPDSpm)) will conjugate onto the HNP surface. In concentration of 25 μgmL^{-1} at 37 °C, the temperature of the particles increased up to 44.5 °C and in concentration of 50 μgmL^{-1} at

37 °C, the temperature of the particles increased up to 48°C, which is enough for our therapeutic agent to be released inside the tumour cells (will be described in Chapter Three).

Some of drugs linkers such as BNIPDSpm derivetives can frequently contain of long chains or polymers, which may exist in some distance from the particle surface. The heat distribution from the HNP needs to be such that the thermally labile linker experiences the temperature rise for payload release, otherwise the system would be impractical. Additionally, the heating effects must be manageable, in that the thermal rise must be adequate for drug release but not for cellular stress or damage (Curtis *et al.,* 2015). Consequently lower concentration would be more suitable for these purposes. Not only the heating generation was not significant different with higher concentration, but the heat effect did not occur or with a small increase (1 ^{o}C) after 10 mm for 25 µgmL^{-1}.It can decrease possibility of surrounding tissues.

2.5. Conclusion

Novel iron oxide-silver core-shell HNPs have been successfully synthesised and characterised by using different techniques such as ICP, PCS, TEM and UV-Vis. The results have shown the HNP which has coated with silver is 90 nm. The laser mediated heating confirmed that the HNPs possessed surface plasmon resonance and hence highlights the potential of new HNP capability in thermo-responsive drug delivery.

Chapter Three

Drug conjugations and characterisation of new formulations

3.1. Introduction

Nanoparticles (NPs) are colloidal particles with core diameter between 10- 100 nm. NPs can be unstable and easily react with active substances and change their structure to reach a relatively stable state in some cases. High reactivity and small particle size of NPs can lead to make them unstable and also the main reason of the aggregation (Xu *et al*., 2018). The main factors which influence NP aggregation are the presence of electrolytes, temperature, pH, ionic strength, type of NPs, duration and of storage and the zeta potential. Increasing NPs stability is main solution for preventing from NPs high reactivity and aggregation (Bhadra *et al.,* 2002; Jokerst *et al.,* 2011).

A common method of stabilizing NPs is the utilization of the electrostatic repulsion among NPs, which are modified with charged ligands such as citrate (Dong *et al.,* 2007) and triphenyl phosphine (Pan *et al*., 2007) or using amphiphilic polymers such as polyethylene glycol (Thiol-PEG) (Wang and Nie, 2008).

Polyethylene glycol thiol (SH-PEG)

SH-PEG is most widely applied in various studies due to its good solubility, biocompatibility and also its antifouling properties (Dreaden *et al*., 2009; Liu *et al*., 2007; Simpson *et al*., 2012) and (Jiang *et al*. 2002). Many studies have shown that conjugating PEG on surface of NPs has significant effect on the particle stability and sensitivity of NPs (Durgadas *et al*., 2010) and circulation times (Maus *et al*., 2010). In order to conjugate PEG onto gold or silver nanoparticles a thiol (-SH) functionality is required to form a dative covalent bond between the metallic surface and PEG residue; hence SH-PEG is commonly used. Many researchers have used PEGylated NPs for increasing drug targeting and as biosensors under physiological

conditions. These PEG-Thiol effects on delivery systems have many advantages including prolonging the blood circulation time as well as mimicking biological molecules and hence allowing the NPs to evade macrophage capture and clearance (Dreaden *et al*., 2010). The Thiol-PEG also can encapsulate anticancer drug and control drug release (Maus *et al*., 2010).

Wang *et al.* studied the effect on the performance of PEG-modified gold nanoparticles (AuNPs) (Wang *et al.,* 2013). According to Wang and colleagues studies, PEG plays important roles in improving the AuNP system. These roles include: use as an antifouling spacer arm between the functional ligands and gold surface, as a steric stabilizer for AuNPs under complicated conditions, for screening the charge on the AuNPsto avoid unexpected effects between sodium citrate and other electrolytes which implies that the PEG capping densities crucial to the saturation amount of functional ligands on AuNPs (Figure 32) (Wang *et al.,* 2013).

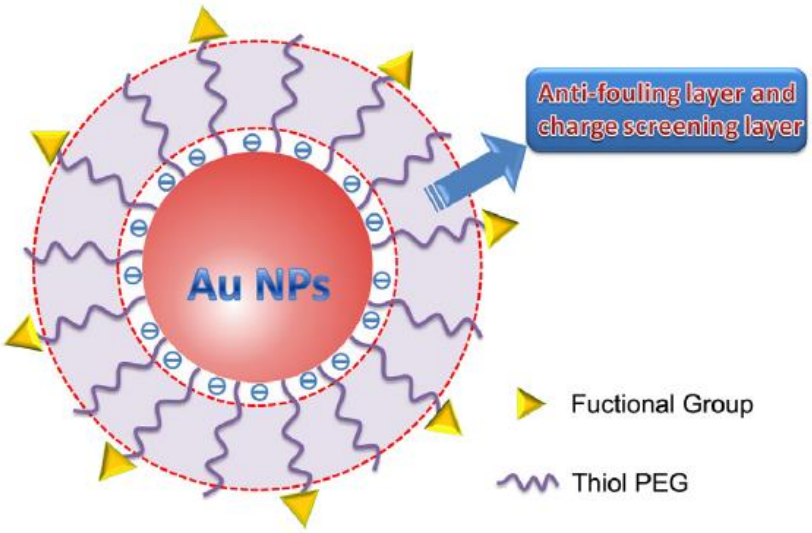

Figure 32: Structure of thiol-PEG-modified AuNPs (Wang *et al*., 2013).

Silver colloids are usually chemically stable against auto-aggregation which is essential for materials in antibacterial and anticancer medicine. However, silver nanoparticles have high

surface area which leads to poor colloidal stability and aggregation in solution. Stabilizing and capping agents such as polymers have been used in the synthesis process of AgNPs to overcome this instability (Wu *et al*., 2010; Maccuspie, 2011; Prathna *et al*., 2011; Tejamaya *et al*., 2012). Polymers are applied to form an outer shell coating to the silver cores or a carrier to loading AgNPs on their surface and providing a steric barrier to aggregation. Moreover, the types of polymers have some effect on the size, shape and properties of AgNPs (Batista *et al.,* 2018; Hu *et al.,* 2012; Krklješ *et al*., 2007; Mallick *et al*., 2004; Wu *et al*., 2010).

Mengda *et al*. studied the effect of SH-PEG on the AgNPs stability and antimicrobial properties (Mengda *et al*., 2018). According the research, silver-polyethylene glycol (Ag-PEG) nanoparticles were synthesized with the thiol-functionalized polyethylene glycol (SH-PEA) as the coating, reducing and stabilizing agent. Moreover, the results of antibacterial activities demonstrated that the Ag-PEG nanoparticles exhibited strong antibacterial activity against *Staphylococcus* aureus, *Escherichia* coli and *Bacillus* subtilis. The results of cytotoxicity showed the Janus Ag-PEG nanoparticles had lower toxicity for healthy cells than the multi-core shell nanoparticles (Mengda *et al*., 2018).

Naphthalimide derivatives

Brana and Ramos synthesized the 1,8-naphthalimide derivatives in 2001 (Brana and Ramos, 2001). According to their research, “naphthalimide derivatives can connect to DNA by intercalation of the chromophore and two of them, mitonafide and amonafide, were used in clinical trials. The therapeutic properties of these drugs can improve by designing new bis intercalating agents. In this case, elinafide, demonstrated powerful activities against solid tumors” (Brana and Ramos, 2001).

Quaquebeke *et al.* assessed effect of new naphthalimides as anti-cancer against for breast cancer MCF-7, pancreatic cancer (BxPC-3) and colon cancer HCT15 Cell Lines in 2007 (Quaquebeke *et al.,* 2007). They synthesised naphthalimides with modified linker alkyl chain with 2, 3 and 4 carbons and the terminal groups include amino, imino, pyrrole, nitrobenzene and ureas. These compounds were assessed against breast cancer MCF-7, colon cancer HCT-15 and pancreatic cancer BxPC-3 cell lines. The new compounds demonstrated very good GI50 values towards MCF-7, HCT-15, and BxPC-3 cancer cell lines. By changing the alkyl chain length in 1,8-naphthalimido derivatives they could increase anticancer activity against different type of cancer cells (Quaquebeke *et al.,* 2007).

Clinical reports displayed that adding free amine group amonafide can switch it to N-acetyl derivative. Mateusz *et al.* added groups such as amides, ureas, thio-amides, amines, and imines to make new compound to increase the activity and to prevent the metabolism that provoke the hematotoxicity (Mateusz *et al*., 2018). The greatest effective complex demonstrated amines group have higher tolerated dose compare with amonafide and did not cause hematotoxicity in mice at doses that displayed strong antitumour results. Even though, 5-fold compound weaker intercalating power than amonafide, it is able to restrain its strand-passage activity (Mateusz *et al*., 2018).

Naphthalimide derivatives signify as a class of DNA-binding agents. These agents have been broadly studied as antitumor agents (Paull *et al.,* 1984) like some of the naphthalimide derivatives, such as bisnafide, amonafide and elinafide (Figure 33) (National Cancer Institute, 1984). Elinafide and bisnafide were formed by a polyamine linker and two naphthalimide groups. Naphthalimide derivatives have ability to bind with the DNA and anticancer activity of the intercalation (Marshall *et al.,* 1994). Amonafide has entered phase

II clinical trials. Amonafide showed activity towards breast and prostate cancer (Isabella *et al.,* 1995). Amonafide acts as a Topo II poison by perturbing the cleavage-relegation equilibrium, which consequences in store of DNA-Topo II covalent adducts (Nishio *et al.,* 1983). Blocking the relegation step after DNA cleavage makes of double-strand breaks. Despite its activity, Amonafide is no longer in clinical trials because of unexpected toxicity begun by one of its metabolite, N-acetyl-amonafide (Felder *et al.,* 1987).

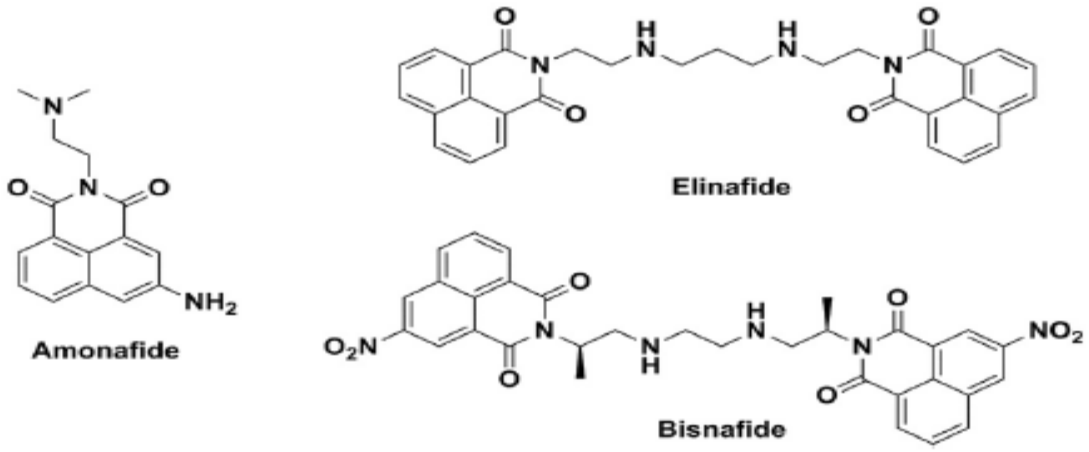

Figure 33: Representative naphthalimide derivatives in clinical trial (National Cancer Institute, 1984).

Bis-naphthalimido compounds can attach to DNA double helix via the major groove (Bailly *et al.,* 1995) The cytotoxicity of these compounds are much greater than higher monomeric compounds. Bis-naphthalimido compounds can be extremely insoluble in aqueous solutions depending on their linker. Many attempts were carried out for increasing their solubility and decreasing cytotoxicity activity. Eight bis-naphthalimido compounds were modified with adding one or two nitrogen atoms in the linker chain (Brana *et al.,* 1996). The Bis-naphthalimido modified could simply react the corresponding alkyltetraamine with 1,8-naphthalic anhydride (Brana *et al.,* 1996).

Naphthalimide-based anti-tumour drugs may cause serious side effects, including dose limiting toxicity and central neurotoxicity. In order to develop their efficacy and decrease the side effects, naphthalimide derivatives, adapted with imide substituents, fused aromatic rings and various side chains (Tabor, 1984). Recently, the studies have been published in design of novel drugs for sequence-specific binding of naphthalimides to DNA (Tomczyk *et al*., 2018). The trisubstituted naphthalimide derivatives can bind telomeric G-quadruplexes with extraordinary anti proliferation activity against different cell lines (Barron *et al.,* 2010). The substituents at naphthalimide skeleton and linkers play crucial roles in determining the cytotoxic activity, photophysical properties and sequence selectivity of bisnaphthalimides derivatives (Filosa *et al.,* 2009).

In 2000, Thoo Lin and colleagues synthesised of bis-naphthalimidopropyl polyamine derivatives, which contain 2, 3 and 4 nitrogen atoms in the linker chain (Thoo Lin *et al.,* 2000). They increased the aqueous solubility of bis-naphthalimido compounds with adding more heteroatoms (N-alkylation reaction) in the linker chain (Thoo Lin *et al.,* 2000; Paul *et al.,* 2000). The new bis-naphthalimidopropyl polyamine derivatives was involve oxa-putrescine (BNIPOPut), bis-naphthalimido- propyl putrescine (BNIPPut), Bis(naphthalimidopropyl) spermidine (BNIPSpd) and Bis(naphthalimidopropyl)spermine (BNIPSpm). The general intermediate for the synthesis of BNIPPut, BNIPSpd, BNIPSpm and BNIPOPut is toluene- nesulfonyloxypropylnaphthalimide (Figure 34) (Dance *et al.,* 2004). This was formulated by first reacting 1,8-naphthalic anhydride with aminopro- panol to give N-(3-hydroxypropyl) naphthalimide which upon reaction with tosyl chloride in 60% yield (Dance *et al.,* 2004). Thoo Lin *et al.* discovered that using four times excess of tosyl chloride in a small volume of solvent could make best situation to achieve a maximum yield. On the

other hands (e.g., with equimolar or 2 molar quantities of tosyl chloride), a combination of 2 and 3, N-(3-chloropro pyl)naphthalimide is constantly formed so reducing the overall yield of the reaction and also, renders purification very complex (Figure 34) (Dance *et al.,* 2004).

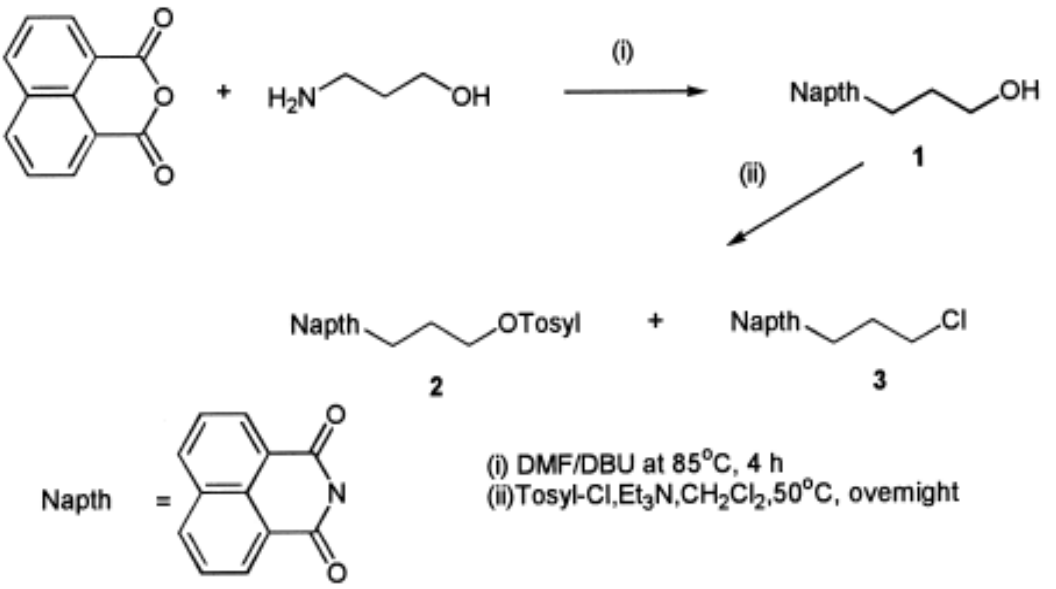

Figure 34: The steps of bis-naphthalimidopropyl polyamine derivatives preparation (Dance *et al.,* 2004).

According to the Dance *et al.* studies "To obtain bis-naphthalimides such as oxa-putrescine (BNIPOPut), bis-naphthalimido- propyl putrescine (BNIPPut), Bis (naphthalimidopropyl) spermidine (BNIPSpd) and Bis(naphthalimidopropyl) spermine (BNIPSpm) (Figure 35), polyamines (4,5,6 and 7) were covered with 2,4,5-trimethylsulphonyl chloride (Mts-Cl) in pyridine followed by their N-alkylation with compound 2 to yield the fully protected bisnaphthalimido compounds which, on subsequent deprotection with hydrobromic acid/glacial acetic acid in dichloromethane. The BNIPPut, BNIPSpd, BNIPSpm and BNIPO were made as their hydrobromide salts" (Dance *et al.,* 2004). Their research was

demonstrated that BNIPSpd and BNIPSpm have stronger bind to DNA and have more potential to contribute to their cytotoxic action than the other compounds. Consequently BNIPSpd and BNIPSpm were better basis for their further development as anticancer drugs (Dance *et al.,* 2004).

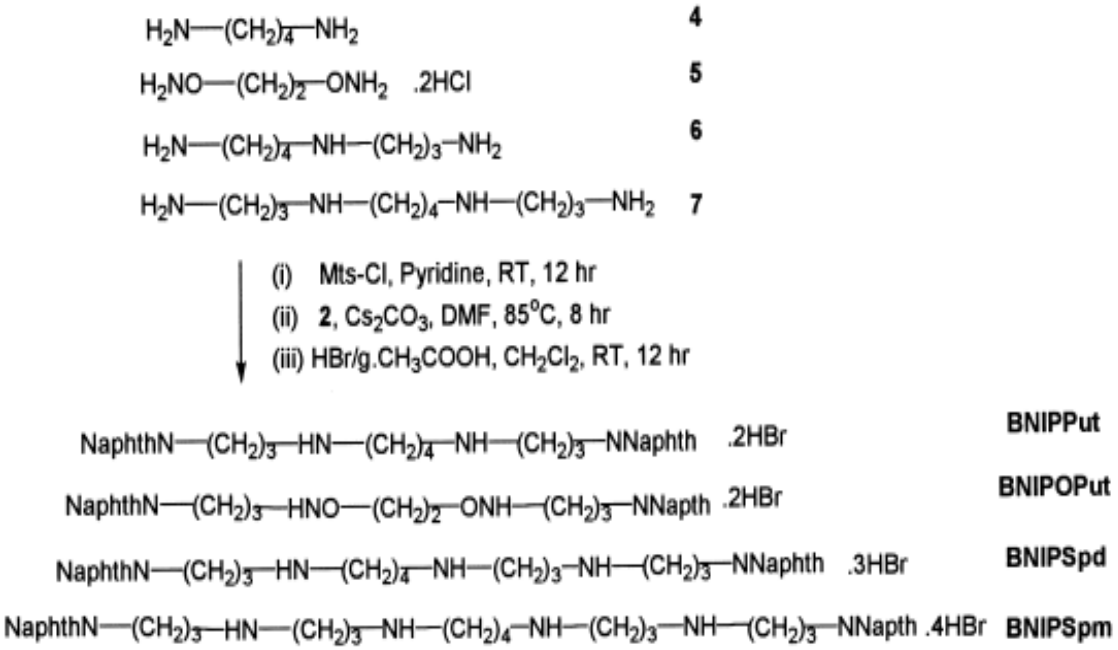

Figure 35: BNIPPut, BNIPOPut, BNIPSpd and BNIPSpm formulations (Dance *et al.,* 2004).

National Cancer Institute (NCI) compered cytotoxic properties of BNIPSpd and BNIPSpm against 60 standard human cell lines derived from nine different tumours including breast cancer. BNIPSpd and BNIPSpm were indicated to be very active against all panels of cell lines, with mean IC_{50} values (drug concentration that causes 50% growth inhibition) ranging from 0.25 to 7.43mM and demonstrating considerable selectivity depending on the panel and cell line tested (Thoo Lin *et al.,* 2000).

Malekigorji *et al.* researched the interaction between bisnaphthalamide derivatives and novel HNPs with using gold nanoparticles for pancreatic cancer treatment.

The impact of conjugation ability, stability and drug release pattern of hybrid formulations were assessed in their study. The bisnaphthalamide derivatives were compared between bisnaphthalimido 1,12-diaminododecane (BNIPd), bisnaphthalimidopropyl spermine (BNIPDSpm), bis naphthamimidopropyl -3,3-butane-1,4-diyl, bis sulfanediyl, bispropan-1-amine (BNIPds) and bisnaphthalimido-1,20-diaminoicosane (BNIDi). Their researches illustrated that BNIDi was not able to conjugate with HNP because this compound did not have amine group, resulted in weak electrostatic interactions between the drug and particle. So the amine group could be main reason to conjugate the bisnaphthalamide derivatives to the HNP. Moreover BNIPd to BNIPDSpm had stronger interaction of drug-NPs cause of 4 amine group's existence in the structures. BNIPDSpm (with four amine groups) displayed highest loading capacity, fastest release and greatest stability on the surface of HNP between the other bisnaphthalamide derivatives. According to their research, PEGylated formulations mostly revealed greater release of drug in comparison with their unPEGylated counterparts (Malekigorji *et al.,* 2017).

Malekigorji *et al.* found that BNIPDSpm was the best option in their Fe304-Au system. Therefore, this is the drug of choice for conjugation with the silver HNPs synthesised in the previous chapter (Malekigorji *et al.,* 2017). Additionally, previous SH-PEG was also seen to be advantageous and therefore this will be included onto the HNP surface in combination with the drug molecules (Mengda *et al.,* 2017).

In this chapter, the interaction between BNIPDSpm and BNIPDSpm- PEG Thiol on novel HNPs with using silver nanoparticles was compared together. After formulation they also

were characterised by different analytic instruments such as photon correlation spectroscopy (PSC), fourier transform infrared spectroscopy (FTIR), inductively coupled plasma optical emission spectroscopy (ICP-oes) and reverse phase high performance liquid chromatography (RP-HPLC).

Fourier Transform Infrared spectroscopy (FT-IR)

The Fourier Transform Infrared Spectroscopy (FTIR) can rapidly deduce a chemical finger print with high sensitivity & specificity, in a fast and non-destructive manner (Alvarez-Ordóñez *et al.* 2011).

When molecules are exposed to infra-red radiation the atoms attract particular frequencies and vibrate (Williams & Fleming. 2007). On a typical infra-red (IR) spectrum the frequency is demonstrated in wavenumbers 400-4000 cm^{-1}, which is the reserve of frequency (1/frequency) in cm^{-1}. The percentage transmission of identifiable wavenumbers offers a strong indication to the functional groups (Williams & Fleming, 2007).

The samples expose on IR and absorbance of the infrared light's energy at various wavelengths. FTIR analysis measures the range of wavelengths in the infrared region that are absorbed by a material. This technique is a quick and cost effective method for identifying unknown particles, residues, films or fibres. FTIR can also assess levels of oxidation in some polymers or degrees of cure in other polymers as well as surface contamination or additives in materials (Andersen *et al.,* 2016). Figure 36 demonstrates the schematic diagram of an FTIR spectroscopy (Dost & İdeli, 2012).

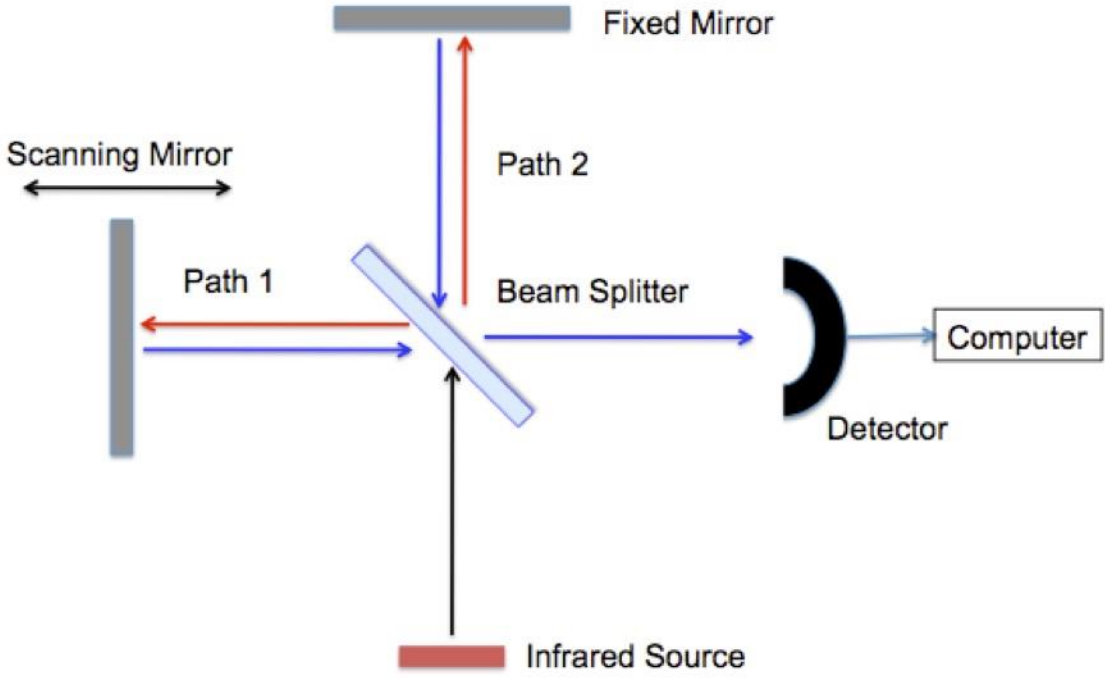

Figure 36: Schematic diagram of a FTIR spectrometer (Dost & İdeli, 2012).

High performance liquid chromatography (HPLC)

High performance liquid chromatography (HPLC) is a great technique for separation and analysis of components within a mixture. HPLC can be utilised to analyse complex mixtures of molecules based on distribution between stationary and mobile phases (Neue, 2007; Dean *et al.,* 2002c; Jared *et al.,* 2015). HPLC basically used for separations and purifications in various areas including biotechnology, polymer, food industries, environment and pharmaceuticals (Hema *et al.,* 2009). Figure 37 illustrates a schematic diagram of an HPLC system (Czaplicki, 2012).

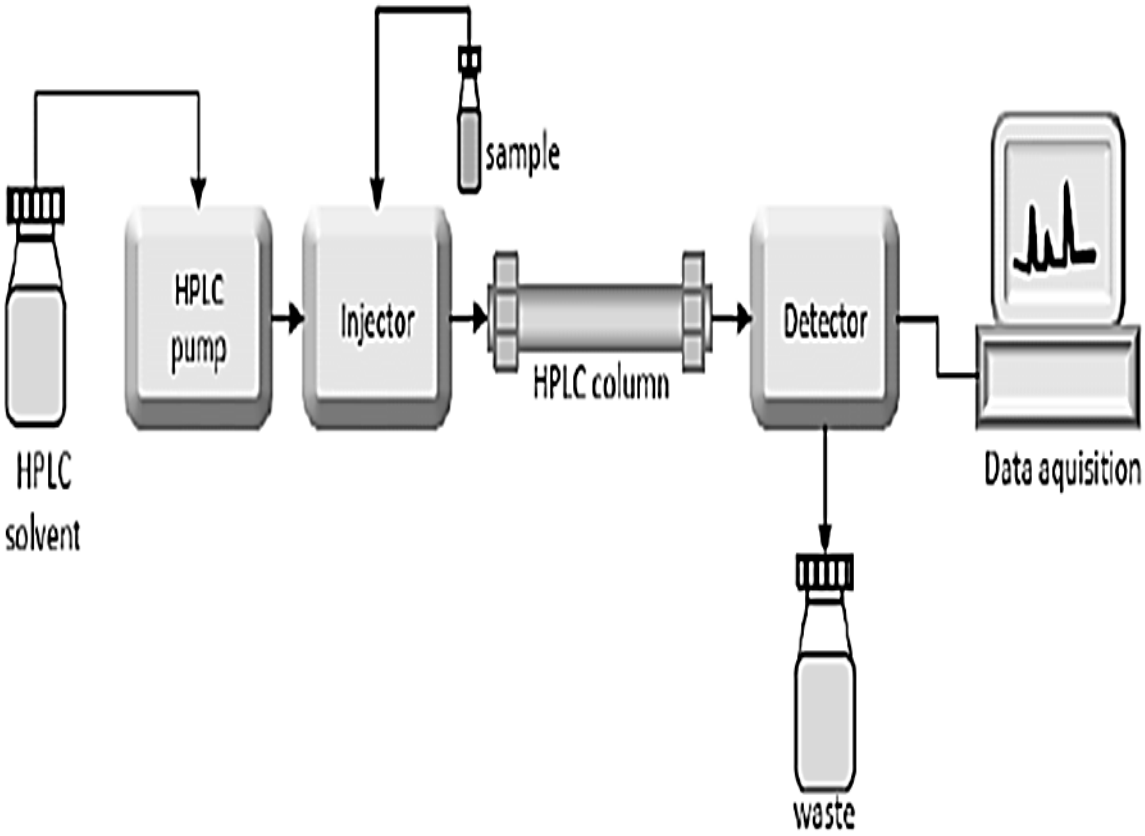

Figure 37: Schematic diagram of High Performance Liquid Chromatographer (HPLC) (Czaplicki, 2012).

After injecting the fixed amount of sample, the sample will incorporate in the mobile phase and pass through the column at a fixed flow rate. The column is packed with stationary phase (usually silica). The sample adsorbs onto the stationary phase dependant on its chemical characteristics and this will alter its retention time. Once the sample is eluted it is detected via fluorescence spectroscopy, UV/Vis spectroscopy, mass spectrometry or electrochemical detectors. The whole system is connected to a built-in computer interface control (Dost & İdeli, 2012; Khare *et al*., 2016; Ansari & Häubl, 2016; Campos *et al.,* 2016).

Chromatographic separation can be classified into number modes such as size exclusion (SE), ion exchange (IE) and reversed-phase (RP) according to the size, polarity and charge of the molecules (Chi-San. 1995; Haddad and Jackson. 1990). Reversed-phase (RP) can separate all substances in various compounds (Snyder et al., 2010). Separation mechanism based on the hydrophobic binding of the solute molecule in the mobile phase (polar) to the immobilised hydrophobic stationary phase such as inorganic polymers with large surface areas, carbon and silica gel (Rubinson, 2000).

Retention time is the particular time taken for passing of a particular mixture component through the column. Various factors can effect on the retention time such as polarity of the column adsorbent. In normal-phase HPLC systems, columns containing polar adsorbents will have a higher affinity for polar components in a separation mixture. So, these polar components move slower during column and the lead to increasing retention time. On the other hands, non-polar solvent travel through the column quicker and cause to shortens their retention time. Moreover, longer columns cause to increase the retention time, as the distance components must travel before reaching the end will increase (Campos, 2016).

Aims and objectives

The aim of this chapter is to study the ability of BNIPDSpm and BNIPDSpm-PEG to conjugate onto the surface of the silver HNPs produced in Chapter 2. In previous chapter the HNP thermal ability were assessed and in this chapter. Laser irradiation, will result in quick drug release from the particles. Then the free drug can enter cells` nucleus and interact with DNA for anticancer effect. We will check drug release in different temperatures. In this case, the release pattern of the formulations inside the pancreatic cancer cells, before and after laser irradiation can be predicted. The nano-formulation will be characterised by PCS, ICP-OES,

FTIR and RP-HPLC. The amount of drug loading and releasing of novel formulation will be assessed at varied temperature and pH and quantified using RP-HPLC. The stability of formulation and physical stability will be tested at different temperatures and forms (dispersed in water or freeze dried) by RP-HPLC and ICP respectively for 4 weeks.

3.2. Materials and methods

Materials used for this chapter

Table7. Materials used in Drug conjugations, synthesis and characterisation of new formulations

Materials	Suppliers
PRMI Medium 1640(1X)	Thermo Fisher, UK
HPLC Grade acetonitrile	Sigma-Aldrich Co., UK
Octane sulfonic acid	Sigma-Aldrich Co., UK
Sodium acetate	ACROS Organics Co., USA
HPLC Grade hydrochloric acid	Sigma-Aldrich Co., UK
HPLC Grade dimethyl sulfoxide	Sigma-Aldrich Co., UK
Hybrid nanoparticles (HNPs)	Synthesised in Chapter Two
Nitric acid	Fisher Scientific, UK
Hydrochloric acid	Fisher Scientific, UK
Thiolated poly ethylene glycol (PEG-thiol)	Sigma-Aldrich Co., UK
Bis(naphthalimidopropyl)spermine (BNIPDSpm)	Provided by Keele Nanopharmaceutics Group

Methods

Drug conjugation

HNPs solutions (1 mg mL^{-1}) were mixed with the drugs in the ratio (HNP: Drug) 1:1, 1:5, 1:10, 5:1 and 10:1 respectively. The solutions were stirred for 3 h at room temperature. Finally the solution was magnetically separated and highly washing with deionised water for three times.

The particles were separated from the supernatant (waste solution) after drug conjugation by using a strong permanent magnet on the outside of a glass vial containing the formulation. One mL of the waste solution (in water) was diluted with 1 mL of DMSO and drug concentrations were analysed via HPLC. All measurements were run in triplicate and recorded as average values.

PEG-thiol was added simultaneously into the drug-HNP reaction at 25 mg, 50 mg and 100 mg of powdered polymer (based on the concentration used in the literature for PEG-thiol) was added with the solution respectively (Barnett *et al*., 2013a; Barnett *et al.,* 2013b). The particles were washed after 3 h as previously described. It was assumed that PEG will coat the surface of HNPs completely if it was added before the drug, thus no free surface would be available for the drug attachment (Barnett *et al*., 2013a; Barnett *et al.,* 2013b).

Drug quantification

RP-HPLC (Prominence, DEGASSER, LC20AD, SHIMADZU) with a fluorescence detector at 234 nm (Excitation) and 394 nm (Emission) (Jasco, PU-980, Japan; column C18 (2), 150×4.60 mm 5 micron, flow rate: 1 $mLmin^{-1}$, injection volume: 20 µL) were used for identifying amount of drug loading and releasing of HNP- BNIPDSpm and HNPs- BNIPDSpm-PEG-Thiol. In this case,

to improve the retention, the buffer used in HPLC mobile phase was made by adding 1.64 g sodium acetate and 0.432 g octane sulfonic acid in 200 mL of deionised water. After dissolving the materials in water, the pH of the solution was decreased to 4.5 by the addition of hydrochloric acid (2 mL). Finally, acetonitrile were added to the solution with ratio of 70:30, respectively. For dissolving BNIPDSpm without sonication DMSO added to the solution before injecting to HPLC. The amount of attached drug was assessed from the amount of free drug in waste solution and distinguished via HPLC.

Characterisation of novel formulations

Zeta potential measurement

Zeta potential measurements of novel formulations were assessed using a photon correlation spectrometer (PCS, Zetasizer nano-ZS, Malvern Instruments, UK) as described in Chapter Two (Section 2.2.2.7.1).

Fourier Transform Infrared Spectroscopy (FT-IR)

HNP, HNP- BNIPDSpm and HNPs- BNIPDSpm-PEG-Thiol with highest drug loading concentrations (5 mL) were freeze dried using a Heto Power Dry LL3000, Thermo-Fisher UK. The freeze dried samples were analysed on the FTIR using a diamond tipped attenuated total reflectance attachment (Nicolet iS5 with iD5 ATR, Thermo-Fisher UK) over 600 scans.

***In vitro* drug release study**

***In vitro* drug release study in aqueous environments**

HNP-drug or HNP-Drug-PEG solution (2 mL) were place into dialysis membrane (12-14 KDa) and the membrane were placed and stirred into conical flask containing 200 mL of deionised

water or RPMI media at varied pH (pH 7.2, pH 4.6 and pH 3.6) and temperatures (37˚C, 44˚C, 50˚C & 60˚C). Different samples (1 mL) were taken from the exterior solution at selected time points (0.017 h, 0.084 h, 0.17 h, 0.33 h, 0.5 h, 1 h, 2 h, 3 h, 4 h, 24 h, 48 h and 72 h). All extracted samples were diluted with 1 mL of Dimethyl sulfoxide (DMSO) and drug concentrations were analysed via HPLC.

Stability study

Formulations Chemical Stability study

HNP-BNIPDSpm and HNP- BNIPDSpm-PEG (1 mL, drug = 0.5 mg mL^{-1}) was kept at room temperature or 4˚C over 5 weeks. The concentration of released drug in samples was monitored each week by magnetic separation and RP-HPLC of the supernatant. Additionally each formulation with the same mentioned concentration was freeze dried. The powder formulations were kept at room temperature or 4 ˚C and each week the powder formulations reconstituted in deionised water and the concentration of released drug analysed via HPLC in the supernatant after magnetic separation. All samples were sonicated with a sonic bath before the separation of particles from the supernatant. All measurements were run in triplicate and recorded as average values.

Stability of HNPs in physiological conditions

Previous researches were carried out for testing HNP stability in physiological conditions (Hoskins *et al*., 2012b). For physical stability, 2mL HNP (100 μgmL^{-1}) were pipetted into dialysis membrane (12-14 KDa) and then placed in 200 mL RPMI (Life Technologies, UK). The samples were taken from stirred particles during 1 h, 4 h, 24 h, 48 h, 72h, 168 h, 336 h, 504 h and 672 h. The media was pH changed to pH 7.2 and 4.5 to mimic blood and lysosomal

physiological conditions respectively. The physical stability of novel formulations was carried out using ICP-OES spectrometer for analysing for amount of Iron in the solution. Iron content in solution was calculated in respect to a calibration as described in Chapter Two (section 2.3.1).

3.3. Results

Drug conjugation

BNIPDSpm was analysed by HPLC. The fellow rate adjusted in 1 $mLmin^{-1}$ and fluorescence detector at Excitation 234 nm and Emission 394 wavelengths. A calibration was run using drug solutions dissolved in 50: 50 H2O: DMSO with the concentration of 31.25 -1000μgmL^{-1} (R^2 = 0.999) (Figure 38).

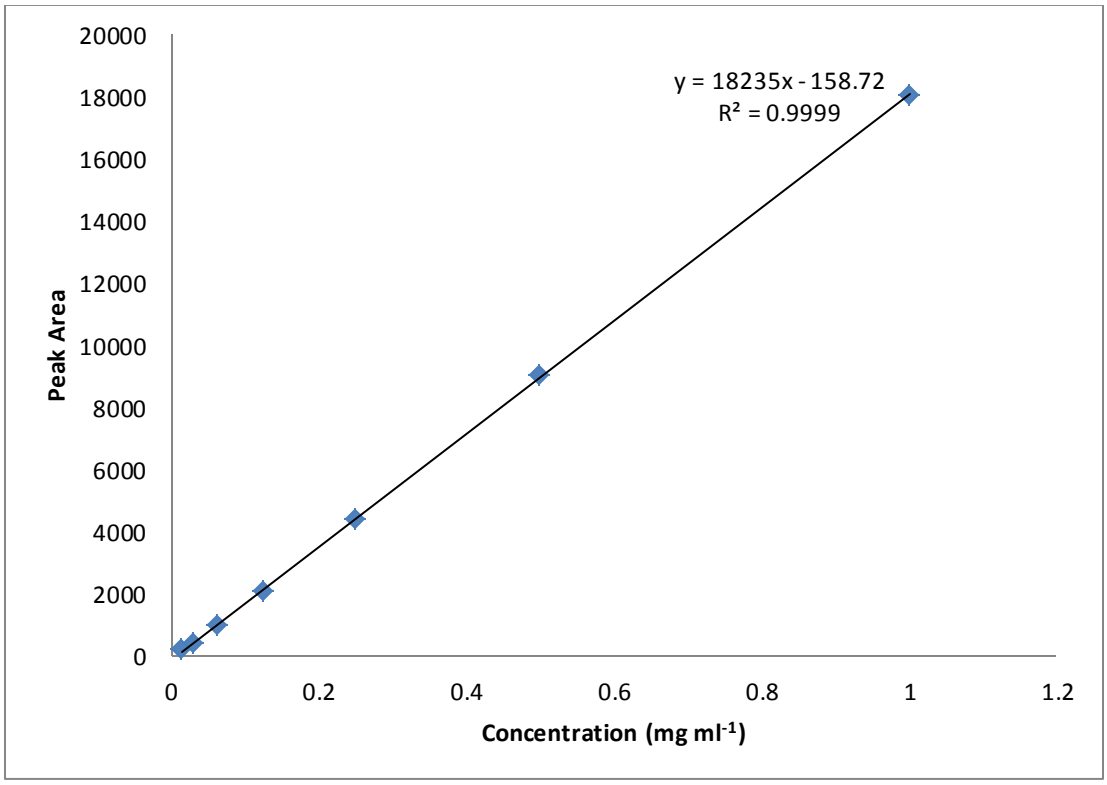

Figure 38: Calibration graph of BNIPDSpm for drug loading.

The drug had sharp peak which observed between 9-10 min (Figure 39).

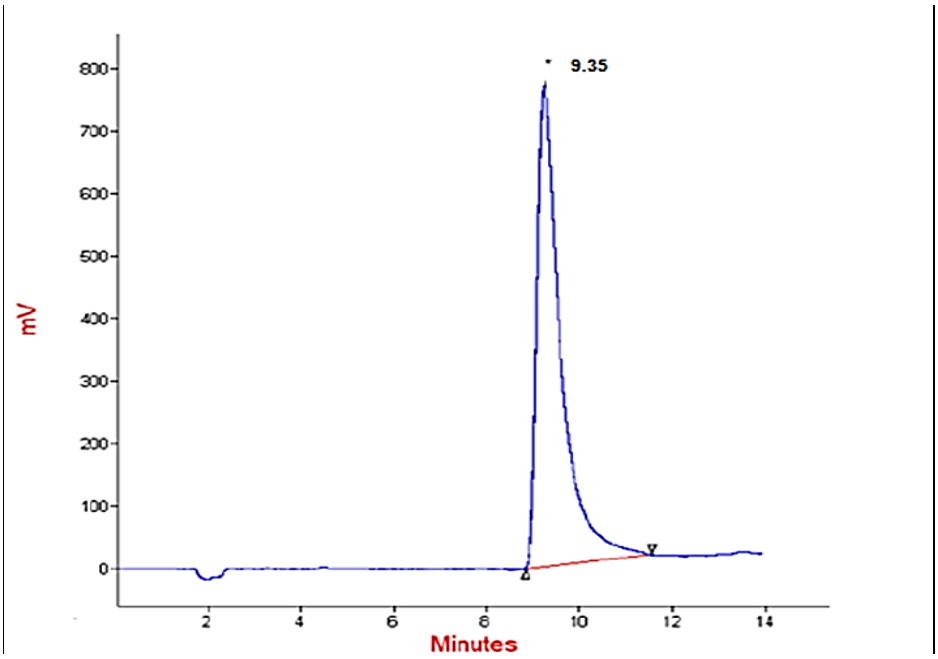

Figure 39: RP-HPLC analysis of 100 µgmL^{-1} BNIPDSpm (dissolved in DMSO/H2O (50:50 v/v)).

The drug conjugation were assessed in different ratios between HNP and the drug according to the Figure 40.

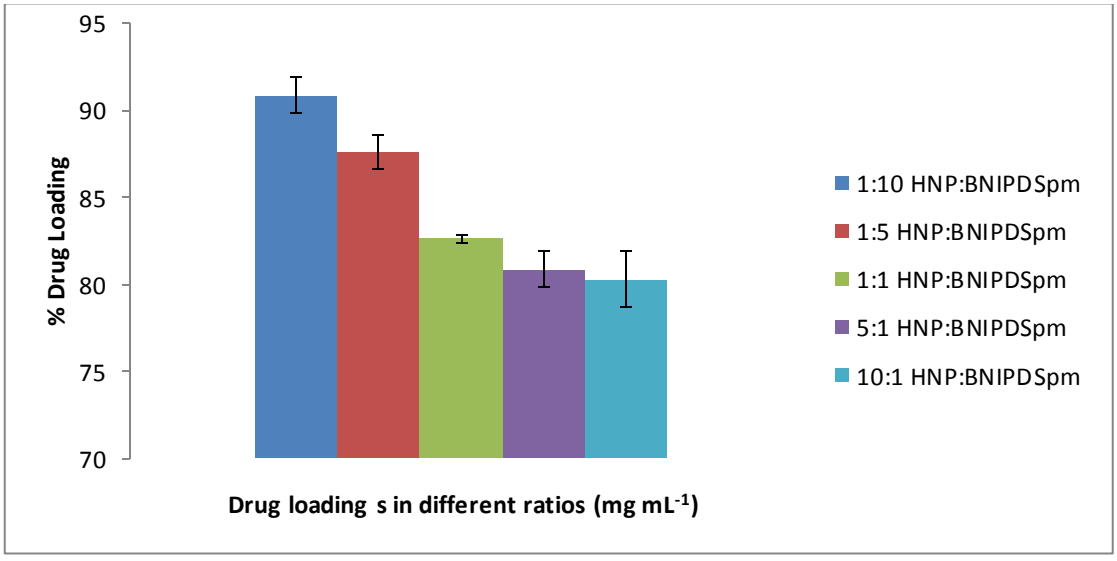

Figure 40: Drug conjugations in different ratios of HNP and BNIPDSpm.

According to the Figure 40, BNIPDSpm conjugated into HNP with 80-90% in different ratios. The existence of 4 positive charged amine groups in BNIPDSpm structure can lead to strong electrostatic interactions between the drug and HNP with negative surface charge. Figure 40 demonstrated that the ratio of 1:10 HNP: BNIPDSpm has the highest percentage of drug conjugation among other concentrations. In this ratio 81.72 mg ± 1.03 (out of 90 mg) of the drug conjugated into the HNP (9 mL, 1 mg mL^{-1}) (Table 8). The percentage of drug conjugation was 90.88 %± 1.03 which means that 1mg mL^{-1} HNP (Fe) conjugated 9 mg mL^{-1} of the drug in optimum ratio.

Table 8. Actual weight of drug conjugations in different ratios. Experiments were performed three times, and data were expressed as mean ± standard errors (n=3, ave ± SD).

Different Ratios (mg.mL-1)	**Drug conjugated (out of 90 mg)**
1:10 HNP:BNIPDSpm	81.72 mg ± 1.03
1:5 HNP:BNIPDSpm	78.31 mg ± 1.17
1:1 HNP:BNIPDSpm	74.69 mg ± 0.27
5:1 HNP:BNIPDSpm	72.93 mg ± 1.06
10:1 HNP:BNIPDSpm	71.10 mg ± 1.93

Different ratios PEG-Thiol was added to the optimum ratio HNP-Drug (1:10 respectively). These ratios were including 1:10:1 HNP:BNIPDSpm:PEG-Thiol, 1:10:5 HNP:BNIPDSpm:PEG-Thiol and 1:10:10 HNP:BNIPDSpm:PEG-Thiol. The drug conjugation was according to the Figure 41.

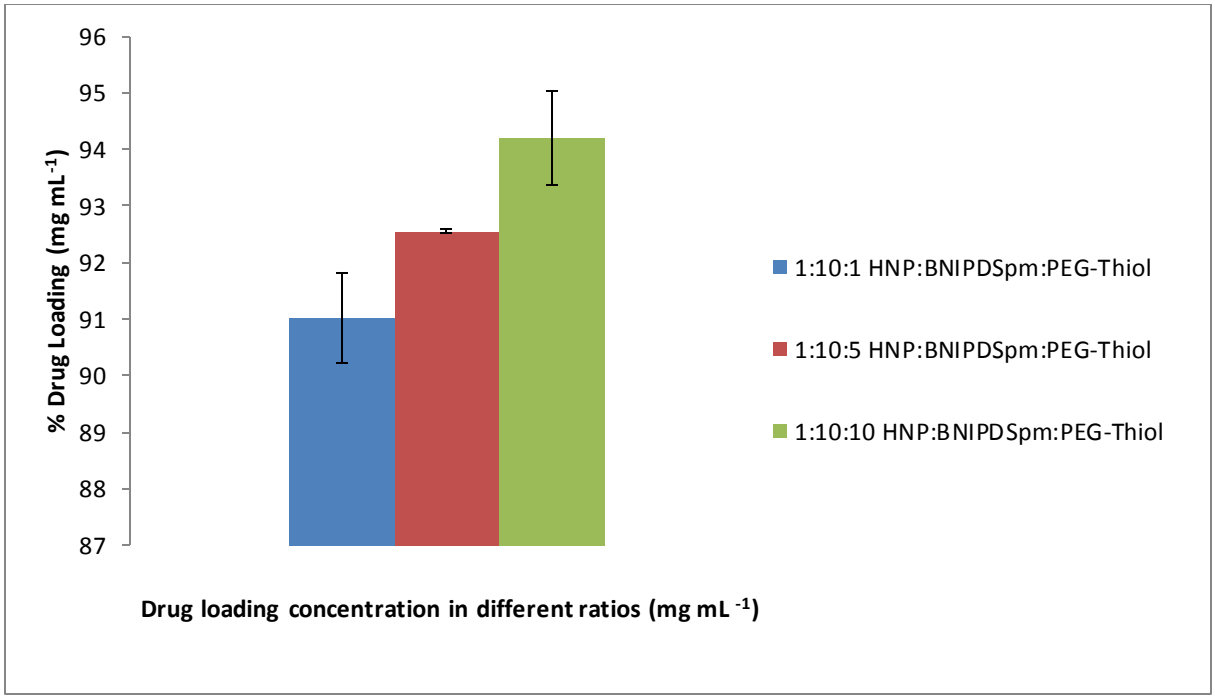

Figure 41: Drug conjugations in different ratios of PEG-Thiol.

According to the Figure 41, ratio of 1:10:10 HNP:BNIPDSpm:PEG-Thiol has the highest percentage of drug loading in compare with the other ratios. In this ratio 84.78 mg ± 0.83 of the drug (out of 90 mg) was attached into the HNP (9 mL, 1mg mL^{-1}) (Table 9). The percentage of drug conjugation was 94.21 %± 0.83 which mean 1mg mL^{-1} HNP (Fe) was conjugated 9.42 mg mL^{-1} of the drug in optimum ratio (Table 9).

Table 9. Drug loading in different ratios of PEG-Thiol. Experiments were performed three times, and data were expressed as mean ± standard errors (n=3, ave ± SD).

Different Ratios ($mg.mL^{-1}$)	**Drug conjugated (out of 90 mg)**
1:10:1 HNP:BNIPDSpm:PEG-Thiol	81.91 ± 0.78
1:10:5 HNP:BNIPDSpm:PEG-Thiol	83.29 ± 0.03
1:10:10 HNP:BNIPDSpm:PEG-Thiol	84.78 ± 0.83

Characterisation of novel formulations

Zeta potential measurement of novel formulations

HNP, BNIPDSpm-HNP and BNIPDSpm-HNP-PEG were characterised by photon correlation spectroscopy (PCS) (Table 10).

Table 10. Zeta potential index of particles measured at 1 mg mL^{-1} (concentration of conjugated drug) in deionised water (n=3, Ave ± SD).

Particle	Zeta Potential (mV ± SD)
HNP	-3.05± 0.29
BNIPDSpm-HNP	+32.51± 0.35
BNIPDSpm-HNP-PEG	+18.77± 0.41

The data showed that the 'naked' HNPs possessed a negative surface charge (-3.05 ± 0.29 mV) before conjugating with the drug. This is probably due to the slight electronegativity of silver surfaces in the colloidal form. BNIPDSpm possessed 4 amine groups so the surface charge shifted to positive (+32.51 ±0.35 mV) after drug conjugation. The surface charge for BNIPDSpm-HNP-PEG was positive but lower than BNIPDSpm-HNP (+18.77±0.41 mV), indicating further modification of PEG. This could be due to the -OH groups in the PEG chains possessing a slight negativity, thus reducing the net surface charge. The decrease of zeta potential confirms the PEG binding.

Fourier transforms infrared spectroscopy of formulations

FTIR were carried out for HNP, BNIPDSpm-HNP and BNIPDSpm-HNP-PEG to confirm whether the drugs/PEG had conjugated onto the HNPs. Before conjugation the drug, the 'naked'

HNPs were characterised (Figure 42). As seen in the spectra, no substantive peaks were observed, as expected.

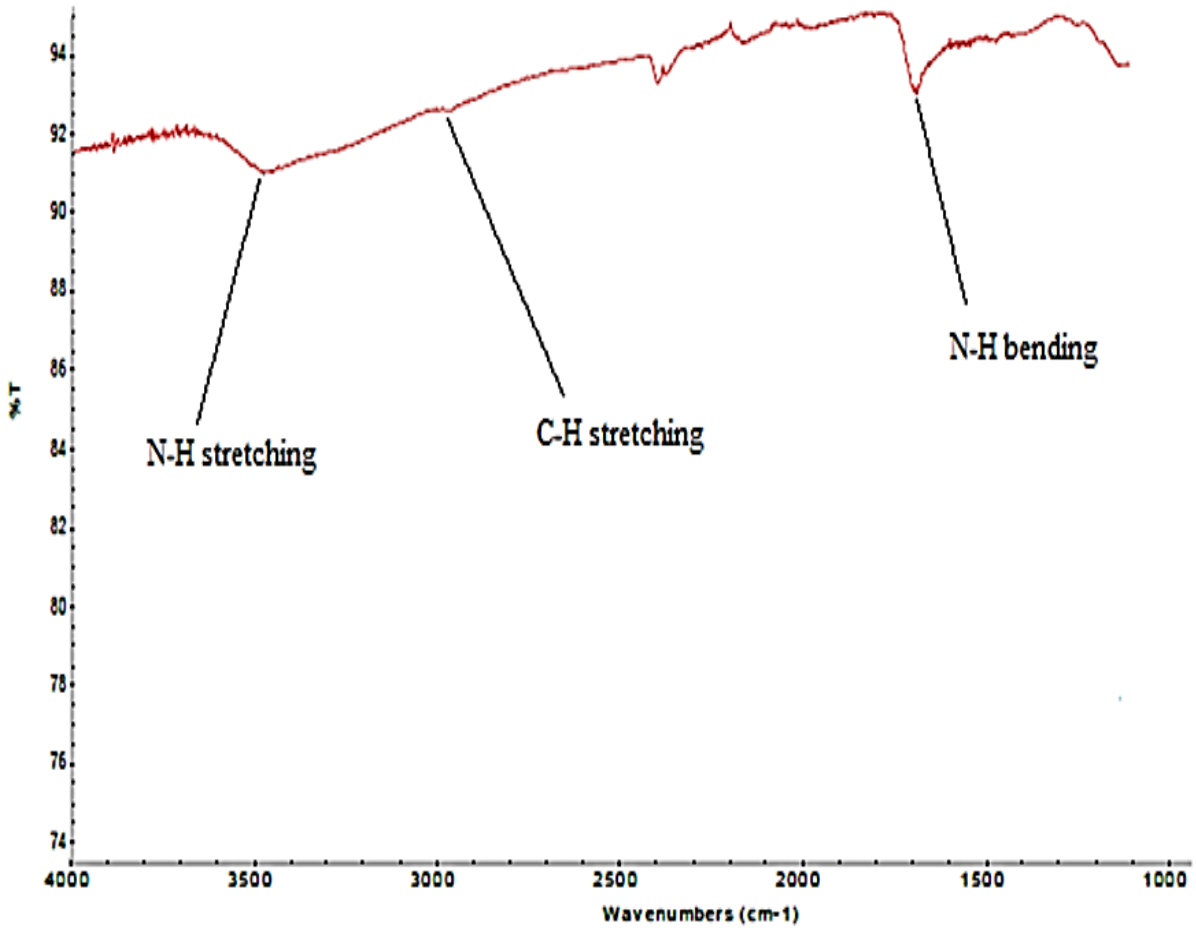

Figure 42: FTIR spectra of HNP, between 1000-4000 cm^{-1}.

The attachment of BNIPDSpm with HNP and HNP-PEG was confirmed by FTIR spectra (Figure 43A and 43B). The series of characteristic IR bands for both formulations are summarised in detail in Tables 11. Bands 1098 cm^{-1} in BNIPDSpm-HNP and 1124 cm^{-1} BNIPDSpm-HNP-PEG approved the presence of aromatic in-plane C-H bending. Bands 1573 cm^{-1} and 1580 cm^{-1} presented aromatic C=C stretching in BNIPDSpm-HNP and BNIPDSpm-HNP-PEG respectively. C=O (Stretching) bands appeared in 1684 cm^{-1} in BNIPDSpm-HNP and 1641 cm^{-1} in

BNIPDSpm-HNP-PEG. Bands in 2910 cm^{-1} and 2989 cm^{-1} area approved existence of C-H (Stretching) in BNIPDSpm-HNP-PEG AND BNIPDSpm-HNP-PEG respectively. Other bigger Peak observed at 1341 cm^{-1} (C–H bending; −CH2 and −CH3) confirm the presence of bound PEG within BNIPDSpm -HNP- PEG formulation (Figures 43A and 43B).

Table 11. Assignment of FTIR spectra for BNIPDSpm-HNP and BNIPDSpm-HNP-PEG.

Samples	**IR bands (cm^{-1})**	**Description**
BNIPDSpm-HNP	1098	Aromatic in-plane C-H (bending)
	1573	Aromatic C=C stretching
	1684	C=O (Stretching)
	2910	C-H (Stretching)
BNIPDSpm-HNP-PEG	1124	Aromatic in-plane C-H (bending)
	1580	Aromatic C=C stretching
	1641	C=O (Stretching)
	2989	C-H (Stretching)

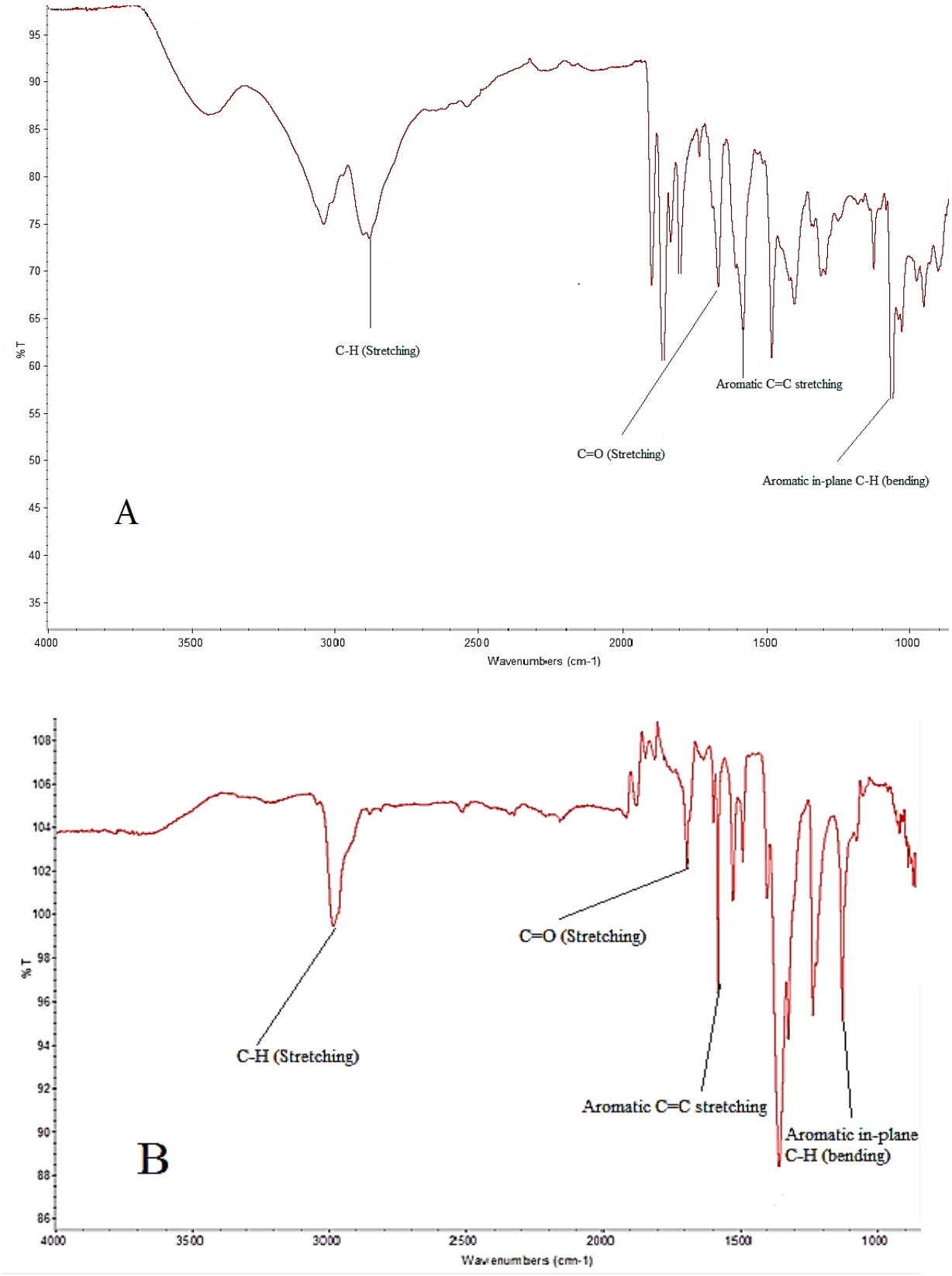

Figure 43: FTIR spectra of A) BNIPDSpm-HNP and B) BNIPDSpm-HNP-PEG, between 1000 - 4000 cm^{-1}.

Stability tests

After optimizing the formulations, the formulations were kept in a dark airtight container at room temperature and under refrigeration (4 °C). Moreover the samples were assessed with 2 different states include freeze dried 'cakes' (reconstituted with water and sonicated) and liquid state for up to 5 weeks (Figures 44 and 45). Both forms (dried and disperse) were sonicated before stability measurement.

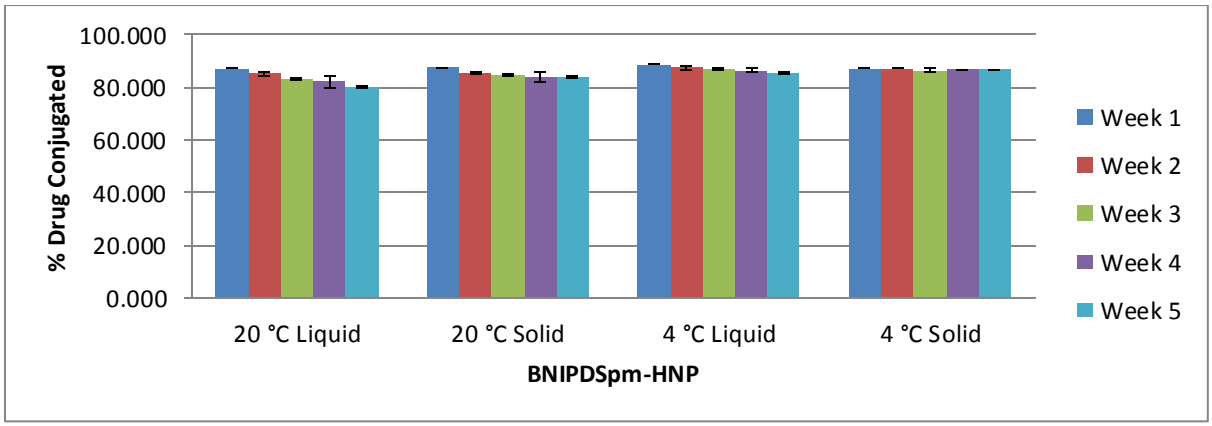

Figure 44: Stability test for BNIPDSpm-HNP at 20 °C and 4 °C in the form of dispersed in water and freeze dried, over the period of 5 weeks (n=3, ave ± SD).

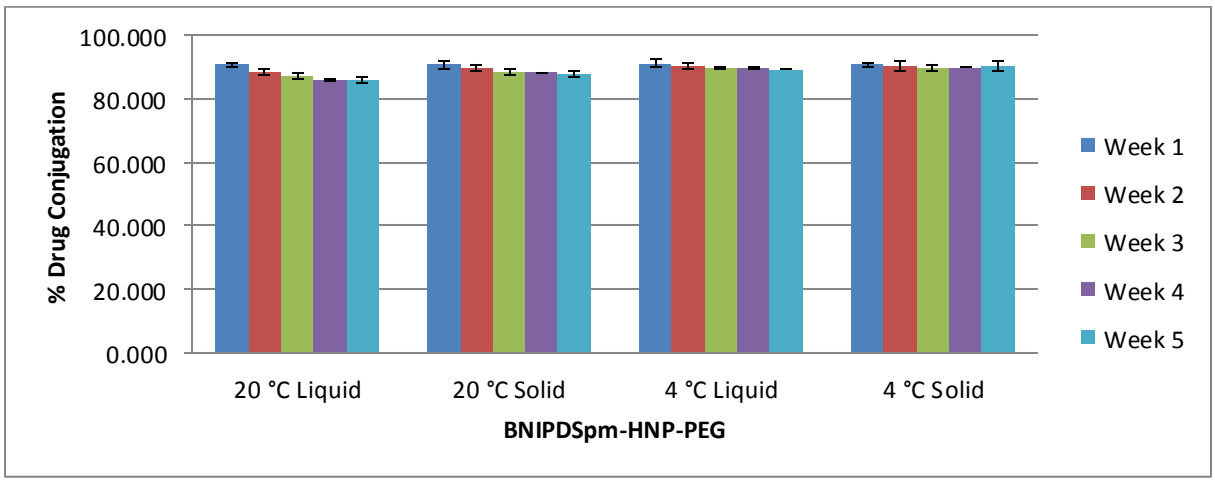

Figure 45: Stability test for BNIPDSpm-HNP-PEG at 20 °C and 4 °C in the form of dispersed in water and freeze dried, over the period of 5 weeks (n=3, ave ± SD).

Figures 44 and 45 demonstrated that formulation state and temperature are two important factors in the stability of HNP. The results were shown that solid state is more stable than liquid state it might be due to the presence of water in in aqueous formulations, which can raise the risk of drug release from the nano-carriers. Moreover decreasing temperature can increase the stability. In comparison between 20 °C and 4 °C, the test result illustrated the new formulations were more stable in 4 °C than 20 °C. Infact, reducing temperature leads to less drug detachment and protects the integrity of the electrostatic bonds and due to the stronger electrostatic binding on the HNP surface**.** Consequently, the new formulations were completely stable in 4 °C and solid state. According to Figures 44 and 45, the test results demonstrated better result for BNIPDSpm-HNP-PEG than BNIPDSpm-HNP. BNIPDSpm-HNP-PEG was reduced lower % drug conjugation during 5 weeks than BNIPDSpm-HNP. The drug stability for BNIPDSpm-HNP was around 80% - 88% and the stability for BNIPDSpm-HNP-PEG was slightly more and around 87 % - 90 %.

***In vitro* drug release study**

The release of the drugs from the optimal formulations were investigated in aqueous environment and culturing media at various temperatures and pH via HPLC. A calibration of the free drug dissolved in DMSO/H_2O (50:50) (R^2 = 0.999) were carried in deionised water (Figures 46). The peak areas for various samples were compared to calibration. All samples were carried out for three times.

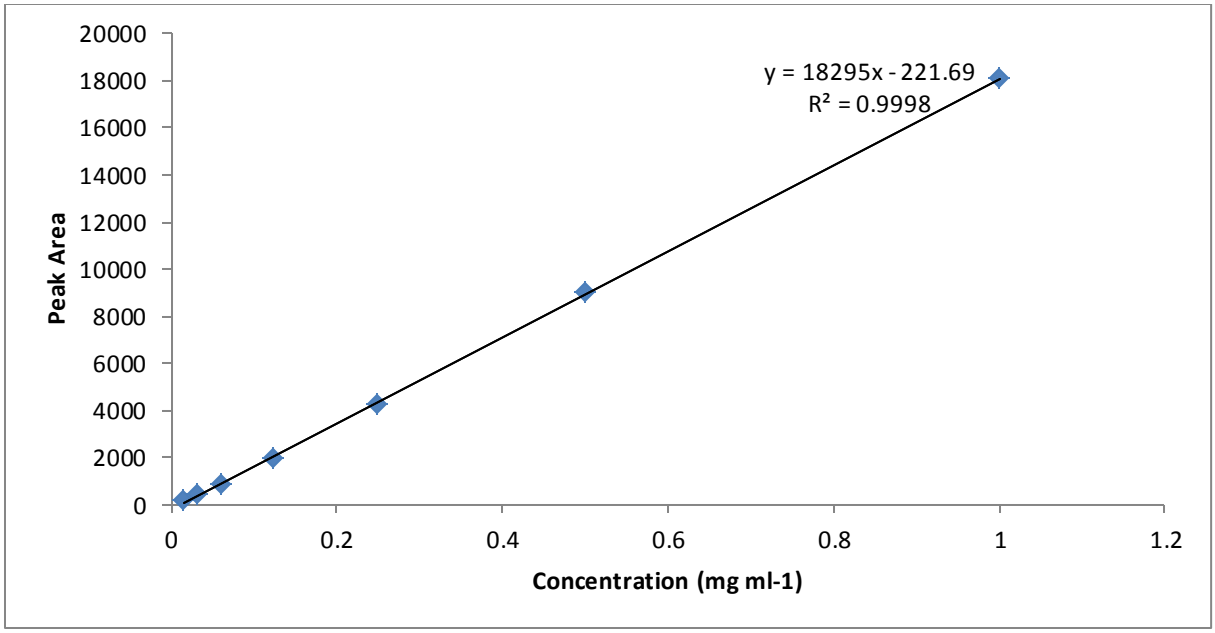

Figure 46: Calibration graphs of BNIPDSpm for drug release in deionised water.

***In vitro* drug release study in aqueous environments in various temperatures**

BNIPDSpm-HNP and BNIPDSpm-HNP-PEG were assessed in terms of the amount of drug release in 20 ˚C, 37 ˚C, 44 ˚C, 50 ˚C and 60 ˚C in deionised water (Figures 47A and 47B) ($p > 0.05$). BNIPDSpm release for both formulations measured over 72 h showed a biphasic release profile due to an initial burst, which is followed by a constant release. According to the HPLC results, drug release in first 4 h was greater that after 4 h. It can be due to 4 amine group in the drug and number of amine groups which can conjugate on HNP surface.

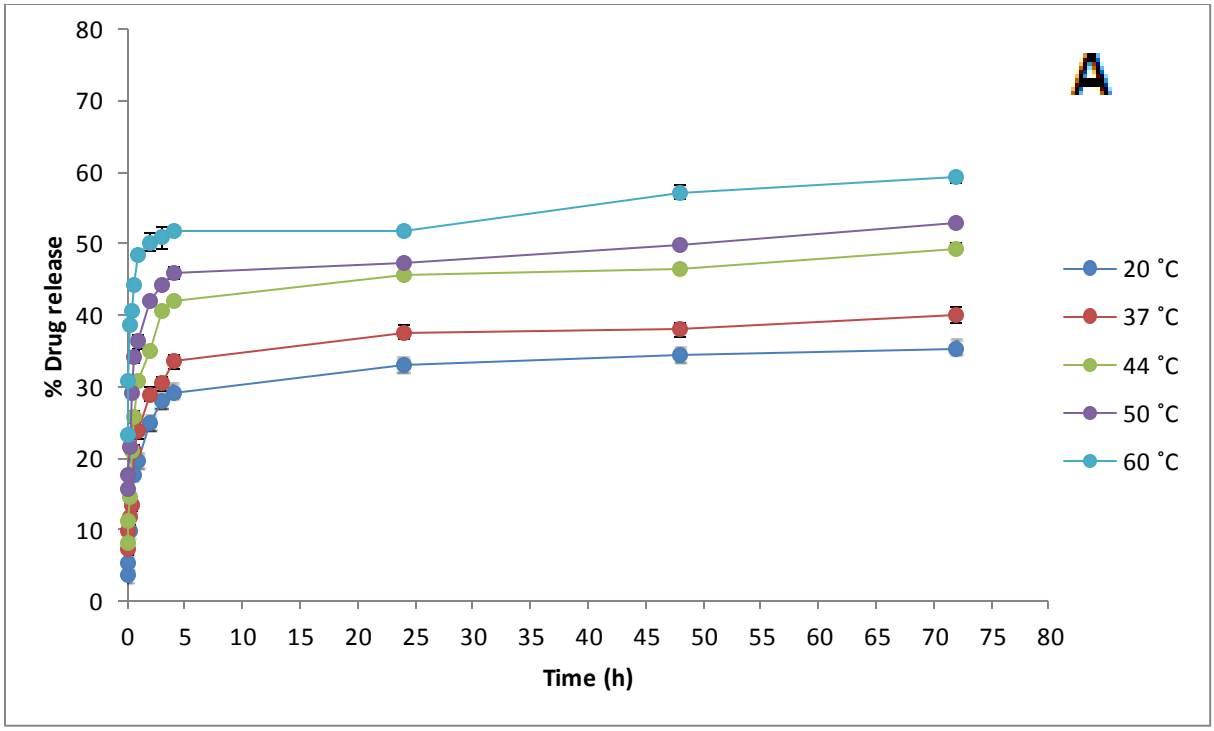

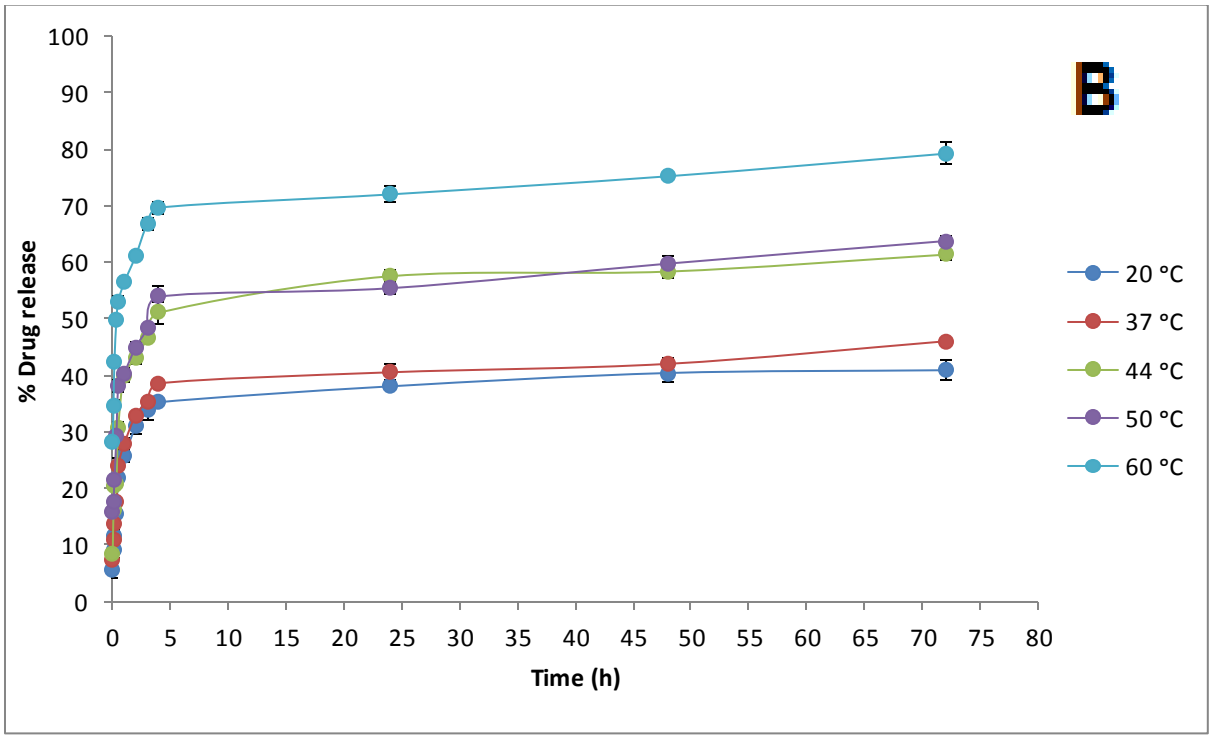

Figure 47: Drug release study of A) BNIPDSpm-HNP and B) BNIPDSpm-HNP-PEG in 20 ˚C, 37 ˚C, 44 ˚C, 50 ˚C and 60 ˚C in deionised water ($p < 0.05$). Experiments were performed three times, and data were expressed as mean ± standard errors (n=3, ave ± SD).

In 20˚C the drug was released 9.69 % ± 0.12 in the first 10 minutes for BNIPDSpm-HNP and also 11.73% ± 0.92 in first 10 minutes for BNIPDSpm-HNP-PEG. The drug releasing was increased sharply over 3 h and then slightly increased over 72 h. At 72 h, the drug was released 35.41% ± 0.95 in 20˚C for BNIPDSpm-HNP and also 40.91% ± 1.65 in 20˚C for BNIPDSpm-HNP-PEG. This low drug release over 72 h could be due to the strong electrostatic interactions between the drug and particles, as BNIPDSpm have four amines groups within its structure. However the drug releasing result for BNIPDSpm-HNP-PEG was better than BNIPDSpm-HNP in all temperatures. In the absence of PEG, BNIPDSpm and HNP might have stronger interactions as flattened at the surface of the particles because of the abundance of free space. In the presence of PEG, drug might have challenge with the polymer for the particles surface.

The graphs demonstrated that increasing temperature will increase drug realising. In this case in 60 ˚C, the drug was released 59.22% ± 0.66 over 72 h for BNIPDSpm-HNP and also 78.31% ± 0.91 for BNIPDSpm-HNP-PEG over 72 h for.

***In vitro* drug release study in aqueous environments in various pH.**

The drug release was assessed for BNIPDSpm-HNP and BNIPDSpm-HNP-PEG in 20 ˚C, 37 ˚C, 44 ˚C, 50 ˚C and 60 ˚C at pH=4.6 and pH=3.6 in deionised water (Figures 48 and 49).

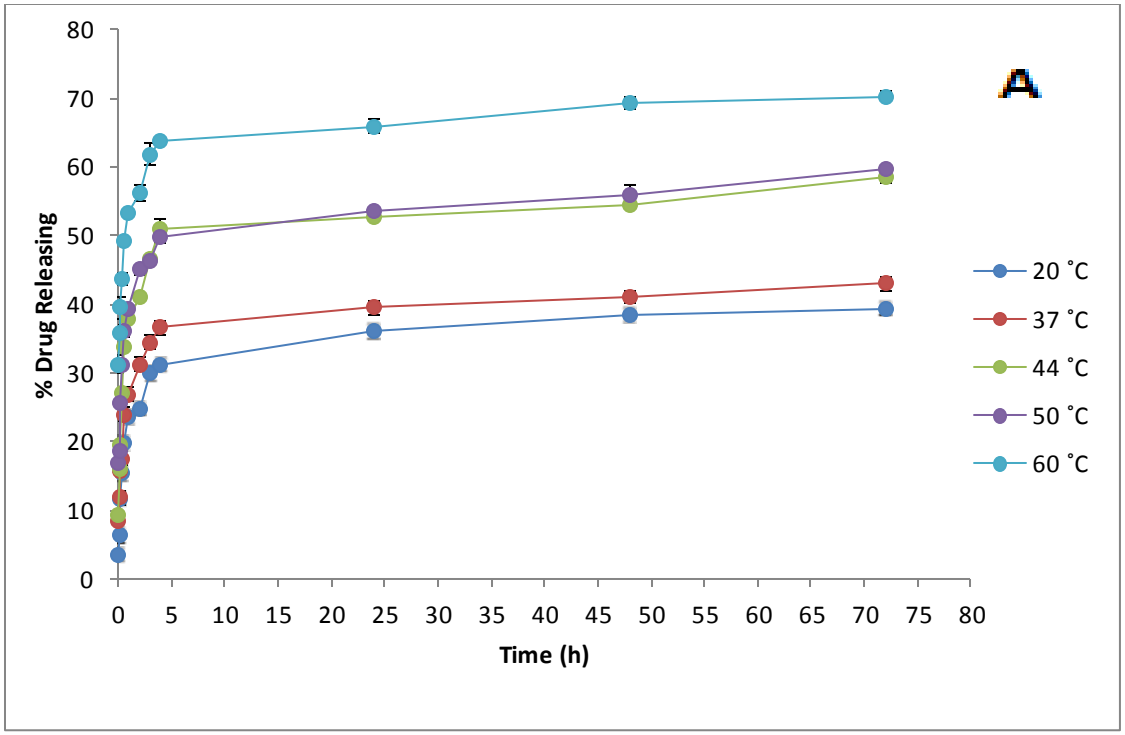

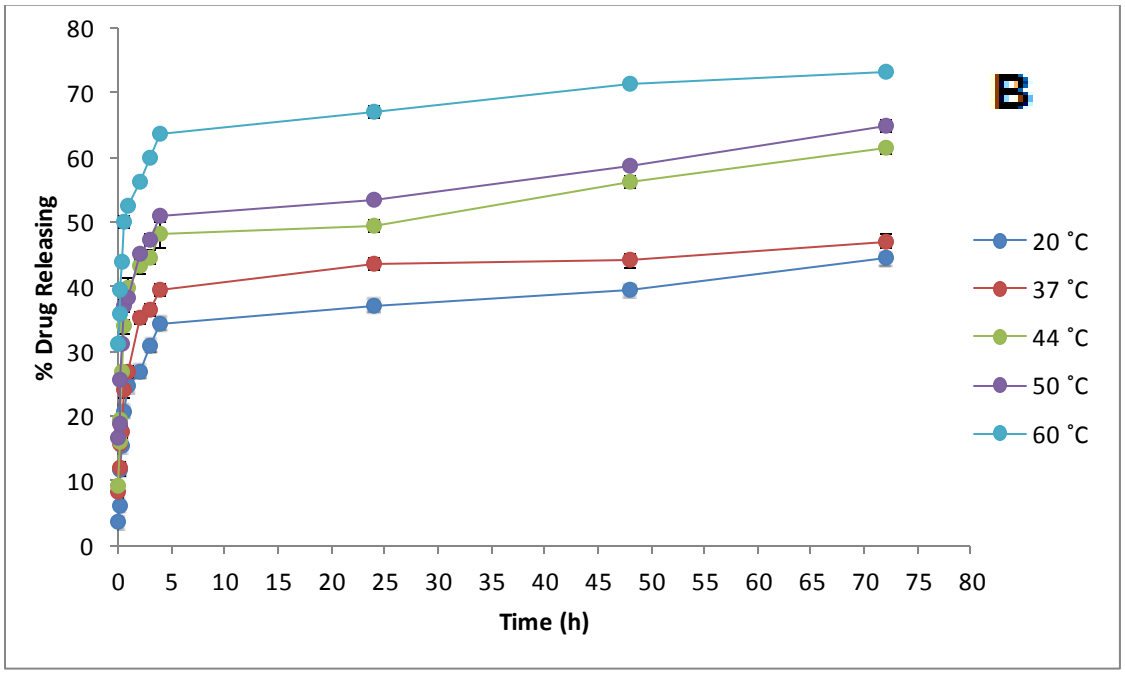

Figure 48: Drug release study of A) BNIPDSpm-HNP and B) BNIPDSpm-HNP-PEG in 20 ˚C, 30 ˚C, 40 ˚C, 50 ˚C and 60 ˚C at pH=4.6 ($p < 0.05$). Experiments were performed three times, and data were expressed as mean ± standard errors (n=3, ave ± SD).

According to Figure 48 the drug release were compared between BNIPDSpm-HNP and BNIPDSpm-HNP-PEG PEG in 20 ˚C, 30 ˚C, 40 ˚C, 50 ˚C and 60 ˚C at pH=4.6 ($p < 0.05$). The graphs demonstrated that the drug releasing were increased in pH=4.6 in compare the previous data's. Also the drug release results for BNIPDSpm-HNP-PEG was more than BNIPDSpm-HNP in same situation.

The drug release for BNIPDSpm-HNP and BNIPDSpm-HNP-PEG in 20 ˚C, 37 ˚C, 44 ˚C, 50 ˚C and 60 ˚C at pH=3.6 were as below graphs as well (Figure 49).

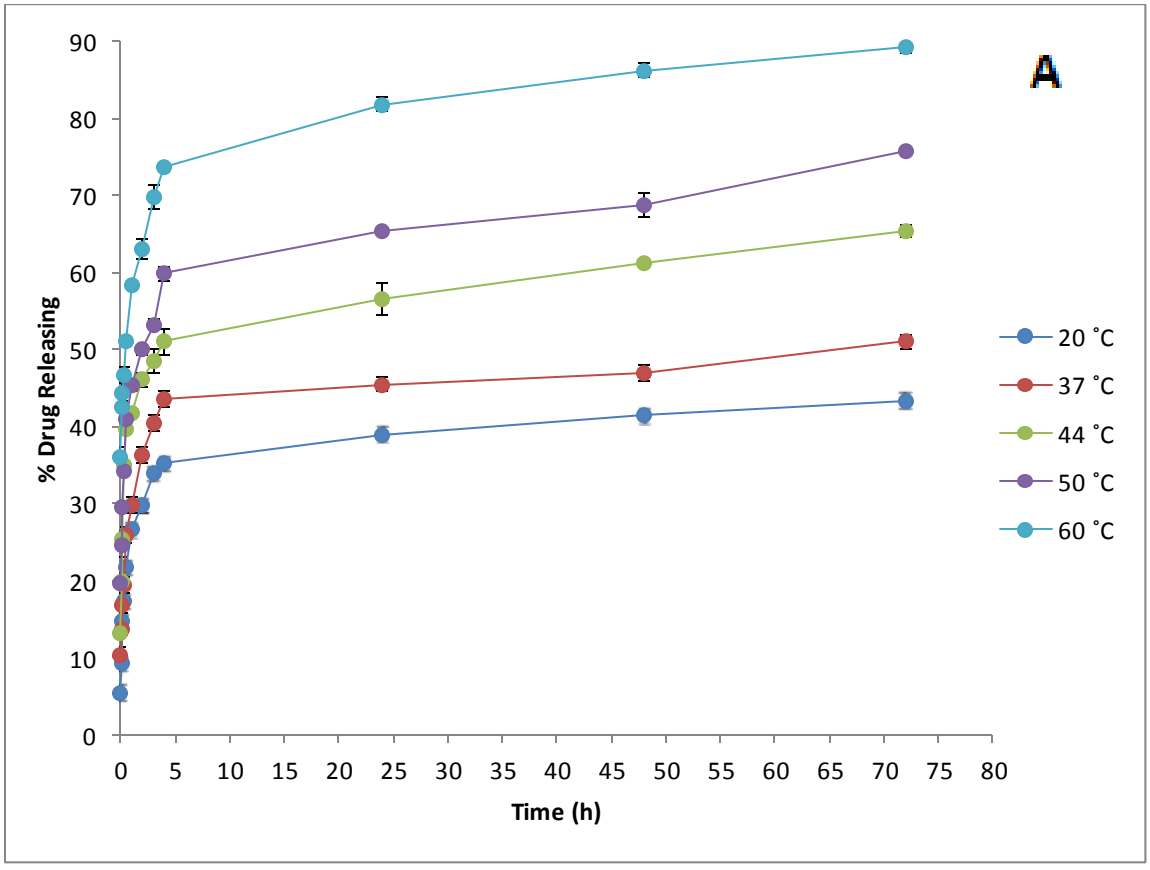

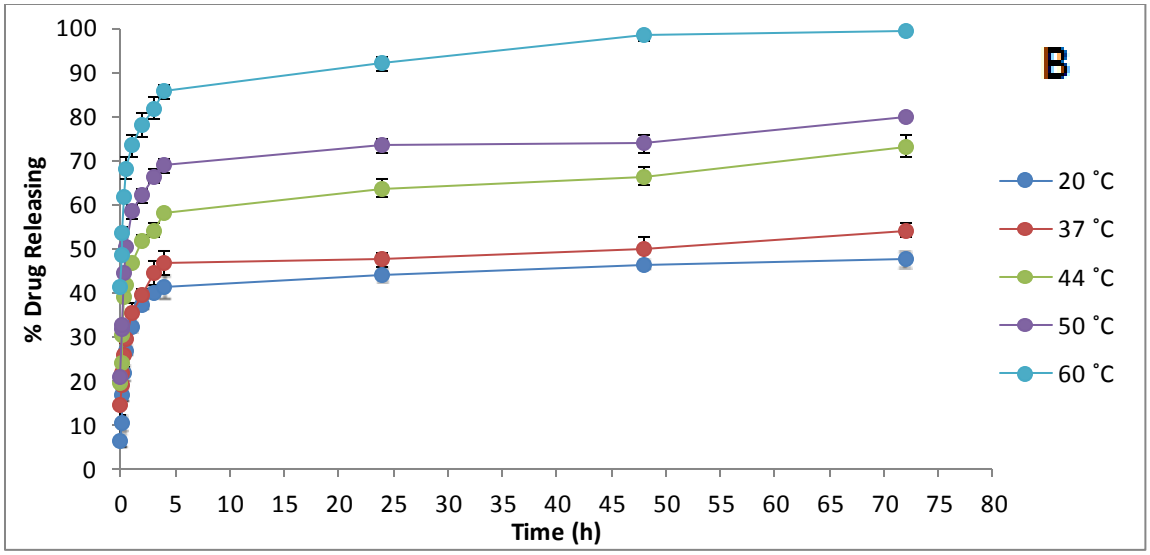

Figure 49: Drug release study of A) BNIPDSpm-HNP and B) BNIPDSpm-HNP-PEG in 20 ˚C, 30 ˚C, 40 ˚C, 50 ˚C and 60 ˚C at pH=3.6 ($p < 0.05$). Experiments were performed three times, and data were expressed as mean ± standard errors (n=3, ave ± SD).

The graphs demonstrated that the drug release rate of BNIPDSpm from PEGylayed formulation is significantly higher than the release from unPEGylated formulation ($p < 0.05$). Moreover reducing pH considerably increased the release rate of drug from both formulations as electrostatic interactions can be broken faster in lower pH ($p < 0.05$). The data's were shown that in first 4h the drug release rate were significantly higher than after that. In BNIPDSpm-HNP-PEG the drug completely released after 75 h at 60 ^{O}C and drug release was higher than lower temperatures ($p <0.05$).

As we discussed in chapter 2 (achieved by laser irradiation), we assessed the drug release in different pH and temperatures. The results demonstrated that release of BNIPDSpm from the particles in 44 ˚C was greater/faster at lower pH and PEGylated formulation always possessed more release compared to the unPEGylated formulation. In pH=3.6 almost 73% ± 1.22 of the drug was released after 75 h. By considering these data we suggest that when

the BNIPDSpm-HNP-PEG particles cross the pancreatic cancer cell membrane and accumulate inside the lysosome (pH=3.6), at 44 ˚C (achieved by laser irradiation), about 46.72 %± 0.97 of drug will be released in the first 1 h ($p < 0.05$). BNIPDSpm drug release pattern was investigated at 44 ^{O}C, as this is the optimum temperature generated by HNPs upon the laser irradiation, described in Chapter Two (Section 2.3.5).

***In vitro* drug release in biological media**

The drug release were analysed in in culture media at pH= 7.5, pH=4.6 and pH=3.6 at 20 ˚C, 37 ˚C and 44 ˚C and 50 ˚C up to 312 h to mimic cytoplasm (pHi =7.42), endosome and lysosome environment in pancreatic cancer cells, respectively (Preissler and Williams, 1981) as below graphs. A calibration of the free drug dissolved in DMSO/H_2O (50:50) (R^2 = 0.999) were carried in RPMI (Figures 50). The peak areas for various samples were compared to calibration. All samples were carried out for three times.

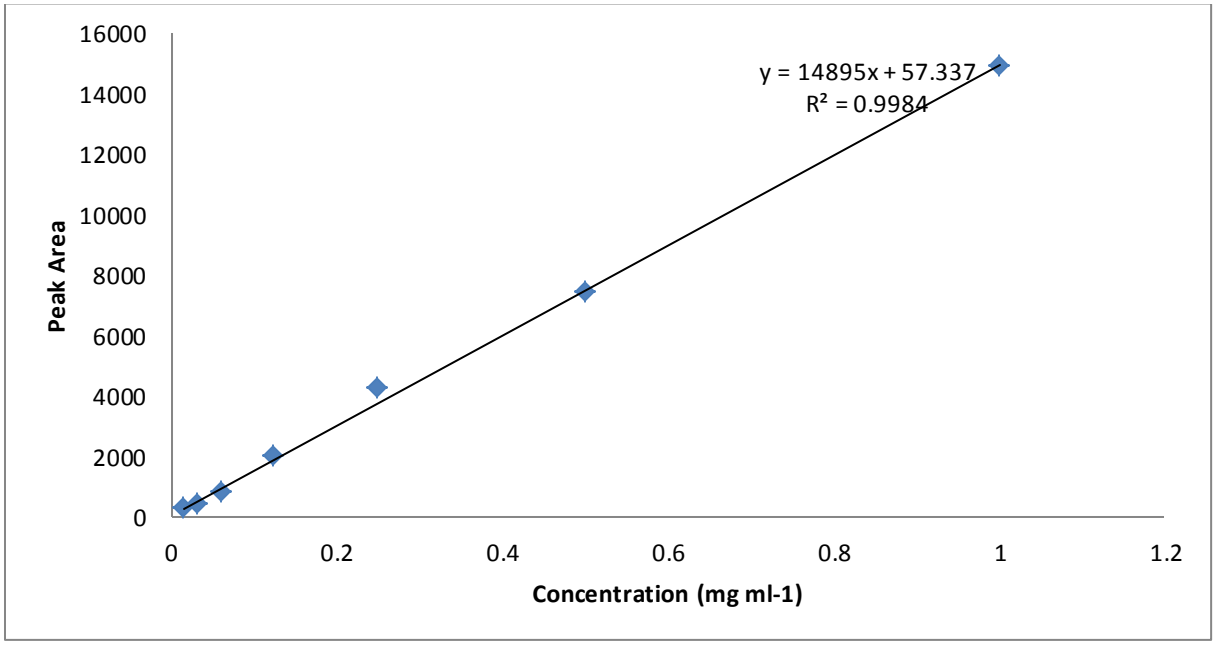

Figure 50: Calibration graphs of BNIPDSpm for drug release in RPMI

According to Figure 51, in 20 ˚C, 30-40 % of release from BNIPSDpm-HNP and BNIPDSpm-HNP-PEG respectively occurred in pH=3.6, 4.6 and 7.5 before 4 h.

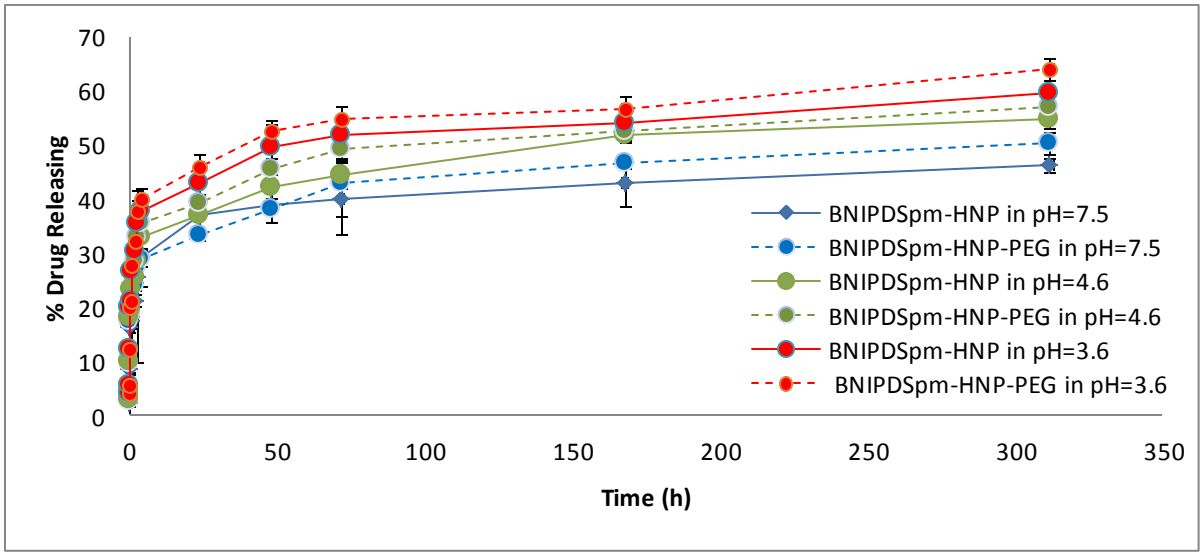

Figure 51: Drug release BNIPDSpm-HNP and BNIPDSpm-HNP-PEG in 20˚C at pH=7.5, pH=4.6 and pH=3.6 ($p < 0.05$). Experiments were performed three times, and data were expressed as mean ± standard errors (n=3, ave ± SD).

The drug release was increased with decreasing pH because the lower pH was broken the electrostatic interactions in NPs and can separate the drug from NPs amine groups. Moreover the drug release in formulation with PEG was higher rate in compare with the formulation without PEG as surface charge results demonstrated that BNIPDSpm-HNP-PEG has lower surface charge so the electrostatic interactions can break easier in compare with BNIPSDpm-HNP.

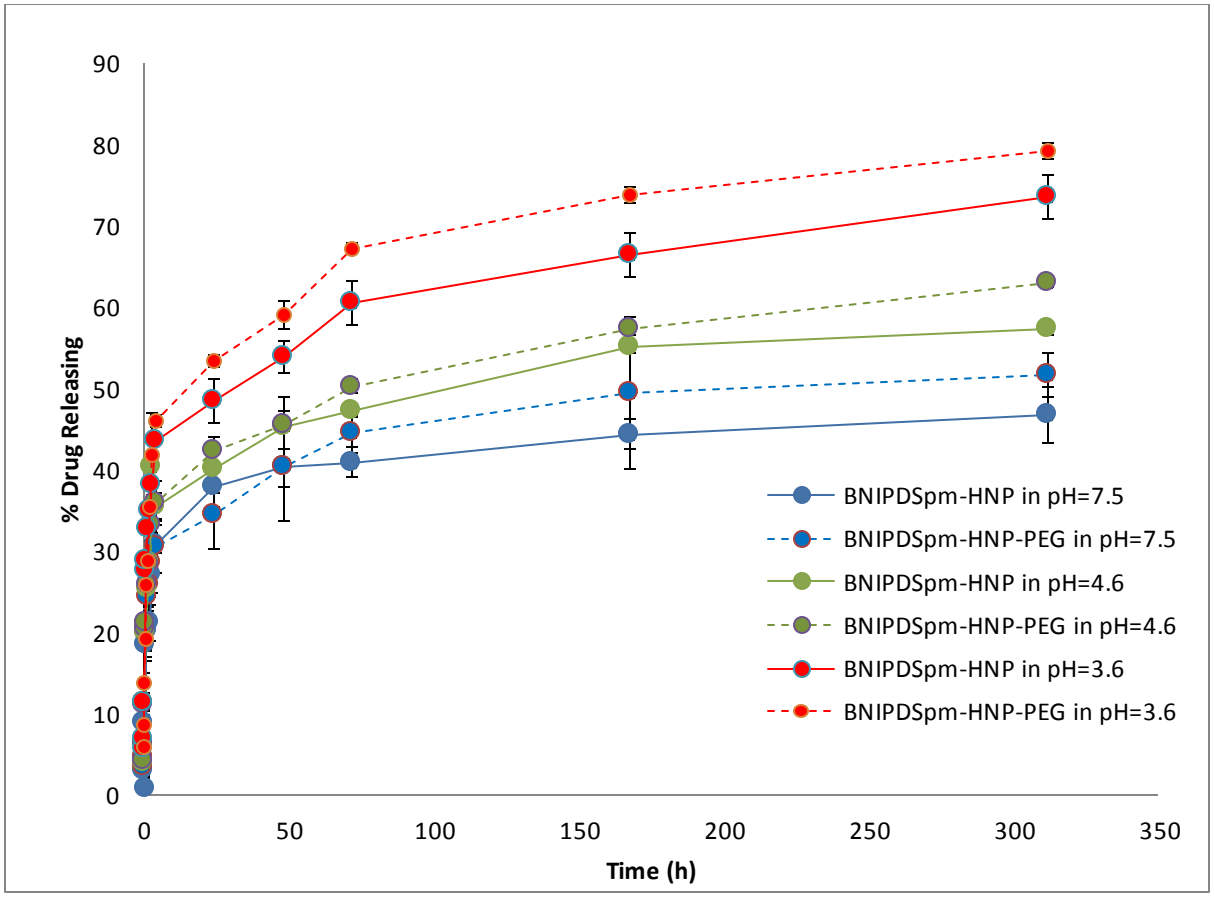

Figure 52: Drug release BNIPDSpm-HNP and BNIPDSpm-HNP-PEG in 37˚C at pH=7.5, pH=4.6 and pH=3.6 ($p < 0.05$). Experiments were performed three times, and data were expressed as mean ± standard errors (n=3, ave ± SD).

In 37 ˚C more drug release was occurred in compare with 20 ˚C. BNIPDSpm-HNP-PEG at pH=3.6 had highest rate of drug releasing. In this pH 20% ± 2.05 of drug release was occurred in first 0.5h and the drug release arrived to the 40% ± 0.715 in first 4 h. The drug release sharply increased in first 4 h and then the rate of increasing was slightly went up until 312h ($p<0.05$). The best drug release rate was for BNIPDSpm-HNP-PEG in pH=3.6. In this formulation 78% ± 1.92 of drug was release before 312 h.

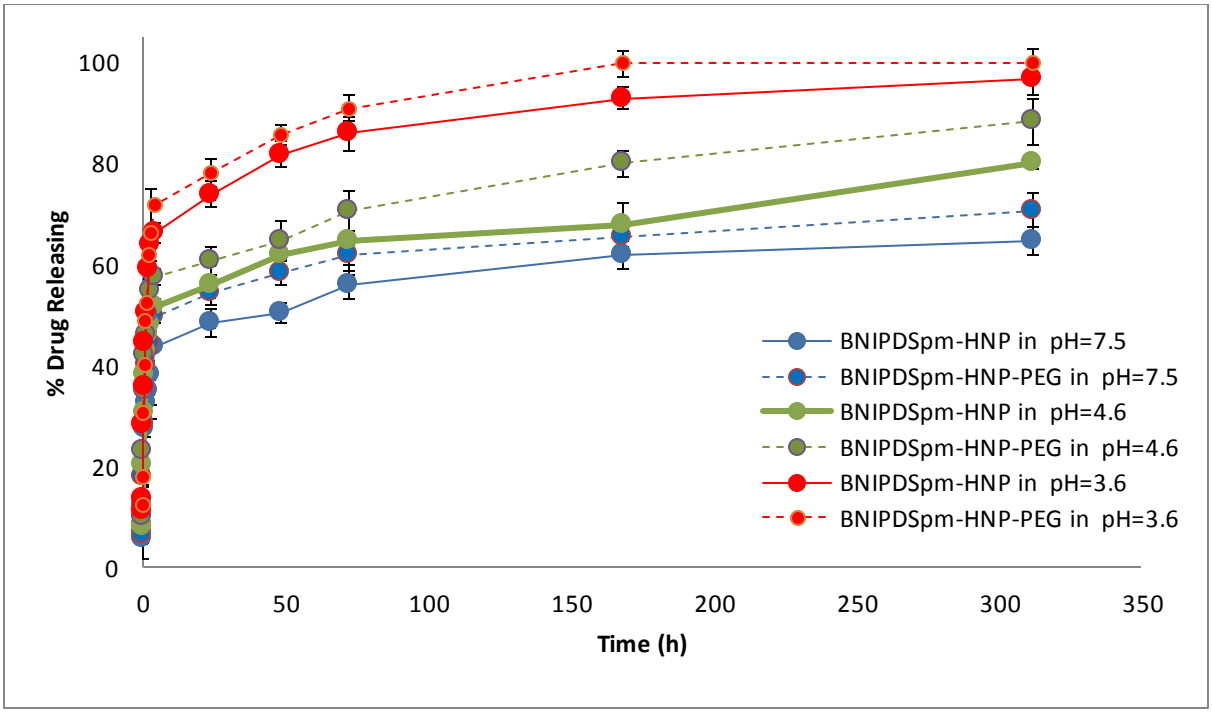

Figure 53: Drug release BNIPDSpm-HNP and BNIPDSpm-HNP-PEG in 44˚C at pH=7.5, pH=4.6 and pH=3.6 ($p < 0.05$). Experiments were performed three times, and data were expressed as mean ± standard errors (n=3, ave ± SD).

The same pattern was observed in 44 ˚C, and again the higher release occurred in lower pH (Figure 53). The release from PEGylated formulation was significantly higher than its unPEGylated counterpart ($p < 0.05$). In first 10 minutes 11.30% ± 1.72, 20.31% ± 3.74 and 25% ± 1.74 of drug release from unPEGylated in pH=7.5, pH= 4.6 and pH=3.6 respectively. In first 10 minutes 18.12% ± 1.90, 22.23% ± 1.71 and 30.26% ± 2.94 of drug release from PEGylated formulation in pH=7.5, pH= 4.6 and pH=3.6 respectively. Half of the drug (0.5 mg) released from BNIPSDpm-HNP-PEG in pH=7.5, pH= 4.6 and pH=3.6 in 3 h, 1 h and 0.5 h, while these amount of drug released from unPEGylated was in 4 h , 3 h and 2 h with the same pH mentioned above, respectively ($p < 0.05$). In 168h almost 100% of drug was release in BNIPDSpm-HNP-PEG in pH=3.6 (Figure 53).

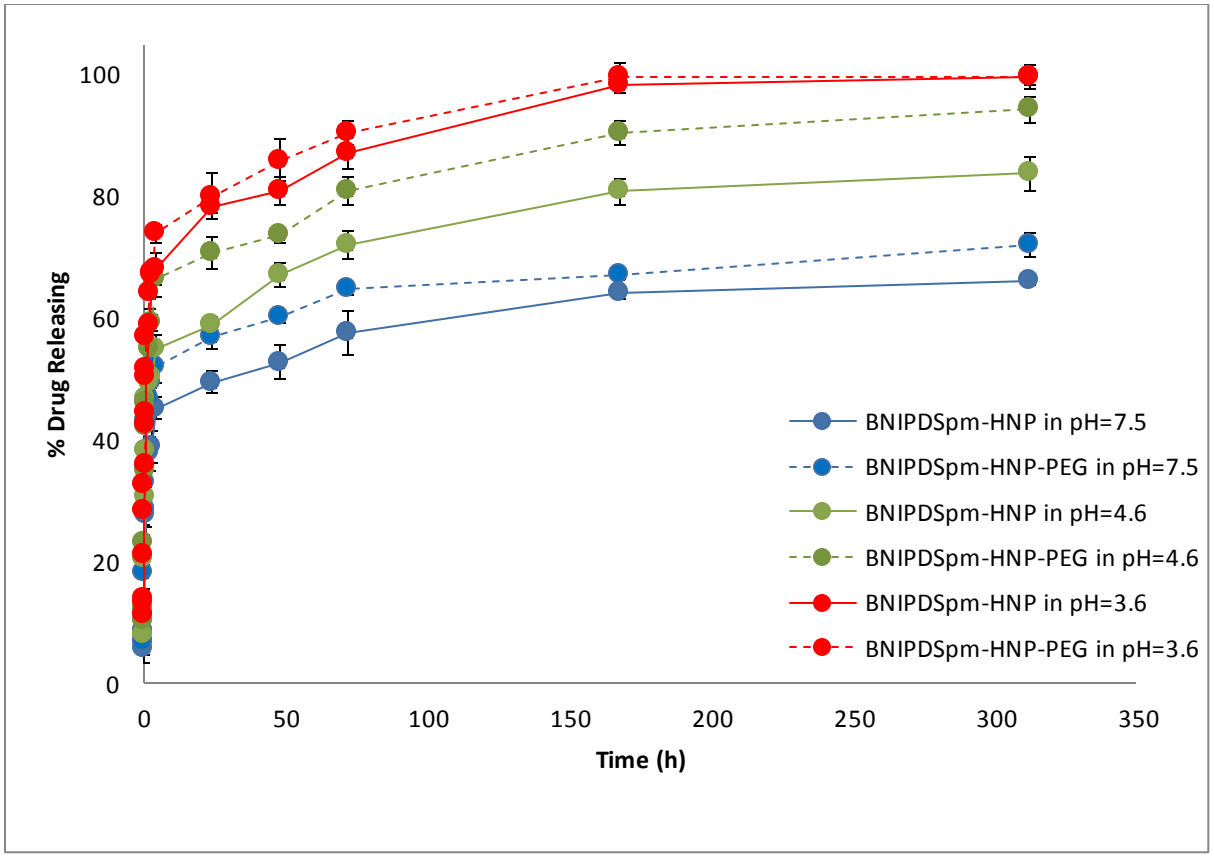

Figure 54: Drug release BNIPDSpm-HNP and BNIPDSpm-HNP-PEG in 50˚C at pH=7.5, pH=4.6 and pH=3.6 ($p < 0.05$). Experiments were performed three times, and data were expressed as mean ± standard errors (n=3, ave ± SD).

At 50 ˚C, 50 % release from BNIPSDpm-HNP in pH=7.5, pH=4.6 and pH=3.6 occurred in 3 h, 1 h and 0.5 h, while this amount of drug released from PEGylated formulations in 2 h , 0.5 h and 0.33 h with the same pH mentioned above, respectively (Figure 54). These data suggest that decreasing pH significantly enhanced the release rate of drug from both formulations ($p < 0.05$). Moreover, release rate of BNIPDSpm from PEGylayed formulation is higher than the release from unPEGylated formulation ($p < 0.05$) (Figure 54). After 168 h the drug completely released from both formulations at 50 ^{o}C in pH=3.6.

Stability of HNPs in physiological conditions

The ICP results represented the chemical stability of HNP and HNP-PEG at pH=7.5, pH=4.6 (Figure 55).

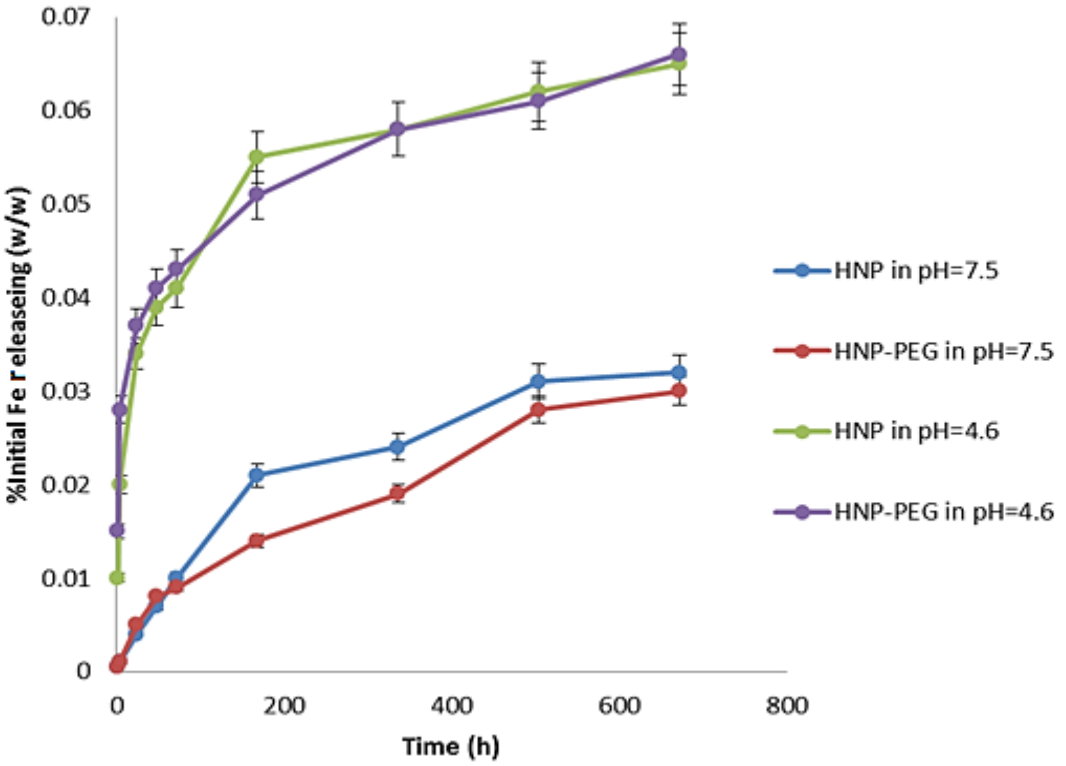

Figure 55: Physical stability of HNP (Fe) and HNP-PEG (Fe) at pH=7.5, pH=4.6 ($p < 0.05$). Experiments were performed three times, and data were expressed as mean ± standard errors (n=3, ave ± SD).

The results were compared with the initial amount of Fe weight at the first of experiment which was 100 $\mu g mL^{-1}$. At pH 7.2 a maximum of 0.032% ± 0.52 of the iron concentration was observed in the media for the HNP and 0.030% ± 1.35 of iron were released for HNP-PEG in same pH. The graph demonstrated that the results for HNP was slightly more than HNP-PEG as the matter of fact the HNP-PEG was more stable than HNP however the results was not significantly different ($p > 0.05$). At pH 4.6, particle degradation was bigger than pH 7.5

($p < 0.05$). At pH 4.6 an initial burst release of iron (0.034% ± 1.25) was observed in the first 24 h for HNP followed by a slow incline over the duration to a maximum of 0.065%± 1.37 and 0.066%± 0.77 for HNP and HNP- PEG respectively ($p > 0.05$). The increased degradation compared with at higher pH can be attributed to the iron core being slowly dissolved in acidic environments (Hoskins *et al*., 2012b).

3.4. Discussion

In previous studies, the ability of conjugation of different bisnaphthalamide based drugs onto their surface via electrostatic interactions or covalent bonds onto the surface of HNPs with gold nanoparticles were assessed and compared (Malekigorji *et al.,* 2017). In that research the conjugation ability of BNIDi, BNIPd, BNIPds and BNIPDSpm were compared together (Malekigorji *et al.,* 2017). According their test results by FTIR spectra the BNIDi could not be conjugated to the surface of HNPs (even with the highest loading concentration). BNIDi does not have amine group in the structure and amine group is very important and critical for making electrostatic interaction between the drug and HNPs (Malekigorji *et al.,* 2017). The BNIPd formulations were not stable and most of attached drug on the HNP were released easily in initial minutes. In fact, the low number of amine group made BNIPd formulation unsuitable for drug delivery system (Malekigorji *et al.,* 2017). On the other hands, due to the low release rate of BNIPds from formulations in different pH and temperatures, BNIPds could not be good option for conjugating the drug on HNP surface (Malekigorji *et al.,* 2017). Consequently the best drug loading, releasing and stability was BNIPDSpm-HNP due to the BNIPDSpm molecule possessing the greatest number of amine groups (four amines) compared with other drugs. The amine group is a crucial factor for electrostatic interaction to the surface of HNPs, as two central amines in

bisnaphthalmide chain seem to have more affinity to the gold surface (Malekigorji *et al.,* 2017).

In the other research Barnett and co-works proved that the thiol-containing pendant group can raise the connection of HNPs by dative covalent bonding (Barnett *et al.,* 2013b). The PEG-Thiol effects were assessed on delivery systems by Dreaden and colleagues and the test results confirmed that PEG-Thiol can circulate in the blood for a long time and can avoid the killing by mononuclear macrophages (Dreaden *et al.,* 2010). The Thiol-PEG also can encapsulate anticancer drug and control drug release (Maus *et al.,* 2010).

In first step, different ratio of HNP and the drug were mixed together and the solution was stirred for 3 h at room temperature (20 ^{o}C). After separating the solution and highly washing with deionised water for three times, the amount drug loading were assessed by HPLC. The results demonstrated that the ratio of 1: 10 HNP: BNIPDSpm had the highest level of drug loading which was 90.88%± 1.03. In fact, 1mg.mL^{-1} HNP (Fe) was conjugated 9 mg.mL^{-1} of the drug in optimum ratio. In next step, various ratios of powdered polymer (based on the concentration used in the literature for PEG-thiol) were added with the solution respectively. The particles were washed after 3 h as previously described. It was assumed that PEG will coat the surface of HNPs completely if it was added before the drug, thus no free surface would be available for the drug attachment (Barnett *et al.,* 2013a; Barnett *et al.*, 2013b). The percentage of drug conjugation was 94.21%± 0.83 which mean 1mg.mL^{-1} HNP (Fe) was conjugated 9.42 mg.mL^{-1} of the drug in optimum ratio (1:10:10 HNP:BNIPDSpm:PEG-Thiol) (Table 9).

HNP possess a negative surface charge (-3.05 ± 0.29 mV) before conjugating with the drug. BNIPDSpm have 4 amine groups so the surface charge were shifted to positive (+32.51 ±

0.35 mV) when the drug were conjugated to the HNP. The previous researches demonstrated that the presence of amine groups increased the surface charge of the particles (Kardys *et al.,* 2013). The surface charge for BNIPDSpm-HNP-PEG was positive but lower than BNIPDSpm-HNP (+18.77 ± 0.41 mV), indicating further modification of PEG. This could be due to PEG chains shielding surface charge of silver coating. The decrease of zeta potential confirms also the binding of thiol groups on silver surface. Thiol group and PEG shifted the zeta potential toward negative values (Ku *et al.,* 2010).

FTIR were carried out for HNP, BNIPDSpm-HNP and BNIPDSpm-HNP-PEG to approve the conjugation of drugs onto the HNPs. The presences of peaks for C-H (3442 cm^{-1}), N-H stretching (2930 cm^{-1}) and N-H bending (1651 cm^{-1}) proved the presence of PEI in HNP. The FTIR Bands demonstrated the presence of aromatic in-plane C-H bending, aromatic C=C stretching, C=O (Stretching) bands and C-H (Stretching) which presented the existence of BNIPDSpm-HNP and BNIPDSpm-HNP-PEG respectively. On the other hands, bigger peak observed at 1341 cm^{-1} (C–H bending; $-CH_2$ and $-CH_3$) confirm the presence of bound PEG within BNIPDSpm -HNP- PEG formulation (Figures 43 A and 43 B).

HPLC results were shown that formulation state and temperature are two important factors in the stability of HNP. The results were shown that solid state is more stable than liquid state it might be due to the presence of water in in aqueous formulations, which can raise the risk of drug release from the nano-carriers. Moreover decreasing temperature can increase the stability. In comparison between 20 °C and 4 °C, the test result illustrated the new formulations were more stable in 4 °C than 20 °C. Infect, reducing temperature leads to less drug detachment and protects the integrity of the electrostatic bonds and presumably due to the stronger electrostatic binding on the HNP surface.

After finding amount of drug loading by HNPs and HNPs-PEG-Thiol, the amount of drug release were assessed as well. The method followed previous reports revealed linear correlation model between *In vitro* drug release in water and *in vivo* absorption (Bose and Wui, 2013; Cardot *et al.,* 2007). Barnett *et al.* were placed the HNP in dialysis membrane and the volume of dialysis fluid was in excess to mimic the 'sink' conditions experienced after injection into the blood stream (Barnett *et al.,* 2013a). Drug release study for formulations was achieved at different temperatures (37 ˚C, 44 ˚C, 50 ˚C & 60 ˚C) in deionised water and RPMI. This test was carried out to mimic the temperature change upon the laser irradiation. Jelveh and Chithrani used this method to check the release of drug from gold NPs after laser irradiation (Jelveh and Chithrani, 2011). The drug releasing were carried out in pH=4.6 and pH=3.6 in deionised water and PRMI to simulate endosome and lysosome environment as well. In this case the pH was adjusted by using concentrated hydrochloric acid (20 M).

BNIPDSpm-HNP and BNIPDSpm-HNP-PEG were assessed in terms of the amount of drug release in 20 ˚C, 37 ˚C, 44 ˚C, 50 ˚C and 60 ˚C (Figures 47A and 47B) ($p < 0.05$). BNIPDSpm release for both formulations measured over 72 h showed a biphasic release profile due to an initial burst, which is followed by a constant release. In 20 ˚C the drug was released 9.69% ± 0.12 in first 10 minutes for BNIPDSpm-HNP and also 11.73% ± 0.92 in first 10 minutes for BNIPDSpm-HNP-PEG. The drug releasing was increased sharply over 3 h for all temperatures and then slightly increased over 72 h. This low drug release over 72h could be due to the strong electrostatic interactions between the drug and particles, as BNIPDSpm have four amines groups within its structure. However the drug releasing result for BNIPDSpm-HNP-PEG was better than BNIPDSpm-HNP in all temperatures. In the absence of

PEG, BNIPDSpm and HNP might have stronger interactions as flattened at the surface of the particles because of the abundance of free space. In the presence of PEG, drug might have challenge with the polymer for the particles surface.

The graphs demonstrated that increasing temperature will increase drug realising. In this case in 60 ˚C, the drug was released 59.22% ± 0.66 over 72 h for BNIPDSpm-HNP and also 78.31% ± 0.91 for BNIPDSpm-HNP-PEG over 72 h. Moreover reducing pH considerably increased the release rate of drug from both formulations as electrostatic interactions can be broken faster in lower pH ($p < 0.05$). In fact, lower pH was broken the electrostatic interactions in NPs and can separate the drug from NPs amine groups. The data's were shown that in first 4 h the drug release rate were significantly higher than after that ($p <0.05$).

The drug release were analysed in in culture media at pH= 7.5, pH=4.6 and pH=3.6 at 20 ˚C, 37 ˚C and 44 ˚C and 50 ˚C up to 312 h to mimic cytoplasm (pH =7.42), endosome and lysosome environment in pancreatic cancer cells, respectively. The drug release was increased with increasing temperature and decreasing pH because the electrostatic interactions in NPs were broken and can separate the drug from NPs amine groups. Moreover, drug release in BNIPDSpm-HNP-PEG was significantly higher than BNIPDSpm-HNP in culture media.

As we discussed in chapter 2 (achieved by laser irradiation), we assessed the drug release in different pH in 44 ˚C and 37 ˚C. In this case, the release pattern of the formulations inside the pancreatic cancer cells, before and after laser irradiation can be predicted. In body temperature, 64% ± 1.92 of drug was release for BNIPDSpm-HNP-PEG at pH=3.6 before 312 h. Moreover, in 44 ^{O}C, 100% of drug was release in BNIPDSpm-HNP-PEG at pH=3.6 after

168 h ($p < 0.05$). Therefore, it is assumed that after accumulation of the NPs in endosome and lysosome, the low environmental pH and increasing the temperature through laser irradiation, will result in quick drug release from the particles. Then the free drug can enter cells` nucleus and interact with DNA for anticancer effect.

In cancer therapy, many drugs such as small molecule chemotherapeutic agents, siRNA, DNA and proteins have to be delivered by a carrier and released into the particular cellular compartments, which is usually cytoplasm or nucleus of cancer cells. Intracellular environment-responsive NPs, which possess high extracellular stability while rapidly releasing their cargo inside cancer cells have been enormously investigated for improving cancer therapy (Park *et al.,* 2006). The HNP and HNP-PEG physical stability was assessed in cell culture media during 4 weeks at pH=7.2 and pH=4.6. At pH 7.2 a maximum of 0.032% ± 0.52 of the iron concentration was observed in the media for the HNP and 0.030% ± 1.35 of Iron were released for HNP-PEG in same situation. The graph demonstrated that the results for HNP was slightly more than HNP-PEG as the matter of fact the HNP-PEG was more stable than HNP however the results was not significantly different ($p > 0.05$). At pH 4.6, particle degradation was bigger than pH 7.2 ($p < 0.05$). At pH 4.6 an initial burst release of iron (0.034% ± 1.25) was observed in the first 24 h for HNP followed by a slow incline over the duration to a maximum of 0.065%± 1.37 and 0.066%± 0.77 for HNP and HNP- PEG respectively.

3.5. Conclusion

BNIPDSpm was loaded on the HNP surface with high rate in optimum ratio. The drug loading were assessed and confirmed by FTIR and also changing surface charges in HNP, HNP-BNIPDSpm and HNP-BNIPDSpm-PEG. The HPLC and ICP demonstrated that HNP and HNP-

PEG have high physical and formulation stabilities. Drug release study of BNIPDSpm formulations demonstrated that quicker release was occured by increasing the temperature and reducing the pH in water and culture media (close to the pH of intracellular organelles). Moreover, PEGylated formulations mostly revealed greater release of drug in comparison with their unPEGylated counterparts.

Chapter Four

Drug loading and release from linker targeted formulation

4.1. Introduction

Arginine-glycine-aspartic acid (RGD) peptides

Targeting drugs to tumour cells is a significant way to improve existing cancer therapies. Directing therapeutic agents like such as toxins, viruses for gene therapy, enzymes for prodrug therapy chemo- or radiotherapeutic drugs can increase the ability of anticancer drugs and to reduce side effects (DeNardo, 1998). In the 1970s, it was reported that arginine–glycine–aspartic acid (RGD) tripeptide could be used cell recognition molecule and adhesion ligand for targeting (Ruoslahti and Pierschbacher, 1987).

RGD peptides ares integrin antagonist whichlinks to integrin αvβ3, which plays a significant role in tumour angiogenesis (Wang *et al.,* 2013; Chakravarty *et al.,* 2015; Cai and Conti, 2013). Integrin αvβ3, is a receptor for the extracellular matrix proteins with the exposed RGD tripeptide sequence. Integrin αvβ3 receptor has been reported on several types of cancer cells, including pancreatic cancer and plays an important role in tumour growth and metastasis (Hwang and Varner, 2004). The cell adhesion molecule, integrin αvβ3, is highly prevalent in tumour cells and much less prevalent on normal healthy tissue (Wu *et al.,* 2005). The ability to target the integrin αvβ3 receptor on cancer cells increases the efficacy of targeted therapy and reduces the side effects (Xiong *et al.,* 2006). RGD and RGD derivatives have been extensively used in studies of adhesion, cell migration, apoptosis and growth by RGD-integrin interactions (Hwang and Varner, 2004).

RGD analogues are used in antiangiogenics approaches (Haubner *et al.,* 2001) in tumour targeting with radio nucleotides (Hagen *et al.,* 2000), in tumour imaging (Pasqualini *et al.,* 2000) and or chemotherapeutic drugs (Arap *et al.,* 1998). Subsequently, RGD and different

cyclic RGD (cRGDfK, cRGDyK, cRGDfC and iRGD) (Figure 56) have been developed and significantly studied (Sheldrake and Patterson, 2009), (Mas-Moruno *et al*., 2010), (Paolillo *et al.,* 2009) and (Auzzas *et al.,* 2010).

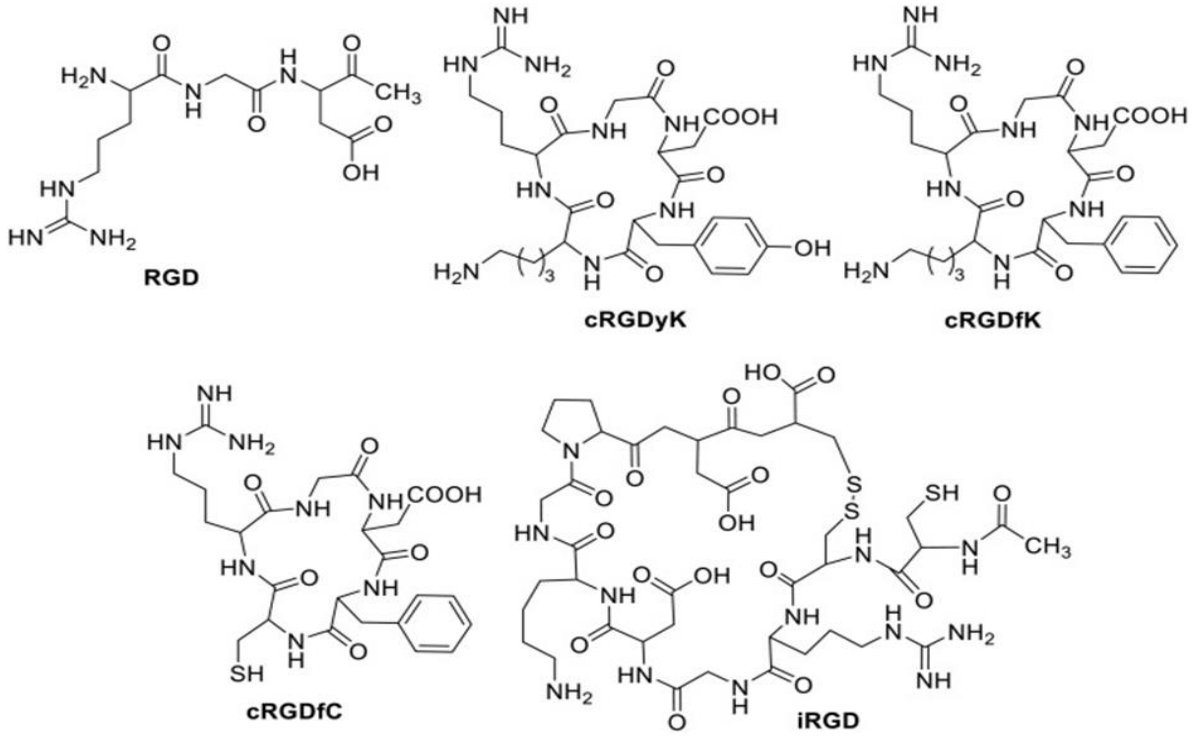

Figure 56: Schematic representation of the most commonly employed RGD peptide sequences (Cheng and Yuanhui, 2018).

In comparing linear RGD and cyclic RGD, The cyclic RGD has been shown to be more selective and stabile than linear RGD and has been widely used to increase binding to certain integrin (e.g. αvβ3). iRGD can undertake as both a cell penetrating peptide and an integrin-homing peptide to improve the drug delivery to the tumour microenvironment and increase tumour penetration (Duro-Castano *et al.,* 2017). In recent years, RGD-modified polymers, liposomes and other nano vehicles have been used for cancer therapy including photodynamic therapy, gene therapy, combination therapy, photo thermal therapy and chemotherapy. Many studies have been carried out to use RGD-modified nano-vehicles for

transporting drugs. In comparison with efficiency of monotherapy, the mixture of multiple treatments helps more overcome drug resistance through different mechanisms (Mas-Moruno *et al.,* 2010).

Cyclo (Arg–Gly–Asp–D-Phe–Cys) (c(RGDfC)) is the cyclic RGD peptide which can inhibite αvβ3 integrin. c(RGDfC) functionalised with an aminooxy functionality via a suitable linkage (Xiang-Guo *et al.,* 2012). The c(RGDfc) peptide was made by solid phase synthesis and functionalised by aminooxy conjugation with various sugars include D-ribose, 2-FDG, 6-FDG and D-Glucose under acid conditions (Figure 57) (Xiang-Guo *et al.,* 2012).

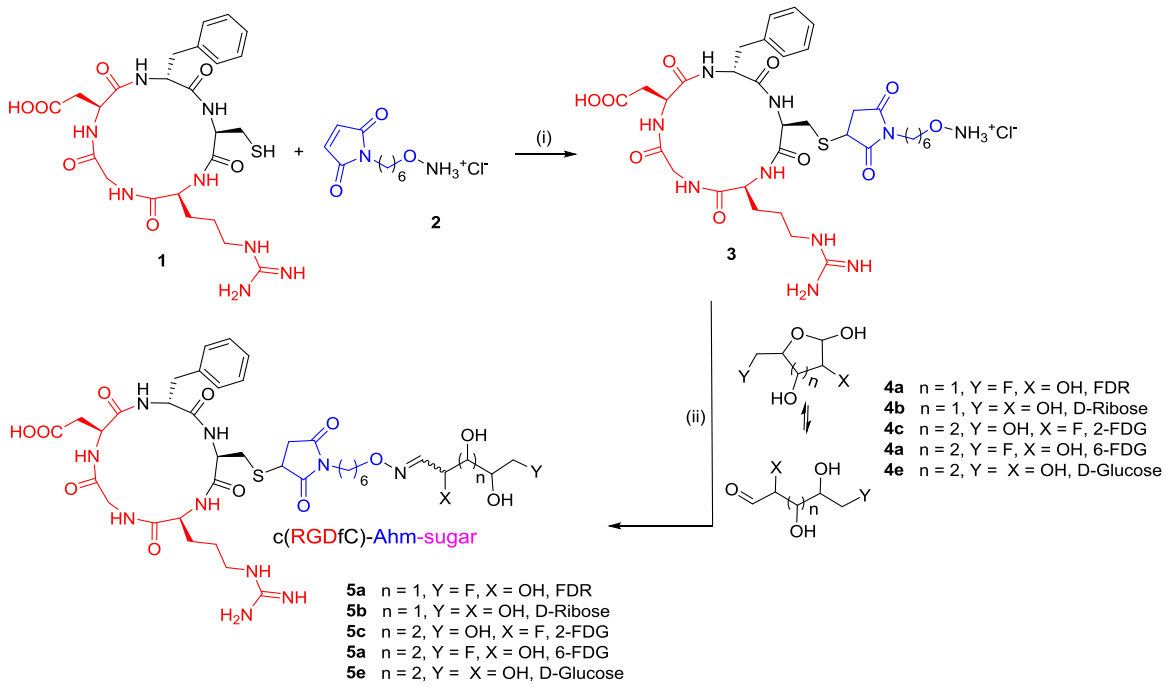

Figure 57: Functionalisation of c(RGDfC) (Xiang-Guo *et al.,* 2012).

c(RGDfC)) can attach to αvβ3 integrin and connect on the surface of polymeric micelle as the targeting group. c(RGDfC)) increased endocytosis mediated by the αvβ3 integrin in the surface of tumour cells in micelle body. Shen and his group studied on three types of colon tumour-bearing models consist of subcutaneous implantation, in situ induction and in situ

surgery transplantation models, in BALB/c mice were created for *in vivo* tumour inhibition assesses. Targeting delivery system c(RGDfC)) displayed advanced tumour tissue accumulation and antitumor abilities in comparison with those of the non-targeting platform in all three different tumour models. Consequently, c(RGDfC)-decorated targeting drug delivery systems have extensive clinical application prospect (Shen *et al*., 2015).

Ji *et al.* studied on RGD-conjugated albumin nanoparticles as a novel delivery vehicle in pancreatic cancer therapy in 2012 (Ji *et al.,* 2012). According to their research, RGD peptide was conjugated to albumin nanoparticle to increase the intracellular uptake of anticancer drug into the pancreatic cancer cells (BxPC-3). In the cellular uptake reports, the fluorescent signal of RGD-conjugated bovine serum albumin nanoparticles (BSANPs) in BxPC3 cells was greater than alone BSANPs according fluorescence spectrophotometer results.

The uptake of RGD-conjugated BSANPs by pancreatic cancer cells was constrained by an excess amount of free RGD peptide, indicating that the binding and/or uptake were intercedes by the αvβ3 receptor (Ji *et al.*2012). Moreover, the nanoparticles were initiated to be placed close to the nuclei by using laser scanning confocal microscopy. Furthermore, no major *in vitro* cytotoxicity was found as measured with MTT assay. Both *in vitro* and *in vivo* antitumor ability was increased by targeting gemcitabine-loaded nanoparticles to BxPC-3 cells using RGD peptides. Consequently, the RGD-conjugated BSANPs hold high potential as an effective drug delivery system to deliver therapeutic agents to pancreatic cancer (Ji *et al.,* 2012).

Aims and objectives

In this Chapter the c(RGDfC) peptide will be conjugated onto the achieved optimum ratio of BNIPDSpm-HNP-PEG and the drug uptake will comprise between gemcitabine (described in Chapter 1) and different BNIPDSpm formulations.The drug optimum loading will assess by HPLC in order to characterising BNIPDSpm-HNP-PEG- c(RGDfC) peptide conjugation and also Drug uptake potentials will assess in human epithelial-like pancreatic carcinoma (PANC-1).

4.2. Materials and methods

Materials used

Table12. Materials used in RGD characterization and drug uptake

Materials	Suppliers
Cyclo(-Arg-Gly-Asp-D-Phe-Cys) peptide	Bachem Co., Switzerland
HPLC Grade ethanol	Fisher Scientific, UK
Thiolated poly ethylene glycol (PEG-thiol)	Sigma-Aldrich Co., UK
PRMI culture medium	Life technologies Co., UK
Penicillin streptomycin	Life technologies Co., UK
Phosphate buffered saline	Fisher Scientific, UK
Foetal bovine serum	Fisher Scientific, UK
Trypsin-EDTA	Life technologies Co., UK
Highly purified water	MillexQ system (UK)
Acetonitrile	Sigma-Aldrich Co., UK
Bis(naphthalimidopropyl)spermine (BNIPDSpm)	Synthesised by Keele nanopharmaceutics Research group
BxPC-3 cell line (Passage number:10)	LGC Standards Co., UK
Gemcitabine	Sigma-Aldrich Co., UK
Octane sulfonic acid	Sigma-Aldrich Co., UK
Sodium acetate	ACROS Organics Co., USA

Methods

Peptide conjugation to HNP-BNIPDSpm-PEG thiol and characterisation of the new formulation

HNPs (2.5 mL, 1 mg mL^{-1}), 25mg BNIPDSpm (dissolved in 5 mL deionised water), 25 mg PEG-thiol (1:10:10 HNP:BNIPDSpm: PEG Thiol) and 1 mg c(RGDfC) peptide were added together. The mixture was stirred for 3 h and then magnetically separated and highly washed for 3 times with deionised water. The amount of the attached drug and conjugated peptide was identified by RP-HPLC (Prominence, DEGASSER, LC20AD, SHIMADZU). For drug conjugation quantification the method which was described in Chapter 3, section 3.2.2.3.5.1 was used. In order to determine the amount of conjugated peptide, RP-HPLC with a fluorescence detector at 250 nm (excitation) and 307 nm (emission) (Jasco, PU-980, Japan; column C18(2), 150×4.60 mm 5 micron, flow rate: 1 $mLmin^{-1}$, injection volume: 20µL) was used. The different mobile phase was used for detecting c(RGDfC) peptide in HPLC (Jin *et al*., 2007). The mobile phase was contained 50:50 of two different solvents. First solvent was including 0.09 % trifluoroacetic acid (TFA) and second solvent contained acetonitrile containing 9.91% H_2O and 0.09 % TFA (Jin *et al*., 2007). Before injecting 1 mL of sample was diluted with 1 mL of acetonitrile and then 20µL of the mixture was transferred into the HPLC.

The amount of the peptide conjugated was calculated after assessing the amount of attached drug from the amount of free drug in waste solution. All measurements were carried out for three times.

For finding optimum drug attached, 1:10:10 HNP:BNIPDSpm:PEG-Thiol which has highest percentage of drug loading in compare with the other ratios HNPs solutions (1 mg mL^{-1}) (described in Chapter 3 section 3.2.2.3.5.1) were mixed with the c(RGDfC) peptide in the ratio (HNP: c(RGDfC) peptide) 1:1, 1:5, 1:10 respectively. The solutions were stirred for 3 h at room temperature. Finally the solution was magnetically separated and highly washing with deionised water for three times. The particles were separated from the supernatant (waste solution) after drug conjugation by using a strong permanent magnet on the outside of a glass vial containing the formulation. The waste solution (1 mL in water) was diluted with 1 mL of DMSO and drug concentrations were analysed via HPLC. All measurements were run in triplicate and recorded as average values.

Cellular uptake of formulations *in vitro*

For cellular uptake, human primary pancreatic adenocarcinoma cells (BxPC-3) were cultured in Roswell Park Memorial Institute (RPMI) media, with 1 % penicillin/ streptomycin and 10 % foetal bovine serum. Cells were seeded 150000 cells/ well in their exponential growth phase into 6-well plates and incubated for 24 h at 37° C with 5 % CO_2. The media was removed and 3 mL of 25 μgmL^{-1} & 50 μgmL^{-1} gemcitabine, BNIPDSpm, HNP-BNIPDSpm, HNP-BNIPDSpm-PEG Thiol and HNP-BNIPDSpm-PEG Thiol- c(RGDfC) peptide were replaced and incubated for 1 h and 4 h. The medium was removed and each well was washed with 1 mL phosphate buffered saline (PBS) and removed again. Trypsin (185µL) was added into each well. The wells were incubated for 3 min to detach the cells from the monolayer and 815µLof fresh media was added to the each well. This solution (50µL) was added to 50µL blue trypan and mixed in an Eppendorf tubes. The number of dead, live and total cells were counted using an automated cell counter (Invitrogen countess®, UK).

Cells were aliquoted (100,000) and diluted in DMSO: water (1:1) (for samples containing bisnaphthalamide derivatives) or water (for samples containing gemcitabine). The concentration of the drugs in different samples was measured using reverse phase high performance liquid chromatography (HPLC). Gemcitabine characterizing was carried out with HPLC with UV detector (Perkin Elmer, Flexar Autosampler and column: SPHERISORB ODS 2 5µm, length 250 mm, internal diameter 4.6 mm). Gemcitabine mobile phase was contained 30% H_2O and 70% acetonitrile (Losa *et al.* 2006). The standard solutions of gemcitabine were scanned in the range of 200-400 nm against mobile phase as a blank. Gemcitabine demonstrated maximum absorbance at 234 nm with flow rate of 1 mL (Losa *et al.,* 2006).

Characterisation of bisnaphthalamide by reverse phase HPLC (Prominence, Degasser, LC20AD, Shimadzu) was described in Chapter Three (Section 3.2.2.2).

4.3. Results

Conjugation of targeting peptide onto the optimal formulation

HPLC peak indicate that c(RGDfC) peptide was conjugated on the HNP successfully. Also amount of drug and targeting peptide were analysed by RP-HPLC. A calibration was carried out in rang of 0.03 – 0.96 μgmL^{-1} (R^2 = 0.9999) (Figure 58).

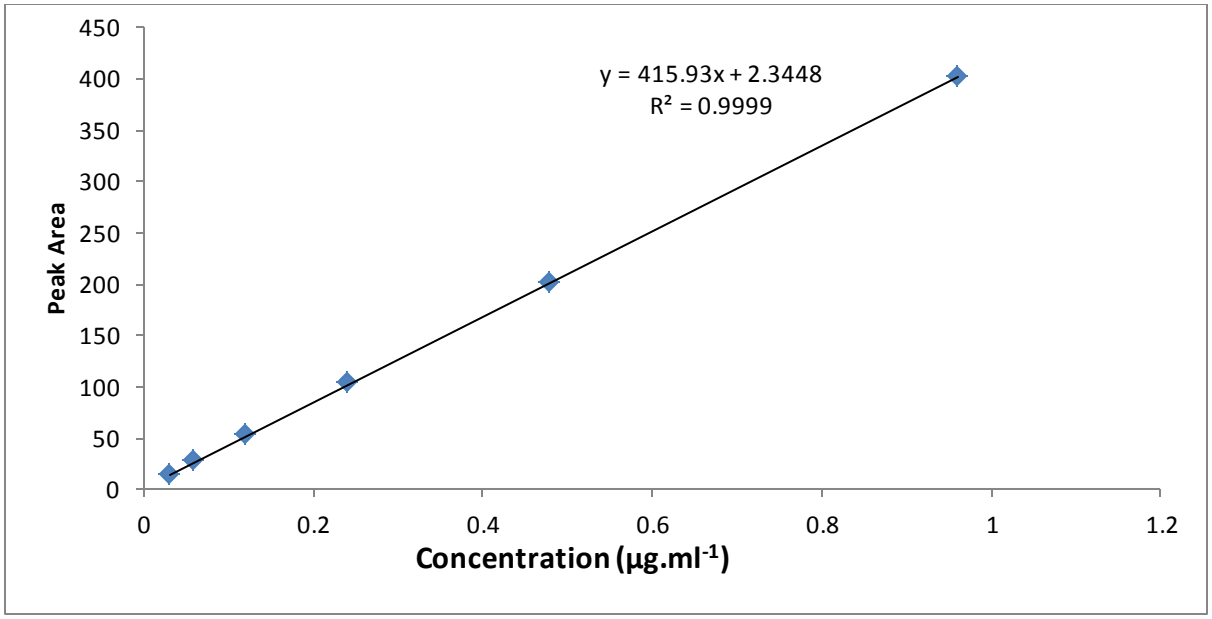

Figure 58: Calibration graph of RGD peptide.

The c(RGDfC) peptide sharp peak was observed at around 17 min at the concentration of 0.683 µgmL^{-1} of c(RGDfC) (Figure 59).

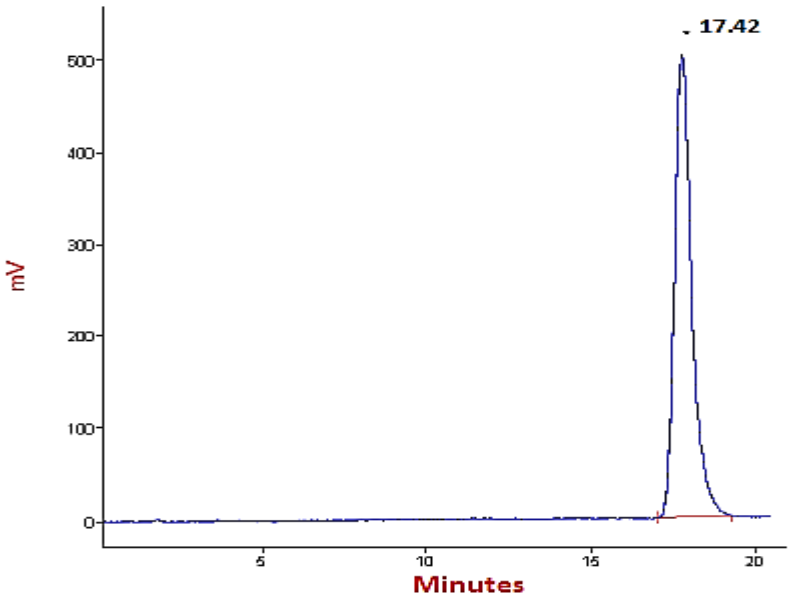

Figure 59: Reverse phase HPLC analysis (with fluorescence detector) of 0.183 µgmL^{-1} c(RGDfC).

The drug had sharp peak which observed between 9-10 min and same as the peak which described in Chapter 3 in Figure 39 (section 3.2.2.3.5.1).

The concentration of the BNIPDSpm and c(RGDfC) peptide in BNIPDSpm-HNP-PEG-c(RGDfC) formulation was characterized and calculated by HPLC. The HPLC test result demonstrated that 4.113 ± 0.032 mg mL^{-1} of BNIPDSpm and 0.204 ± 0.011 mg mL^{-1} of c(RGDfC) peptide were conjugated in BNIPDSpm-HNP-PEG-c(RGDfC) formulation. Consequently 51 % of the initial amount of peptide was able to conjugate to the surface of HNPs.

Different ratios c(RGDfC) peptide were added to the optimum ratio HNP-Drug-PEG Thiol (1:10:10 respectively). These ratios were including 1:10:10:1 HNP:BNIPDSpm:PEG-Thiol:c(RGDfC), 1:10:10:5 HNP:BNIPDSpm:PEG-Thiol:c(RGDfC) and 1:10:10:10 HNP:BNIPDSpm:PEG-Thiol:c(RGDfC). The drug conjugation was according to the Figure 60.

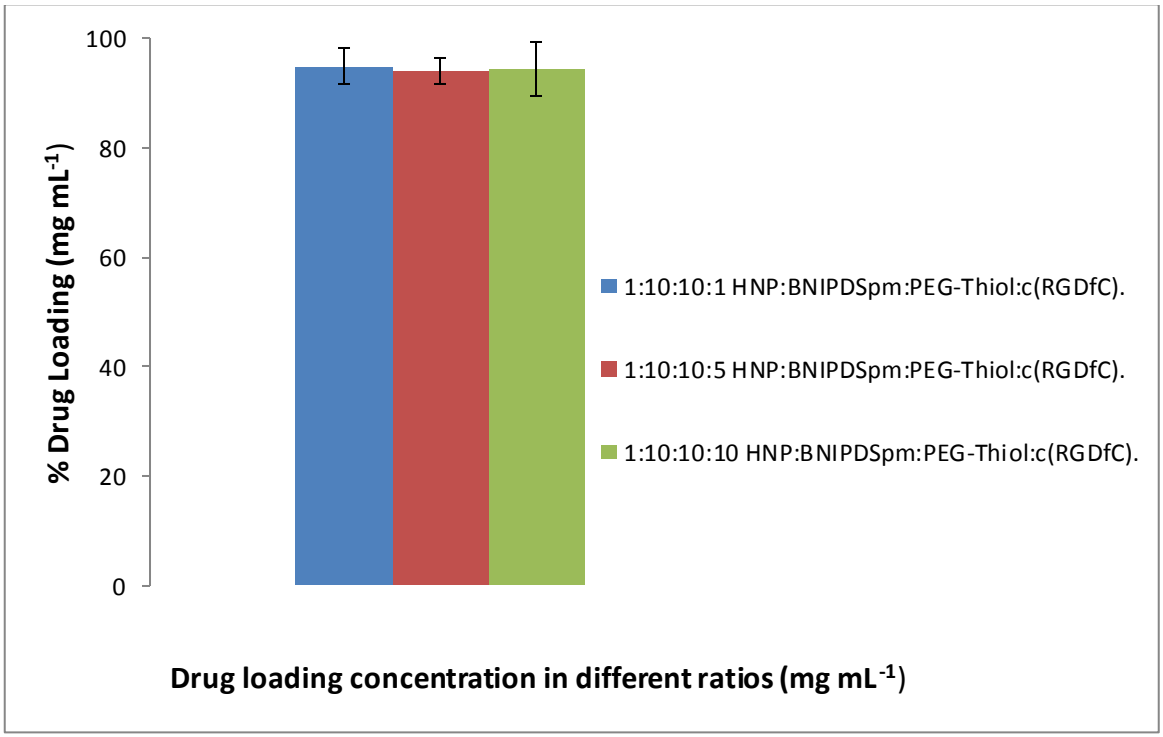

Figure 60: Drug conjugations in different ratios of c(RGDfC).

According to the Figure 60, increasing ratios of c(RGDfC) did not have effect in drug conjugation. In ratio of 1:10:10:1 HNP:BNIPDSpm:PEG-Thiol: c(RGDfC), 95.03% ± 3.25 of drug was attached into the HNP. Almost same result was observed in different ratios of RGD as well. Table 13 was demonstrated that 23.75 mg ± 3.25 of the drug (out of 25 mg) was attached into the HNP (2.5 mL, 1mg mL^{-1}) (Table 13) ($p < 0.05$).

Table 13: Drug loading with different ratios of c(RGDfC). Experiments were performed three times, and data were expressed as mean ± standard errors (n=3, ave ± SD).

Different Ratios ($mg.mL^{-1}$)	**Drug conjugated (out of 25 mg)**
1:10:10:1 HNP:BNIPDSpm:PEG-Thiol:RGD	23.75 ± 3.25
1:10:10:5 HNP:BNIPDSpm:PEG-Thiol:RGD	23.11 ± 2.45
1:10:10:10 HNP:BNIPDSpm:PEG-Thiol:RGD	23.59 ± 4.01

Drug uptake investigations on BxPC-3 Cell line

Drug uptake was investigated and compared between control anticancer drug (gemcitabine), BNIPDSpm and novel hybrid formulations at different concentrations and times. The amount of accumulated free drug was quantified by RP-HPLC. A calibration was run using gemcitabine solutions, dissolved in H2O with the concentration of 18.75 - 300µgmL^{-1} (R^2 = 0.999) (Figure 61)

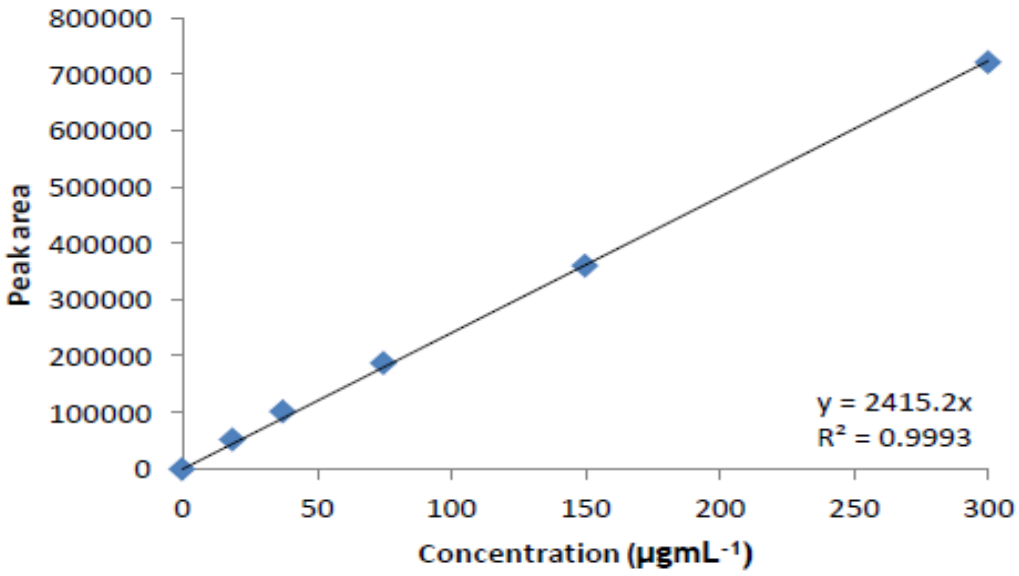

Figure 61: Calibration graph of Gemcitabine in HPLC.

Drug uptake was investigated as a control anticancer drug at 25 µgmL^{-1} and 50 µgmL^{-1} concentrations for 1 h and 4 h for gemcitabine (Figure 62). The amount of accumulated free drug was quantified by RP-HPLC.

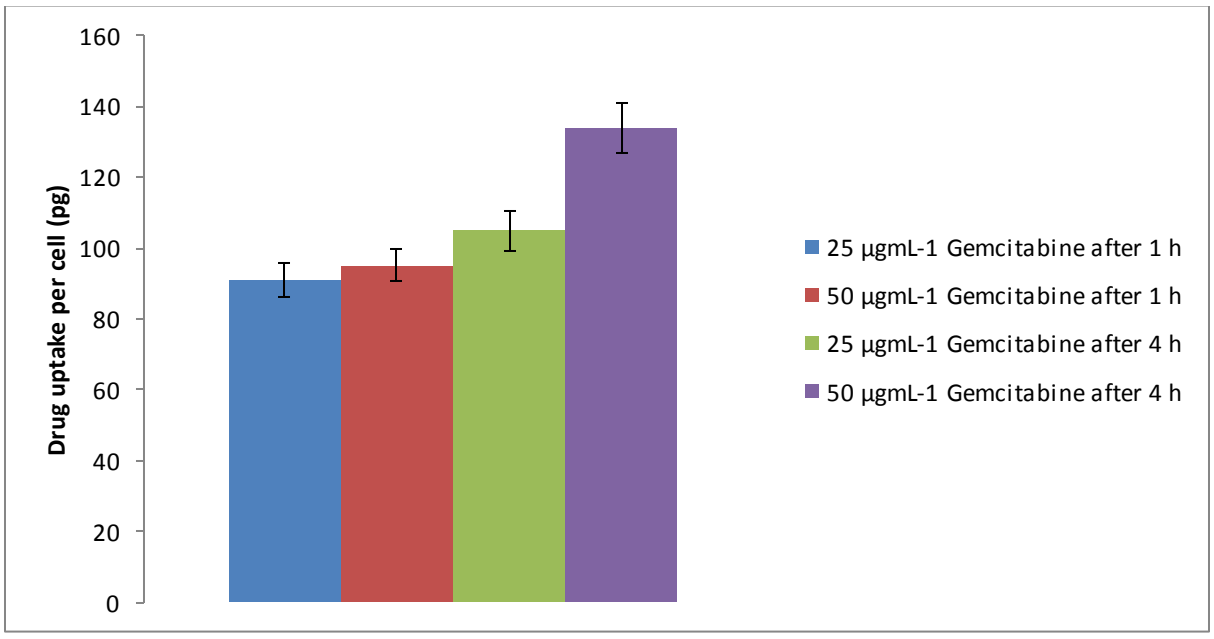

Figure 62: Drug uptake with Gemcitabine at 25 µgmL^{-1} and 50 µgmL^{-1} concentrations for 1 h and 4 h (n=3, ave ±SD).

Figure 62 demonstrates time and concentration are two important factors in increasing level of drug up taking. The drug uptake for 25 μgmL^{-1} gemcitabine on BxPC-3 cells was 91pg per cell after 1h ($p < 0.05$). The drug uptake on BxPC-3 cells was increased slightly to 95pg per cell for 50 μgmL^{-1} gemcitabine at same time ($p < 0.05$). After 4h incubation with 25μgmL^{-1} and 50 μgmL^{-1} of gemcitabine with BxPC-3 cells, amount of 105pg per cell and 134pg per cell of drug was taken up by the cells, respectively ($p < 0.05$).

BNIPDSpm (free drug), BNIPDSpm-HNP, BNIPDSpm-HNP-PEG and BNIPDSpm-HNP-PEG-RGD were incubated on BxPC-3 cells at 25 μgmL^{-1} and 50μgmL^{-1} concentrations for 1 h and 4 h (Figure 63).

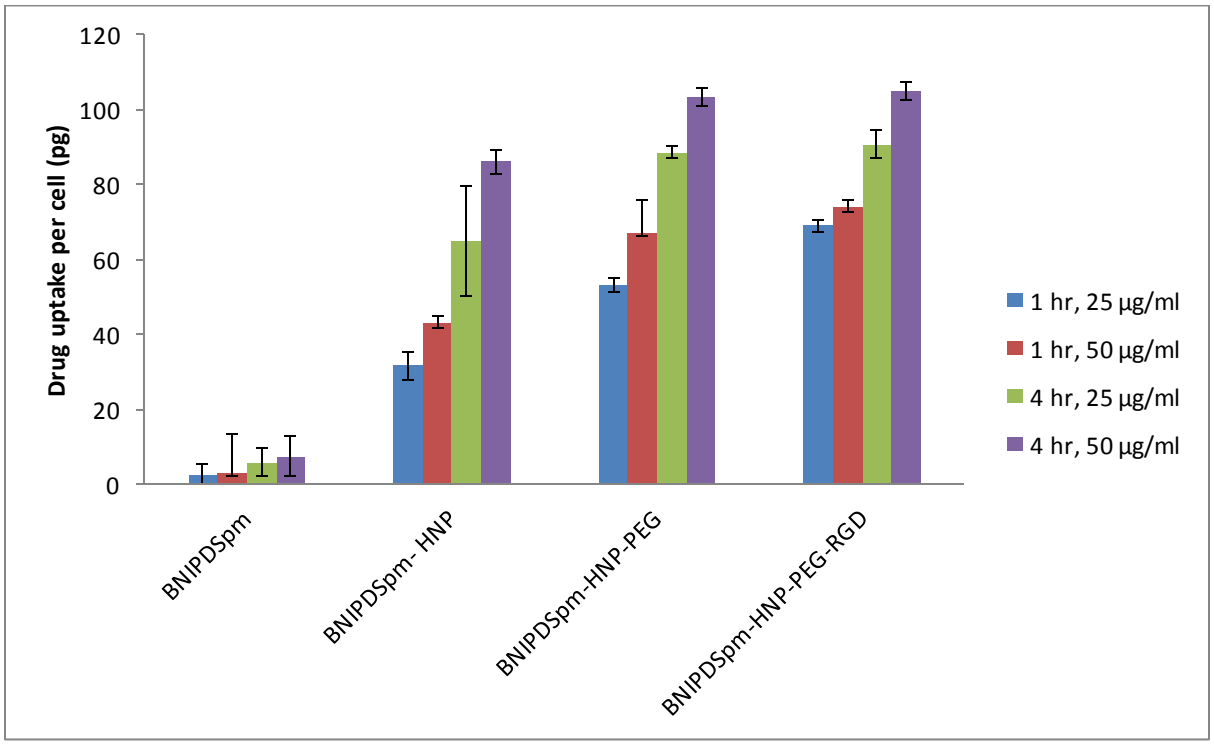

Figure 63: Drug uptake with BNIPDSpm and its formulations at 25 μgmL^{-1} and 50 μgmL^{-1} concentrations for 1 h and 4 h (n=3, ave ±SD) ($p < 0.05$).

The data showed that the lowest drug uptake for free drug in compared with the formulations. At 25μgmL^{-1}, 3pg per cell of BNIPDSpm was taken up from free drug after 1h

and 7pg per cell of the free drug was taken by cell after 4 h. Also at 50µgmL^{-1}, 5pg per cell and 9pg per cell of free drug were taken on BxPC-3 Cell line after 1 h and 4 h respectively ($p < 0.05$). As BNIPDSpm formulations (with four amine groups in drug`s chemical structure) were more positive (discussed in Chapter Three), they were taken up more by BxPC-3 cells which might be related with the charge-charge interactions of positive formulation with the negative cell membrane. The test results demonstrate that by increasing time the drug uptake will increase significantly and also raising concentration can increase the drug uptake as well. BNIPDSpm-HNP drug uptake was significantly higher result in compare with BNIPDSpm ($p < 0.05$).

The test result was demonstrated that during first hour around 31pg and 41pg of drug was taken by cells at 25 µgmL^{-1} and 50 µgmL^{-1}. On the other hand, 62pg per cell and 84pg per cell of the drug attached by BxPC-3 Cells at 25 µgmL^{-1} and 50 µgmL^{-1} after 4h ($p < 0.05$). At 25 µgmL^{-1} HNP-BNIPDSpm-PEG, after 1 h incubation, 55 pg of BNIPDSpm was taken up from free drug and after 4h incubation 82 pg per cell of the drug was attached by the cells. At 50 µgmL^{-1} HNP-BNIPDSpm-PEG, after 1 h incubation, 65 pg per cell of BNIPDSpm was taken up from free drug and after 4 h incubation 104 pg per cell of the drug was attached by the cells. The HNP-BNIPDSpm-PEG test result was higher than free drug and HNP-BNIPDSpm but lower than Gemcitabine drug up taken ($p < 0.05$).

Consequently the target formulation had the highest drug uptake in compare with free drug and the formulations although the test result was slightly lower than Gemcitabine. The target formulation test result was demonstrated that during first hour around 67 pg per cell and 71 pg per cell of drug was taken by cells at 25 µgmL^{-1} and 50 µgmL^{-1}. On the other hand, 87 pg per cell and 108pg per cell of the drug attached by BxPC-3 Cells at 25 µgmL^{-1} and 50

μgmL^{-1} after 4 h ($p < 0.05$). As discussed before, free BNIPDSpm enters to cells through cell membrane pores/channels which is not energy dependant, but particles internalise by endocytosis, thus slower proliferation resulted in a bit less uptake of hybrid formulations compared to the Gemcitabine ($p > 0.05$).

4.4. Discussion

$\alpha v\beta_3$ integrin receptor which has been effective with different types of cancer including breast, ovarian, prostate, melanoma, glioblastoma, cervical, colon and pancreatic cancer (Demircioglu and Hodivala-Dilke, 2016). $\alpha v\beta_3$ integrin receptor is a selective target with high potential for diagnosis and therapy of cancer (Demircioglu and Hodivala-Dilke, 2016). RGD peptide has high potential to act as a tumour-targeting moiety for decreasing adverse effects and enhancing anti-tumour activity (Verrier *et al.,* 2012).

Expansion of novel RGD peptides against integrin αvβ3 with greater affinity, better specificity, and improved stability represents a new trend in this field (Verrier *et al.,* 2012). Novel RGDs such as cRGDfK, cRGDyK, cRGDfC and iRG were investigated to expand the anti-tumor activity (Sheldrake and Patterson, 2009; Paolillo *et al.,* 2009; Auzzas *et al.,* 2010).

Zuo and colleagues conjugated iRGD peptide (CRGDK/RGPD/EC) to the surface of super paramagnetic iron oxide nanoparticles (SPIONs) to enhance labelling of PANC-1 cells in cancer imaging. They suggested that SPIONs with iRGD peptide can raise the uptake and labelling rate of PANC-1 (Zuo *et al.,* 2014).

The concentration of the BNIPDSpm and c(RGDfC) peptide in BNIPDSpm-HNP-PEG-c(RGDfC) formulation was characterized and calculated by HPLC. c(RGDfC) peptide was successfully conjugated to the surface of BNIPDSpm-HNP-PEG (PEGylatedbformulation was used in order

to increase biocompatibility) and the amount of attached BNIPDSpm and peptide were analysed by RP-HPLC. The HPLC test result demonstrated that 4.113 ± 0.032 mg mL^{-1} of BNIPDSpm and 0.102 ± 0.011 mg mL^{-1} of c(RGDfC) peptide were conjugated in BNIPDSpm-HNP-PEG-c(RGDfC) formulation. Consequently 51 % of the initial amount of peptide was able to conjugate to the surface of HNPs. For RGD optimum drug conjugation, 1:10:10 HNP:BNIPDSpm:PEG-Thiol which has highest percentage of drug loading were mixed with the c(RGDfC) peptide in the ratio (HNP: c(RGDfC) peptide) 1:1, 1:5, 1:10 respectively. In ratio of 1:10:10:1 HNP:BNIPDSpm:PEG-Thiol:c(RGDfC), we observed the maximum drug conjugation (95.03% ± 3.25 of drug was attached into the HNP). Almost same result was observed in different ratios of RGD as well.

Drug uptake of gemcitabine, BNIPDSpm and HNP formulations were investigated and compared at 25 μgmL^{-1} and 50 μgmL^{-1} concentrations for 1 h and 4 h for BxPC-3. The amount of accumulated free drug was quantified by RP-HPLC. Drug uptake study of BNIPDSpm on BxPC-3 cells showed that hybrid formulations were taken up significantly higher than free drug ($p < 0.05$) (Figure 63). The drug uptake for 25 μgmL^{-1} gemcitabine on BxPC-3 cells was 91pg per cell after 1h. The drug uptake on BxPC-3 cells was increased slightly to 95pg per cell for 50 μgmL^{-1} gemcitabine at same time. After 4h incubation with 25μgmL^{-1} and 50 μgmL^{-1} of gemcitabine with BxPC-3 cells, amount of 105pg per cell and 134pg per cell of drug was taken up by the cells, respectively ($p < 0.05$). The test results demonstrated that the drug uptake for free drug and its formulations was BNIPDSpm<HNP-BNIPDSpm<HNP-BNIPDSpm-PEG<HNP-BNIPDSpm-PEG-RGD.

The best result was for the target formulations which has the highest drug uptake after 4 h. The target formulation test result was demonstrated that during first hour around 67pg per

cell and 71pg per cell of drug was taken by cells at 25µgmL^{-1} and 50µgmL^{-1}. On the other hand, 87pg per cell and 108pg per cell of the drug attached by BxPC-3 Cells at 25 µgmL^{-1} and 50 µgmL^{-1} after 4 h ($p < 0.05$).

The test results demonstrated that the drug uptake for HNP-BNIPDSpm-PEG-RGD was significantly greater than free drug in different concentrations and times ($p < 0.05$). It can prove that the target peptide play important role for efficient delivery of the drug into cancer cells. The RGD formulation was also higher than HNP-BNIPDSpm and BNIPDSpm-PEG However the HNP formulation with RGD was not significantly higher than HNP-BNIPDSpm-PEG. It might be because this is a monolayer cell culture and not representative of 3D *in vivo* physiology. As the matter of fact in monolayer cell culture many challenges remain, including the mechanical microenvironment, the tissue-tissue interface and the spatiotemporal distributions of oxygen, nutrients, and metabolic wastes. These challenges may lead to affect in RGD formulation for uptaking drug in the cancer cells (Duval *et al.,* 2017).

The presence of targeting peptide within the formulations resulted in comparable uptake rate to gemcitabine. Gemcitabine has not significant increase in compare with target formulation, however previous researches was shown that the cytotoxicity of Gemcitabine was more than BNIPDSpm and its formulations (Malekigorji *et al*., 2017). In next Chapter the cytotoxicity of free drug and its formulation and also Gemcitabine will compare together.

4.5. Conclusion

The target peptide successfully conjugated in the novel drug formulations. *In vitro* drug uptake study also validated that hybrid formulations internalise and accumulate inside

pancreatic cancer cells significantly higher than free drugs. The target formulations had the highest drug uptake after 1 h and 4 h in from free drug and its formulations.

Chapter Five

Biological characterisation of bisnaphthalmide based formulations

5.1. Introduction

Cytotoxic drugs

Cytotoxic drugs or cytostatic (also cytotoxic chemotherapy) are drugs which are used to destroy cancerous cells. Cytotoxic prevent the prolific cancer cell division and are commonly used either before or after surgery depending on the stage of the cancer. Cytotoxic drugs also reduce instances of metastases and can stop cancer progression or remove total cancer in patients. Using types of cytotoxic drugs depend on type of tumour, its mechanism, rate of development and ratio of cells in the distribution stage (Joensuu *et al.,* 2013).

Cytotoxic drugs are transported in the bloodstream throughout the body, which often poses a problem for the already sick patients which require them. Although cytotoxic drugs are valuable for cancer treatment, they are highly toxic and therefore kill healthy cells as well as their cancerous targets.

As a result almost all chemotherapie possess very unpleasant side effects which patients must endure including hair loss, damage to the mouth and pharynx mucosa, bone marrow depletion, fatigue, diarrhoea and nausea. For instance, in their effect on bone marrow, the cytoxicity can lead to a drop in white blood cell, blood platelet and haemoglobin counts. Damage to the bone marrow enhances the risks of infection and communicable disease (Joensuu *et al.,* 2013).

The other disadvantages of chemotherapy also include swelling, changes to fingernails and toenails, symptoms affecting the mucous membranes of the eyes, muscle pain, hypersensitivity, constipation, premature menopause symptoms in women due to oestrogen deficiency and numbness in the hands and soles of the feet (Joensuu *et al.,* 2013).

There are numerous techniques which have been studied in order to increase the efficacy of anticancer agents such as enhancing the solubility or uptake rate of drugs by cancer cells, mitochondria targeted drugs delivery (Modica-Napolitano and Weissig, 2015) and targeted delivery to tumour (Jeanbart *et al*., 2014). However, many of these methods failed to increase the site specific delivery of chemotherapeutic agents. The main reason is most of new compounds detected are insufficiently soluble in aqueous media or lack the ability for preferential uptake in cancerous cells (Lindenberg *et al.,* 2004).

In pancreatic cancer the first line treatment in the UK is with gemcitabine, or gemcitabine in combination with capecitabine. Gemcitabine side effects include flu-like symptoms (muscle pain, fever, headache, chills, and fatigue), Fever (within 6-12 hours of first dose), fatigue, nausea (mild), vomiting, poor appetite, skin rash, low blood counts (Kasuya *et al*., 2012). Moreover, the resistance of pancreatic ductal adenocarcinoma (PDAC) cells to the chemotherapeutic agents remains a significant obstruction to effective chemotherapy (Chakraborty and Rahman, 2012).

Recent studies have demonstrated that the epithelial and stromal compartments interact to enhance the aggressive nature of this cancer (Rasheed *et al.,* 2012). Consequently, it is important to improve anticancer therapies targeting the stroma and epithelial cells, which may play a key role in clinical outcome development for cancer treatment (Rasheed *et al.,* 2012). In this chapter cytotoxicity of new formulations were determined *in vitro* as it is important to confirm the biocompatibility before introducing to *in vivo* environments.

Cytotoxicity assay

MTT assay

3-(4,5-Dimethylthiazol-2-yl)-2,5-diphenyltetrazolium bromide (MTT) is extensively applied for cell viability and cytotoxicity assays (Lamprecht *et al.,* 2000). The enzymatic reduction of 3-[4,5-dimethylthiazole-2-yl]-2,5-diphenyltetrazolium bromide (MTT) to MTT-formazan has been catalyzed by mitochondrial succinate dehydrogenase (Figure 64) (Carmichael *et al.,* 1987).

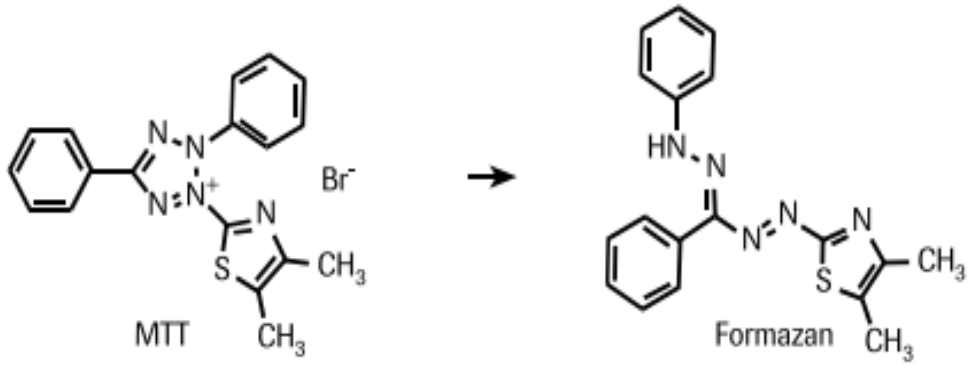

Figure 64: MTT to formazan mechanism (Carmichael *et al.,* 1987).

The MTT assay is a colorimetric reaction. The mono layers cell can be counted in different plates such as 35 mm dishes or multi well plates. The test is according to the treating cells in their exponential growth phase to the MTT solution (Lamprecht *et al.,* 2000). The assay relies on the reduction of MTT, a yellow water-soluble tetrazolium dye, primarily by the mitochondrial dehydrogenases, to purple coloured formazan crystals. The formazan product is analysed spectrophotometrically (550 nm) after dissolution in DMSO, the spectra of nanoparticle-treated and untreated cells giving validate of the extent of cytotoxicity (Lu *et al.,* 2012). It's been studied that 4 h is the optimal time for cells to be incubated with MTT.

After 4 h, the accurate viability determination by dissolving the formazan crystal in dimethyl sulfoxide (DMSO), following calculating the absorbance formazan solutions by a microplate reader. Consequently, the percentage of cell viability can be analysed and half maximal inhibitory concentration (IC_{50}) can be identified (Carmichael *et al.,* 1987).

Trypan blue assay

Trypan blue exclusion (TB) is a test used to distinguish the number of viable cells existing in a cell population compared with those which are dead (Tennant, 1964). The viable cells are displayed refractive, small and rounded while dead cells are presented dark blue, swollen and large (Tennant, 1964). In the TB test, a cell suspension should mix with same amount trypan blue and then visually tested to identify whether cells take up or exclude the dye. The solution move into the plate and cells can be measured by an automated cell counter or by a microscope. The IC_{50} value can be identify regarding the number of control cells (Tennant, 1964).

Aims and objectives

In this chapter the toxicity of BNIPDSpm, HNP-BNIPDSpm, HNP-BNIPDSpm-PEG and HNP-BNIPDSpm-PEG-RGD and Gemcitabine were characterised using MTT and Trypan Blue assays. *In vitro* testing is an essential step in order to determine whether the novel formulations tested were better than existing drug therapies.

5.2. Materials and methods

Materials used for this chapter

Table14. Materials used for toxicity assay.

Materials	Suppliers
Cyclo(-Arg-Gly-Asp-D-Phe-Cys) peptide	Bachem Co., Switzerland
3-[4,5-dimethylthiazol-2-yl]-2,5-diphenyltetrazolium bromide (MTT)	Sigma-Aldrich Co., UK
Thiolated poly ethylene glycol (PEG-thiol)	Sigma-Aldrich Co., UK
RPMI culture medium	Life technologies Co., UK
Penicillin streptomycin	Life technologies Co., UK
Phosphate buffered saline	Fisher Scientific, UK
Foetal bovine serum	Fisher Scientific, UK
Trypsin-EDTA 0.05 %	Life technologies Co., UK
Highly purified water	MillexQ system (UK)
Bis(naphthalimidopropyl)spermine (BNIPDSpm)	Synthesised by Keele nanopharmaceutics Research group
BxPC-3 cell line	LGC Standards Co., UK
Gemcitabine	Sigma-Aldrich Co., UK
Dimethyl sulfoxide	Sigma-Aldrich Co., UK
phosphate buffered saline (PBS)	Sigma-Aldrich Co., UK

Methods

Cell culture and sub culturing

BxPC-3 cells were cultured in Roswell Park Memorial Institute (culture medium) (RPMI cell culture medium) supplemented with 1 % penicillin streptomycin and 10 % foetal bovine serum. BxPC-3 cells grown in RPMI were incubated in an ESCO CO_2 Incubator at 5% CO_2 at 37 °C for 3-4 days. The BxPC-3 cells were monitored under microscope to monitor cell growth; cells were allowed to grow to 70% confluency before being sub cultured. The media was removed and 10mL phosphate buffered saline (PBS) added to the flask. The PBS was subsequently removed and 2.5mL trypsin added to the cells and the flasks where incubated for 5 min. Trypsin can separate the cells from the flask, once the cells were detached, 7.5mL RPMI was added to the flasks for further cell growth.

Cytotoxicity Assay

Cytotoxicity of free drugs, hybrid nanoparticles (HNP) naked and new formulations was investigated by using two different cytotoxicity assays: MTT and Blue trypan.

MTT assay procedure

BxPC-s cells (100µL, 15000 cells/ well) in exponential growth phases were seeded into 96 well flat bottomed plate and incubated for 24 h at 37 °C with 5 % CO2. After 24 h, the media was replaced with various concentrations of gemcitabine, BNIPDSpm, naked HNPs, BNIPDSpm-HNP, BNIPDSpm-HNP-PEG Thiol and BNIPDSpm-HNP-PEG-RGD diluted in cellular growth medium. In 96 wells, Serial dilution solutions were made from these stock solutions ($1x10^{-1}$ - $1x10^{-5}$ mg mL^{-1}) using media as the diluent (Table 15).

Table15. Preparation of Excipient Solutions for MTT assay.

Drug concentration (mg mL^{-1})	**Volume of 20 mg mL^{-1} drug stock solution (µL)**	**Total volume of media (ml)**
0.1	22.5	4.5
0.05	11.5	4.5
0.025	5.6	4.5
0.01	2.25	4.5
0.005	1.125	4.5
*0.001	90	4.5
*0.0001	9	4.5
*0.00001	1	4.5

* Sample was made from 0.05 mg mL^{-1} concentration as a stock solution and the same concentrations of drug discussed in Table 14 were prepared. Furthermore, the concentrations made for naked HNP presents the concentration of iron oxide in hybrid formulations (HNP-drug).

A 20 mg mL^{-1} of each free drug solution was prepared using 50:50 of sterile water: DMSO as the diluent to form a stock solution. MTT well plates have 12 rows which including eight dilutions (0.1 - 1×10^{-5} mg mL^{-1}) were made using media as the diluent, Media which is positive control and deionised water which is negative control. Several 96 well plates were carried out with same MTT method. Samples were incubated for 24 h, 48 h and 72 h to check the effect of time on the cell viability.

After incubating the cells in different times (24 h, 48 h and 72 h) the drug solutions were removed and washed with fresh media to remove any excess drug. Fresh media was replaced into the wells (100µL). 3-[4, 5-dimethylthiazole-2-yl]-2, 5-diphenyl tetrazolium (MTT, 50µL, 5 mg mL^{-1} in PBS) was added to the wells and plate was incubated (37 °C with 5 % CO_2) for 4 h. After 4 h, the MTT solution was removed from the wells and 100µL of DMSO was replaced to dissolve the purple formazan crystals trapped in cells. The light absorbance of the resultant purple colour was identified at 570 nm by the using a microplate reader (Tecan, infinite 200 pro, GmbH 5082, Australia). All assays were carried out in triplicate. Percentage of cell viability and IC_{50} was calculated according to the microplate reader result for samples, negative and positive controls data. Percentage of cell viability and IC_{50} was calculated according to below equation.

$$\% \text{ Cell Viability} = \frac{Abs\ of\ sample - Abs\ of\ negative\ control}{Abs\ of\ Positive\ control - Abs\ of\ negative\ control} \times 100$$

Trypan blue cytotoxicity test

BxPC-3 cells (1 mL, 50000 cells/ well) in exponential growth phase was placed and seeded into 12 well flat bottomed plates. The plates were incubated for 24 h at 37°C with 5 % CO_2. The samples such as drug, HNPs and novel formulations were placed in the plates with different concentrations with same method which described for MTT assay. The plates were incubated for 24 h, 48 h, and 72 h to check the effect of time on toxicity of different samples. Then the media was soaked from plates and cells were washed 3 times with PBS. The cells were trypsinised and re-suspended in fresh media. The sample and trypan blue solution were mixed together with ratio of 1:1 (50µL: 50µL) and the mixture was placed in

an automated cell counter (Invitrogen Countess®, UK) to count the variable cells. Percentage of cell viability and IC_{50} was calculated according to below equation.

$$\% \text{ Cell Viability} = \frac{Number\ of\ live\ cells\ in\ sample}{Number\ of\ control\ cells} \times 100$$

***In vitro* thermo-responsive cytotoxicity assay**

Thermal responsive cytotoxicity assay was carried out on 96 wells plate for MTT assay and 12 well flat bottomed plates for trypan blue test on BxPC-3 cells. The cells were seeded in free drug, HNPs and new formulations with same methods as described before and pre-incubated for 4 h at 37°C in a humidified atmosphere of 95% air and 5% CO_2. After this time, 96-well (MTT) and 12-well (blue trypan) plates were removed and placed into a pre-warmed incubator type Memmert IN-30 and heated at 44°C (to mimic the heat generated by the SPR of laser irradiated HNP silver coatings) and 60°C respectively for half an hour. After 0.5 h the plates were incubated again for 24 h, 48 h and 72 h respectively. Calculation cell viability was calculated as described in MTT and blue trypan sections. The % cell viability and IC_{50} was identified for all the plates and the results were compared to the non-activated plates in order to investigate the effect of temperature and time on cell cytotoxicity.

5.3. Results

MTT and Trypan blue Cytotoxicity of drugs, naked HNP and novel formulations

MTT and trypan blue assays were carried out to check and compare free drugs, naked HNP and new formulations toxicity. Cell viability of BxPC-3 incubated with unloaded HNPs were identified by the MTT cytotoxicity test and trypan blue exclusion assay in 24 h, 48 h and 72 h

(Figure 65 A and B). The concentrations illustrate in the graph for HNP are exactly same as the concentration of hybrid formulations but definitely without drug (the concentrations of Fe in HNP and hybrid formulations are the same). There was no significant difference between the MTT and trypan blue test results ($p>0.05$). In (1.0×10^{-5} - 0.005 mg mL^{-1}) the cell viability was around 98% in MTT and 96% in trypan blue ($p > 0.05$). Between 0.05mg mL^{-1} – 0.01 mg mL^{-1} slight decreased was observed and the cell viability around 91% in MTT and Trypan blue tests. Consequently at 0.1 mg mL^{-1}, the cell viability was 87% and 85% in MTT and Trypan Blue respectively ($p > 0.05$) However, this is much more concentrated than would ever be expected to be managed in the drug formulation to a patient in the clinic (Cortajarena *et al.* 2014). The test results were demonstrated that increasing time did not have significant effect on HNP cell viability. After 48 h the test results were almost same as 24 h and. The cell viability was decreased for 14%-18% at highest concentration in MTT and Trypan blue respectively ($p > 0.05$). After 72 h, the cell viability was around 84% and 80% in MTT and Trypan blue respectively. The cell viability decreased for 16%-20% in highest concentration and after 72 h. ($p > 0.05$) (Figure 65A and 65B).

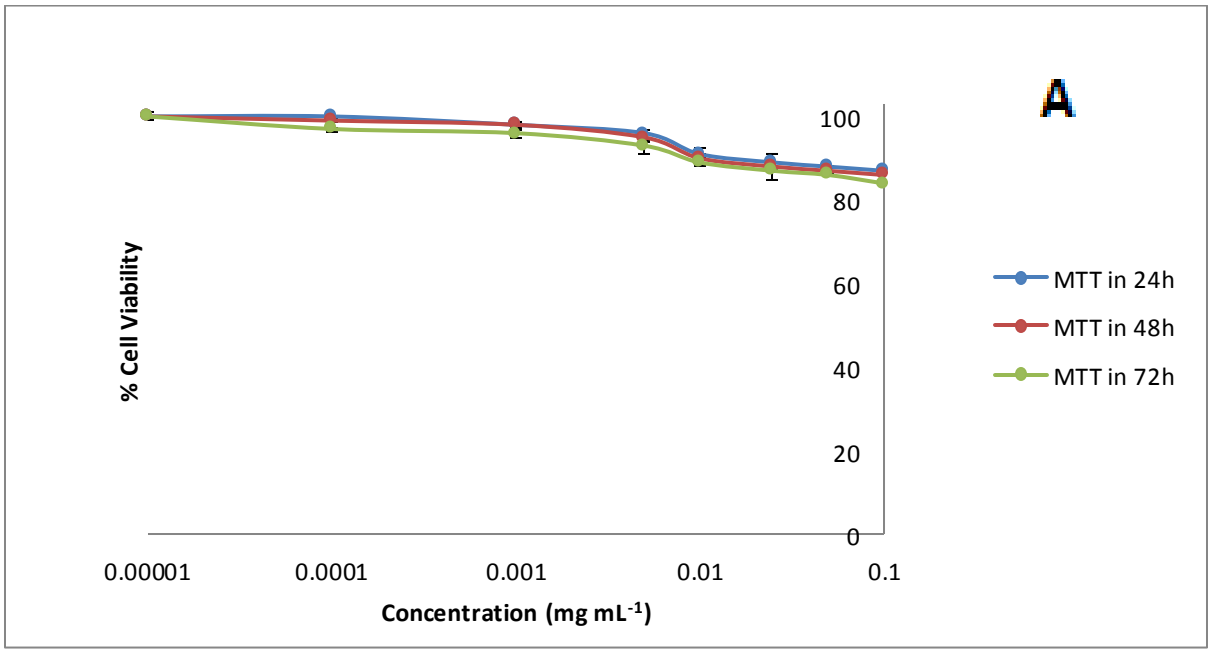

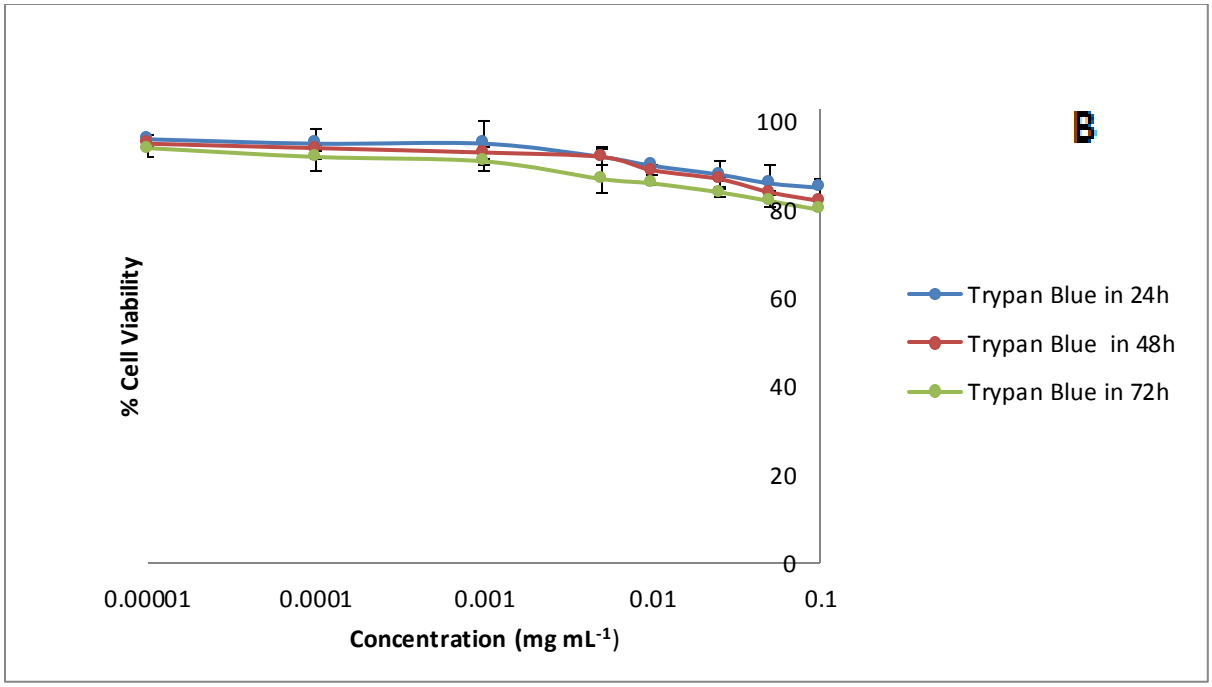

Figure 65: Cell viability of BxPC-3 exposed to HNPs and measured with MTT (A) and Trypan blue (B) tests in 24 h, 48 h and 72 h (n=3,±SD).

The cell viability of BxPC-3 cells incubated with BNIPDSpm (free drug) measured using the MTT cytotoxicity test and trypan blue exclusion assay in 24 h, 48 h and 7 2h (Figure 66A and 66B). In 1.0×10^{-5} mg mL^{-1} to 0.005 mg mL^{-1}, the cell viability was decreased for around 6% - 8% in MTT and Trypan blue respectively after 24 h. Also at this concentration, the cell viability was decreased around 12% - 13% in MTT and Trypan blue respectively after 48 h and around 14% - 17% in MTT and Trypan blue respectively after 72 h. The significant decrease was observed between 0.05mg mL^{-1} to 0.1mg mL^{-1} in MTT and trypan blue in 24 h, 48 h and 72 h ($p < 0.05$). In 0.1 mg mL^{-1} concentration, 31% and 21% of cells were alieved in MTT and Trypan Blue respectively after 24 h ($p < 0.05$). The test results were demonstrated that increasing time slightly decreased the cell viability of BxPC-3. After 48 h, the cell viability was decreased for 73% - 85% at highest concentration in MTT and Trypan blue

respectively ($p > 0.05$). The cell viability decreased for 77% - 90% in highest concentration and after 72 h. ($p > 0.05$) (Figure 66A and 66B).

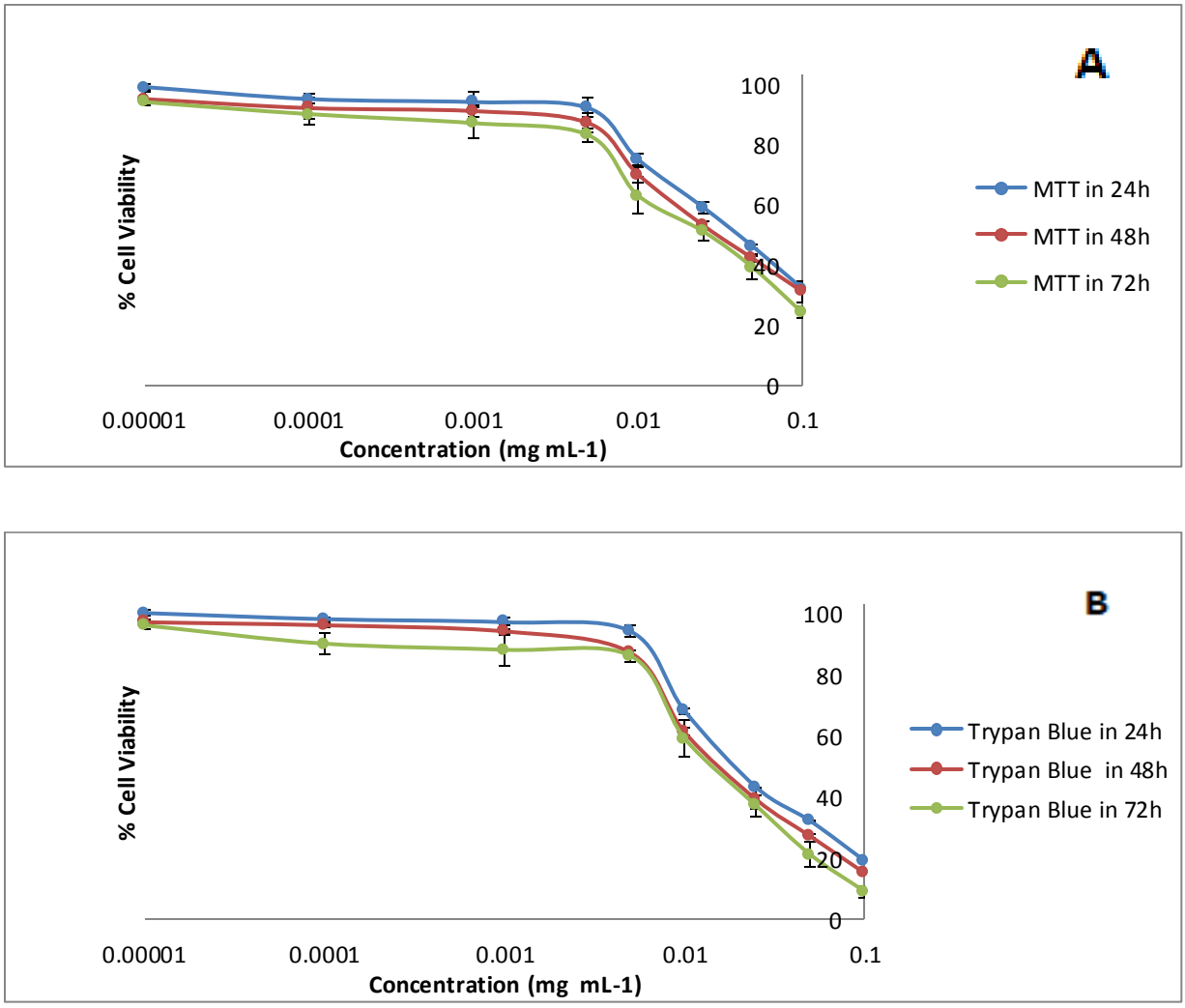

Figure 66: Cell viability of BxPC-3 exposed to BNIPDSpm in different times for MTT (A) and Trypan blue (B) (n=3, ±SD).

The cytotoxic effect of hybrid formulations, BNIPDSpm and Gemcitabine (IC_{50}) was tested and compared together with MTT cytotoxicity test and trypan blue exclusion assay on BxPC-3 cells for 24 h, 48 h and 72 h by GraphPad Prism 6 software (Figure 67). The IC_{50} achieved within the concentrations tested from 1.0×10^{-5} mg mL^{-1} to 0.1mg mL^{-1}. Gemcitabine IC_{50} was calculated over 100µgmL^{-1} with MTT cytotoxicity test and trypan blue exclusion assay

on BxPC-3 cells for all different times (24 h, 48 h and 72 h). Therefore, no IC_{50} was noticeable using both the MTT assay and trypan blue cytotoxicity test for gemcitabine after 24 h, 48 h and 72 h. The MTT test results demonstrated, the IC_{50} for BNIPDSpm was 17.31±0.72µgmL^{-1}, 17.11 ± 0.11µgmL^{-1} and 16.48 ± 0.91 µgmL^{-1} after 24 h, 48 h and 72 h respectively. Moreover the trypan blue test results demonstrated the IC_{50} for BNIPDSpm was 24.57 ± 0.91 µgmL^{-1}, 23.97 ± 1.06µgmL^{-1} and 23.41 ± 0.02µgmL^{-1} after 24 h, 48 h and 72 h respectively. The IC_{50} of the free drugs was around 10, 13 and 14 times greater than HNP-BNIPDSpm, HNP-BNIPDSpm-PEG and HNP-BNIPDSpm-PEG-RGD respectively after 24 h and these differences were increased significantly with increasing time ($p < 0.05$). This specifies that hybrid formulation was able to enhance the therapeutic effect of the drug compared with the free BNIPDSpm. MTT assay was demonstrated that, IC_{50} value of HNP-BNIPDSpm-PEG was 0.83µgmL^{-1}, 0.92µgmL^{-1} and 0.93 µgmL^{-1} lower than HNP-BNIPDSpm in 24 h, 48 h and 72 h respectively. Moreover in trypan blue IC50 value of HNP-BNIPDSpm-PEG was 1.16µgmL^{-1}, 1.17 µgmL^{-1} and 0.97 µgmL^{-1} lower than HNP-BNIPDSpm in 24 h, 48 h and 72 h respectively. The target formulation had the lowest IC_{50} value in compare with free drugs and non-targeted formulations. The MTT test results demonstrated, the IC_{50} for HNP-BNIPDSpm-PEG-RGD was 1.18 ± 0.02 µgmL^{-1}, 0.99 ± 0.55 µgmL^{-1} and 0.79 ± 0.48 µgmL^{-1} after 24 h, 48 h and 72 h respectively. Moreover the trypan blue test results demonstrated the IC_{50} for target formulation was 1.62 ± 0.15 µgmL^{-1}, 1.32 ± 0.17 µgmL^{-1} and 1.11 ± 0.33 µgmL^{-1} after 24 h, 48 h and 72 h respectively ($p > 0.05$).These results confirm that the hybrid formulations have significantly higher efficacy compared with free drugs ($p < 0.05$) (Figure 67).

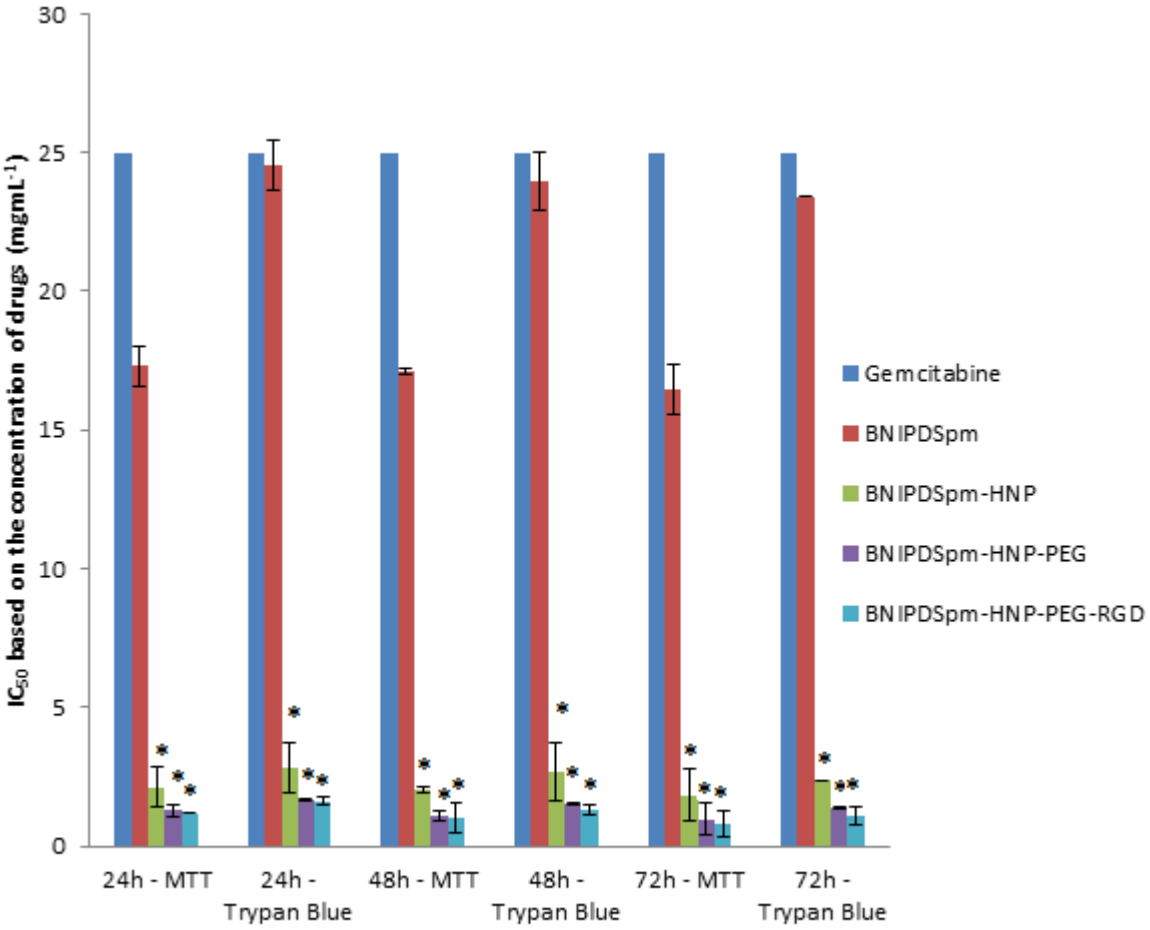

Figure 67: IC_{50} value of drugs and hybrid formulations on BxPC-3 cells obtained by MTT cytotoxicity test and trypan blue exclusion assay after 24 h, 48 h and 72 h ($p < 0.05$) (n=3, ave ± SD). IC_{50} achieved within the concentrations tested ($0.1 – 1.0 \times 10^{-5}$ mg mL^{-1}) and for Gemcitabine IC_{50} achieved over 100 µgmL^{-1} by GraphPad Prism 6 software. * denotes significant decrease in IC50 from hybrid formulations compared with drug alone.

***In vitro* thermo-responsive cytotoxicity assay**

The cytotoxicity assay for free drug, HNP and new formulations were carried out to assess the effect of time and temperature on cell toxicity. In this case MTT and trypan blue tests (triple times for each test) were carried to check and compare the test results in 37 ^{o}C, 44 ^{o}C

and 60 ^{o}C at 24 h, 48 h and 72 h. The test results were demonstrated that the MTT and trypan blue results were almost same as each other. In this case the average data's of MTT and trypan blue were used for identifying thermos responsive cytotoxicity assay. Figure 68A, 68B and 68C demonstrated the effect of temperature on HNP, BNIPDSpm, HNP-BNIPDSpm, HNP-BNIPDSpm-PEG and HNP-BNIPDSpm-PEG-RGD at 24 h, 48 h and 72 h respectively. Test results were demonstrated that time and temperatures are two main factors in cytotoxicity assay however in general, the result indicated that increasing the temperature and time had no significant impact on cytotoxicity of HNPs in compare with free drug and the other formulations ($p > 0.05$). After 24 h the cell viability of highest concentration of HNPs (0.1mg mL^{-1}) decreased for 87%, 85% and 76% in 37 ^{o}C, 44 ^{o}C and 60 ^{o}C respectively. The cell viability in same concentration of HNPs was 86%, 81% and 71% in 37 ^{o}C, 44 ^{o}C and 60 ^{o}C after 48h respectively. At 72 h, the cell viability in same concentration of HNPs was 84%, 78% and 67 % in 37 ^{o}C, 44 ^{o}C and 60 ^{o}C respectively. The test results demonstrated that time and temperature has significant effect on free drug and the new formulations. In comparison, after 24h the cell viability of highest concentration of BNIPDSpm (0.1 mg mL^{-1}) decreased for 21%, 10% and 9% in 37 ^{o}C, 44 ^{o}C and 60 ^{o}C respectively. The cell viability in same concentration of HNPs was 17%, 9% and 5% in 37 ^{o}C, 44 ^{o}C and 60 ^{o}C after 48h respectively. In 72, the cell viability in same concentration of HNPs was 9%, 3% and 1 % in 37 ^{o}C, 44 ^{o}C and 60 ^{o}C respectively ($p < 0.05$) (Figure 68 A, 68B and 68C).

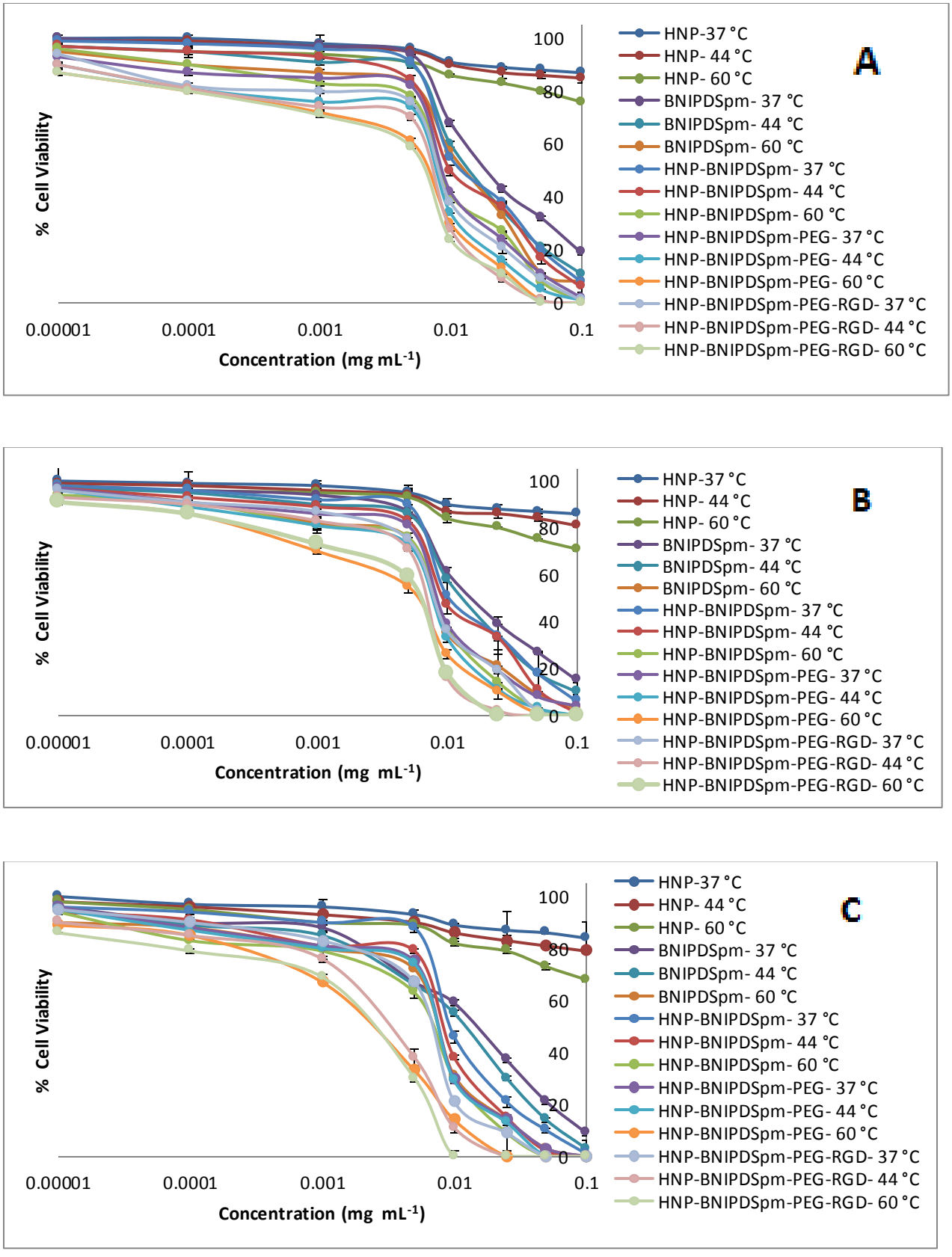

Figure 68: *In vitro* thermo-responsive cytotoxicity test on BxPC-3 cell line at (A) 24 h, (B) 48 h and (C) 72 h (n=3,±SD).

According Figure 68A, 68B and 68C cytotoxicity of hybrid formulations on BxPC-3 cells considerably increased upon the time and temperature increase. The target formulation indicated the highest cytotoxicity on BxPC-3 cells. The viability of BxPC-3 cells treated with BNIPDSpm-HNP-PEG-RGD at 25 ^{o}C, 44 ^{o}C and 60 ^{o}C were 1 %, 0 % in 0.1 mg mL^{-1} and 0 % from 0.05mg mL^{-1} after 24 h, respectively (Figure 68A). The viability of BxPC-3 cells treated with BNIPDSpm-HNP-PEG-RGD at 25 ^{o}C, 44 ^{o}C and 60 ^{o}C were 0 % in 0.1mg mL^{-1}, 0 % from 0.05 mg mL^{-1} and 0 % from 0.025 mg mL^{-1} after 48 h, respectively (Figure 68 B). Finally, the viability of BxPC-3 cells treated with BNIPDSpm-HNP-PEG-RGD at 25 ^{o}C, 44 ^{o}C and 60 ^{o}C were 0 % from 0.05 mg mL^{-1}, 0 % from 0.025 mg mL^{-1} and 0 % from0.01mg mL^{-1} after 72 h, respectively ($p > 0.05$) (Figure 68C).

Further reduction in cell viability and IC_{50} was achieved upon the treating of BxPC-3 with BNIPDSpm in comparison with new formulations in different times and temperatures. Cell viability of BxPC-3 treated with new formulations was considerably smaller than free drug in different time and temperatures (Table 16). The cell viability and IC_{50} test results illustrated that on BxPC-3 cells, Cytotoxicity of HNP-BNIPDSpm-PEG-RGD> HNP-BNIPDSpm-PEG> HNP-BNIPDSpm > BNIPDSpm. The IC_{50} of free drug was almost 10, 14 and 15 times bigger than HNP-BNIPDSpm, HNP-BNIPDSpm-PEG and HNP-BNIPDSpm-PEG-RGD respectively ($P < 0.05$) (Table 16).

Table16. IC_{50} of hybrid formulations at different temperature and time in comparison with free BNIPDSpm on BxPC-3 cell line (n=3, ± SD).

Time (h)	Incubation Temperature (^oC)	BNIPDSpm (μgmL^{-1})	HNP-BNIPDSpm (μgmL^{-1})	HNP-BNIPDSpm-PEG (μgmL^{-1})	HNP-BNIPDSpm-PEG – RGD (μgmL^{-1})
24	37	20.94 ± 0.72	2.47 ± 1.21	1.47 ± 1.67	1.41 ± 0.11
	44	19.67 ± 0.37	2.02 ± 0.99	1.20 ± 0.64	1.32 ± 0.92
	60	17.29 ± 0.81	1.39 ± 0.05	0.91 ± 2.59	0.86 ± 1.21
48	37	20.54 ± 1.03	2.34 ± 0.94	1.31 ± 0.07	1.25 ± 0.63
	44	19.01 ± 1.21	1.91 ± 2.67	1.16 ± 0.77	1.07 ± 0.85
	60	16.99 ± 0.54	1.01 ± 0.57	0.59 ± 0.68	0.46 ± 1.92
72	37	19.94 ± 0.15	2.01 ± 0.09	1.18 ± 0.41	0.95 ± 0.03
	44	18.64 ± 1.11	1.83 ± 0.69	1.01 ± 0.29	0.79 ± 1.22
	60	16.05 ± 3.83	0.79 ± 0.81	0.25 ± 1.21	0.08 ± 0.73

The temperature and time have significant effect on cytotoxicity of free drug and hybrid formulations. Although the lowest IC_{50} and cell viability of hybrid formulations on BXPC3 cell line was occurred in 60 ^oC, The cell viability of BXPC3 cell in expose of 0.1mg mL^{-1} naked HNPs was decreased to 76%, 71% and 67% at 24h, 48h and 72h respectively. In comparison, in 44 ^oC had lower effect of HNPs on BXPC3 cell line. In this temperature, the cell viability of BXPC3 cell in expose of 0.1mg mL^{-1} naked HNPs was decreased to 85%, 81% and 78% at 24 h, 48 h and 72 h respectively.

5.4. Discussion

Pancreatic ductal adenocarcinoma (PDAC) is related with poor survival as often diagnosed when they have metastasised. Radiotherapy and chemotherapy of PDAC is still largely consisting of classical cytotoxic chemotherapy agents (Zuo *et al.,* 2014). The PDAC chemotherapy drugs side effects are including Flu-like symptoms (muscle pain, fever, headache, chills, and fatigue), Fever (within 6-12 hours of first dose), fatigue, nausea (mild), vomiting, poor appetite, skin rash, low blood counts (Kasuya *et al*., 2012). It is essential to improve anticancer therapies targeting the stroma and epithelial cells, which may play a key role in clinical outcome development for cancer treatment (Rasheed *et al.,* 2012). General toxicity tests, such as MTT cytotoxicity assay and trypan blue exclusion cytotoxicity test are require to identify the biological activity of drugs and formulations, which can be carried out on many cell types.

Brana *et al.* reported bisnaphthalimides as powerful chemotherapeutic agents (Brana *et al.,* 1980). Bisnaphthalimide derivatives are detected to have considerable anti-tumour activity in both human cancerous cells and murine (Brana *et al.,* 2001). Existence of planar aromatic moieties in these molecules can insert within the DNA by entry via the major groove (Sami *et al.,* 2000). In this research, MTT and trypan blue assays were carried out to check and compare free drugs, naked HNP and new formulations toxicity. Cell viability of BxPC-3 incubated with unloaded HNPs were identified by the MTT cytotoxicity test and trypan blue exclusion assay in 24h, 48h and 72h (Figure 65 A and B). There were not significant different between MTT and trypan blue test results. In 0.1 mg mL^{-1} HNP concentration 87% and 85% of cells were alieved in MTT and Trypan Blue respectively ($p > 0.05$) However This is much more concentrated than would ever be expected to be managed in the drug formulation to

a patient in the clinic (Cortajarena *et al*., 2014). Barnett and colleagues reported that there was no significant cytotoxic effect for cells incubated with the high concentration of HNPs (100µg mL^{-1}) with both BxPC-3 and differentiated U937 cells for up to 1 week (Barnett *et al.,* 2013a). In this research, test results were demonstrated that increasing time did not have significant effect on HNP cell viability. The cell viability decreased for 16%-20% in highest concentration and after 72 h. ($p > 0.05$). In comparison, the BXPC3 cell viability in expose of free drug (BNIPDSpm) was decreased for 77% - 90% in highest concentration and after 72h ($p < 0.05$).

Gemcitabine IC_{50} was calculated over 100µgmL^{-1} with MTT cytotoxicity test and trypan blue exclusion assay on BxPC-3 cells for all different times (24 h, 48 h and 72 h). Therefore, no IC_{50} was noticeable using both the MTT assay and trypan blue cytotoxicity test for gemcitabine after 24 h, 48 h and 72h. The MTT test results demonstrated, the IC_{50} for BNIPDSpm was 17.31 ± 0.72 µgmL^{-1}, 17.11 ± 0.11 µgmL^{-1} and 16.48 ± 0.91 µgmL^{-1} after 24 h, 48 h and 72 h respectively. Moreover, the trypan blue test results demonstrated the IC_{50} for BNIPDSpm was 24.57 ± 0.91 µgmL^{-1}, 23.97 ± 1.06 µgmL^{-1} and 23.41 ± 0.02 µgmL^{-1} after 24 h, 48 h and 72 h respectively. The IC_{50} of the free drugs was around 10, 13 and 14 times greater than HNP-BNIPDSpm, HNP-BNIPDSpm-PEG and HNP-BNIPDSpm-PEG-RGD respectively after 24 h and these differences were increased significantly with increasing time ($p < 0.05$).

The cytotoxicity assay for free drug, HNP and new formulations were carried out to assess the effect of time and temperature on cell toxicity. In this case MTT and trypan blue tests (triple times for each test) were carried to check and compare the test results in 37 ^{o}C, 44 ^{o}C and 60 ^{o}C at 24h, 48h and 72h. Test results were demonstrated that time and temperatures

are two main factors in cytotoxicity assay however in general, the result indicated that increasing the temperature and time had no significant impact on cytotoxicity of HNPs in compare with free drug and the other formulations ($p > 0.05$). After 72h, the BXPC3 cell viability expose 100 μgmL^{-1} HNP was 84%, 78% and 67 % in 37 ^{o}C, 44 ^{o}C and 60 ^{o}C respectively. The cell viability and IC_{50} test results illustrated that on BxPC-3 cells, Cytotoxicity of HNP-BNIPDSpm-PEG-RGD> HNP-BNIPDSpm-PEG> HNP-BNIPDSpm > BNIPDSpm. The IC_{50} of free drug was almost 10, 14 and 15 times biger than HNP-BNIPDSpm, HNP-BNIPDSpm-PEG and HNP-BNIPDSpm-PEG-RGD respectively.

In previous studies, the cytotoxicity iron oxide-gold HNPs, BNIPDSpm-HNP-PEG and also BNIPDSpm-HNP-PEG-c(RGDfC) were compared with different bisnaphthalamide based drugs such as BNIPDSpm and gemcitabine (Malekigorji *et al.,* 2017). According their research, in the highest concentration of HNPs (100 μgmL^{-1}) 19-23 % decrease in viability was occurred after 24 h incubation. In comparison, at 0.1 mg mL^{-1}, the cell viability of iron oxide-silver HNPs was 13% and 15% in MTT and Trypan Blue respectively. Although silver is more toxic than gold, our test results represented that the silver not effecting it and that this formulation may have benefits over hers such as antimicrobial nature as very recent studies have shown that bacteria in pancreatic tumour hinders therapy (McAllister *et al*., 2019).

Although our HNP cytotoxicity tests represented lower toxicity results than iron oxide-gold HNPs, almost same results were observed between target formulations. Previous research demonstrated that after 24h incubation of BxPC-3 cells with BNIPDSpm-HNP-PEG-c(RGDfC), the IC50 was 1.15 μgmL^{-1} by MTT cytotoxicity test (Malekigorji *et al.,* 2017). In this research, the IC_{50} for RGD was 1.18μgmL^{-1} after 24 h by MTT cytotoxicity test. The previous studies

demonstrated that silver nanoparticles play important role in increasing cancer drugs activities (Gavamukulya *et al*. 2019).

It is assumed (in relation to the drug release studies) that by increasing the particles temperature (accumulated inside the pancreatic cancer cells) via laser irradiation, drug will be released from HNP inside the cells; thus the hybrid formulations are able to kill pancreatic cancer cells in a more efficient way. In 44 ^{o}C had lower effect of HNPs on BXPC3 cell line than 60 ^{o}C. In this temperature, the cell viability of BXPC3 cell in expose of 0.1mg mL^{-1} naked HNPs was decreased for 15%, 19% and 22% at 24 h, 48 h and 72 h respectively. In comparison, the viability of BxPC-3 cells treated with target formulation (BNIPDSpm-HNP-PEG-RGD) in 44 ^{o}C was 0% after 24h ($p > 0.05$).

5.5. Conclusion

This study demonstrates the potential ability of BNIPDSpm novel formulations to accumulate and kill pancreatic cancer cells in compare with free drugs such as Gemcitabine and BNIPDSpm. However there was not significant toxicity effect with naked HNP pancreatic cancer cells. Test results has shown that increasing time and temperature are two main factors for increasing killing pancreatic cancer cells by new HNP formulations. Further research has to be performed *in vitro* and *in vivo* to fully exploit the properties of these nanoparticles for image guided thermally triggered drug delivery.

Chapter Six

General conclusions

Hybrid iron oxide-silver core-shell nanostructures (HNPs) were successfully designed, synthesised and characterised. For the synthesis of HNPs, iron oxide nanoparticles were synthesised and coated with PEI. Colloidal silver seeds were synthesised and attached electrostatically onto the Fe_3o_4-PEI forming Fe_3O_4-PEI-AgNPseed. After this, acidic silver was reduced onto the surface forming to complete coating of the HNPs. These particles were characterised by different techniques such as their magnetic properties, particle size, zeta potential, inductively coupled plasma (ICP), ultraviolet light (UV) and transmission electron microscopy (TEM). The colour was changed in each stage of iron oxide coating which can indicate the status of each step. In each step of synthesising the sample was characterised by photon correlation spectroscopy and zeta potential measurement. The surface charge constantly shifted between positive and negative between the iron oxide, silver and PEI during coating. PEI caused to shift surface charge to positive as the presence primary amine groups in the structure. The changing zeta surface charge demonstrates that the coating was successful. The particle sizes were measured in each step for checking nanoparticle size and confirming that the particle was not aggregated. The particle size was shift to smaller size as the coatings in each step reduced the aggregation of the particles. The ICP data demonstrates that iron oxide core was successfully coated with silver forming the HNPs with a ratio between Fe and Ag of 3:1. The TEM images indicated that the silver seeds were successfully anchored onto the surface of the Fe_3O_4-PEI and also that subsequent coating had been achieved. TEM image of Silver nanoparticles were indicated the size of 5nm. The TEM images demonstrated that AgNPs were not aggregated after 6 weeks from synthesising. TEM image of the fully coated Fe_3O_4-PEI coated with Ag seeds displayed unique shape and different from the iron oxide core and the size was 85 nm. According to the UV data there was no plasmon resonance appears for Fe_3O_4 and Fe_3O_4-PEI which was

expected. Ag seeds have λ_{max} of 400 nm. The Fe_3O_4-PEI-Ag seeds indicated λ_{max} shift to 450 nm which might be due to the interaction between solute and solvent or Ag shell and PEI polymer. Finally, the λ_{max} of 490 nm was observed for HNP. Ideally a laser around 490 nm may result in better heating of the particles – however caution is advised as this sits below the biological near infrared window whereby tissue is not damaged.

Silver-iron oxide HNPs demonstrates greater thermal capability in lower concentrations (25µgmL^{-1}) in comparison with gold-iron oxide HNPs which have been previously reported in the literature (Malekigorji *et al.,* 2017). The laser results demonstrate that there are significant changes between times, concentration between different HNPs in compare with the control. At concentrations of 25µgmL^{-1}, ΔT was 7 °C ± 0.35 and at 50µgmL^{-1}, ΔT was 11 °C ± 0.56 at 37 °C in 30 s. The Laser data demonstrates high increasing temperature in first 5 sec followed by a more discrete rise up to 15 s, after which a plateau was observed.

The heat dissipation analysis away from the laser culmination point was measured and analysed for different times. The heat dissipation results clearly demonstrated that there is not differ between 2 points in any concentrations or times. At 25 µgmL^{-1} and 50 µgmL^{-1}, the heat dissipation changes were not significant for 0 - 2 mm but the changes were dropped significantly from 2 mm to 10 mm. The SPR optimal wavelength of the particles was 500 nm and our HNPs observed heat generation up to 11 °C at 50 µgmL^{-1} and dissipation up to 10 mm away from radiation site for 25µgmL^{-1} (0 s and 10 s). Consequently lower concentration would be more suitable for these purposes. Not only the heating generation was not significant different with higher concentration, but the heating effect was not occurred or with a small increase (1 ^{o}C) after 10 mm for 25 µgmL^{-1}. It can decrease possibility of surrounding tissues damage.

HNPs were coated using thiolated poly (ethylene glycol) (PEG-thiol) to increase biocompatibility. The presence of and BNIPDSpm and PEG-Thiol in HNP was characterised by photon correlation spectrometer, Fourier transforms infrared spectroscopy (FTIR) and High performance liquid chromatography (HPLC). The surface charge results demonstrated that the 'naked' HNPs possessed a negative surface charge (-3.05 ± 0.29 mV) before conjugating with the drug. The surface charge shifted to positive (+32.51 ± 0.35 mV) after drug conjugation as BNIPDSpm possessed 4 amine groups. The surface charge for BNIPDSpm-HNP-PEG was positive but lower than BNIPDSpm-HNP (+18.77± 0.41 mV), indicating further modification of PEG.

FTIR were carried out for HNP, BNIPDSpm-HNP and BNIPDSpm-HNP-PEG to approve the conjugation of drugs onto the HNPs. The presences of peaks for C-H (3442 cm^{-1}), N-H stretching (2930 cm^{-1}) and N-H bending (1651 cm^{-1}) proved the presence of PEI in HNP. The FTIR Bands demonstrated the presence of aromatic in-plane C-H bending, aromatic C=C stretching, C=O (Stretching) bands and C-H (stretching) which presented the existence of BNIPDSpm-HNP and BNIPDSpm-HNP-PEG respectively. On the other hands, bigger Peak observed at 1341 cm^{-1} (C–H bending; $-CH_2$ and $-CH_3$) confirm the presence of bound PEG within BNIPDSpm -HNP- PEG formulation.

The ability of BNIPDSpm and BNIPDSpm-PEG to conjugate onto the surface of the silver HNPs, optimum drug releasing and physical and chemical drug stability were carried out by HPLC and ICP. HPLC results demonstrated that the ratio of 1:10 HNP:BNIPDSpm have highest percentage of drug conjugation. In this ratio, the percentage of drug conjugation was 90.88 %± 1.03 which means that 1 mg mL^{-1} HNP (Fe) conjugated 9 mg mL^{-1} of the drug in optimum ratio. Moreover the ratio of 1:10:10 HNP:BNIPDSpm:PEG-Thiol has highest

percentage of drug loading in compare with the other ratios. In this ratio, the percentage of drug conjugation was 94.21 %± 0.83 which mean 1mg mL^{-1} HNP (Fe) was conjugated 9.42 mg mL^{-1} of the drug in optimum ratio.

HPLC results were shown that formulation state and temperature are two important factors in the physical stability of HNP. The results were shown that solid state is more stable than liquid state. It might be due to the presence of water in in aqueous formulations, which can raise the risk of drug release from the nano-carriers. Moreover decreasing temperature can increase the stability.

The HPLC results demonstrated that increasing temperature will increase drug realising. In this case in 60 ˚C, the drug was released in deionised water at 59.22% ± 0.66 over 72 h for BNIPDSpm-HNP and also 78.31% ± 0.91 for BNIPDSpm-HNP-PEG over 72 h. Moreover reducing pH considerably increased the release rate of drug from both formulations as electrostatic interactions can be broken faster in lower pH. In fact, lower pH was broken the electrostatic interactions in NPs and can separate the drug from NPs amine groups. The HPLC data's were shown that in first 4 h the drug release rate were significantly higher than after that. In BNIPDSpm-HNP-PEG the drug completely released after 75 h at 60 ^{o}C. The drug release in BNIPDSpm-HNP and BNIPDSpm-HNP-PEG were analysed in in culture media at pH= 7.5, pH=4.6 and pH=3.6 at 20 ^{o}C, 37 ^{o}C and 44 ^{o}C and 50 ^{o}C up to 312 h to mimic cytoplasm (pHi =7.42), endosome and lysosome environment in pancreatic cancer cells, respectively. The drug release was increased with increasing temperature and decreasing pH because the electrostatic interactions in NPs were broken and can separate the drug from NPs amine groups. Moreover, drug release in BNIPDSpm-HNP-PEG was significantly higher than BNIPDSpm-HNP in culture media.

We assessed the drug release in various pH in 44 ^{o}C and 37 ^{o}C (achieved by laser irradiation). In this case, the release pattern of the formulations inside the pancreatic cancer cells, before and after laser irradiation can be predicted. In body temperature, 64% ± 1.92 of drug was release for BNIPDSpm-HNP-PEG at pH=3.6 before 312 h. Moreover, in 44 ^{o}C, 100% of drug was release in BNIPDSpm-HNP-PEG at pH=3.6 before 168 h. Therefore, it is assumed that after accumulation of the NPs in endosome and lysosome, the low environmental pH and increasing the temperature through laser irradiation, will result in quick drug release from the particles. Then the free drug can enter cells` nucleus and interact with DNA for anticancer effect.

The HNP and HNP-PEG physical stability was assessed in cell culture media during 4 weeks at pH=7.2 and pH=4.6. At pH 7.2 a maximum of 0.032% ± 0.52 of the iron concentration was observed in the media for the HNP and 0.030% ± 1.35 of Iron were released for HNP-PEG in same situation. The graph demonstrated that the results for HNP was slightly more than HNP-PEG as the matter of fact the HNP-PEG was more stable than HNP however the results was not significantly different. At pH 4.6, particle degradation was bigger than pH 7.2. At pH 4.6 an initial burst release of iron (0.034% ± 1.25) was observed in the first 24 h for HNP followed by a slow incline over the duration to a maximum of 0.065%± 1.37 and 0.066%± 0.77 for HNP and HNP- PEG respectively.

HPLC peak represented that the c(RGDfC) peptide conjugation to the HNP successfully and present and amount of drug and targeting peptide were analysed by RP-HPLC. In ratio of 1:10:10:1 HNP:BNIPDSpm:PEG-Thiol: c(RGDfC), 95.03% ± 3.25 of drug was attached into the HNP. Almost same result was observed in different ratios of RGD as well.

HPLC results demonstrate increasing time and concentration are two important factors in increasing level of drug up taking. The target formulation had the highest drug uptake in compare with free drug and HNP-BNIPDSpm and HNP-BNIPDSpm-PEG formulations. Free BNIPDSpm enters to cells through cell membrane pores/channels which are not energy dependant, but particles internalise by endocytosis, thus slower proliferation resulted in a bit less uptake of hybrid formulations compared to the Gemcitabine. However MTT cytotoxicity test and trypan blue exclusion assay on BxPC-3 cells for gemcitabine demonstrated that gemcitabine cytotoxicity is significantly higher than BNIPDSpm and new formulations.

MTT and trypan blue assays were carried out to check and compare free drugs, naked HNP and new formulations toxicity. The BXPC-3 cell viability in expose of 0.1 mg mL^{-1} naked HNP concentration was decreased to 16% and 20% of in MTT and Trypan Blue respectively after 72h. In comparison, the BXPC-3 cell viability in expose of free drug (BNIPDSpm) was decreased for 77% - 90% at concentration 0.1 mg mL^{-1} and after 72h. The IC_{50} of the free drugs was around 10, 13 and 14 times greater than HNP-BNIPDSpm, HNP-BNIPDSpm-PEG and HNP-BNIPDSpm-PEG-RGD respectively after 24h and these differences were increased with increasing time.

MTT and trypan blue tests were carried to check and compare the test results in 37 ^{o}C, 44 ^{o}C and 60 ^{o}C at 24 h, 48 h and 72 h. Test results were demonstrated that increasing time and temperatures are two main factors in increasing cytotoxicity however, the result indicated that increasing the temperature and time had no significant impact on cytotoxicity of naked HNPs in compare with free drug and the other formulations. The cell viability and IC_{50} test results illustrated that on BxPC-3 cells, Cytotoxicity of HNP-BNIPDSpm-PEG-RGD> HNP-

BNIPDSpm-PEG> HNP-BNIPDSpm > BNIPDSpm. The IC_{50} of free drug was almost 10, 14 and 15 times biger than HNP-BNIPDSpm, HNP-BNIPDSpm-PEG and HNP-BNIPDSpm-PEG-RGD respectively.

In conclusion, the HNPs conjugated with BNIPDSpm and have been presented for pancreatic cancer therapy. BNIPDSpm novel formulations have high potential to act as thermo-responsive drug carriers and could help to increase killing pancreatic cancer cells. The data indicated that the presence of PEG and RGD targeting peptide increase the ability of the BNIPDSpm-HNP to act as biocompatible multimodal platforms with higher affinity to pancreatic cancer cells as an anticancer formulation.

The aim of the thesis was preparation and evaluation of novel HNPs based silver nano structure in order to produce thermos-responsive drug carriers for pancreatic cancer therapy. Further work is required in order to fully defined the biological activity and safety of these systems first *in vitro* in terms of cellular uptake, cellular stress, degradation etc and *in vivo* particularly related to target ability, accumulation, clearance and off target effects.

Using our novel HNP in carbon nanotubes sensors structures in the future may help in the rapid detection and distinction of bacterial pathogens, early availability of information of their antimicrobial susceptibility underpin the necessity for the continued development of novel bacterial sensors. Moreover using our novel HNP in carbon nano tubes structures can led to preventing bacteria growing and development, therapeutic, and diagnostic functions. In particular, nano-carbons become high potential sensors against bacterial pathogens which have thermos-responsive drug carriers' ability for destroying them.

By considering the high potential of our HNP which has studied in this research, It also would be advantageous idea to study laser effect on our novel HNP in pancreatic tumour and explore reduced growth in xenograft mice over longer time periods to confirm the potential of the novel formulation for pharmaceutical therapies.

References

Acar, C., Garaas, S., Syud, F., Bonitatebus, P., Kulkarni, A. (2005). **Superparamagnetic nanoparticles stabilized by polymerized PEGylated coatings.** Journal of Magnetism and Magnetic Materials, Volume 293, Issue 1. pp 1-7.

Achkar, I.W., Abdulrahman, N., Al-Sulaiti, H., Joseph, J.M., Uddin, S., Mraiche, F. (2018). **Cisplatin based therapy: the role of the mitogen activated protein kinase signalling pathway**, Journal of Transl. Med, 16 (1): 94-96.

ACS, Blecher, E., Chaney-Graves, K., DeSantis, C., Edwards, B., *et al.* (2011). **Global Cancer Facts & Figures**. American Cancer Society, 2nd Edition. Atlanta.

Agnihotri, S., Mukherji, S., Mukherji,S. (2012). **Antimicrobial chitosan–PVA hydrogel as a nanoreactor and immobilizing matrix for silver nanoparticles.** Journal of Nanosci, (2): 179–188.

Agnihotri, S., Mukherji, S., Mukherji, S. (2013). **Immobilized silver nanoparticles enhance contact killing and show highest efficacy: elucidation of the mechanism of bactericidal action of silver5**, Journal of Nanoscale, 7328–7340.

Agnihotria, S., Mukherjiabc, S., Mukherji, S. (2014). **Size-controlled silver nanoparticles synthesized over the range 5–100 nm using the same protocol and their antibacterial efficacy**. Journal of RSC Advances, (4): 3974-3983.

Aguiar, JC., Mittmann, J., Ferreira, I., Ferreira-Strixino, J., Raniero, L. (2015). **Differentiation of Leishmania species by FT-IR spectroscopy, Spectrochim**. Journal of Spectrochim Acta A Mol Biomol Spectrosc, (142): 80–85.

Ahamed, M., Alsalhi, M., Siddiqui, M. (2010). **Silver nanoparticle applications and human health.** Journal of Clin Chim Acta, 411 (23), 1841–1848.

Ahlberg, S., Meinke, M.C., Werner, L., Epple, M., Diendorf, J., Blume-Peytavi, U., Lademann, J., Vogt, A., Rancan, F. (2014). **Comparison of silver nanoparticles stored under air or argon with respect to the induction of intracellular free radicals and toxic effects toward keratinocytes.** Eur. Journal of Pharm. Biopharm, 88 (3), 651–657.

Ajani, A. (2008). **Optimizing docetaxel chemotherapy in patients with cancer of the gastric and gastroesophageal junction: evolution of the docetaxel, cisplatin, and 5- fluorouracil regimen.** American Cancer Society, 113 (5): 945–955.

Ajitha, B., Ashok-Kumar-Reddy Y., Sreedhara-Reddy P. (2015). **Enhanced antimicrobial activity of silver nanoparticles with controlled particle size by pH variation**. Journal of Powder Technology, 269: 110–117

Akitake, S., Miyamoto, F., Nakamura, T., Horimatsu, Y., Ezoe, M., Muto, T., Chiba. (2011). **Early detection of 5-FU-induced acute leukoencephalopathy on diffusion-weighted MRI.** Journal of Clin Oncol, pp. 121-124, 10.1093.

Allen, S.L. & Lundberg, A.S. (2011). **Amonafide: A potential role in treating acute myeloid leukemia.** Journal of Investigational Drugs, 20(7).

Alvarez-Ordóñez, A., Mouwen, DJ., López, M., Prieto. M. (2011). **Fourier Transform InfraredSpectroscopy as a tool to characterize molecular composition and stress response infoodborne pathogenic bacteria**. Journal of Microbiol Methods, (84): 369–378.

Andersen, A.J., López, M., Prieto. M. (2016). **Nanomechanical IR spectroscopy for fast analysis of liquid dispersed engineered nanomaterials**. Journal of Sensors and Actuators B: Chemical, 233, pp.667–673.

Ansari, P., Häubl, G. (2016). **Determination of cyclopiazonic acid in white mould cheese by liquid chromatography–tandem mass spectrometry (HPLC–MS/MS) using a novel internal standard**. Journal of Food Chemistry, 211, pp.978–982.

Ansari, A., Hussain, Q. (2011). **Immobilization of kluyveromyces lactis b galactosidase on concanavalin A layered aluminium oxide nanoparticles—its future aspects in biosensor applications**. Journal of Mol Catal B Enzymatic, 70:119-126.

Ansari, A., Hussain, Q., Qayyum, S., Azam, A. (2011). **Designing and surface modification of zinc oxide nanoparticles for biomedical applications.** Journal of Food Chem Toxicol, 49:2107-2115.

Arruebo, M., Fernández-Pacheco, R., Ibarra, MR., Santamaría, J. (2007). **Magnetic nanoparticles for drug delivery.** Journal of Nanoscience Institute of Aragon, 2(3):22-32.

Arumugam, S., Muthaiah, A., Shen-Ming, C., Paramasivam, B., Mahalingam, S. (2019). **Synthesis of silver nanoparticles decorated on core-shell structured tannic acid-coated iron oxide nanospheres for excellent electrochemical detection and efficient catalytic reduction of hazardous 4-nitrophenol.** Journal of Composites Part B 162 (2019) 33–42.

Arvizo, R.R., Bhattacharyya, S., Kudgus, R.A., Giri, K., Bhattacharya R., Mukherjee, P. (2012). **Intrinsic therapeutic applications of noble metal nanoparticles: past, present and future.** Journal of Chem. Soc. Rev., (41): 2943–2970.

Asghari, S., Johari, S.A., Lee, J.H., Kim, Y.S., Jeon, Y.B., Choi, H.J., Moon, M.C., Yu, I.J. (2012). **Toxicity of various silver nanoparticles compared to silver ions in Daphnia magna.** Journal of Nanobiotechnol, 1186/1477-3155-10-14.

AshaRani, P.V, Low-Kah-Mun, G., Hande, M.P., Valiyaveettil S. (2009). **Cytotoxicity and genotoxicity of silver nanoparticles in human cells.** Journal of ACS Nano, 2009; 3(2):279–290.

Auzzas, L., Zanardi, F., Battistini, L., Burreddu, P., Carta, P., Rassu, G., Curti, C., Casiraghi, G. (2010). **Targeting αvβ3 integrin: design and applications of mono- and multifunctional RGD-based peptides and semipeptides**. Journal of Curr Med Chem, (17):1255–1299.

Avendano, C., Menendez, J.C. (2008). **Medicinal Chemistry of Anticancer Drugs, Bachrach, 2008. The early history of polyamine research.** Journal of Plant Physiology and Biochemistry, 48(7), pp.490–495.

Baik, J.M., Lee, S.J., Moskovits, M. (2009) **Polarized surface-enhanced Raman spectroscopy from molecules adsorbed in nanogaps produced by electromigration in silver nanowires.** Journal of Nano Lett, 2009; 9 (2):672–676.

Banerjee, S., Veale, E.B., Phelan, C.M., Murphy, S.A., Tocci, G.M., Gillespie, L.J., Frimannsson, Kelly, D.O., Gunnlaugsson. T. 2013). **Recent advances in the development of 1,8-naphthalimide based DNA targeting binders, anticancer and fluorescent cellular imaging agents**, Journal of Chem. Soc. Rev, (42): 1601e1618.

Barnett, C.M., Gueorguieva, M., Less, M.R., McGarvey, D.J., Darton, R.J., Hoskins, C. (2012). **Effect of the hybrid composition on the physicochemical properties and morphology of iron oxide** – Journal of nanoparticles, 14:1170.

Barnett, C., Gueorguieva, M., Lees, M., McGarvey, D., Hoskins, C. (2013). **Physical stability, biocompatibility and potential use of hybrid iron oxide-gold nanoparticles as drug carriers.** Journal of Nano Res, 15(6):1076.

Barnett, C., Lees, M., Curtis, ADM., Kong Thoo Lin, P., Cheng, P., Hoskins, C. (2013b). **Poly (allylamine) magnetomicelles for image guided drug delivery.** Journal of nanoparticles, 14:1170.

Barron, G.A. (2010). **Novel bisnaphthalimidopropyl polyamine derivatives: their mode of action in a breast cancer cell system**. Journal of *Chem. Soc. Rev, (42): 1601e1618.*

Beik, J., Khateri, M., Khosravi, Z., Kamran-Kamrava, S., Kooranifar, S., Ghaznavi, H., Shakeri-Zadeh, A. (2019). **Gold nanoparticles in combinatorial cancer therapy strategies.** Journal of Coordination Chemistry Reviews, 387 (4): 299–324.

Bhattacharjee, S. (2016). **DLS and zeta potential – What they are and what they are not?** Journal of Controlled Release, 235, pp.337–351.

Bharde, A.A., Parikh, R.Y., Baidakova, M., Jouen, S., Hannoyer, B., Enoki, T., *et al.* (2008). **Magnetic nanoparticle activated carbon.** Journal of ACS Nano, 3; 24 (11):87-94.

Bhadra, D., Bhadra, S., Jain, P. (2002). **Pegnology: a review of PEG-ylated systems**. Journal of Pharmazie, (57):5-29.

Bomatı´-Miguel, O., Mazeina, L., Navrotsky, A., VeintemillasVerdaguer, S. (2008). **Calorimetric Study of Maghemite Nanoparticles Synthesized by Laser-Induced Pyrolysis.** Journal of Chem Mater, (20): 591.

Boonkaew, B., Kempf, M., Kimble, R., Cuttle, L. (2014). **Cytotoxicity testing of silver containing burn treatments using primary and immortal skin cells.** Journal of Chem Mater 40 (8), 1562–1569.

Bois, L., Chassagneux, F., Desroches, C., Battie, Y., Destouches, N., Gilon, N., Parola S., St´ephan, O. (2010). **Electroless growth of silver nanoparticles into mesostructured silica - block copolymer films.** Journal of Langmuir, 2010, 26, 8729–8736.

Bragg, W.H., (1915). **The structure of magnetite and the spinels,** Journal of Nature (95): 515-561.

De-Wilde, R.F., Edil, B.H., Hruban, R.H. (2012). **Well-differentiated pancreatic neuroendocrine tumors: from genetics to therapy**. Journal of Nat Rev Gastroenterol Hepatol, (12): 240 -262.

Brana, M.F., Castellano, J.M., Jimenez, A., Lombart, A., Rabadan, F.P., Roldan, M.C., Santos, A., Vazquez, D. (1978). **Synthesis, cytostatic activity and mode of action of a new series of imide derivatives of 3-nitro-11a naphthalic acid.** Journal of Current Chemother, (2): 1216-1217.

Brana, MF., Castellano, JM., Moran, M., Perea de vega, MJ., Qjan, XD., Romerdahl, CA., Keilhauer, G. (1995). **Bisnaphthalimides. 2. Synthesis and Biological Activity of 5, 6-**

acenaphthalimidoalkyl-1, 8-naphthalimidoalkyl amines. Journal of Medicinal Chemistry, 30:235-239.

Brana, MF., Castellano, JM., Roldán, CM., Santos, A., Vázquez, D., Jiménez, A. (1980). **Cancer Chemotherapy and Pharmacology**. Journal of Front Pharmacol, (4): 61-66

Brana, M.F. & Ramos, A. (2001). **Naphthalimides as Anticancer Agents: Synthesis and Biological Activity.** Journal of Current Medicinal Chemistry -Anti-Cancer Agents, 1(3), pp.237–255

Brazzale, C., Canaparo, R., Racca, L., Foglietta, F., Durando, G., Fantozzi, R,. Caliceti, P., Salmaso, S., Serpe, L. (2016). **Treatment by targeted gold nanoparticles as ultrasound sensitizers for the treatment of cancer.** Journal of Nanomedicine, 12 (2016) 3053–3070.

Bose, M., Wui. E.(2013). **Convolution and validation of in vitro-in vivo correlation of waterinsoluble sustained-release drug (domperidone) by first-order pharmacokinetic onecompartmental model fitting equation**. Europian Journal of Drug Metab Pharmacokinet, 38(3):191-200.

Boss, B., Fredeen J. (1997), **Instrumentation and Techniques in Inductively Coupled Plasma Optical Emission Spectrometry**, Journal of the Perkin-Elmer Corporation, 115:11147-11190.

Browning, L., Lee, K., Nallathamby, P., Xu, X.-H.N. (2013). **Silver nanoparticles incite size- and dose-dependent developmental phenotypes and nanotoxicity in zebrafish embryos.** Journal of Chem. Res. Toxicol, 26, 1503–1513.

Bulte, J.W.M., Douglas, T., Witwer,B. *et al.* (2001). **Magnetodendrimers allow endosomal magnetic labeling and in vivo tracking of stem cells.** Journal of Nature Biotechnol, 19: 1141-1147.

Cabrera, L., Gutierrez, S., Menendezb, N., Morales, M.P., Herrasti, P. (2008). **Magnetic Iron Oxide Nanoparticles: Synthesis and Surface Functionalization Strategies.** Journal of Electrochim Acta, 53, 3436.

Cai, H., Conti, PS. (2013). **RGD-based PET tracers for imaging receptor integrin alphav beta3 expression.** Journal of Labelled Comp Rad, 56 (5), pp. 264-279.

Cai, W., Gao, T., Hong, H., Sun, J. (2008). **Applications of gold nanoparticles in cancer nanotechnology.** Journal of Nanotechnology, Science and Applications, 1:17-32.

Campos, PS., Praça, FS., Bentley, MV. (2016). **Quantification of lipoic acid from skin samples by HPLC using ultraviolet, electrochemical and evaporative light scattering detectors.** Journal of Chromatography B, 1019, pp.66–71.

Cardot, JM., Beyssac, E., Alric, M. (2007). **In Vitro–In Vivo Correlation: Importance of dissolution in IVIVC**. Journal of Dissolution Technologies, 15-19.

Carmichael, J., DeGraff, WG., Gazdar, AF., Minna, JD., Mitchell, JB. (1987). **Evaluation of a tetrazolium-based Semiautomated Colorimetrie Assay: Assessment of Chemosensitivity testing**. Journal of Cancer research, 47:936-942.

Casadei, R. *et al*. (2015**). Neoadjuvant Chemoradiotherapy and Surgery Versus Surgery Alone in Resectable Pancreatic Cancer: A Single-Center Prospective, Randomized,**

Controlled Trial Which Failed to Achieve Accrual Targets. Journal of Gastrointestinal Surgery, 19(10), pp.1802–1812.

Caswell, K.K., Bender, C.M., Murphy, C.J. (2003). **Seedless, surfactantless wet chemical synthesis of silver nanowires.** Journal of Nano Lett, 2003, 3, 667–669.

Cembrowski, S., Clarke, G. (2015). **Quality Control of Automated Cell Counters.** Journal of Clin Lab Med, 35(1): 59-71.

Chairuangkitti, P., Lawanprasert, S., Roytrakul, S., Aueviriyavit, S., Phummiratch, D., Kulthong, K., Chanvorachote, P., Maniratanachote, R., (2013). **Silver nanoparticles induce toxicity in A549 cells via ROS-dependent and ROS-independent pathways.** Journal of Toxicol in Vitro, 27 (1), 330–338.

Chakra, P., Joshi, Megalamane, S., Bootharaj, u., Alhilaly Osman, M. (2015). **The Golden and Silver Nanoparticle.** Journal of the American Chemical Society, Volume 16, 625-631.

Chakravarty, R., Chakraborty, S., Dash, A. (2015). **Molecular imaging of breast cancer: role of RGD peptides.** Journal of Mini Rev Med Chem, 15 (13), pp. 1073-1094.

Chakraborty, S., Rahman, T. (2012). **The difficulties in cancer treatment.** Journal of cancer medical science, 14; 6: ed16.

Chen, D.X., Sanchez, A., Taboada, E., Roig, A., Sun, N., GuChen, H.C. (2009). **Size determination of superparamagnetic nanoparticles from magnetization curve.** Journal of Appl. Phys, 105 (2009) 083924.

Cheng, Y., and Yuanhui, Y. (2018). **RGD-modified polymer and liposome nano vehicles: Recent research progress for drug delivery in cancer therapeutics**. Journal of Eur J Pharm Sci, 1(128): 8-17.

Chen, H., *et al.,* (2014). **A novel brain targeted 5-fU derivative with potential antitumor efficiency and decreased acute toxicity: synthesis, in vitro and in vivo evaluation**. Journal of Pharmazie, 69 (4): 271–276.

Chen, Y., Gao, N., Jiang, J. (2013). **Surface matters: enhanced bactericidal property of core–shell Ag–Fe2O3 nanostructures to their heteromer counterparts from one-pot synthesis**. Journal of PubMed, 11; 9 (19): 3242-6.

Chi-San, C., Wu, E. (1995). **Handbook of Size Exclusion Chromatography, Chrom.** Journal of Science Series, Marcel Dekker, New York, Volume 6, 128.

Christopher, P., Linic, S. (2008). **Engineering selectivity in heterogeneous catalysis: Ag nanowires as selective ethylene epoxidation catalysts.** Journal of Am Chem Soc, 130(34):11264–11265.

Claus, P., Hofmeister, H., Phys, J. (1999). **Electron Microscopy and Catalytic Study of Silver Catalysts: Structure Sensitivity of the Hydrogenation of Crotonaldehyde.** Journal of Chem, (10): 2766–2775.

Comfort, K.K., Maurer, E.I., Hussain, S.M., (2014)**. Slow release of ions from internalized silver nanoparticles modifies the epidermal growth factor signalling response.** Journal of Colloid Surface B, 123, 136–142.

Comoucka, J., Drbohlavova, J., Huska, D., Adam, V., Kizek, R., Hubalek, J. (2010). **Magnetic Nanoparticles and Targeted Drug Delivering.** Journal of Pharmacol Res, 62:144-149.

Compagnini, G., Pignataro, B., Pelligra, B. (1997). **Nanomorphology and SERS activity in plasma prepared silver,** Journal of Chem. Phys. Lett, 272 (1): 453–458.

Costanza, M.E., Berry, D., Henderson, I.C., Ratain, M., Wu, K., Shapiro, C., Duggan, D., Kalra, J., Berkowitz, I., Lyss, A.P. (1995). **Amonafide: an active agent in the treatment of previously untreated advanced breast cancerda cancer andleukemia group B study.** Journal of Clin Cancer Res, (7):699-704.

Corot C, et al. (2004). **Nanomedicine in Drug Delivery**. Journal of Radiol Invest, 39(10):619.

Cortajarena, AL., Ortega, D., Ocampo, SM., Gonzalez-García,A., Couleaud, P., Miranda, R., Belda-Iniesta, C., Ayuso-Sacido, A. (2014). **Engineering Iron Oxide Nanoparticles for Clinical Settings.** Journal of Nanobiomedicine, DOI: 10.5772/58841.

Creighton, J.A., Blatchford, C.G., and Albrecht, M.G. (1979). **Plasma resonance enhancement of Raman scattering by pyridine adsorbed on silver or gold sol particles of size comparable to the excitation wavelength** Journal of Faraday Trans, 2, 1979, 75, 790–798.

Cunha, A.S., Rault, A., Laurent, C., Adhoute, X., Vendrely, V., Bellannee, G., Brunet, R., Collet, D., Masson, B. (2005). **Surgical resection after radiochemotherapy in patients with unresectable adenocarcinoma of the pancreas.** Journal of Am Coll Surg, 201(3):359-365.

Curtis, A., Malekigorji, M., Holman, J., Skidmore, M., Hoskins, C. (2015), **Heat Dissipation of Hybrid Iron Oxide-Gold Nanoparticles in an Agar Phantom**. Journal of Nanomed Nanotechnol, Volume 6, Issue 6.

Czaplicki. C. (2012). **Chromatography in Bioactivity Analysis of Compounds.** Journal of Nanobiomedicine, DOI: 10.5772/55620.

Dai, C.H. , Chen, P., Li, J., Lan, T., Chen, Y.C., Qian, H., Chen, K., Li, M.Y. (2016) **Co-inhibition of pol θ and HR genes efficiently synergize with cisplatin to suppress cisplatinresistant lung cancer cells survival**, Journal of Oncotarget, 7 (40): 65157–65170.

Dall'Angelo, S., Zhang, Q., Fleming, IN., Piras, M., Schweiger, LF., Hagan, D., Matteo Zandaa, M. (2018). **Efficient bio conjugation of 5-Fluoro-5-Deoxy-Ribose (FDR) to RGD Peptides for Positron Emission Tomography (PET).** Journal of Org Biomol Chem, 11(27): 4551-8.

Dance, AM., Ralton, L., Fuller, Z., Milne, L., Duthie, S., Bestwick, CS., Lin, PK. (2005). **Synthesis and biological activities of bisnaphthalimido polyamines derivatives: cytotoxicity, DNA binding, DNA damage and drug localization in breast cancer MCF 7 cells.** Journal of Biochem Pharmacol, 169(1):19-27.

Danilcauk, M., Lund, A., Saldo, J., Yamada, H., Michalik, J. (2006). **Conduction electron spin resonance of small silver particles.** Journal of Spectrochimaca. Part A. 2006, 63: 189–191. 10.1016/j.saa.2005.05.002

Denardo, RK. (1998). **The next frontier of molecular medicine: delivery of therapeutics**. Journal of Nat Med, 4: 655-657.

Díaz, M.R., Vivas-Mejia, P.E. (2013) **Nanoparticles as drug delivery systems in cancer medicine: emphasis on RNAi-containing nanoliposomes.** Journal of Pharmaceuticals, 6(11): 1361-1380.

Dictor, R.A., Bell, A.T. (1986). **Fischer–Tropsch synthesis over reduced and unreduced dironoxide catalysts.** Journal of Catal, (97): 121–136.

Dilnawaz, F., Singh, A., Mohanty, C., Sahoo, S.K., (2010). **Dual drug loaded superparamagnetic iron oxide nanoparticles for targeted cancer therapy,** Journal of ACS Nano**,** 31 (2): 3694–3706.

Doria, G., Conde, J., Veigas, B., Giestas, L., Almeida, C. (2012). **Noble metal nanoparticles for biosensing applications.** Journal of Sensors, 12(2): 1657-1687.

Dost, K., Ideli, C. (2012). **Determination of polycyclic aromatic hydrocarbons in edible oils and barbecued food by HPLC/UV–Vis detection**. Journal of Food Chemistry, 133(1), pp.193–199.

Dreaden, E.C., Alkilany, A.M., Huang, X., Murphy, C.J., El-Sayed, M.A., (2012). **The golden age: gold nanoparticles for biomedicine.** Journal of Chem. Soc. Rev, 41 (2012) 2740–2779.

Dreaden, E.C., Mwakwari, S.C., Sodji, Q.H., Oyelere, A.K., El-Sayed, M.A. (2009**). Tamoxifen poly (ethylene glycol)-thiol gold nanoparticle conjugates: enhanced potency and selective delivery for breast cancer treatment.** Journal of Bioconjugate Chem, (20): 2247.

Durgadas, C.V., Kaladhar, K., Divya, P., Sreenivasan, K., Sharma, C.P. (2010). **Preliminary Studies on Blood Compatibility and Langmuir Monolayer Stability of Gold Nanoparticles**

Stabilized Through Amino-PEG Functionality. Journal of Trends Biomater Artificial Organs, (23): 203-210.

Duval, K., Grover, L., Li-Hsin Han, LH., Mou, Y., Pegoraro, AF., Fredberg, J., Modeling, J. (2017). **Physiological Events in 2D vs. 3D Cell Culture.** Journal of Physiology (Bethesda), 32(4):266-277.

Edelman R.D, (1996). *et al.* **MRI: Clinical Magnetic Resonance Imaging.** Journal of Philadelphia, Pennsylvania, p. 1150.

Elechiguerra, J.L., Burt, J.L., Morones, J.R., Bragado, A.C., Gao, X., Lara, H.H., Yacaman, M.J. (2005). **Interaction of silver nanoparticles with HIV-1.** Journal of Nano biotechnol, 3 (23): 6–12.

Eugênia, M., Brollo, F., López-Ruiz, R., Muraca, D., Figueroa, S.J.A., Kleber, R., Knobel, P.M. (2014). **Compact Ag-Fe3O4 Core-shell Nanoparticles by Means of Single-step Thermal decomposition Reaction.** Journal of Scientific Reports volume, 4, Article number: 6839 (2014).

Fang, Y., Zhang, C., Wu, T., Wang, Q., Liu, J., Dai, P. (2017). **Transcriptome sequencing reveals key pathways and genes associated with cisplatin resistance in lung adenocarcinoma A549 cells,** Journal of PLoS One, 12 (1) 170-209.

Farias, S., Smichowski, P. (1999). **Determination of germanium at trace levels in environmental matrices by chloride generation-inductively coupled plasma atomic emission spectrometry.** Journal of Analytical Atomic Spectrometry, 14(5): 809-814 ·

Ferrari, M., Wang, P., Yoo, B. (2005). **Cancer nanotechnology: opportunities and challenges.** Journal of Nat Rev Cancer, 5:161-171.

Fernández-López, C., Mateo-Mateo, C., Alvarez-Puebla, R., Pérez-Juste, J., Pastoriza- Santos, I., Liz-Marzán, L. (2009). **Highly controlled silica coating of PEG-capped metal nanoparticles and preparation of SERS-encoded particles.** Journal of Langmuir, 25, 13894–13899.

Ferrone, C.R., *et al.* (2012). **Pancreatic ductal adenocarcinoma: long-term survival does not equal cure.** Journal of Surgery, 152(3 Suppl 1), pp.S43-9.

Feynman, R. (1959). **Engineering and Science. California Institute of Technology**, Journal of American Physical Society, (67): 47-84.

Filosa, R., Peduto, A., Micco, SD., Caprariis, P., Festa, M., Petrella, A., Capranico, G., Bifulco, G. (2009). **Molecular modelling studies, synthesis and biological activity of a series of novel bisnaphthalimides and their development as new DNA topoisomerase II inhibitors**. Journal of Bioorg Med Chem, (17): pp.13-24.

Foldbjerg, R., Irving, E., Hayashi, Y., Sutherland, D., Thorsen, K., Autrup, H., Beer, C. (2012). **Global gene expression profiling of human lung epithelial cells after exposure to nanosilver.** Journal of Toxicol, Sci, 130, 145–157.

Felder, T.B., McLean, M.A., Vestal, M.L., Lu, K., Farquhar, D., Legha, S.S., Shah, R., Newman, R.A. (1987). **Pharmacokinetics and metabolism of the antitumor drug amo-nafide (NSC 308847) in humans.** Journal of Drug Metab Dispos, (15): 773e778.

Frankel, R.B., Blakemore, R., Wolfe, R.S. (1979). **Magnetite in fresh water magnetotactic bacteria.** Journal of Science, (203): 1355–1356.

Galluzzi, L., Senovilla, L., Vitale, I., Michels, J., Martins,I., Kepp,O., Castedo, M., Kroemer, G. (2012). **Molecular mechanisms of cisplatin resistance**. Journal of Oncogene, 31 (15) (2012) 1869–1883.

Galluzzi, L., Vitale, I., Michels, J., Brenner, C., Szabadkai, G., Harel-Bellan, A., Castedo, M., Kroemer, G. (2014). **Systems biology of cisplatin resistance: past, present and future.** Journal of Cell Death Dis, 5 (2014) e1257.

Gavamukulya, Y., Esther, E., Maina, A., Amos, H., Meroka, G., Hany, A. et al. (2019). **In search of new anticancer drugs: Data for cytotoxic activities of green synthesized silver nanoparticles from ethanolic extracts of fruits and leaves of Annona muricata and 5-Fluorouracil against HeLa, PC3 and PNT1A cell lines**. Journal of Oncogene, 31 (15) (2012) 1869–1883.

Ghaznavi, H., Hosseini-Nami, S., Kamrava, S.K., Irajirad, R., Maleki, S., Shakeri- Zadeh, A., Montazerabadi, A. (2018). **Folic acid conjugated PEG coated gold-iron oxide core-shell nanocomplex as a potential agent for targeted photothermal therapy of cancer.** Journal of Cells Nanomed Biotechnol, 46 (20): 1594– 1604.

Gellerman, G. (2016). **Recent developments in the synthesis and applications of anticancer amonafide derivatives, A Mini Review**. Journal of Lett Drug Des. Discov, (13): 47e63.

Ghosh, P., Han, G., De, M., Kim, C.K., Rotello, V.M. (2008). **Gold nanoparticles in delivery applications.** Journal of Adv. Drug Deliv, (60): 1307–1315.

Gliga, A., Skoglund, S., Odnevall-Wallinder, I., Fadeel, B., Karlsson, H. (2014). **Sizedependent cytotoxicity of silver nanoparticles in human lung cells: the role of cellular uptake, agglomeration and Ag release.** Journal of Part Fibre Toxicol, 11 (11), 11–17.

Goon, I.Y., Lai, L.M.H., Lim, M., Munroe, P., Gooding, J.J., Amal, R. (2009). **Fabrication of goldshell-protected magnetite nanoparticles: systematic control using polyethyleneimine**. Journal of ChemMater, 21:673-681.

Granqvist, C.G, Buhrman, R.A., (1976). **Ultrafine metal particles.** Journal of applied Physics, 10 (47): 2200-2219.

Grosse, S., Evje, L., Syversen, T. (2013). **Silver nanoparticle-induced cytotoxicity in rat brain endothelial cell culture.** Journal of Toxicol *in Vitro*, 27, 305–313.

Guia-Christopher, P., Juliena, Suehyb, G., *et al*. (2019). **An indolent pancreatic ductal adenocarcinoma with psammoma bodies and a coincidental neuroendocrine tumor.** Journal of Human Pathology: Case Reports, Volume 16, 100286.

Gunawan, P., Guan, C., Song, X., Zhang, Q., Leong, S.S.J., Tang,C., Chen, Y., Chan-park, M.B., Chang, M.W., Wang, K., and Xu, R. (2011). **Nanoscale Materials in Water Purification.** Journal of ACS Nano, (5): 10033–10040.

Gurunathan, S., Han, J.W., Eppakayala, V., Jeyaraj, M., Kim, J.H. (2013) **Cytotoxicity of biologically synthesized silver nanoparticles in MDA-MB-231 human breast cancer cells.** Journal of Biotechnology Reports, Volume 4, Pages 42-49.

Haberl, N., Hirn, S., Wenk, A., Diendorf, J., Epple, M., Johnston, B., Krombach, F., Kreyling, W., Schleh, C. (2013). **Cytotoxic and proinflammatory effects of PVP- coated silver nanoparticles after intratracheal instillation in rats.** Journal of Nanotechnol, 4 (1): 933–940.

Haddad P.R, Jackson P.E. (1990). **Ion Chromatography. Principles and Applications, J. Chromatogr**. Journal of Libr, Volume 46, Elsevier, Amsterdam.

Harish-Kumar, K., Nagasamy, V., Himangshu, B., and Anuttam, K. (2018). **Metallic Nanoparticle.** Department of Pharmaceutics, A Constituent College of JSS University, India, Volume 4, Issue 2, 258-259.

Hema, S., Vijayalakshmi, N., Srilatha, KP. (2009). **High performance liquid chromatography and its role in identification of mycobacteriae: An overview**. Journal of NTI Bulletin, Volume 45, 1-4.

Heinig, U., Scholz, S., Jennewein, S. (2013). **Getting to the bottom of Taxol biosynthesis byfungi.** Journal of Fungal Divers, 60: 161–70.

Her, S., Jaffray, D.A., Allen, C. (2017). **Gold nanoparticles for applications in cancer radiotherapy: Mechanisms and recent advancements.** Journal of Drug Delivery, (10): 84–101.

Hornyak, G.L., Moore, J.J., Tibbals, H.F., Dutta, J. (2008). **Nanoscience- Fundamentals of Nanotechnology.** Journal of CRC Press, 211 (22): 258-300.

Hoskins, C., Cuschieri, A., Wang, L. (2012a). **Cytotoxicity of polycationic iron oxide nanoparticles: Common endpoint assays and alternative approaches for improved understanding of cellular response mechanism**. Journal of Nanobiotechnol, (22): 128-130.

Hoskins, C., Min, Y., Gueorguieva, M., McDougall, C., Volovick, A., Prentice, P., Wang, Z., Melzer, A., Cuschieri, A., Wang, L. (2012b). **Hybrid gold-iron oxide nanoparticles as a multifunctional platform for biomedical application**. Journal of Nanobiotechnology, 60: 61–63.

Hoskins, C., Ouaissi, M., Lima, SC., Cheng, WP., Loureirio, I., et al. (2010). **In vitro and in vivo anticancer activity of a novel nano-sized formulation based on self-assembling polymers against pancreatic cancer**. Journal of Pharm Res, 27(12):2694-2703.

Hoskins, C., Wang, L., Cheng, WP., Cuschieri, A. (2012c). **Dilemmas in the reliable estimation of the in-vitro cell viability in magnetic nanoparticle engineering: which tests and what protocols?** Journal of Nanoscale Res Letts, 7:77.

Hou, X., Jones, B. (2000). **Inductively Coupled Plasma/Optical Emission Spectrometry.** Journal of Encyclopedia of Analytical Chemistry, (11): 9468-9485.

Hua, M., Zhang, S., Pan, B., Zhang, W., Zhang, L. (2012). **Heavy metal removal from water/waste water by Nano sized metal oxides.** Journal of Hazardous Materials, Volumes 211–212, Pages 317-331

Hu, J., Chen, G., Lo, I. (2006). **Selective removal of heavymetals from industrial Waste water using magnetite nanoparticle: performance and mechanisms.** Journal of Environmental Engineering, 709–715.

Hu, J., Zhou, S., Sun, Y., Fang, X., Wu, L. (2012). **Fabrication, properties and applications of Janus particles.** Journal of Chemical Society Reviews, (41):4356–4378.

Hu, Y., Zhu, Q.N., Deng, J.L., Li, Z.X., Wang, G., Zhu, Y.S. (2018). **Emerging role of long noncoding RNAs in cisplatin resistance.** Journal of Onco Targets Ther, (11): 3185–3194.

Hwang, G., Varner. H. (2004). **The role of integrins in tumor angiogenesis**. Journal of Hematol Oncol Clin North Am, (18):991-1006.

Isabella, P., Zunino, Z., Capranico. G. (1995). **Base sequence determinants of amonafide stimulation of topoisomerase II DNA cleavage.** Journal of Nucleic Acids Res, (23): 223e229.

Ingrassia, l., Lefranc, F., Kiss, R., Mijatovic, T. (2009). **Naphthalimides and azonafides as promising anti-cancer agents**. Journal of Curr Med Chem, (16): 1192e1213.

Jain, S., Hirst, D.G., O'Sullivan, J.M., (2012). **Gold nanoparticles as novel agents for cancer therapy.** Journal of Radiol, 85(1010):101-113.

Jared, L., Anderson, A., Berthod, A., Estévez, V. (2015), **Analytical Separation Science.** Journal of Wiley-VCH Verlag GmbH & Co. KGaA.

Jau-Rung, C., Bo-Hung, L., Kai-Chih, H., Dong-Hwang, C. (2013). **One-pot green synthesis of silver/iron oxide composite nanoparticles for 4-nitrophenol reduction.** Journal of Hazardous Materials, Volumes 248–249, Pages 394-400.

Jawahar, N., & Meyyanathan, S.N. (2012). **Polymeric nanoparticles for drug delivery and targeting.** International Journal of Health & Allied Sciences, 1 (4): PP.217-223.

Jelveh, S., Chithrani, DB. (2011). **Gold Nanostructures as a Platform for Combinational therapy in Future Cancer Therapeutics.** Journal of Cancers, 3(1):1081-1110.

Jemal, A., Siegel, R., Ward, E., Murray, T., X.u., J., Thun, M.J. (2007). **Cancer statistics,** Journal of Cancer Clin, 57: 43–66.

Jeanbart, L., Ballester, M., de Titta, A., Corthésy, P., Romero, P., Hubbell, JA., Swartz, MA. (2014). **Enhancing efficacy of anticancer vaccines by targeted delivery to tumor-draining lymph nodes**. Journal of Cancer Immunol Res, 2(5):436-447.

Jianga, k., Huaixiang, Z., Chao, N., Xiaoge, H., Yiping, M., Dongsheng, H., Liu, Y.B. (2019). **Immunotherapy in pancreatic cancer: New hope or mission impossible.** Journal of Cancer Letters, Volume 445, Pages 57-64.

Jin, L., Chun,J., Pan,C., Li, D., Lin,R., Alesi,G.N., Wang,X., Kang, H.B., Song,L., Wang, D., Zhang,G., Fan, J., Boggon, T.J., Zhou, L., Kowalski, J., Qu, C.K., Steuer, C.E., Chen, G.Z., Saba,N.F., Boise,L.H., Owonikoko, T.K., Khuri,F.R., Magliocca,K.R., Shin, D.M., Lonial, S. Kang, S. (2018). **MAST1 drives cisplatin resistance in human cancers by rewiring cRaf-Independent MEK activation,** Journal of Cancer Cell, 34 (2) (2018) 315–330 e7.

Jin, ZH., Razkin, J., Josserand, V., Boturyn, D., Grichine, A., Texier, I., Favrot, MC., Dumy, P., Coll, JL. (2007). **In Vivo Noninvasive Optical Imaging of Receptor-Mediated RGD Internalization Using Self-Quenched Cy5-Labeled RAFT-c(-RGDfK-)4**. Journal of Molecular Imaging, 6(1):43-55.

Ji, S., Xu, J., Zhang, B., Yao, W., Xu, W., Wu, W., Xu, Wang, H., Ni, Q., Hou, H., Yu, H. (2012). **RGD-conjugated albumin nanoparticles as a novel delivery vehicle in pancreatic cancer therapy**. Journal of Cancer Biol Ther, 13(4): 206-15.

Jokerst, J., Lobovkina, T., Gambhir, S.S. (2011). **Nanoparticle PEGylation for imaging and therapy.** Journal of Nanomedicine (Lond), 6(4):715-728.

, John F., Carpenter , Anette Schneemann. (2009). **Preface to nanotechnology special issue of journal of microbiological methods.** Journal of Microbiological Methods. Volume 167, December 2009, 105744

Joyce, J., Sung, Neha N., Pardeshi, Anke M., Mulder, Sean K., Mulligan, Joel Quispe, Kathy On, Bridget Carragher, Clinton S., Potter, John F., Carpenter , Anette Schneemann. (2015), **Transmission electron microscopy as an orthogonal method to characterize protein aggregates**, Journal of Pharm Sci, Volume 104, Issue 2, 750–759.

Kamal, A., Bolla, N.R., Srikanth, P.S., Srivastava, A.K. (2013). **Naphthalimide derivatives with therapeutic characteristics: a patent review.** Journal of Opin Ther Pat, (23): 299e317.

Kang, H. *et al.* (2015). **Synergistic antiviral activity of gemcitabine and ribavirin against enteroviruses.** Journal of Antiviral Research, (124): pp.1–10.

Kalishwaralal, K., Barath-Mani-Kanth, S., Pandian, S.R.K., Deepak, V., Gurunathan, S. (2010). **Silver nano – a trove for retinal therapies.** Journal of Control Release, 145(2):76–90.

Kalska-Szostko, B., Kropniewicka, K. (2012). **The influence of the transition metal substitution on chemically prepared ferrite nanoparticles.** Journal of Mossbauer studies, Curr. Appl. Phys, (12): 869–902.

Kalska, B., Paggel, J.J., Fumagalli, P., Rybczynski, J., Satula, D., Hilgendorff, M., Giersig, M. (2004). **Magnetite particles studied by Mossbauer and magneto-optical Kerr effect**. Journal of Appl. Phys, 95 (3): 1343–1350.

Kalska-Szostko, B., Wykowska, U., Satuła, D. (2014). **Core–shell and multi-layered magnetic nanoparticles.** Journal of Appl. Surf. Sci, 306: 7–15.

Kang, H., Chen, S.,*et al.* (2018). **Magnesium lithospermate B loaded PEGylated solid lipid nanoparticles for improved oral bioavailability**. Journal of Colloids Surf. B Biointerfaces, 161 (2018), pp. 597-605

Kapildeva, G., Manickavasagama, M., Thajuddinb, N., Premkumarc, K., Ganapathi, A. (2013). **Biogenic silver nanoparticles for cancer treatment.** Journal of experimental report, Colloids and Surfaces Biointerfaces, 106 (3): 86–92.

Kardys, AY., Bharali, DJ., Mousa, SA. (2013). **Amino-Functionalized Silica Nanoparticles: In vitro evaluation for targeted delivery and therapy of Pancreatic cancer**. Journal of Nanotechnology, Article ID 768724, 8 pages.

Kasuya, K., Tsuchida, A., Nagakawa, Y., Suzuki, Y., Suzuki, M., Aoki, T., Abe, Y., Shimazu, M., Itoi, T., Sofuni. A. (2012). **Prediction of a side effect and efficacy of adjuvant chemotherapy with gemcitabine for post-operative patient of pancreatic cancer by a genetic polymorphism analysis**. Journal of Hepato-Gastroenterology, 59, pp. 1609-1613

Khan, A.K., Rashid, R., Murtaza, G., Zahra, A. (2014). **Gold Nanoparticles: Synthesis and Applications in Drug Delivery.** Journal of Tropical J Pharmaceutical Research, 13(7):1169-1177.

Khana, S., Setuaa, S., Kumaria, S., Dana, N., Masseya, A., Hafeeza, B.B., Yallapua, M.M., Stilesa, Z.E., Alabkaaa, A., Yueb, J., Ganjua, A., Behrmanc, S., Jaggia, M., Chauhana, S.C.

(2019). **Superparamagnetic iron oxide nanoparticles of curcumin enhance gemcitabine therapeutic response in pancreatic cancer.** Journal of Biomaterials, (20): 83–97.

Khande, P., Kumar-Shahi, S. (2016). **Microbes mediated synthesis of metal nanoparticles: current status and future prospects.** Biosynthesis of metallic nanoparticle, (23): 5243–5249.

Khare, V. *et al*. (2016). **Long-circulatory nanoparticles for gemcitabine delivery: Development and investigation of pharmacokinetics and in-vivo anticancer efficacy.** European Journal of Pharmaceutical Sciences, 92, pp.183–193.

Kholoud, M.M., El-NouraAla'a E., Al-Warthanb, R., Ammarb, A.A. (2010). **Synthesis and applications of silver nanoparticles**. Arabian Journal of Chemistry, 3, 135–140.

Kim, T.H., Kim, M., Park, H.S., Shin, U.S., Gong, M.S., Kim, H.W. (2012). **Size-dependent cellular toxicity of silver nanoparticles.** Journal of Biomed. Mater, 100A, 1033–1043.

Kirschvink, J.L., Kobayashi-Kirschvink, A., Woodford, B.J. (1992) **Magnetite bromine realization in the human brain.** Journal of Natl Acad Sci U S A, 89(16): 7683–7687.

Kishkinev, D.A., Chernetsov, N.S., (2015). **Magnetoreception systems in birds: areview of current research**. Journal of Biol. Bull. Rev, 5 (2015) 46–62.

Knox, J.J., Hedley, D., Oza, A., Feld, R., Siu, L.L., Chen, E. (2005). **Nematollahi, M., Pond, G.R., Zhang, J., and Moore, M.J., Combining Gemcitabine and Capecitabine in Patients With Advanced Biliary Cancer.** Journal of clinical Oncology, Volume 23, number 10, 121 131.

Konwarh, R., Karak, N., Rai, S.K., Mukherjee, A.K. (2009). **Polymer-assisted iron oxide magnetic nanoparticle immobilized keratinase.** Journal of Nanotechnology, (20): 107-225.

Krklješ, k., Nedeljković, J.M., Kačarević-Popović, Z.M. (2007). **Fabrication of Ag-PVA hydrogel nanocomposite by γ-irradiation.** Journal of Polymer Bulletin, (58):271–279.

Ku, M., Yan, I., Wang, R., Sun, I., Yang, W. (2010). T**he blood– brain barrier penetration and distribution of PEGylated fluorescein-doped magnetic silica nanoparticles in rat brain.** Journal of Biochem Bioph Res Co, 394:871-876.

Kumagai, M., Sarma, T.K., Cabral, H., Kaida, S., Sekino, M., Herlambang, N., Osada, K., Kano, M.R., Nishiyama, N., Kataoka, K. (2010). **Enhanced in vivo Magnetic Resonance Imaging of Tumors by PEGylated Iron-Oxide–Gold Core–Shell Nanoparticles with Prolonged Blood Circulation Properties.** Journal of Macromol Rapid Commun, (17): pp1521-1528.

Lamprecht, G., Torres, H., Schäfer, K. (2000). **Biodegradable microparticles as a two-drug controlled release formulation: a potential treatment of inflammatory bowel disease.** Journal of Controlled Release, 69:445-454.

Lee, K.S., El-Sayed, M.A. (2006). **Gold and silver nanoparticles in sensing and imaging: sensitivity of plasmon response to size, shape, and metal composition.** Journal of Phys Chem B, 2006; 110 (39): 19220–19225.

Lee, S.H., Kim, H.T. (2016). **Reliability of thermal conductivity measurement of liquids by using transient hot-wire, photon-correlation spectroscopy and the laser flash method.** Korean Journal of Physical Society, 68(10):1145-1155.

Li, C., Shuford, K.L., Park, Q., Cai, W., Li, Y., *et al*. (2007) **High-Yield Synthesis of Single-Crystalline Gold Nano-octahedra.** Journal of Angewandte Chemie, 46(18): 3264-3268.

Lin, k.t., Pavlov. V.A. (2000). **The synthesis and in vitro cytotoxic studies of novel bis-naphthal-imidopropyl polyamine derivatives, Bioorg**. Journal of Med Chem Lett, (10): 1609–1611.

Lindenberg, M., Kopp, S., Dressman, JB. (2004). **Classification of orally administered drugs on the World Health Organization Model list of Essential Medicines according to the bio pharmaceutics classification system**. Europian Journal of Pharm Biopharm, 58(2):265-78.

Tennant, JR. (1964). **Evaluation of the trypan blue technique for determination of cell viability**. Journal of Transplantation, 2:685-694.

Liu, Y., Shipton, M.K., Ryan, J., Kaufman, E.D., Franzen, S., Feldheim, D.L. (2007). **Synthesis, stability, and cellular internalization of gold nanoparticles containing mixed peptide-poly(ethylene glycol) monolayers.** Journal of Anal Chem, (79):2221.

Li, Z., Li, Y., Qian, X.F., Yin, J., Zhu, Z.K. (2005). **Nanotubes and NanowiresAppl**. Journal of Surf Sci, (39): 109–116.

Lockhart, A.C., Rothenberg, M.L., Berlin, J.D. (2005). **Treatment for pancreatic cancer: current therapy and continued progress.** Journal of Gastroenterology, 128(6):1642-1654.

Lok, C.N., Ho, C.M., Chen, R., He,Q.Y., Yu, W.Y., Sun,H., Tam, P.K.H., Chiu,J.F., and Che, C.M., (2006). **Analysis of the mode of antibacterial action of silver nanoparticles.** Journal of Proteome, J., Res., 5, 916–924.

Long, H., Mengdi, L., Marie-Pier, D., Philippe, B., Wei, P., Hongya, G., Francois, M. (2018). **Hybridization conditions of oligonucleotide-capped gold nanoparticles for SPR sensing of microRNA.** Journal of ACS Publications, Volume 109, 30 June 2018, Pages 230-236.

Longley, D.B., Harkin, D.P., Johnston, P.G. (2003). **5-fluorouracil: mechanisms of action and clinical strategies**. Journal of Cancer, 3 (5): 330–338.

Lordick, F., Lorenzen, S., Yamada, Y., Ilson, D. (2014). **Optimal chemotherapy for advancedgastric cancer: is there a global consensus?** Journal of Gastric Cancer, 17(2):213–25.

Losa, R., Sierra, MI., Gión, MO., Esteban, E., Buesa. JM. (2006). **Simultaneous determination of gemcitabine di- and triphosphate in human blood mononuclear and cancer cells by RP-HPLC and UV detection.** Journal of Chromatogr B Analyt Technol Biomed Life Sci, 840(1):44-9.

Lu, L., Zhang, W., Wang, D., Xu, X., Miao, J., Jiang, Y. (2010). **Fe_3O_4/Au/Ag core–shell nanoparticles with both sensitive plasmonic properties and tunable magnetism**, Journal of Mater. Lett, 64 (2010) 1732–1734.

Lowenfels, A.B., Maisonneuve, P. (2006). **Epidemiology and risk factors for pancreatic cancer.** Journal of Best Pract Res Clin Gastroenterol, 20: 197–209.

Lyon, JL., Fleming, DA., Stone, MB., Schiffer, P., Williams, ME (2004). **Synthesis of Fe Oxide Core/Au Shell Nanoparticles by Iterative Hydroxylamine Seeding**. Journal of Nano Lett, 4(403):719-723.

Maccuspie, R. (2011). **Colloidal stability of silver nanoparticles in biologically relevant conditions**. Journal of Nanopart, (13):2893–2908.

Maeda, H., Wu, J., Sawa, T., Matsumura, Y., Hori, K. (2000). **Tumor vascular permeability and the EPR effect in macromolecular therapeutics Control.** Journal of Release, 65 (2): 271–284.

Maiti, A., Nemati-Shafaee, M., Msaouel, P., Pagliaro, L., Jonasch, E. (2018). **Phase 2 trial of Capecitabine, Gemcitabine, and Bevacizumab in Sarcomatoid Renal-Cell Carcinoma**. Journal of Clin Genitourin Cancer, Volume 16, Issue 1, Pages e47-e57.

Majoube, M. (1984). **Vibrational spectra of guanine. A normal coordinate analysis**. Journal of Mol Struct, (114): 403–406.

Malekigorji, M., (2016). **Preparation and evaluation of hybrid gold-iron oxide nanoparticles as a multifunctional platform for diagnosis and therapy of pancreatic cancer.** P.h.D thesis of Keele University. 250 (Aim), 40-41.

Malekigorji, M., Alfahad, M., Lin, P.K.T., Jones, S., Curtis, A., Hoskins, C. (2017). **Thermally triggered theranostics for pancreatic cancer therapy.** Journal of Nanoscale, Volume 9, 12735-12745.

Malekigorji, M., Curtis A., Hoskins, C. (2014). **The Use of Iron Oxide Nanoparticles for Pancreatic Cancer Therapy.** Journal of Nanomedicine Research, Volume 1 Issue 1 – 2014.

Mallick, K., Witcomb, M.J., Scurrell, M.S. (2004). **Polymer stabilized silver nanoparticles: A photochemical synthesis route.** Journal of Mater Science, (39): 4459–4463.

Marshall, M., Blumenstein, B., Crawford, E.D., Thompson, I.M., Craig, J.B., Eisenberger, M., Ahmann, F. (1994). **Phase II trial of amonafide for the treatment ofadvanced, hormonally refractory carcinoma of the prostate**, Am. Journal of Clin.Oncol, 17 514e515.

Mas-Moruno, C., Rechenmacher, F., Kessler Cilengitide, H. (2010). **The first anti-angiogenic small molecule drug candidate design, synthesis and clinical evaluation.** Journal of Anti Cancer Agents Med Chem, 10, pp. 753-768.

Maus, L., Dick, O., Bading, H., Spatz, J.P., Fiammengo, R. (2010). **Conjugation of peptides to the passivation shell of gold nanoparticles for targeting of cell-surface receptors.** Journal of ACS Nano, (4): 6617.

Mazzucchelli, L., Burritt, J. B., Jesaitis, A. J., Nusrat, A., Liang, T. W., Gewirtz, A. T., Schnell, F. J., Parkos, C. A. (1999). **Cell-specific peptide binding by human neutrophils.** Journal of Blood, 93: 1738-1748.

McAllister, A., WadudKhan, V., Helmink, H., Wargo. E. (2019). **The Tumor Microbiome in Pancreatic Cancer: Bacteria and Beyond**. Journal of Transplantation, 2:685-694.

Mejías, R., Pérez-Yagüe, S., Gutiérrez, L. Cabrera, L.I., Spada, R., Acedo, P., Serna, C.J., Lázaro, F.J., Villanueva, A., Morales, M.D.P., Barber, D.F., (2011). **Dimercaptosuccinic acid coated magnetite nanoparticles for magnetically guided in vivo delivery of interferon gamma for cancer immunotherapy.** Journal of Biomaterials, (32): 2938–2952.

Mengda, X., Liu, J., Peterka, F., Ren, Y., and Zhu, X. (2018). **Synthesis and Comparative Biological Properties of Ag-PEG Nanoparticles with Tunable Morphologies from Janus to Multi-Core Shell Structure.** Journal of Materials Basel, 11(10): 1787.

Mermet, J.M. (2005). **"Is it still possible, necessary and beneficial to perform research in ICPatomic emission spectrometry?"** Journal of Spectrom, 20:11-16.

Michalke, B. (2010). **Platinum speciation used for elucidating activation or inhibition of Pt-containing anti-cancer drugs**, Journal of Trace Elem. Med. Biol, 24 (2): 69–77.

Modica-Napolitano, JS., Weissig, V. (2015). **Treatment Strategies that Enhance the Efficacy and Selectivity of Mitochondria-Targeted Anticancer Agents**. Journal of Mol Sci, 16(8):17394-17421.

Mohamed, E.T., & Safwat, G.M. (2016). **Evaluation of cardioprotective activity of Lepidium sativum seed powder in albino rats treated with 5-fluorouracil.** Beni-Suef University Journal of Basic and Applied Sciences, 5(2), pp.208–215.

Moiseeva, E.P. & Manson, M.M., (2009). **Dietary chemopreventive phytochemicals: Too little or too much.** Journal of Cancer Prevention Research, 2(7): pp.611–616.

Monteiro, D.R., Gorup, O.F., Takamia, A.S., Ruvolo- Filho, A.C., De-Camargo E.R., and Barbosa, D.B., Int. J.(2009). **Diversity of bacterial endophytes in roots of Mexican husk tomato plants (Physalis ixocarpa) and their detection in the rhizosphere.** Journal of Antimicrob Agents, 34, 103–110.

Montes-Ruiz-Cabello, F.J., et al. (2014). **Electric double-layer potentials and surface regulation properties measured by colloidal-probe atomic force microscopy**. Journal of Physical Review E, 90(1), p.12301.

Morones, J.R., Elechiguerra, J.L., Camacho, A., Holt, K., Kouri, J.B., Ram´ırez, J.T., Yacaman, M.J. (2005). **The bactericidal effect of silver nanoparticles.** Journal of Nanotechnology, 16, 2346–2353.

Mukherji, S., Ruparelia J.P., Agnihotri, S., Cioffi, N., Rai, M., Verlag, S. (2012). **In Nano-Antimicrobials: Progress and Prospects**. Journal of Berlin Heidelberg, (10): 225–251.

Munoz, M., dePedro, Z.M., Casas, J.A., Rodriguez, J.J. (2015). **Preparation of magnetite-based catalysts and their application in heterogeneous Fenton oxidation**. Journal of Appl.Catal.B: Environ, (17): 249–265.

Murphy, D.B. (2002). **Fundamentals of Light Microscopy and Electronic Imaging.** Journal of John Wiley & Sons, New York, ISBN: 9780471234296.

Nadagouda, M.N., Varma, R.S. (2008). **Green synthesis of silver and palladium nano particles at room temperature using coffee and tea extract**, Journal of Green Chem, (10): 859–862.

Nagasamy-Venkatesh, D. (2018). **Metallic Nanoparticle.** Biomed Journal of Sci & Tech Res, Volume 4- Issue 2, 3767

Nasrollahzadeh, M.S., Sajadi, M., AIssaabadi, Z., (2019). **Chapter 1 - An Introduction to Nanotechnology**. Journal of Interface Science and Technology, V (28), pp.1-27.

National Cancer Institute, Clinical Brochure, (1984) **Nafidimide,** Journal of NSC 308847, pp. 6e22.

Naughton, M. (2010). **Evolution of capecitabine dosing in breast cancer.** Washington University School of Medicine, Clin BreastCancer, 10(2):130–5.

Neethirajan, S., Jayas, D., (2010). **Nanotechnology for the Food and Bioprocessing Industries, Food and Bioprocess Technology**. Journal of cancer, volume 4, pages39–47(2011)

Neoptolemos, J.P., *et al.* (2010). **Adjuvant chemotherapy with fluorouracil plus folinic acid vs gemcitabine following pancreatic cancer resection: a randomized controlled trial.** Journal of JAMA, 304(10): pp.1073–81.

Neoptolemos, J.P., et al., (2012). **Effect of adjuvant chemotherapy with fluorouracil plus folinic acid or gemcitabine vs observation on survival in patients with resected periampullary adenocarcinoma: The espac-3 periampullary cancer randomized trial.** Journal of JAMA, 308(2): pp.147.

Neue, E. (2007). **Stationary phase characterization and method development**. Journal of Separation Science, 30(11), pp.1611–1627.

Ng, C.N., Yen, H., Hsiao, H.Y., Su, S.C. (2018). **Phytochemicals in skin Cancer prevention and treatment**: updated review of Journal of Int. J. Mol. Sci, 19 (4): 13-21.

Nguyen, M.T., Seriani, N., Gebauer, R. (2013). **Water adsorption and dissociation on α Fe2O3 calculations**. Journal of Chem.Phys, (13): 194-197.

Nishio, A., Uyeki, E.M. (1983). **Induction of DNA strand breaks and chromosome abnormalities by an imide derivative of 3-Nitro-1,8-naphthalic acid (mitonafide) in Chinese hamster ovary cells.** Journal of Natl. Cancer Inst, (70): 1097e1102.

Novich, B.E., Ring, T.A. (1984). **Colloid stability of clays using photon correlation spectroscopy,** Journal of Clays and Clay Minerals, Volume 32, Issue 5, 400-406.

Nurgali, K., Jagoe, R., Abalo, R. (2018). Editorial: **Adverse Effects of Cancer Chemotherapy: Anything New to Improve Tolerance and Reduce Sequelae?** Journal of Front Pharmacol. 9: 245.

Nymark, P., Catalán, J., Suhonen, S., Järventaus, H., Birkedal, R., Clausen, P., Jensen, K., Vippola, M., Savolainen, K., Norppa, H. (2013). **Genotoxicity of polyvinylpyrrolidone-coated silver nanoparticles in BEAS 2B cells.** Journal of Toxicology, 313, 38–48.

Ojha, S., Venkataraman, B., Kurdi, A., Mahgoub, E., Sadek, B., Rajesh, M. (2016). **Plant-derived agents for counteracting cisplatin-induced nephrotoxicity,** Journal of Oxide Med Cell, (4): 320-374.

Okines, A.F., Norman, A.R., McCloud, P., Kang, Y.K., Cunningham, D. (2009). **Meta-analysis of the REAL-2 and ML17032 trials: evaluating capecitabine-based combination chemotherapy and infused 5-fluorouracil-based combination chemotherapy for the treatment of advanced oesophago-gastric cancer.** Journal of Ann Oncol, 20(9): 1529–34.

O'Reilly, R.K., Joralemon, M.J., Wooley, K.L., Hawker, C.J. (2005) **Functionalization of micelles and shell cross-linked nanoparticles using click chemistry.** Journal of Chem. Mater, (17): 5967–5988.

Pal, S., Tak, Y.K., Song, J.M. (2007). **Does the antibacterial activity of silver nanoparticles depend on the shape of the nanoparticle? A study of the gram-negative bacterium Escherichia coli Appl.** Journal of Environ Microbiol, (73): 1712–1720.

Palneedi, h., Hwan-Park, j., Maurya, d., Peddigari, m., Hwang, t., Annapureddy, v., Kim, j., Jong, J., Byung, C., and Hahn, D. (2018) **Laser Irradiation of Metal Oxide Films and Nanostructures: Applications and Advances.** Journal of Advanced Materials, Volume30, Issue14, 1705148.

Pan, F., Tao, K., Liu, B.X., (1993). **Enhancement of magnetic moment of iron atoms in the Fe/Au nanomultilayers.** Journal of Appl. Phys, 74. 1929.

Pan,Y., Neuss,S., Leifert,A., Fischler,M., Wen,F., Simon,U., Schmid,G., Brandau,W., Jahnen-Dechent,W. (2007). **Size-dependent cytotoxicity of gold nanoparticles**. Journal of Environ Microbiol, (3): 1941.

Paolillo, Russo, Serra, Colombo, Schinelli, 2009. **Small molecule integrin antagonists in cancer therapy**. Journal of Environ Microbiol Mini Rev. Med. Chem. 9, 1439–1446.

Pascal, C., Pascal, J.L, Favier, F., Moubtassim, M.L.E., Payen, C. (1999). **Magnetic Iron Oxide Nanoparticles: Synthesis and Surface Functionalization**. Journal of Nanoscale Research Letters, 11, 141 (3): 397-400.

Pasqualini, P. (1999). **Vascular targeting with phage peptide libraries**. Journal of Nucl Med, (43): 159-162.

Pasqualini, R., Koivunen, E., Ruoslahti, E. 1997). **αv integrins as receptors for tumor targeting by circulating ligands.** Nat Biotechnol, (15): 542-546.

Parham, H., Pourreza, N. & Rahbar, N. (2009). **Solid phase extraction of lead and cadmium using solid sulfur as a new metal extractor prior to determination by flame atomic absorption spectrometry.** Journal of hazardous materials, 163(2–3): pp.588–92.

Patel, V.R., Agrawal, Y.K. (2011). **Nanosuspension: An approach to enhance solubility of drugs.** Journal of advanced pharmaceutical technology & research, 2(2): pp.81–7.

Paull, K.D., Nasr,M., Narayanan, V.L. (1984). **Computer Assisted Structure-Activity Correlations. Evaluation of benzo(de)isoquinoline-1,3-diones and related compounds as antitumor agents,** Journal of Arzneim.-Forsch, 34, 1243e1246.

Petrelli, F., Cabiddu, M., Barni, S. (2012). **5-Fluorouracil or capecitabine in the treatmentof advanced colorectal cancer: a pooled-analysis of randomized trials.** Journal of MedOncol, 29(2):1020–9.

Pissuwan, D., Valenzueka, SM., Cortie, MB. (2006). **Therapeutic possibilities of plasmonically heated gold nanoparticles.** Journal of Trends Biotechnol, (24): 62-67.

Povoski, S.P., Davis, P.D., Colcher, D., Martin, E.W. (2013). **Single molecular weight discrete PEG compounds: emerging roles in molecular diagnostics, imaging and therapeut ics**. Journal of Expert Rev. Mol. Diagn, (13): 315–319.

Prathna, T.C., Chandrasekaran, N., Mukherjee, A. (2011). **Studies on aggregation behaviour of silver nanoparticles in aqueous matrices: Effect of surface functionalization and matrix composition.** Journal of Colloid Surf, 390: 216–224.

Preissler, M., Williams, JA. (1981). **Pancreatic acinar cell function: measurement of intracellular ions and pH and their relation to secretion.** Journal of Physiol, 321:437-448.

Pyatenko A., Yamaguchi, M., and Suzuki, M., Phys, J. (2007). **Synthesis of spherical silver nanoparticles** Journal of Chem, 2007, 111, 7910–7917.

Qian, X., Peng, XH., Ansari, DO., Yin-Goen, Q., Chen, GZ., Shin, DM., Yang, LA., Young, N. (2012). **Nanoparticle Electromagnetic Properties for Sensing Applications.** Journal of Advances in Nanoparticles, (2): 9-14.

Quaquebeke, T., Dumont P., Dewelle, J., Ribaucour, F., Simon G, *et al*. (2007). **2,2,2-Trichloro-N-({2-[2-(dimethylamino)ethyl]-1,3-dioxo-2,3-dihydro-1H-benzo[de] isoquinolin-5-yl}carbamoyl)acetamide (UNBS3157), a novel nonhematotoxic naphthalimide derivative with potent antitumor activity**. Journal of Med Chem, 50(17):4122-34.

Ralton, L.D., Bestwick, C.S., Milne, L., Duthie, S., Kong-Thoo-Lin, P. (2009). **Bisnaphthalimidopropyl spermidine induces apoptosis within colon carcinoma cells.** Journal of ChemBiol Interact, (177):1-6.

Rasheed, A., Matsui, W., Maitra, A. (2012). **Pathology of pancreatic stroma in PDAC.** Journal of Pancreatic Cancer and Tumor Microenvironment, 50(17):4122-34.

Roh, Y., Vali, H., Phelps, T.J., Moon, J.W. (2006).**Extracellular Synthesis of Magnetite and Metal-Substituted Magnetite Nanoparticles.** Journal of Nanosci Nanotechnol. (11): 35-47.

Roldan, M.C., Brana, M.F., Berlanga, J.M.C., (1973). **4-acylamino-n-phenylbutyramides useful as Pharmaceuticals**. Journal of Microenvironment, 50(17):4122-34.

Roldan, M., Brana, M.F., Berlanga, J.M.C. (1979). **N-Aminoethyl-substituted-3-nitronaphthalimides,** Journal of Current Pharmaceutical Design, 7(17):1745-80.

Ross, W.E., Bradley, M.O. (1981). **DNA double-strand breaks in mammalian cells after exposure to intercalating agents**, Journal of Biochim Biophys Acta Nucleic Acids Protein Synth, 654 (1): 129-134.

Rubinson, B.M. (2015).**Therapeutic approaches for metastatic pancreatic adenocarcinoma.** Journal of Hematol Oncol Clin, North America, 29 (4): 761–776.

Rubinson, KA. (2000). **Contemporary Instrumental Analysis.** Journal of Upper Saddle River, NJ, Prentice Hall.

Ruoslahti, E. (1996). **RGD and other recognition sequences for integrins.** Journal of Annu Rev Cell Dev Biol, (12): 697-715, 1996.

Ruoslahti, E., Pierschbacher, MD. (1987). **New perspectives in cell adhesion: RGD and integrins.** Journal of Science, 238, pp. 491-497.

Salameh, S. *et al.,* (2014). **Contact behavior of size fractionated TiO2 nanoparticle agglomerates and aggregates**. Journal of Powder Technology, (25) 345–351.

Samadian, H., Hosseini-Nami, S., Kamrava, S.K., Ghaznavi, H., Shakeri-Zadeh A., (2016). **Diagnostic, Prognostic and Predictive Biomarkers in Prostate Cancer.** Journal of Res Clin Oncol, 142 (4): pp. 2217-2229.

Sanvicens, N., Pila-Marco, M. (2015). **Multifunctional nanoparticles – properties and prospects for their use in human medicine.** Journal of Trends Biotechnol, 26 (8): 425–533.

Sassen, E.A., Miska, C. (2008). **MicroRNA: implications for cancer.** Journal of Virchows Arch, (10): 432-452.

Seil, J.T., Webster, J. (2012). **Antimicrobial applications of nanotechnology: methods and literature.** Journal of Int J Nanomedicine, (7): 2767.

Shahid, F., Farooqui, Z., Khan, F. (2018) **Cisplatin-induced gastrointestinal toxicity: An update on possible mechanisms and on available gastroprotective strategies.** Journal of Pharmacol, 827 (2018) 49–57.

Shakeri-Zadeh, A., Mansoori, G.A., Hashemian, A.R., Eshghi, H., Sazgarnia, A., Montazerabadi, A.R. (2010). **Biochem Process Biotechnol Mol**. Journal of Controlled Release, 4 (2010), pp. 06-12.

Shakeri-Zadeh, A., Mansoori, G.A., Hashemian, A.R., Eshghi, H., Sazgarnia, A., Montazerabadi, A.R. (2010). **Cancerous cells targeting and destruction using folate conjugated gold nanoparticles.** Journal of Biochem Process Biotechnol, Mol. Biol, 06–12.

Sharma, V., Yngard, R., Lin, Y. (2009). **Silver nanoparticles: green synthesis and their antimicrobial activities.** Journal of Colloid Interface, 145 (1), 83–96.

Sheldrake, M., Patterson, H. (2009). **Function and antagonism of β integrins in the development of cancer therapy.** Journal of Cancer Drug Targets, (9): 519–540.

Shen, K., Zhang, Y., Ding. J. (2015). **c(RGDfC)-decorated micelle as nanocarrier for targeting therapeutic of colon cancer.** Journal of Control Release, (10): 213- 266.

Shirtcliffe, N., Nickel, U., and Schneider, S. (1999). **Reproducible Preparation of Silver Sols with Small Particle Size Using Borohydride Reduction: For Use as Nuclei for Preparation of Larger Particles.** Journal of Colloid Interface Sci, (21): 122–129.

Shrikhande, S.V. *et al.,* (2007). **Pancreatic resection for M1 pancreatic ductal adenocarcinoma.** Journal of Annals of surgical oncology, (14): 118–127.

Shu, Y., Pi, F., Sharma, A., Rajabi, M., Haque, F., Shu, D., Leggas, M., Evers, B.M., Guo, P. (2014). **Stable RNA nanoparticles as potential new generation drugs for cancer therapy.** Journal of Advanced Drug Delivery Reviews, 66, pp.74–89.

Sibilia, J.P. (1996). **A Guide to Materials Characterization and Chemical Analysis.** 2nd Edition, USA, VCH, (5): 408 Pages.

Siddik, Z.H. (2003). **Cisplatin: mode of cytotoxic action and molecular basis of resistance**. Journal of Oncogene, 22 (47): 7265–7279.

Siegel, R.L., Miller, K.D., Jemal, A., (2016). **Cancer statistics**. Ca - Cancer Journal of Clin, 66: 7e30.

Simpson, A., Agrawal, A., Kellen, M., Harkness, D. (2011). **Short-Chain PEG Mixed Monolayer Protected Gold Clusters Increase Clearance and Red Blood Cell Counts**. Journal of ACS Nano, 5, 5, 3577-3584.

Sivula, K., Le-Formal, F., Grätzel, M. (2011). **Solar Water Splitting: Progress Using Hematite (α-Fe2O3) Photoelectrodes**. Journal of ChemSusChem, 4 (2011) 432–449.

Snyder, H.R., Miyake, A., Hankin, B.L. (2015). **Advancing understanding of executive function impairments and psychopathology: bridging the gap between clinical and cognitive approaches**, Journal of Front Psychol, volume 6, 1170.

Snyder, L.R., Kirkland, J.W. Dolan, L. (2011). **Introduction to modern liquid chromatography, 3 Ed**. Journal of John Wiley & Sons, Volume 8, Issue 1, 139-144.

Sondi, I., Salopek-Sondi, B. (2004). **Silver nanoparticles as antimicrobial agent: a case study on E. coli as a model for Gram-negative bacteria**. Journal of Colloid Interface Sci. 2004, 275: 177–182. 10.1016/j.jcis.2004.02.012.

Song, X., Chen, H., Zhang, C., Yu, Y., Chen, Z., Liang, H., *et al.,* (2019). **SRC-3 inhibition blocks tumor growth of pancreatic ductal adenocarcinoma**. Journal of Pubmed Elsevier, (4): 310-319.

Sotiriou, G. A., Pratsinis, S. E. (2010) **Antibacterial activity of Nano silver ions and particles**. Journal of Environ Sci Technol, (4): 49-56 (2010).

Sperling, R.A., Parak, W.J. (2010). **Surface modification, functionalization and bioconjugation of colloidal inorganic nanoparticles**. Journal of Phil. Trans. R. Soc, 368, 1333–1383.

Sriram, M.I., Kanth, S.B., Kalishwaralal, K., Gurunathan, S. (2010). **Antitumor activity of silver nanoparticles in Dalton's lymphoma ascites tumour model.** Internationa Journal of Nanomedicine. (5): 753–762.

Steinigeweg, D., Schlücker S., (2012). **Monodispersity and size control in the synthesis of 20–100 nm quasi-spherical silver nanoparticles by citrate and ascorbic acid reduction in glycerol–water mixtures**. Journal of Chem. Commun, 48 (2012), pp. 8682–8684.

Sugimoto, T., Matijevic,E. (1980). **Formation of Uniform Spherical Magnetite Particles by Crystallization from Ferrous Hydroxide Gel.** Journal of Colloid Interface Science, (74): 227–243.

Suk, J.S., Lai, S.K., Boylan, N.J., Dawson, M.R., Boyle, M.P., Hanes, J. (2011). **Rapid transport of muco-inert nanoparticles in cystic fibrosis sputum treated with Nacetyl cysteine**. Journal of Nanomedicine, (6): 365–375.

Sun, T., Zhang, Y.S., Pang, B., Hyun, D.C., Yang, M., Xia, Y. (2014). **Engineered nanoparticles for drug delivery in cancer therapy.** Journal of Angew Chem Int Ed, (53): 12320–12364.

Sun, W. (2010). **Evolution of capecitabine dosing in colorectal cancer**. Journal of Clin Colorectal Cancer, 9(1): 31–9.

Surh, Y.J. (2003). **Cancer chemoprevention with dietary phytochemicals.** Journal of Nature reviews Cancer, (10): 768–780.

Sun, Y. Xia., Y. (2002) **Shape-Controlled Synthesis of Gold and Silver Nanoparticles.** Journal of Science, (29): 2176–2179.

Takahari, D. (2017). **Second-line chemotherapy for patients with advanced gastric cancer.** Journal of Gastric Cancer, 20 (3) (2017) 395–406.

Takeshi, T., Makoto, T., Takuya, K., Hiroaki, A., Masaharu, T. (2017). **Morphological changes from spherical silver nanoparticles to cubes after laser irradiation in acetone–water solutions via spontaneous atom transportation process.** Journal of American Chemical Society, (5): 33-37.

Tanaka, Y., Matsuo, K., Yuzuriha, S. (2011). **Objective assessment of skin rejuvenation using near-infrared 1064-nm neodymium: YAG laser in Asians**. Journal of Clin Cosmet Investig Dermatol, (4):123-130.

Tan, Y., Dai, X., Li, Y., Zhu, D. (2003). **Preparation of gold, platinum, palladium and silver nanoparticles by the reduction of their salts with a weak reductant–potassium bitartrate.** Journal of Materials Chemistry, (13): 1069–1075.

Tao, X., Ning, Z., Heather, L.N., Donglu, S., Xuejun, W. (2007). **Modification of nanostructured materials for biomedical applications.** Journal of Mater Science, 27 (3), 579–594.

Tartaj, P., Morales, M.P., Gonzalez-Carreño, T., Veintemillas-Verdaguer, S., Serna, C.J. (2011). **The iron oxides strike back: from biomedical applications to energy storage devices and photo electrochemical water.** Journal of Splitting Adv Mater, 23(2011): 5243–5249.

Tejamaya, A., Römer, H., Merrifield, L., Lead, J.R. (2012). **Stability of citrate, PVP, and PEG coated silver nanoparticles in ecotoxicology media**. Journal of Environ. Sci. Technology, (46): 7011–7017.

Theimer, S. (2016). **Non-Narcotic Nerve Block Controls Children's Pain, Shortens Hospital Stays.** Journal of Mayo Clinic Public Affairs, (50): 284-505.

Todolí, J.L. & Mermet, J.M. (2006). **Sample introduction systems for the analysis of liquid microsamples.** Journal of Spectrochimica Acta Part B Atomic Spectroscopy, 61(3): 239–283.

Tsuji, T., Watanabe, N., Tsuji, M. (2003).**Laser induced morphology change of silver colloids: formation of nano-size wires.** Journal of Appl Surf Sci, 211 (81): 189–193.

Tran, S., Puhar, A., Camus, M., Ramarao. N. (2011). **Trypan Blue Dye Enters Viable Cells Incubated with the Pore-Forming Toxin HlyII of Bacillus cereus**. Journal of PLoS One, 6(9): e22876.

U.S. National Library of Medicine's. (2004). **Toxicology and Environmental Health Information Program.** Journal of of Appl Surf Sci, Volume 198, Issues 1–3, 20 May 2004, Pages 161-168.

Vekas, L., Bica, D., Marinica, O. (2006). **Magnetic nanofluids stabilized with various chain length surfactants.** Journal of Appl, 58 (2006) 257–267.

Verbruggen, S., Keulemans, M., Marten, J., Lenaerts, S. (2013). **Predicting the Surface Plasmon Resonance Wavelength of Gold–Silver Alloy Nanoparticles.** Journal of American Chemical Society, (37): 19142-19145.

Verwey, E.J.W., (1939). **Electronic conduction of magnetite (Fe3O4) and itstransition point at low temperatures.** Journal of Nature, 144 (1939): 327.

Vincent, A. et al., (2011). **Pancreatic cancer.** Journal of Lancet, 378(9791): 607–720.

Vincent, A. Herman J, Schulick R, Hruban RH, Goggins M. (2011). **Pancreatic cancer.** Journal of Lancet, 378(91): 607–720.

Wang, L., Park, H,Y., Im-Lim H.I., Schadt, M.J., Mott,D., Luo, J., Wang, X., Zhong, C.J. (2008). **Core–shell nanomaterials: gold-coated magnetic oxide nanoparticles,** Journal of Mater. Chem, 18 (2008) 2629–2635.

Wang M.D., Nie, S. (2008). **In vivo tumour targeting and spectroscopic detection with surfaceenhanced Raman nanoparticle tags.** Journal of Nat Biotechnol, (26):83-90.

Wang, Z, Mohamed, M.B, Link, S., EL-Sayed, M.A. (1999). **Crystallographic facets and shapes of gold Nanorods of different aspect ratios.** Journal of Surface science, 440(1): 809-814.

Wang, E., Wei, W., Zhang, R., Yuan, A. (2013). **Role of thiol-containing polyethylene glycol (thiol-PEG) in the modification process of gold nanoparticles (AuNPs): Stabilizer or coagulant.** Journal of Colloid and Interface Science, 404, 223–229.

Warra, A.A., JIMOH, W.L.O. (2011). **Overview of an inductively coupled plasma (ICP) system**. International Journal of Chemical Research, (2): 41-48.

Wei, K., Li, J., Liu, J., Chen, G., Jiang, M. (2012). **Reversible vesicles of supramolecular hybrid nanoparticles.** Journal of Soft Matter, (8): 300-303.

Weiss, W., Ranke, W. (2002). **Surface chemistry and catalysis on well-defined epitaxial iron oxide layers.** Progress in Surface Science, (70): 147–151.

Wei, W., Zhaohui, W., Taekyung, Y., Changzhong, J., Woo-Sik, K. (2015). **Recent progress on magnetic iron oxide nanoparticles: synthesis, surface functional strategies and biomedical applications.** Journal of Science Techno Mater, (16): 423-501.

Weller, H., Eychmüller, A., Vogel, R., Katsikas, L., Hässelbarth, A., Giersig, M. (1993). **Synthesis and photochemistry of quantum-size semiconductor particles in solution and in modified layers**, Journal of Chem, 33 (1): 107–113.

Widmann, D., Behm, R.J., (2014). **Activation of molecular oxygen and the nature of the active oxygen species for CO oxidation on oxide supported Au catalysts,** Journal of Acc.Chem.Res, 47 (2014)740–749.

Wang, H., Word, BR., Lyn-Cook, BD. (2005). **Enhanced Efficacy of Gemcitabine by Indole-3 carbinol in Pancreatic Cell Lines: The Role of Human Equilibrative Nucleoside Transporter.** Journal of Anticancer Research, 31(10):3171-3180.

Williams, D., & Fleming, I. (2007). **Spectroscopic Methods in Organic**. Journal of Nano Lett, 4(403): 719-723.

Wang, W., Nie, J. (2008). **In vivo tumour targeting and spectroscopic detection with surfaceenhanced Raman nanoparticle tags**. Journal of Nat. Biotechnol, (26):83-90.

Wang, W., Shen, E., Wang, W., Xie C. (2013). **The functions and applications of RGD in tumor therapy and tissue engineering.** International Journal of Mol. Sci., 14 (7), pp. 13447-13462.

Woodrow, W. (2011). **An inventory of nanotechnology based consumer products currently on the market.** Beilstein Journal of Nanotechnol, 6: 1769–1780.

Wu, W., Zhou, Z., Berliner, B., Banerjee, B., Zhou, Z. (2010). **Smart core– shell hybrid nanogels with Ag nanoparticle core for cancer cell imaging and gel shell for pH-regulated drug delivery**. Journal of Chem. Mater, (22):1966–1976.

Wu, Y., Zhang, X., Xiong. Z. (2005). **MicroPET imaging of glioma integrin {alpha}v{beta}3 expression using (64)Cu-labeled tetrameric RGD peptide**. Journal of Acta Biomaterialia, 46 (10): pp. 1707-1718.

Xiong, X.-B. *et al*. (2012). **Amphiphilic block co-polymers: Preparation and application in nanodrug and gene delivery**. Journal of Acta Biomaterialia, 8(6): pp.2017–2033.

Xu, C., Cheng, P., Sun, L., Zhang, S., Huang, H., Chen, Y., Shi, J. (2015). **Distinctive effects of TiO2 and CuO nanoparticles on soil microbes and their community structures in flooded paddy soil**. Journal of Nanomaterials (Basel), 8(10): 839.

Xu, C., Wang, B., Sun, S. (2009). **Dumbbell-like Au-Fe3O4 Nanoparticles for Target-Specific Platin Delivery**. Journal of Am. J. Chem. Soc, 131:4216-4217.

Xu, H. (2009). **Overview of naphthalimide analogs as anticancer agents**. Journal of Curr Med Chem, (16): 4797e4813.

Xu, L., HW, L., Yang.Y. (2018). **Stability and Reactivity: Positive and Negative Aspects for Nanoparticle Processing.** Journal of Chem Rev, (7):3209-3250.

Yancik, R. (2005). **Population aging and cancer: a cross-national concern.** Journal of Cancer journal, 11(6): 437–441.

Yang, E.H. (2010). **Engineered low-dimensional nanomaterials for sensors, actuators and electronics.** Journal of Micro Nanolith Mem, (4): 41-103.

Yang, J., Yin, H., Jia, J., Wei, Y. (2011). **Facile Synthesis of High-Concentration, Stable Aqueous Dispersions of Uniform Silver Nanoparticles Using Aniline as a Reductant.** Journal of Langmuir, (27): 5047– 5053.

Yavuz, C.T., Mayo, J.T., Yu, W.W., Prakash, A., Falkner, J.C., Yean, S., Cong, L., Shipley, H.J., Kan, A., Tomson, M., Natelson, D., Colvin, V.L. (2006). **Low-field magnetic separation of mono disperses Fe_3O_4 nanocrystals**. Journal of Science, 314(2006)964–967.

Yen-Ang, C., Yu-Tan, S., Lu, Y., Bai, L., Li, M., Li, P., Zhang, Q., Tamil-Selvan, S., Zhao, Y. (2014). **Turn-on fluorescence probe integrated polymer nanoparticles for sensing biological thiol molecules.** Journal of Scientific Reports, 7(2):189-217.

Yun, S.I. *et al.,* (2009). **Japanese encephalitis virus-based replicon RNAs/particles as an expression system for HIV-1 Pr55Gag that is capable of producing virus-like particles.** Journal of Virus Research, 144(12) 298–305.

Zhang, T., Wang, L., Chen, Q., Chen, C. (2014). **Cytotoxic potential of silver nanoparticles.** Journal of Yonsei Med Journal, (55): 283–291.

Zhi, X. *et al.,* (2014). **MUC4-induced nuclear translocation of β-catenin: a novel mechanism for growth, metastasis and angiogenesis in pancreatic cancer.** Journal of Cancer letters, 346(1), 104–113.

Zijlstra, P., Orrit, M. (2011). **Single metal nanoparticles: optical detection, spectroscopy and applications.** Journal of Rep Prog Phys, (74):106401-106456.

Zsigmondy, R. (1926). **Properties of colloid.** Nobel Foundation Lecture, (15): 108-132.

Zuo, HD., Yao, W., Chen, W., Zhu J., Zhang, J., Pu, Y., Liu, G., Zhang, XM. (2014). **The effect of superparamagnetic iron oxide with iRGD peptide on the labeling of pancreatic cancer cells in vitro: a preliminary study**. Journal of Biomed Res Int. 2014:852352 (8 pages).